

Contents

Glossary	xiii
Acronyms	xiv
1 Introduction	1
1.1 Cancer Research in the Post-Genomic Era	1
1.1.1 Cancer as a Global Health Concern	2
1.1.1.1 The Genetics and Molecular Biology of Cancers	3
1.1.2 The Human Genome Revolution	6
1.1.2.1 The First Human Genome Sequence	6
1.1.2.2 Impact of Genomics	7
1.1.3 Technologies to Enable Genetics Research	7
1.1.3.1 DNA Sequencing and Genotyping Technologies	7
1.1.3.2 Microarrays and Quantitative Technologies	8
1.1.3.3 Massively Parallel “Next Generation” Sequencing	9
1.1.3.3.1 Molecular Profiling with Genomics Technology .	11
1.1.3.3.2 Sequencing Technologies	11
1.1.3.4 Bioinformatics as Interdisciplinary Genomic Analysis .	12
1.1.4 Follow-up Large-Scale Genomics Projects	13
1.1.5 Cancer Genomes	14
1.1.5.1 The Cancer Genome Atlas Project	15
1.1.5.1.1 Findings from Cancer Genomes	15
1.1.5.1.2 Genomic Comparisons Across Cancer Tissues .	17
1.1.5.1.3 Cancer Genomic Data Resources	18
1.1.6 Genomic Cancer Medicine	18
1.1.6.1 Cancer Genes and Driver Mutations	18
1.1.6.2 Personalised or Precision Cancer Medicine	19
1.1.6.2.1 Molecular Diagnostics and Pan-Cancer Medicine	20
1.1.6.3 Targeted Therapeutics and Pharmacogenomics	21
1.1.6.3.1 Targeting Oncogenic Driver Mutations	21
1.1.6.4 Systems and Network Biology	22
1.1.6.4.1 Network Medicine, and Polypharmacology	24
1.2 A Synthetic Lethal Approach to Cancer Medicine	25
1.2.1 Synthetic Lethal Genetic Interactions	26
1.2.2 Synthetic Lethal Concepts in Genetics	26
1.2.3 Studies of Synthetic Lethality	27

1.2.3.1	Synthetic Lethal Pathways and Networks	28
1.2.3.1.1	Evolution of Synthetic Lethality	29
1.2.4	Synthetic Lethal Concepts in Cancer	29
1.2.5	Clinical Impact of Synthetic Lethality in Cancer	31
1.2.6	High-throughput Screening for Synthetic Lethality	33
1.2.6.1	Synthetic Lethal Screens	34
1.2.7	Computational Prediction of Synthetic Lethality	37
1.2.7.1	Bioinformatics Approaches to Genetic Interactions . .	37
1.2.7.2	Comparative Genomics	38
1.2.7.3	Analysis and Modelling of Protein Data	41
1.2.7.4	Differential Gene Expression	43
1.2.7.5	Data Mining and Machine Learning	44
1.2.7.6	Bimodality	47
1.2.7.7	Rationale for Further Development	48
1.3	E-cadherin as a Synthetic Lethal Target	48
1.3.1	The <i>CDH1</i> gene and it's Biological Functions	48
1.3.1.1	Cytoskeleton	49
1.3.1.2	Extracellular and Tumour Micro-Environment	49
1.3.1.3	Cell-Cell Adhesion and Signalling	49
1.3.2	<i>CDH1</i> as a Tumour (and Invasion) Suppressor	50
1.3.2.1	Breast Cancers and Invasion	50
1.3.3	Hereditary Diffuse Gastric Cancer and Lobular Breast Cancer .	50
1.3.4	Somatic Mutations	52
1.3.4.1	Mutation Rate	52
1.3.4.2	Co-occurring Mutations	52
1.3.5	Models of <i>CDH1</i> loss in cell lines	53
1.4	Summary and Research Direction of Thesis	54
2	Methods and Resources	58
2.1	Bioinformatics Resources for Genomics Research	58
2.1.1	Public Data and Software Packages	58
2.1.1.1	Cancer Genome Atlas Data	59
2.1.1.2	Reactome and Annotation Data	60
2.2	Data Handling	61
2.2.1	Normalisation	61
2.2.2	Sample Triage	61
2.2.3	Metagenes and the Singular Value Decomposition	63
2.2.3.1	Candidate Triage and Integration with Screen Data .	63
2.3	Techniques	64
2.3.1	Statistical Procedures and Tests	64
2.3.2	Gene Set Over-representation Analysis	65
2.3.3	Clustering	66
2.3.4	Heatmap	66
2.3.5	Modeling and Simulations	66
2.3.5.1	Receiver Operating Characteristic (Performance) . .	67
2.3.6	Resampling Analysis	68

2.4	Pathway Structure Methods	69
2.4.1	Network and Graph Analysis	69
2.4.2	Sourcing Graph Structure Data	70
2.4.3	Constructing Pathway Subgraphs	70
2.4.4	Network Analysis Metrics	70
2.5	Implementation	71
2.5.1	Computational Resources and Linux Utilities	71
2.5.2	R Language and Packages	73
2.5.3	High Performance and Parallel Computing	75
3	Methods Developed During Thesis	77
3.1	A Synthetic Lethal Detection Methodology	77
3.2	Synthetic Lethal Simulation and Modelling	80
3.2.1	A Model of Synthetic Lethality in Expression Data	80
3.2.2	Simulation Procedure	84
3.3	Detecting Simulated Synthetic Lethal Partners	87
3.3.1	Binomial Simulation of Synthetic lethality	87
3.3.2	Multivariate Normal Simulation of Synthetic lethality	89
3.3.2.1	Multivariate Normal Simulation with Correlated Genes	92
3.3.2.2	Specificity with Query-Correlated Pathways	99
3.3.2.3	Importance of Directional Testing	99
3.4	Graph Structure Methods	101
3.4.1	Upstream and Downstream Gene Detection	101
3.4.1.1	Permutation Analysis for Statistical Significance	102
3.4.1.2	Hierarchy Based on Biological Context	103
3.4.2	Simulating Gene Expression from Graph Structures	104
3.5	Customised Functions and Packages Developed	108
3.5.1	Synthetic Lethal Interaction Prediction Tool	108
3.5.2	Data Visualisation	109
3.5.3	Extensions to the iGraph Package	112
3.5.3.1	Sampling Simulated Data from Graph Structures	112
3.5.3.2	Plotting Directed Graph Structures	112
3.5.3.3	Computing Information Centrality	113
3.5.3.4	Testing Pathway Structure with Permutation Testing .	113
3.5.3.5	Metapackage to Install iGraph Functions	114
4	Synthetic Lethal Analysis of Gene Expression Data	115
4.1	Synthetic lethal genes in breast cancer	116
4.1.1	Synthetic lethal pathways in breast cancer	118
4.1.2	Expression profiles of synthetic lethal partners	119
4.1.2.1	Subgroup pathway analysis	122
4.2	Comparison of synthetic lethal gene candidates	125
4.2.1	Comparison with siRNA screen candidates	125
4.2.2	Comparison with correlation	126
4.2.3	Comparison with viability	127
4.2.4	Comparison with secondary siRNA screen candidates	130

4.2.5	Comparison of screen at pathway level	130
4.2.5.1	Resampling of genes for pathway enrichment	132
4.3	Metagene Analysis	138
4.3.1	Pathway expression	138
4.3.2	Somatic mutation	141
4.3.3	Synthetic lethal metagenes	142
4.4	Replication in stomach cancer	144
4.4.1	Synthetic Lethal Genes and Pathways	144
4.4.2	Synthetic Lethal Expression Profiles	146
4.4.3	Comparison to Primary Screen	148
4.4.3.1	Resampling Analysis	149
4.4.4	Metagene Analysis	150
4.5	Global Synthetic Lethality	150
4.5.1	Hub Genes	152
4.5.2	Hub Pathways	153
4.6	Replication in cell line encyclopaedia	154
4.7	Discussion	157
4.7.1	Strengths of the SLIPT Methodology	157
4.7.2	Synthetic Lethal Pathways for E-cadherin	158
4.7.3	Replication and Validation	160
4.7.3.1	Integration with siRNA Screening	160
4.7.3.2	Replication across Tissues and Cell lines	160
4.8	Summary	161
5	Synthetic Lethal Pathway Structure	166
5.1	Synthetic Lethal Genes in Reactome Pathways	166
5.1.1	The PI3K/AKT Pathway	167
5.1.2	The Extracellular Matrix	169
5.1.3	G Protein Coupled Receptors	172
5.1.4	Gene Regulation and Translation	172
5.2	Network Analysis of Synthetic Lethal Genes	173
5.2.1	Gene Connectivity and Vertex Degree	174
5.2.2	Gene Importance and Centrality	175
5.2.2.1	Information Centrality	175
5.2.2.2	PageRank Centrality	177
5.3	Relationships between Synthetic Lethal Genes	179
5.3.1	Hierarchical Pathway Structure	179
5.3.1.1	Contextual Hierarchy of PI3K	179
5.3.1.2	Testing Contextual Hierarchy of Synthetic Lethal Genes	179
5.3.2	Upstream or Downstream Synthetic Lethality	183
5.3.2.1	Measuring Structure of Candidates within PI3K	183
5.3.2.2	Resampling for Synthetic Lethal Pathway Structure . .	185
5.4	Discussion	187
5.5	Summary	189

6 Simulation and Modeling of Synthetic Lethal Pathways	192
6.1 Comparing methods	193
6.1.1 Performance of SLIPT and χ^2 across Quantiles	194
6.1.1.1 Correlated Query Genes affects Specificity	197
6.1.2 Alternative Synthetic Lethal Detection Strategies	199
6.1.2.1 Correlation for Synthetic Lethal Detection	200
6.1.2.2 Testing for Bimodality with BiSEp	201
6.2 Simulations with Graph Structures	203
6.2.1 Performance over a Graph Structure	204
6.2.1.1 Simple Graph Structures	204
6.2.1.2 Constructed Graph Structures	206
6.2.2 Performance with Inhibitions	210
6.2.3 Synthetic Lethality across Graph Structures	216
6.2.4 Performance within a Simulated Human Genome	220
6.3 Simulations over pathway-based graphs	226
6.3.1 Pathway Structures in a Simulated Human Genome	228
6.4 Discussion	231
6.4.1 Simulation Procedure	231
6.4.2 Design and Performance of SLIPT	232
6.4.3 Simulations from Graph Structures	234
6.5 Summary	235
7 Discussion	238
7.1 Significance	238
7.2 Future Directions	239
7.3 Conclusion	240
8 Conclusion	244
References	245
A Sample Quality	271
A.1 Sample Correlation	271
A.2 Replicate Samples in TCGA Breast	274
B Software Used for Thesis	278
C Secondary Screen Data	287
D Mutation Analysis in Breast Cancer	289
D.1 Synthetic Lethal Genes and Pathways	289
D.2 Synthetic Lethal Expression Profiles	292
D.3 Comparison to Primary Screen	295
D.3.1 Resampling Analysis	297
D.4 Compare SLIPT genes	299
D.5 Metagene Analysis	301
D.6 Mutation Variation	302

D.6.1	Mutation Frequency	302
D.6.2	PI3K Mutation Expression	303
E	Metagene Expression Profiles	306
F	Stomach Expression Analysis	312
F.1	Synthetic Lethal Genes and Pathways	312
F.2	Comparison to Primary Screen	315
	F.2.1 Resampling Analysis	317
F.3	Metagene Analysis	319
G	Stomach Mutation Analysis	320
G.1	Synthetic Lethal Genes and Pathways	320
G.2	Synthetic Lethal Expression Profiles	323
G.3	Comparison to Primary Screen	326
	G.3.1 Resampling Analysis	328
G.4	Metagene Analysis	330
H	Global Synthetic Lethality in Stomach Cancer	331
H.1	Hub Genes	333
H.2	Hub Pathways	334
I	Replication in cell line encyclopaedia	335
J	Synthetic Lethal Genes in Pathways	340
K	Pathway Connectivity for Mutation SLIPT	348
L	Information Centrality for Gene Essentiality	352
M	Pathway Structure for Mutation SLIPT	355
N	Performance of SLIPT and χ^2	358
N.0.1	Correlated Query Genes affects Specificity	364
O	Graph Structures	370
O.1	Simulations from Graph Structures	376
O.2	Simulations from Inhibiting Graph Structures	381
O.3	Simulation across Graph Structures	391
O.4	Graph Structure Simulations with 20K genes	395
	O.4.1 Inhibiting Graph Structure Simulations with 20K genes	402
O.5	Simations from Pathway Graph Structures	414

List of Figures

1.1	Synthetic genetic interactions	27
1.2	Synthetic lethality in cancer	30
2.1	Read count density	62
2.2	Read count sample mean	62
3.1	Framework for synthetic lethal prediction	78
3.2	Synthetic lethal prediction adapted for mutation	79
3.3	A model of synthetic lethal gene expression	81
3.4	Modeling synthetic lethal gene expression	82
3.5	Synthetic lethality with multiple genes	83
3.6	Simulating gene function	85
3.7	Simulating synthetic lethal gene function	85
3.8	Simulating synthetic lethal gene expression	86
3.9	Performance of binomial simulations	88
3.10	Comparison of statistical performance	88
3.11	Performance of multivariate normal simulations	90
3.12	Simulating expression with correlated gene blocks	93
3.13	Simulating expression with correlated gene blocks	94
3.14	Synthetic lethal prediction across simulations	95
3.15	Performance with correlations	96
3.16	Comparison of statistical performance with correlation structure	97
3.17	Performance with query correlations	98
3.18	Statistical evaluation of directional criteria	99
3.19	Performance of directional criteria	100
3.20	Simulated graph structures	104
3.21	Simulating expression from a graph structure	106
3.22	Simulating expression from graph structure with inhibitions	107
3.23	Demonstration of violin plots with custom features	110
3.24	Demonstration of annotated heatmap	110
3.25	Simulating graph structures	113
4.1	Synthetic lethal expression profiles of analysed samples	121
4.2	Comparison of SLIPT to siRNA	125
4.3	Compare SLIPT and siRNA genes with correlation	126
4.4	Compare SLIPT and siRNA genes with correlation	127
4.5	Compare SLIPT and siRNA genes with viability	128

4.6	Compare SLIPT and siRNA genes with siRNA viability	129
4.7	Resampled intersection of SLIPT and siRNA candidates	133
4.8	Pathway metagene expression profiles	139
4.9	Somatic mutation against PI3K metagene	141
4.10	Synthetic lethal expression profiles of stomach samples	147
4.11	Synthetic lethal partners across query genes	151
5.1	Synthetic Lethality in the PI3K Cascade	168
5.2	Synthetic Lethality in the Elastic Fibre Formation Pathway	170
5.3	Synthetic Lethality in the Fibrin Clot Formation	171
5.4	Synthetic Lethality and Vertex Degree	174
5.5	Synthetic Lethality and Centrality	177
5.6	Synthetic Lethality and PageRank	178
5.7	Hierarchical Structure of PI3K	180
5.8	Hierarchy Score in PI3K against Synthetic Lethality in PI3K	181
5.9	Structure of Synthetic Lethality in PI3K	183
5.10	Structure of Synthetic Lethality Resampling in PI3K	184
6.1	Performance of χ^2 and SLIPT across quantiles	195
6.2	Performance of χ^2 and SLIPT across quantiles with more genes	196
6.3	Performance of χ^2 and SLIPT across quantiles with query correlation .	197
6.4	Performance of χ^2 and SLIPT across quantiles with query correlation and more genes	198
6.5	Performance of negative correlation and SLIPT	200
6.6	Performance of simulations on a simple graph	205
6.7	Performance of simulations is similar in simple graphs	206
6.8	Performance of simulations on a constructed graph	207
6.9	Performance of simulations on a large graph	209
6.10	Performance of simulations on a simple graph with inhibition	211
6.11	Performance is higher on a simple inhibiting graph	212
6.12	Performance of simulations on a constructed graph with inhibition . . .	214
6.13	Performance is affected by inhibition in graphs	215
6.14	Detection of Synthetic Lethality within a Graph Structure	217
6.15	Detection of Synthetic Lethality within a Graph Structure with Inhibitions	219
6.16	Performance of simulations including a simple graph	221
6.17	Performance on a simple graph improves with more genes	222
6.18	Performance on an inhibiting graph with more genes	223
6.19	Performance on an inhibiting graph improves with more genes	225
6.20	Performance of simulations on the PI3K cascade	227
6.21	Performance of simulations including the PI3K cascade	229
6.22	Performance on pathways improves with more genes	230
A.1	Correlation profiles of removed samples	272
A.2	Correlation analysis and sample removal	273
A.3	Replicate excluded samples	274
A.4	Replicate samples with all remaining	275

A.5	Replicate samples with some excluded	276
D.1	Synthetic lethal expression profiles of analysed samples	293
D.2	Comparison of mtSLIPT to siRNA	295
D.3	Compare mtSLIPT and siRNA genes with correlation	299
D.4	Compare mtSLIPT and siRNA genes with correlation	299
D.5	Compare mtSLIPT and siRNA genes with siRNA viability	300
D.6	Somatic mutation locus	302
D.7	Somatic mutation against PIK3CA metagene	303
D.8	Somatic mutation against PI3K protein	304
D.9	Somatic mutation against AKT protein	305
E.1	Pathway metagene expression profiles	307
E.2	Expression profiles for constituent genes of PI3K	308
E.3	Expression profiles for p53 related genes	309
E.4	Expression profiles for estrogen receptor related genes	310
E.5	Expression profiles for BRCA related genes	311
F.1	Comparison of SLIPT in stomach to siRNA	315
G.1	Synthetic lethal expression profiles of stomach samples	324
G.2	Comparison of mtSLIPT in stomach to siRNA	326
H.1	Synthetic lethal partners across query genes	332
J.1	Synthetic Lethality in the PI3K/AKT Pathway	340
J.2	Synthetic Lethality in the PI3K/AKT Pathway in Cancer	341
J.3	Synthetic Lethality in the Extracellular Matrix	342
J.4	Synthetic Lethality in the GPCRs	343
J.5	Synthetic Lethality in the GPCR Downstream	344
J.6	Synthetic Lethality in the Translation Elongation	345
J.7	Synthetic Lethality in the Nonsense-mediated Decay	346
J.8	Synthetic Lethality in the 3' UTR	347
K.1	Synthetic Lethality and Vertex Degree	348
K.2	Synthetic Lethality and Centrality	349
K.3	Synthetic Lethality and PageRank	350
L.1	Information centrality distribution	354
M.1	Synthetic Lethality and Heirarchy Score in PI3K	355
M.2	Heirarchy Score in PI3K against Synthetic Lethality in PI3K	356
M.3	Structure of Synthetic Lethality in PI3K	356
M.4	Structure of Synthetic Lethality Resampling	357
N.1	Performance of χ^2 and SLIPT across quantiles	358
N.2	Performance of χ^2 and SLIPT across quantiles	360
N.3	Performance of χ^2 and SLIPT across quantiles with more genes	362
N.4	Performance of χ^2 and SLIPT across quantiles with query correlation	364

N.5 Performance of χ^2 and SLIPT across quantiles with query correlation	366
N.6 Performance of χ^2 and SLIPT across quantiles with query correlation and more genes	368
O.1 Simple graph structures	370
O.2 Simple graph structure	371
O.3 Constructed graph structure	371
O.4 Large constructed graph structure.	372
O.5 Branching constructed graph structure	372
O.6 Complex constructed graph structure	374
O.7 Performance of simulations on a simple graph	377
O.8 Performance of simulations on a constructed graph	378
O.9 Performance of simulations on a branching graph	379
O.10 Performance of simulations on a complex graph	380
O.11 Performance of simulations on a simple graph with inhibition	382
O.12 Performance of simulations on a simple graph with inhibition	383
O.13 Performance of simulations on a constructed graph with inhibition	384
O.14 Performance of simulations on a large constructed graph with inhibition	385
O.15 Performance of simulations on a large constructed graph with inhibition	386
O.16 Performance of simulations on a branching graph with inhibition	387
O.17 Performance of simulations on a branching graph with inhibition	388
O.18 Performance of simulations on a complex graph with inhibition	389
O.19 Performance of simulations on a complex graph with inhibition	390
O.20 Detection of Synthetic Lethality within a Graph Structure	391
O.21 Detection of Synthetic Lethality within an Inhibiting Graph Structure .	393
O.22 Detection of Synthetic Lethality within an Inhibiting Graph Structure .	394
O.23 Performance of simulations on a simple graph with more genes	396
O.24 Performance of simulations including a simple graph	397
O.25 Performance of simulations including a constructed graph	398
O.26 Performance of simulations including a large graph	399
O.27 Performance of simulations including a branching graph	400
O.28 Performance of simulations including a complex graph	401
O.29 Performance of simulations including a simple graph with inhibition . .	403
O.30 Performance of simulations including a simple graph with inhibition . .	404
O.31 Performance of simulations including a simple graph with inhibition . .	405
O.32 Performance of simulations including a constructed graph with inhibition	406
O.33 Performance of simulations including a constructed graph with inhibition	407
O.34 Performance of simulations including a large graph with inhibition . . .	408
O.35 Performance of simulations including a large graph with inhibition . . .	409
O.36 Performance of simulations including a branching graph with inhibition	410
O.37 Performance of simulations including a branching graph with inhibition	411
O.38 Performance of simulations including a complex graph with inhibition .	412
O.39 Performance of simulations including a complex graph with inhibition .	413
O.40 Performance of simulations on the $G_{\alpha i}$ signalling pathway	414
O.41 Performance of simulations including the $G_{\alpha i}$ signalling pathway	415

List of Tables

1.1	Methods for Predicting Genetic Interactions	38
1.2	Methods for Predicting Synthetic Lethality in Cancer	39
1.3	Methods used by Wu <i>et al.</i> (2014)	40
2.1	Excluded Samples by Batch and Clinical Characteristics	63
2.2	Computers used during Thesis	72
2.3	Linux Utilities and Applications used during Thesis	72
2.4	R Installations used during Thesis	73
2.5	R Packages used during Thesis	73
2.6	R Packages Developed during Thesis	75
4.1	Candidate synthetic lethal gene partners of <i>CDH1</i> from SLIPT	117
4.2	Pathways for <i>CDH1</i> partners from SLIPT	119
4.3	Pathway composition for clusters of <i>CDH1</i> partners from SLIPT	123
4.4	Pathway composition for <i>CDH1</i> partners from SLIPT and siRNA screening	131
4.5	Pathways for <i>CDH1</i> partners from SLIPT	135
4.6	Pathways for <i>CDH1</i> partners from SLIPT and siRNA primary screen	136
4.7	Candidate synthetic lethal metagenes against <i>CDH1</i> from SLIPT	143
4.8	Pathways for <i>CDH1</i> partners from SLIPT in stomach cancer	146
4.9	Query synthetic lethal genes with the most SLIPT partners	152
4.10	Pathways for genes with the most SLIPT partners	154
4.11	Pathways for <i>CDH1</i> partners from SLIPT in CCLE	155
4.12	Pathways for <i>CDH1</i> partners from SLIPT in breast CCLE	156
5.1	Analysis of variance (ANOVA) for Synthetic Lethality and Vertex Degree	175
5.2	ANOVA for Synthetic Lethality and Information Centrality	177
5.3	ANOVA for Synthetic Lethality and PageRank Centrality	179
5.4	ANOVA for Synthetic Lethality and PI3K Hierarchy	182
5.5	Resampling for pathway structure of synthetic lethal detection methods	186
B.1	R Packages used during Thesis	278
C.1	Comparing SLIPT genes against Secondary siRNA Screen in breast cancer	287
C.2	Comparing mtSLIPT genes against Secondary siRNA Screen in breast cancer	288
C.3	Comparing SLIPT genes against Secondary siRNA Screen in stomach cancer	288

D.1	Candidate synthetic lethal gene partners of <i>CDH1</i> from mtSLIPT	290
D.2	Pathways for <i>CDH1</i> partners from mtSLIPT	291
D.3	Pathway composition for clusters of <i>CDH1</i> partners from mtSLIPT	294
D.4	Pathway composition for <i>CDH1</i> partners from mtSLIPT and siRNA	296
D.5	Pathways for <i>CDH1</i> partners from mtSLIPT	297
D.6	Pathways for <i>CDH1</i> partners from mtSLIPT and siRNA primary screen	298
D.7	Candidate synthetic lethal metagenes against <i>CDH1</i> from mtSLIPT	301
F.1	Synthetic lethal gene partners of <i>CDH1</i> from SLIPT in stomach cancer	313
F.2	Pathway composition for clusters of <i>CDH1</i> partners in stomach SLIPT	314
F.3	Pathway composition for <i>CDH1</i> partners from SLIPT and siRNA screening	316
F.4	Pathways for <i>CDH1</i> partners from SLIPT in stomach cancer	317
F.5	Pathways for <i>CDH1</i> partners from SLIPT in stomach and siRNA screen	318
F.6	Candidate synthetic lethal metagenes against <i>CDH1</i> from SLIPT in stomach cancer	319
G.1	Synthetic lethal gene partners of <i>CDH1</i> from mtSLIPT in stomach cancer	321
G.2	Pathways for <i>CDH1</i> partners from mtSLIPT in stomach cancer	322
G.3	Pathway composition for clusters of <i>CDH1</i> partners in stomach mtSLIPT	325
G.4	Pathway composition for <i>CDH1</i> partners from mtSLIPT and siRNA	327
G.5	Pathways for <i>CDH1</i> partners from mtSLIPT in stomach cancer	328
G.6	Pathways for <i>CDH1</i> partners from mtSLIPT in stomach and siRNA screen	329
G.7	Candidate synthetic lethal metagenes against <i>CDH1</i> from mtSLIPT in stomach cancer	330
H.1	Query synthetic lethal genes with the most SLIPT partners	333
H.2	Pathways for genes with the most SLIPT partners	334
I.1	Candidate synthetic lethal gene partners of <i>CDH1</i> from SLIPT in CCLE	336
I.2	Candidate synthetic lethal gene partners of <i>CDH1</i> from SLIPT in breast CCLE	337
I.3	Candidate synthetic lethal gene partners of <i>CDH1</i> from SLIPT in stomach CCLE	338
I.4	Pathways for <i>CDH1</i> partners from SLIPT in stomach CCLE	339
I.5	Pathways for <i>CDH1</i> partners from SLIPT in breast and stomach CCLE	339
K.1	ANOVA for Synthetic Lethality and Vertex Degree	351
K.2	ANOVA for Synthetic Lethality and Information Centrality	351
K.3	ANOVA for Synthetic Lethality and PageRank Centrality	351
L.1	Information centrality for genes and molecules in the Reactome network	353
M.1	ANOVA for Synthetic Lethality and PI3K Hierarchy	355
M.2	Resampling for pathway structure of synthetic lethal detection methods	357

Glossary

synthetic lethal Genetic interactions where inactivation of multiple genes is inviable (or deleterious) when they are viable if inactivated separately.

Acronyms

ANOVA Analysis of Variance.

CCLE Cancer Cell Line Encyclopaedia.

siRNA Short interfering ribonucleic acid.

SLIPT Synthetic lethal interaction prediction tool.

TCGA The Cancer Genome Atlas (genomics project).

References

- Aarts, M., Bajrami, I., Herrera-Abreu, M.T., Elliott, R., Brough, R., Ashworth, A., Lord, C.J., and Turner, N.C. (2015) Functional genetic screen identifies increased sensitivity to wee1 inhibition in cells with defects in fanconi anemia and hr pathways. *Mol Cancer Ther*, **14**(4): 865–76.
- Abeshouse, A., Ahn, J., Akbani, R., Ally, A., Amin, S., Andry, C.D., Annala, M., Aprikian, A., Armenia, J., Arora, A., *et al.* (2015) The Molecular Taxonomy of Primary Prostate Cancer. *Cell*, **163**(4): 1011–1025.
- Adamski, M.G., Gumann, P., and Baird, A.E. (2014) A method for quantitative analysis of standard and high-throughput qPCR expression data based on input sample quantity. *PLoS ONE*, **9**(8): e103917.
- Adler, D. (2005) *vioplot: Violin plot*. R package version 0.2.
- Agarwal, S., Deane, C.M., Porter, M.A., and Jones, N.S. (2010) Revisiting date and party hubs: Novel approaches to role assignment in protein interaction networks. *PLoS Comput Biol*, **6**(6): e1000817.
- Agrawal, N., Akbani, R., Aksoy, B.A., Ally, A., Arachchi, H., Asa, S.L., Auman, J.T., Balasundaram, M., Balu, S., Baylin, S.B., *et al.* (2014) Integrated genomic characterization of papillary thyroid carcinoma. *Cell*, **159**(3): 676–690.
- Akbani, R., Akdemir, K.C., Aksoy, B.A., Albert, M., Ally, A., Amin, S.B., Arachchi, H., Arora, A., Auman, J.T., Ayala, B., *et al.* (2015) Genomic Classification of Cutaneous Melanoma. *Cell*, **161**(7): 1681–1696.
- Akobeng, A.K. (2007) Understanding diagnostic tests 3: receiver operating characteristic curves. *Acta Padiatrica*, **96**(5): 644–647.
- American Cancer Society (2017) Genetics and cancer. <https://www.cancer.org/cancer/cancer-causes/genetics.html>. Accessed: 22/03/2017.

American Society for Clinical Oncology (ASCO) (2017) The genetics of cancer. <http://www.cancer.net/navigating-cancer-care/cancer-basics/genetics/genetics-cancer>. Accessed: 22/03/2017.

Anjomshoaa, A., Lin, Y.H., Black, M.A., McCall, J.L., Humar, B., Song, S., Fukuzawa, R., Yoon, H.S., Holzmann, B., Friederichs, J., *et al.* (2008) Reduced expression of a gene proliferation signature is associated with enhanced malignancy in colon cancer. *Br J Cancer*, **99**(6): 966–973.

Araki, H., Knapp, C., Tsai, P., and Print, C. (2012) GeneSetDB: A comprehensive meta-database, statistical and visualisation framework for gene set analysis. *FEBS Open Bio*, **2**: 76–82.

Ashburner, M., Ball, C.A., Blake, J.A., Botstein, D., Butler, H., Cherry, J.M., Davis, A.P., Dolinski, K., Dwight, S.S., Eppig, J.T., *et al.* (2000) Gene ontology: tool for the unification of biology. The Gene Ontology Consortium. *Nat Genet*, **25**(1): 25–29.

Ashworth, A. (2008) A synthetic lethal therapeutic approach: poly(adp) ribose polymerase inhibitors for the treatment of cancers deficient in dna double-strand break repair. *J Clin Oncol*, **26**(22): 3785–90.

Audeh, M.W., Carmichael, J., Penson, R.T., Friedlander, M., Powell, B., Bell-McGuinn, K.M., Scott, C., Weitzel, J.N., Oaknin, A., Loman, N., *et al.* (2010) Oral poly(adp-ribose) polymerase inhibitor olaparib in patients with *BRCA1* or *BRCA2* mutations and recurrent ovarian cancer: a proof-of-concept trial. *Lancet*, **376**(9737): 245–51.

Babyak, M.A. (2004) What you see may not be what you get: a brief, nontechnical introduction to overfitting in regression-type models. *Psychosom Med*, **66**(3): 411–21.

Bamford, S., Dawson, E., Forbes, S., Clements, J., Pettett, R., Dogan, A., Flanagan, A., Teague, J., Futreal, P.A., Stratton, M.R., *et al.* (2004) The COSMIC (Catalogue of Somatic Mutations in Cancer) database and website. *Br J Cancer*, **91**(2): 355–358.

Barabási, A.L. and Albert, R. (1999) Emergence of scaling in random networks. *Science*, **286**(5439): 509–12.

- Barabási, A.L. and Oltvai, Z.N. (2004) Network biology: understanding the cell's functional organization. *Nat Rev Genet*, **5**(2): 101–13.
- Barrat, A. and Weigt, M. (2000) On the properties of small-world network models. *The European Physical Journal B - Condensed Matter and Complex Systems*, **13**(3): 547–560.
- Barretina, J., Caponigro, G., Stransky, N., Venkatesan, K., Margolin, A.A., Kim, S., Wilson, C.J., Lehar, J., Kryukov, G.V., Sonkin, D., *et al.* (2012) The Cancer Cell Line Encyclopedia enables predictive modelling of anticancer drug sensitivity. *Nature*, **483**(7391): 603–607.
- Barry, W.T. (2016) *safe: Significance Analysis of Function and Expression*. R package version 3.14.0.
- Baryshnikova, A., Costanzo, M., Dixon, S., Vizeacoumar, F.J., Myers, C.L., Andrews, B., and Boone, C. (2010a) Synthetic genetic array (sga) analysis in *saccharomyces cerevisiae* and *schizosaccharomyces pombe*. *Methods Enzymol*, **470**: 145–79.
- Baryshnikova, A., Costanzo, M., Kim, Y., Ding, H., Koh, J., Toufighi, K., Youn, J.Y., Ou, J., San Luis, B.J., Bandyopadhyay, S., *et al.* (2010b) Quantitative analysis of fitness and genetic interactions in yeast on a genome scale. *Nat Meth*, **7**(12): 1017–1024.
- Bass, A.J., Thorsson, V., Shmulevich, I., Reynolds, S.M., Miller, M., Bernard, B., Hinoue, T., Laird, P.W., Curtis, C., Shen, H., *et al.* (2014) Comprehensive molecular characterization of gastric adenocarcinoma. *Nature*, **513**(7517): 202–209.
- Bates, D. and Maechler, M. (2016) *Matrix: Sparse and Dense Matrix Classes and Methods*. R package version 1.2-7.1.
- Bateson, W. and Mendel, G. (1909) *Mendel's principles of heredity, by W. Bateson*. University Press, Cambridge [Eng.].
- Beck, T.F., Mullikin, J.C., and Biesecker, L.G. (2016) Systematic Evaluation of Sanger Validation of Next-Generation Sequencing Variants. *Clin Chem*, **62**(4): 647–654.
- Becker, K.F., Atkinson, M.J., Reich, U., Becker, I., Nekarda, H., Siewert, J.R., and Hfler, H. (1994) E-cadherin gene mutations provide clues to diffuse type gastric carcinomas. *Cancer Research*, **54**(14): 3845–3852.

- Bell, D., Berchuck, A., Birrer, M., Chien, J., Cramer, D., Dao, F., Dhir, R., DiSaia, P., Gabra, H., Glenn, P., *et al.* (2011) Integrated genomic analyses of ovarian carcinoma. *Nature*, **474**(7353): 609–615.
- Benjamini, Y. and Hochberg, Y. (1995) Controlling the false discovery rate: A practical and powerful approach to multiple testing. *Journal of the Royal Statistical Society Series B (Methodological)*, **57**(1): 289–300.
- Berx, G., Cleton-Jansen, A.M., Nollet, F., de Leeuw, W.J., van de Vijver, M., Cornelisse, C., and van Roy, F. (1995) E-cadherin is a tumour/invasion suppressor gene mutated in human lobular breast cancers. *EMBO J*, **14**(24): 6107–15.
- Berx, G., Cleton-Jansen, A.M., Strumane, K., de Leeuw, W.J., Nollet, F., van Roy, F., and Cornelisse, C. (1996) E-cadherin is inactivated in a majority of invasive human lobular breast cancers by truncation mutations throughout its extracellular domain. *Oncogene*, **13**(9): 1919–25.
- Berx, G. and van Roy, F. (2009) Involvement of members of the cadherin superfamily in cancer. *Cold Spring Harb Perspect Biol*, **1**: a003129.
- Bitler, B.G., Aird, K.M., Garipov, A., Li, H., Amatangelo, M., Kossenkov, A.V., Schultz, D.C., Liu, Q., Shih Ie, M., Conejo-Garcia, J.R., *et al.* (2015) Synthetic lethality by targeting ezh2 methyltransferase activity in arid1a-mutated cancers. *Nat Med*, **21**(3): 231–8.
- Blake, J.A., Christie, K.R., Dolan, M.E., Drabkin, H.J., Hill, D.P., Ni, L., Sitnikov, D., Burgess, S., Buza, T., Gresham, C., *et al.* (2015) Gene Ontology Consortium: going forward. *Nucleic Acids Res*, **43**(Database issue): D1049–1056.
- Boettcher, M., Lawson, A., Ladenburger, V., Fredebohm, J., Wolf, J., Hoheisel, J.D., Frezza, C., and Shlomi, T. (2014) High throughput synthetic lethality screen reveals a tumorigenic role of adenylate cyclase in fumarate hydratase-deficient cancer cells. *BMC Genomics*, **15**: 158.
- Boone, C., Bussey, H., and Andrews, B.J. (2007) Exploring genetic interactions and networks with yeast. *Nat Rev Genet*, **8**(6): 437–49.
- Borgatti, S.P. (2005) Centrality and network flow. *Social Networks*, **27**(1): 55 – 71.
- Boucher, B. and Jenna, S. (2013) Genetic interaction networks: better understand to better predict. *Front Genet*, **4**: 290.

- Breiman, L. (2001) Random forests. *Machine Learning*, **45**(1): 5–32.
- Brin, S. and Page, L. (1998) The anatomy of a large-scale hypertextual web search engine. *Computer Networks and ISDN Systems*, **30**(1): 107 – 117.
- Bryant, H.E., Schultz, N., Thomas, H.D., Parker, K.M., Flower, D., Lopez, E., Kyle, S., Meuth, M., Curtin, N.J., and Helleday, T. (2005) Specific killing of *BRCA2*-deficient tumours with inhibitors of polyadprbose polymerase. *Nature*, **434**(7035): 913–7.
- Burk, R.D., Chen, Z., Saller, C., Tarvin, K., Carvalho, A.L., Scapulatempo-Neto, C., Silveira, H.C., Fregnani, J.H., Creighton, C.J., Anderson, M.L., *et al.* (2017) Integrated genomic and molecular characterization of cervical cancer. *Nature*, **543**(7645): 378–384.
- Bussey, H., Andrews, B., and Boone, C. (2006) From worm genetic networks to complex human diseases. *Nat Genet*, **38**(8): 862–3.
- Butland, G., Babu, M., Diaz-Mejia, J.J., Bohdana, F., Phanse, S., Gold, B., Yang, W., Li, J., Gagarinova, A.G., Pogoutse, O., *et al.* (2008) esga: *E. coli* synthetic genetic array analysis. *Nat Methods*, **5**(9): 789–95.
- Cancer Research UK (2017) Family history and cancer genes. <http://www.cancerresearchuk.org/about-cancer/causes-of-cancer/inherited-cancer-genes-and-increased-cancer-risk/family-history-and-inherited-cancer-genes>. Accessed: 22/03/2017.
- Cancer Cell Line Encyclopedia (CCLE) (2014) Broad-Novartis Cancer Cell Line Encyclopedia. <http://www.broadinstitute.org/ccle>. Accessed: 07/11/2014.
- cBioPortal for Cancer Genomics (cBioPortal) (2017) cBioPortal for Cancer Genomics. <http://www.cbioportal.org/>. Accessed: 26/03/2017.
- Cerami, E.G., Gross, B.E., Demir, E., Rodchenkov, I., Babur, O., Anwar, N., Schultz, N., Bader, G.D., and Sander, C. (2011) Pathway Commons, a web resource for biological pathway data. *Nucleic Acids Res*, **39**(Database issue): D685–690.
- Chen, A., Beetham, H., Black, M.A., Priya, R., Telford, B.J., Guest, J., Wiggins, G.A.R., Godwin, T.D., Yap, A.S., and Guilford, P.J. (2014) E-cadherin loss alters cytoskeletal organization and adhesion in non-malignant breast cells but is insufficient to induce an epithelial-mesenchymal transition. *BMC Cancer*, **14**(1): 552.

- Chen, K., Yang, D., Li, X., Sun, B., Song, F., Cao, W., Brat, D.J., Gao, Z., Li, H., Liang, H., *et al.* (2015) Mutational landscape of gastric adenocarcinoma in Chinese: implications for prognosis and therapy. *Proc Natl Acad Sci USA*, **112**(4): 1107–1112.
- Chen, S. and Parmigiani, G. (2007) Meta-analysis of BRCA1 and BRCA2 penetrance. *J Clin Oncol*, **25**(11): 1329–1333.
- Chen, X. and Tompa, M. (2010) Comparative assessment of methods for aligning multiple genome sequences. *Nat Biotechnol*, **28**(6): 567–572.
- Cherniack, A.D., Shen, H., Walter, V., Stewart, C., Murray, B.A., Bowlby, R., Hu, X., Ling, S., Soslow, R.A., Broaddus, R.R., *et al.* (2017) Integrated Molecular Characterization of Uterine Carcinosarcoma. *Cancer Cell*, **31**(3): 411–423.
- Chipman, K. and Singh, A. (2009) Predicting genetic interactions with random walks on biological networks. *BMC Bioinformatics*, **10**(1): 17.
- Christofori, G. and Semb, H. (1999) The role of the cell-adhesion molecule E-cadherin as a tumour-suppressor gene. *Trends in Biochemical Sciences*, **24**(2): 73 – 76.
- Ciriello, G., Gatza, M.L., Beck, A.H., Wilkerson, M.D., Rhie, S.K., Pastore, A., Zhang, H., McLellan, M., Yau, C., Kandoth, C., *et al.* (2015) Comprehensive Molecular Portraits of Invasive Lobular Breast Cancer. *Cell*, **163**(2): 506–519.
- Clark, M.J. (2004) Endogenous Regulator of G Protein Signaling Proteins Suppress G_o-Dependent μ -Opioid Agonist-Mediated Adenylyl Cyclase Supersensitization. *Journal of Pharmacology and Experimental Therapeutics*, **310**(1): 215–222.
- Clough, E. and Barrett, T. (2016) The Gene Expression Omnibus Database. *Methods Mol Biol*, **1418**: 93–110.
- Collingridge, D.S. (2013) A primer on quantitized data analysis and permutation testing. *Journal of Mixed Methods Research*, **7**(1): 81–97.
- Collins, F.S. and Barker, A.D. (2007) Mapping the cancer genome. Pinpointing the genes involved in cancer will help chart a new course across the complex landscape of human malignancies. *Sci Am*, **296**(3): 50–57.
- Collins, F.S., Morgan, M., and Patrinos, A. (2003) The Human Genome Project: lessons from large-scale biology. *Science*, **300**(5617): 286–290.

- Collisson, E., Campbell, J., Brooks, A., Berger, A., Lee, W., Chmielecki, J., Beer, D., Cope, L., Creighton, C., Danilova, L., *et al.* (2014) Comprehensive molecular profiling of lung adenocarcinoma. *Nature*, **511**(7511): 543–550.
- Corcoran, R.B., Ebi, H., Turke, A.B., Coffee, E.M., Nishino, M., Cogdill, A.P., Brown, R.D., Della Pelle, P., Dias-Santagata, D., Hung, K.E., *et al.* (2012) Egfr-mediated reactivation of mapk signaling contributes to insensitivity of *BRAF*-mutant colorectal cancers to raf inhibition with vemurafenib. *Cancer Discovery*, **2**(3): 227–235.
- Costanzo, M., Baryshnikova, A., Bellay, J., Kim, Y., Spear, E.D., Sevier, C.S., Ding, H., Koh, J.L., Toufighi, K., Mostafavi, S., *et al.* (2010) The genetic landscape of a cell. *Science*, **327**(5964): 425–31.
- Costanzo, M., Baryshnikova, A., Myers, C.L., Andrews, B., and Boone, C. (2011) Charting the genetic interaction map of a cell. *Curr Opin Biotechnol*, **22**(1): 66–74.
- Courtney, K.D., Corcoran, R.B., and Engelman, J.A. (2010) The PI3K pathway as drug target in human cancer. *J Clin Oncol*, **28**(6): 1075–1083.
- Creighton, C.J., Morgan, M., Gunaratne, P.H., Wheeler, D.A., Gibbs, R.A., Robertson, A., Chu, A., Beroukhim, R., Cibulskis, K., Signoretti, S., *et al.* (2013) Comprehensive molecular characterization of clear cell renal cell carcinoma. *Nature*, **499**(7456): 43–49.
- Croft, D., Mundo, A.F., Haw, R., Milacic, M., Weiser, J., Wu, G., Caudy, M., Garapati, P., Gillespie, M., Kamdar, M.R., *et al.* (2014) The Reactome pathway knowledge-base. *Nucleic Acids Res*, **42**(database issue): D472D477.
- Crunkhorn, S. (2014) Cancer: Predicting synthetic lethal interactions. *Nat Rev Drug Discov*, **13**(11): 812.
- Csardi, G. and Nepusz, T. (2006) The igraph software package for complex network research. *InterJournal, Complex Systems*: 1695.
- Curtis, C., Shah, S.P., Chin, S.F., Turashvili, G., Rueda, O.M., Dunning, M.J., Speed, D., Lynch, A.G., Samarajiwa, S., Yuan, Y., *et al.* (2012) The genomic and transcriptomic architecture of 2,000 breast tumours reveals novel subgroups. *Nature*, **486**(7403): 346–352.

- Dai, X., Li, T., Bai, Z., Yang, Y., Liu, X., Zhan, J., and Shi, B. (2015) Breast cancer intrinsic subtype classification, clinical use and future trends. *Am J Cancer Res*, **5**(10): 2929–2943.
- Davierwala, A.P., Haynes, J., Li, Z., Brost, R.L., Robinson, M.D., Yu, L., Mnaimneh, S., Ding, H., Zhu, H., Chen, Y., *et al.* (2005) The synthetic genetic interaction spectrum of essential genes. *Nat Genet*, **37**(10): 1147–1152.
- De Leeuw, W.J., Berx, G., Vos, C.B., Peterse, J.L., Van de Vijver, M.J., Litvinov, S., Van Roy, F., Cornelisse, C.J., and Cleton-Jansen, A.M. (1997) Simultaneous loss of E-cadherin and catenins in invasive lobular breast cancer and lobular carcinoma in situ. *J Pathol*, **183**(4): 404–11.
- Demir, E., Babur, O., Rodchenkov, I., Aksoy, B.A., Fukuda, K.I., Gross, B., Sumer, O.S., Bader, G.D., and Sander, C. (2013) Using biological pathway data with Paxtools. *PLoS Comput Biol*, **9**(9): e1003194.
- Deshpande, R., Asiedu, M.K., Klebig, M., Sutor, S., Kuzmin, E., Nelson, J., Piotrowski, J., Shin, S.H., Yoshida, M., Costanzo, M., *et al.* (2013) A comparative genomic approach for identifying synthetic lethal interactions in human cancer. *Cancer Res*, **73**(20): 6128–36.
- Dickson, D. (1999) Wellcome funds cancer database. *Nature*, **401**(6755): 729.
- Dienstmann, R. and Tabernero, J. (2011) *BRAF* as a target for cancer therapy. *Anti-cancer Agents Med Chem*, **11**(3): 285–95.
- Dijkstra, E.W. (1959) A note on two problems in connexion with graphs. *Numerische Mathematik*, **1**(1): 269–271.
- Dixon, S.J., Andrews, B.J., and Boone, C. (2009) Exploring the conservation of synthetic lethal genetic interaction networks. *Commun Integr Biol*, **2**(2): 78–81.
- Dixon, S.J., Fedyshyn, Y., Koh, J.L., Prasad, T.S., Chahwan, C., Chua, G., Toufighi, K., Baryshnikova, A., Hayles, J., Hoe, K.L., *et al.* (2008) Significant conservation of synthetic lethal genetic interaction networks between distantly related eukaryotes. *Proc Natl Acad Sci U S A*, **105**(43): 16653–8.
- Dorogovtsev, S.N. and Mendes, J.F. (2003) *Evolution of networks: From biological nets to the Internet and WWW*. Oxford University Press, USA.

- Dorsam, R.T. and Gutkind, J.S. (2007) G-protein-coupled receptors and cancer. *Nat Rev Cancer*, **7**(2): 79–94.
- Erdős, P. and Rényi, A. (1959) On random graphs I. *Publ Math Debrecen*, **6**: 290–297.
- Erdős, P. and Rényi, A. (1960) On the evolution of random graphs. In *Publ. Math. Inst. Hung. Acad. Sci*, volume 5, 17–61.
- Eroles, P., Bosch, A., Perez-Fidalgo, J.A., and Lluch, A. (2012) Molecular biology in breast cancer: intrinsic subtypes and signaling pathways. *Cancer Treat Rev*, **38**(6): 698–707.
- Ezkurdia, I., Juan, D., Rodriguez, J.M., Frankish, A., Diekhans, M., Harrow, J., Vazquez, J., Valencia, A., and Tress, M.L. (2014) Multiple evidence strands suggest that there may be as few as 19 000 human protein-coding genes. *Human Molecular Genetics*, **23**(22): 5866.
- Farmer, H., McCabe, N., Lord, C.J., Tutt, A.N., Johnson, D.A., Richardson, T.B., Santarosa, M., Dillon, K.J., Hickson, I., Knights, C., et al. (2005) Targeting the dna repair defect in BRCA mutant cells as a therapeutic strategy. *Nature*, **434**(7035): 917–21.
- Fawcett, T. (2006) An introduction to ROC analysis. *Pattern Recognition Letters*, **27**(8): 861 – 874. {ROC} Analysis in Pattern Recognition.
- Fece de la Cruz, F., Gapp, B.V., and Nijman, S.M. (2015) Synthetic lethal vulnerabilities of cancer. *Annu Rev Pharmacol Toxicol*, **55**: 513–531.
- Ferlay, J., Soerjomataram, I., Dikshit, R., Eser, S., Mathers, C., Rebelo, M., Parkin, D.M., Forman, D., and Bray, F. (2015) Cancer incidence and mortality worldwide: sources, methods and major patterns in GLOBOCAN 2012. *Int J Cancer*, **136**(5): E359–386.
- Fisher, R.A. (1919) Xv.the correlation between relatives on the supposition of mendelian inheritance. *Earth and Environmental Science Transactions of the Royal Society of Edinburgh*, **52**(02): 399–433.
- Fong, P.C., Boss, D.S., Yap, T.A., Tutt, A., Wu, P., Mergui-Roelvink, M., Mortimer, P., Swaisland, H., Lau, A., O'Connor, M.J., et al. (2009) Inhibition of poly(adp-ribose) polymerase in tumors from BRCA mutation carriers. *N Engl J Med*, **361**(2): 123–34.

- Fong, P.C., Yap, T.A., Boss, D.S., Carden, C.P., Mergui-Roelvink, M., Gourley, C., De Greve, J., Lubinski, J., Shanley, S., Messiou, C., *et al.* (2010) Poly(adp)-ribose polymerase inhibition: frequent durable responses in BRCA carrier ovarian cancer correlating with platinum-free interval. *J Clin Oncol*, **28**(15): 2512–9.
- Forbes, S.A., Beare, D., Gunasekaran, P., Leung, K., Bindal, N., Boutselakis, H., Ding, M., Bamford, S., Cole, C., Ward, S., *et al.* (2015) COSMIC: exploring the world's knowledge of somatic mutations in human cancer. *Nucleic Acids Res*, **43**(Database issue): D805–811.
- Fraser, A. (2004) Towards full employment: using RNAi to find roles for the redundant. *Oncogene*, **23**(51): 8346–52.
- Futreal, P.A., Coin, L., Marshall, M., Down, T., Hubbard, T., Wooster, R., Rahman, N., and Stratton, M.R. (2004) A census of human cancer genes. *Nat Rev Cancer*, **4**(3): 177–183.
- Futreal, P.A., Kasprzyk, A., Birney, E., Mullikin, J.C., Wooster, R., and Stratton, M.R. (2001) Cancer and genomics. *Nature*, **409**(6822): 850–852.
- Gao, B. and Roux, P.P. (2015) Translational control by oncogenic signaling pathways. *Biochimica et Biophysica Acta*, **1849**(7): 753–65.
- Gatza, M.L., Kung, H.N., Blackwell, K.L., Dewhirst, M.W., Marks, J.R., and Chi, J.T. (2011) Analysis of tumor environmental response and oncogenic pathway activation identifies distinct basal and luminal features in HER2-related breast tumor subtypes. *Breast Cancer Res*, **13**(3): R62.
- Gatza, M.L., Lucas, J.E., Barry, W.T., Kim, J.W., Wang, Q., Crawford, M.D., Datto, M.B., Kelley, M., Mathey-Prevot, B., Potti, A., *et al.* (2010) A pathway-based classification of human breast cancer. *Proc Natl Acad Sci USA*, **107**(15): 6994–6999.
- Gatza, M.L., Silva, G.O., Parker, J.S., Fan, C., and Perou, C.M. (2014) An integrated genomics approach identifies drivers of proliferation in luminal-subtype human breast cancer. *Nat Genet*, **46**(10): 1051–1059.
- Gentleman, R.C., Carey, V.J., Bates, D.M., Bolstad, B., Dettling, M., Dudoit, S., Ellis, B., Gautier, L., Ge, Y., Gentry, J., *et al.* (2004) Bioconductor: open software development for computational biology and bioinformatics. *Genome Biol*, **5**(10): R80.

- Genz, A. and Bretz, F. (2009) Computation of multivariate normal and t probabilities. In *Lecture Notes in Statistics*, volume 195. Springer-Verlag, Heidelberg.
- Genz, A., Bretz, F., Miwa, T., Mi, X., Leisch, F., Scheipl, F., and Hothorn, T. (2016) *mvtnorm: Multivariate Normal and t Distributions*. R package version 1.0-5. URL <https://CRAN.R-project.org/package=mvtnorm>.
- Gilbert, W. and Maxam, A. (1973) The nucleotide sequence of the lac operator. *Proceedings of the National Academy of Sciences*, **70**(12): 3581–3584.
- Git, A., Dvinge, H., Salmon-Divon, M., Osborne, M., Kutter, C., Hadfield, J., Bertone, P., and Caldas, C. (2010) Systematic comparison of microarray profiling, real-time PCR, and next-generation sequencing technologies for measuring differential microRNA expression. *RNA*, **16**(5): 991–1006.
- Globus (Globus) (2017) Research data management simplified. <https://www.globus.org/>. Accessed: 25/03/2017.
- Graziano, F., Humar, B., and Guilford, P. (2003) The role of the E-cadherin gene (*CDH1*) in diffuse gastric cancer susceptibility: from the laboratory to clinical practice. *Annals of Oncology*, **14**(12): 1705–1713.
- Güell, O., Sagus, F., and Serrano, M. (2014) Essential plasticity and redundancy of metabolism unveiled by synthetic lethality analysis. *PLoS Comput Biol*, **10**(5): e1003637.
- Guilford, P. (1999) E-cadherin downregulation in cancer: fuel on the fire? *Molecular Medicine Today*, **5**(4): 172 – 177.
- Guilford, P., Hopkins, J., Harraway, J., McLeod, M., McLeod, N., Harawira, P., Taite, H., Scouler, R., Miller, A., and Reeve, A.E. (1998) E-cadherin germline mutations in familial gastric cancer. *Nature*, **392**(6674): 402–5.
- Guilford, P., Humar, B., and Blair, V. (2010) Hereditary diffuse gastric cancer: translation of *CDH1* germline mutations into clinical practice. *Gastric Cancer*, **13**(1): 1–10.
- Guilford, P.J., Hopkins, J.B., Grady, W.M., Markowitz, S.D., Willis, J., Lynch, H., Rajput, A., Wiesner, G.L., Lindor, N.M., Burgart, L.J., et al. (1999) E-cadherin germline mutations define an inherited cancer syndrome dominated by diffuse gastric cancer. *Hum Mutat*, **14**(3): 249–55.

- Guo, J., Liu, H., and Zheng, J. (2016) SynLethDB: synthetic lethality database toward discovery of selective and sensitive anticancer drug targets. *Nucleic Acids Res*, **44**(D1): D1011–1017.
- Hajian-Tilaki, K. (2013) Receiver Operating Characteristic (ROC) Curve Analysis for Medical Diagnostic Test Evaluation. *Caspian J Intern Med*, **4**(2): 627–635.
- Hall, M., Frank, E., Holmes, G., Pfahringer, B., Reutemann, P., and Witten, I.H. (2009) The weka data mining software: an update. *SIGKDD Explor News*, **11**(1): 10–18.
- Hamerman, P.S., Lawrence, M.S., Voet, D., Jing, R., Cibulskis, K., Sivachenko, A., Stojanov, P., McKenna, A., Lander, E.S., Gabriel, S., *et al.* (2012) Comprehensive genomic characterization of squamous cell lung cancers. *Nature*, **489**(7417): 519–525.
- Han, J.D.J., Bertin, N., Hao, T., Goldberg, D.S., Berriz, G.F., Zhang, L.V., Dupuy, D., Walhout, A.J.M., Cusick, M.E., Roth, F.P., *et al.* (2004) Evidence for dynamically organized modularity in the yeast protein-protein interaction network. *Nature*, **430**(6995): 88–93.
- Hanahan, D. and Weinberg, R.A. (2000) The hallmarks of cancer. *Cell*, **100**(1): 57–70.
- Hanahan, D. and Weinberg, R.A. (2011) Hallmarks of cancer: the next generation. *Cell*, **144**(5): 646–674.
- Hanna, S. (2003) Cancer incidence in new zealand (2003-2007). In D. Forman, D. Bray F Brewster, C. Gombe Mbalawa, B. Kohler, M. Piñeros, E. Steliarova-Foucher, R. Swaminathan, and J. Ferlay (editors), *Cancer Incidence in Five Continents*, volume X, 902–907. International Agency for Research on Cancer, Lyon, France. Electronic version <http://ci5.iarc.fr> Accessed 22/03/2017.
- Heiskanen, M., Bian, X., Swan, D., and Basu, A. (2014) caArray microarray database in the cancer biomedical informatics grid™ (caBIG™). *Cancer Research*, **67**(9 Supplement): 3712–3712.
- Heiskanen, M.A. and Aittokallio, T. (2012) Mining high-throughput screens for cancer drug targets-lessons from yeast chemical-genomic profiling and synthetic lethality. *Wiley Interdisciplinary Reviews: Data Mining and Knowledge Discovery*, **2**(3): 263–272.

- Hell, P. (1976) Graphs with given neighbourhoods i. problémes combinatorics at theorie des graphes. *Proc Coll Int CNRS, Orsay*, **260**: 219–223.
- Herschkowitz, J.I., Simin, K., Weigman, V.J., Mikaelian, I., Usary, J., Hu, Z., Rasmussen, K.E., Jones, L.P., Assefnia, S., Chandrasekharan, S., *et al.* (2007) Identification of conserved gene expression features between murine mammary carcinoma models and human breast tumors. *Genome Biol*, **8**(5): R76.
- Hillenmeyer, M.E. (2008) The chemical genomic portrait of yeast: uncovering a phenotype for all genes. *Science*, **320**: 362–365.
- Hoadley, K.A., Yau, C., Wolf, D.M., Cherniack, A.D., Tamborero, D., Ng, S., Leiserson, M.D., Niu, B., McLellan, M.D., Uzunangelov, V., *et al.* (2014) Multiplatform analysis of 12 cancer types reveals molecular classification within and across tissues of origin. *Cell*, **158**(4): 929–944.
- Hoehndorf, R., Hardy, N.W., Osumi-Sutherland, D., Tweedie, S., Schofield, P.N., and Gkoutos, G.V. (2013) Systematic analysis of experimental phenotype data reveals gene functions. *PLoS ONE*, **8**(4): e60847.
- Holm, S. (1979) A simple sequentially rejective multiple test procedure. *Scandinavian Journal of Statistics*, **6**(2): 65–70.
- Holme, P. and Kim, B.J. (2002) Growing scale-free networks with tunable clustering. *Physical Review E*, **65**(2): 026107.
- Hopkins, A.L. (2008) Network pharmacology: the next paradigm in drug discovery. *Nat Chem Biol*, **4**(11): 682–690.
- Hu, Z., Fan, C., Oh, D.S., Marron, J.S., He, X., Qaqish, B.F., Livasy, C., Carey, L.A., Reynolds, E., Dressler, L., *et al.* (2006) The molecular portraits of breast tumors are conserved across microarray platforms. *BMC Genomics*, **7**: 96.
- Huang, E., Cheng, S., Dressman, H., Pittman, J., Tsou, M., Horng, C., Bild, A., Iversen, E., Liao, M., Chen, C., *et al.* (2003) Gene expression predictors of breast cancer outcomes. *Lancet*, **361**: 1590–1596.
- Illumina, Inc (Illumina) (2017) Sequencing and array-based solutions for genetic research. <https://www.illumina.com/>. Accessed: 26/03/2017.

- International HapMap 3 Consortium (HapMap) (2003) The International HapMap Project. *Nature*, **426**(6968): 789–796.
- Internationl Human Genome Sequencing Consortium (IHGSC) (2004) Finishing the euchromatic sequence of the human genome. *Nature*, **431**(7011): 931–945.
- Jerby-Arnon, L., Pfetzer, N., Waldman, Y., McGarry, L., James, D., Shanks, E., Seashore-Ludlow, B., Weinstock, A., Geiger, T., Clemons, P., *et al.* (2014) Predicting cancer-specific vulnerability via data-driven detection of synthetic lethality. *Cell*, **158**(5): 1199–1209.
- Joachims, T. (1999) Making large-scale support vector machine learning practical. In S. Bernhard, lkopf, J.C.B. Christopher, and J.S. Alexander (editors), *Advances in kernel methods*, 169–184. MIT Press.
- Ju, Z., Liu, W., Roebuck, P.L., Siwak, D.R., Zhang, N., Lu, Y., Davies, M.A., Akbani, R., Weinstein, J.N., Mills, G.B., *et al.* (2015) Development of a robust classifier for quality control of reverse-phase protein arrays. *Bioinformatics*, **31**(6): 912.
- Kaelin, Jr, W. (2005) The concept of synthetic lethality in the context of anticancer therapy. *Nat Rev Cancer*, **5**(9): 689–98.
- Kaelin, Jr, W. (2009) Synthetic lethality: a framework for the development of wiser cancer therapeutics. *Genome Med*, **1**: 99.
- Kakiuchi, M., Nishizawa, T., Ueda, H., Gotoh, K., Tanaka, A., Hayashi, A., Yamamoto, S., Tatsuno, K., Katoh, H., Watanabe, Y., *et al.* (2014) Recurrent gain-of-function mutations of RHOA in diffuse-type gastric carcinoma. *Nat Genet*, **46**(6): 583–587.
- Kamada, T. and Kawai, S. (1989) An algorithm for drawing general undirected graphs. *Information Processing Letters*, **31**(1): 7–15.
- Kandoth, C., Schultz, N., Cherniack, A.D., Akbani, R., Liu, Y., Shen, H., Robertson, A.G., Pashtan, I., Shen, R., Benz, C.C., *et al.* (2013) Integrated genomic characterization of endometrial carcinoma. *Nature*, **497**(7447): 67–73.
- Kawai, J., Shinagawa, A., Shibata, K., Yoshino, M., Itoh, M., Ishii, Y., Arakawa, T., Hara, A., Fukunishi, Y., Konno, H., *et al.* (2001) Functional annotation of a full-length mouse cDNA collection. *Nature*, **409**(6821): 685–690.

- Kelley, R. and Ideker, T. (2005) Systematic interpretation of genetic interactions using protein networks. *Nat Biotech*, **23**(5): 561–566.
- Kelly, S., Chen, A., Guilford, P., and Black, M. (2017a) Synthetic lethal interaction prediction of target pathways in E-cadherin deficient breast cancers. Submitted to *BMC Genomics*.
- Kelly, S.T. (2013) *Statistical Predictions of Synthetic Lethal Interactions in Cancer*. Dissertation, University of Otago.
- Kelly, S.T., Single, A.B., Telford, B.J., Beetham, H.G., Godwin, T.D., Chen, A., Black, M.A., and Guilford, P.J. (2017b) Towards HDGC chemoprevention: vulnerabilities in E-cadherin-negative cells identified by genome-wide interrogation of isogenic cell lines and whole tumors. Submitted to *Cancer Prev Res*.
- Kozlov, K.N., Gursky, V.V., Kulakovskiy, I.V., and Samsonova, M.G. (2015) Sequence-based model of gap gene regulation network. *BMC Genomics*, **15**(Suppl 12): S6.
- Kranthi, S., Rao, S., and Manimaran, P. (2013) Identification of synthetic lethal pairs in biological systems through network information centrality. *Mol BioSyst*, **9**(8): 2163–2167.
- Lander, E.S. (2011) Initial impact of the sequencing of the human genome. *Nature*, **470**(7333): 187–197.
- Lander, E.S., Linton, L.M., Birren, B., Nusbaum, C., Zody, M.C., Baldwin, J., Devon, K., Dewar, K., Doyle, M., FitzHugh, W., et al. (2001) Initial sequencing and analysis of the human genome. *Nature*, **409**(6822): 860–921.
- Langmead, B., Trapnell, C., Pop, M., and Salzberg, S.L. (2009) Ultrafast and memory-efficient alignment of short DNA sequences to the human genome. *Genome Biol*, **10**(3): R25.
- Latora, V. and Marchiori, M. (2001) Efficient behavior of small-world networks. *Phys Rev Lett*, **87**: 198701.
- Laufer, C., Fischer, B., Billmann, M., Huber, W., and Boutros, M. (2013) Mapping genetic interactions in human cancer cells with RNAi and multiparametric phenotyping. *Nat Methods*, **10**(5): 427–31.

- Law, C.W., Chen, Y., Shi, W., and Smyth, G.K. (2014) voom: precision weights unlock linear model analysis tools for RNA-seq read counts. *Genome Biol*, **15**(2): R29.
- Lawrence, M.S., Sougnez, C., Lichtenstein, L., Cibulskis, K., Lander, E., Gabriel, S.B., Getz, G., Ally, A., Balasundaram, M., Birol, I., et al. (2015) Comprehensive genomic characterization of head and neck squamous cell carcinomas. *Nature*, **517**(7536): 576–582.
- Le Meur, N. and Gentleman, R. (2008) Modeling synthetic lethality. *Genome Biol*, **9**(9): R135.
- Le Meur, N., Jiang, Z., Liu, T., Mar, J., and Gentleman, R.C. (2014) Slgi: Synthetic lethal genetic interaction. r package version 1.26.0.
- Lee, A.Y., Perreault, R., Harel, S., Boulier, E.L., Suderman, M., Hallett, M., and Jenna, S. (2010a) Searching for signaling balance through the identification of genetic interactors of the rab guanine-nucleotide dissociation inhibitor gdi-1. *PLoS ONE*, **5**(5): e10624.
- Lee, I., Lehner, B., Vavouri, T., Shin, J., Fraser, A.G., and Marcotte, E.M. (2010b) Predicting genetic modifier loci using functional gene networks. *Genome Research*, **20**(8): 1143–1153.
- Lee, I. and Marcotte, E.M. (2009) Effects of functional bias on supervised learning of a gene network model. *Methods Mol Biol*, **541**: 463–75.
- Lee, M.J., Ye, A.S., Gardino, A.K., Heijink, A.M., Sorger, P.K., MacBeath, G., and Yaffe, M.B. (2012) Sequential application of anticancer drugs enhances cell death by rewiring apoptotic signaling networks. *Cell*, **149**(4): 780–94.
- Lehner, B., Crombie, C., Tischler, J., Fortunato, A., and Fraser, A.G. (2006) Systematic mapping of genetic interactions in *caenorhabditis elegans* identifies common modifiers of diverse signaling pathways. *Nat Genet*, **38**(8): 896–903.
- Li, X.J., Mishra, S.K., Wu, M., Zhang, F., and Zheng, J. (2014) Syn-lethality: An integrative knowledge base of synthetic lethality towards discovery of selective anticancer therapies. *Biomed Res Int*, **2014**: 196034.
- Linehan, W.M., Spellman, P.T., Ricketts, C.J., Creighton, C.J., Fei, S.S., Davis, C., Wheeler, D.A., Murray, B.A., Schmidt, L., Vocke, C.D., et al. (2016) Comprehen-

- sive Molecular Characterization of Papillary Renal-Cell Carcinoma. *N Engl J Med*, **374**(2): 135–145.
- Lokody, I. (2014) Computational modelling: A computational crystal ball. *Nature Reviews Cancer*, **14**(10): 649–649.
- Lord, C.J., Tutt, A.N., and Ashworth, A. (2015) Synthetic lethality and cancer therapy: lessons learned from the development of PARP inhibitors. *Annu Rev Med*, **66**: 455–470.
- Lu, X., Kensche, P.R., Huynen, M.A., and Notebaart, R.A. (2013) Genome evolution predicts genetic interactions in protein complexes and reveals cancer drug targets. *Nat Commun*, **4**: 2124.
- Lu, X., Megchelenbrink, W., Notebaart, R.A., and Huynen, M.A. (2015) Predicting human genetic interactions from cancer genome evolution. *PLoS One*, **10**(5): e0125795.
- Lum, P.Y., Armour, C.D., Stepaniants, S.B., Cavet, G., Wolf, M.K., Butler, J.S., Hinchshaw, J.C., Garnier, P., Prestwich, G.D., Leonardson, A., et al. (2004) Discovering modes of action for therapeutic compounds using a genome-wide screen of yeast heterozygotes. *Cell*, **116**(1): 121–137.
- Luo, J., Solimini, N.L., and Elledge, S.J. (2009) Principles of Cancer Therapy: Oncogene and Non-oncogene Addiction. *Cell*, **136**(5): 823–837.
- Machado, J., Olivera, C., Carvalh, R., Soares, P., Berx, G., Caldas, C., Sercuca, R., Carneiro, F., and Sorbrinho-Simoes, M. (2001) E-cadherin gene (*CDH1*) promoter methylation as the second hit in sporadic diffuse gastric carcinoma. *Oncogene*, **20**: 1525–1528.
- Masciari, S., Larsson, N., Senz, J., Boyd, N., Kaurah, P., Kandel, M.J., Harris, L.N., Pinheiro, H.C., Troussard, A., Miron, P., et al. (2007) Germline E-cadherin mutations in familial lobular breast cancer. *J Med Genet*, **44**(11): 726–31.
- Mattison, J., van der Weyden, L., Hubbard, T., and Adams, D.J. (2009) Cancer gene discovery in mouse and man. *Biochim Biophys Acta*, **1796**(2): 140–161.
- Maxam, A.M. and Gilbert, W. (1977) A new method for sequencing DNA. *Proceedings of the National Academy of Science*, **74**(2): 560–564.

- McCourt, C.M., McArt, D.G., Mills, K., Catherwood, M.A., Maxwell, P., Waugh, D.J., Hamilton, P., O’Sullivan, J.M., and Salto-Tellez, M. (2013) Validation of next generation sequencing technologies in comparison to current diagnostic gold standards for BRAF, EGFR and KRAS mutational analysis. *PLoS ONE*, **8**(7): e69604.
- McLachlan, J., George, A., and Banerjee, S. (2016) The current status of parp inhibitors in ovarian cancer. *Tumori*, **102**(5): 433–440.
- McLendon, R., Friedman, A., Bigner, D., Van Meir, E.G., Brat, D.J., Mastrogiannakis, G.M., Olson, J.J., Mikkelsen, T., Lehman, N., Aldape, K., *et al.* (2008) Comprehensive genomic characterization defines human glioblastoma genes and core pathways. *Nature*, **455**(7216): 1061–1068.
- Miles, D.W. (2001) Update on HER-2 as a target for cancer therapy: herceptin in the clinical setting. *Breast Cancer Res*, **3**(6): 380–384.
- Mortazavi, A., Williams, B.A., McCue, K., Schaeffer, L., and Wold, B. (2008) Mapping and quantifying mammalian transcriptomes by RNA-Seq. *Nat Methods*, **5**(7): 621–628.
- Muzny, D.M., Bainbridge, M.N., Chang, K., Dinh, H.H., Drummond, J.A., Fowler, G., Kovar, C.L., Lewis, L.R., Morgan, M.B., Newsham, I.F., *et al.* (2012) Comprehensive molecular characterization of human colon and rectal cancer. *Nature*, **487**(7407): 330–337.
- Nagalla, S., Chou, J.W., Willingham, M.C., Ruiz, J., Vaughn, J.P., Dubey, P., Lash, T.L., Hamilton-Dutoit, S.J., Bergh, J., Sotiriou, C., *et al.* (2013) Interactions between immunity, proliferation and molecular subtype in breast cancer prognosis. *Genome Biol*, **14**(4): R34.
- Neeley, E.S., Kornblau, S.M., Coombes, K.R., and Baggerly, K.A. (2009) Variable slope normalization of reverse phase protein arrays. *Bioinformatics*, **25**(11): 1384.
- Novomestky, F. (2012) *matrixcalc: Collection of functions for matrix calculations*. R package version 1.0-3.
- Oliveira, C., Senz, J., Kaurah, P., Pinheiro, H., Sanges, R., Haegert, A., Corso, G., Schouten, J., Fitzgerald, R., Vogelsang, H., *et al.* (2009) Germline CDH1 deletions in hereditary diffuse gastric cancer families. *Human Molecular Genetics*, **18**(9): 1545–1555.

- Oliveira, C., Seruca, R., Hoogerbrugge, N., Ligtenberg, M., and Carneiro, F. (2013) Clinical utility gene card for: Hereditary diffuse gastric cancer (HDGC). *Eur J Hum Genet*, **21**(8).
- Pandey, G., Zhang, B., Chang, A.N., Myers, C.L., Zhu, J., Kumar, V., and Schadt, E.E. (2010) An integrative multi-network and multi-classifier approach to predict genetic interactions. *PLoS Comput Biol*, **6**(9).
- Parker, J., Mullins, M., Cheung, M., Leung, S., Voduc, D., Vickery, T., Davies, S., Fauron, C., He, X., Hu, Z., et al. (2009) Supervised risk predictor of breast cancer based on intrinsic subtypes. *Journal of Clinical Oncology*, **27**(8): 1160–1167.
- Peltonen, L. and McKusick, V.A. (2001) Genomics and medicine. Dissecting human disease in the postgenomic era. *Science*, **291**(5507): 1224–1229.
- Pereira, B., Chin, S.F., Rueda, O.M., Vollan, H.K., Provenzano, E., Bardwell, H.A., Pugh, M., Jones, L., Russell, R., Sammut, S.J., et al. (2016) Erratum: The somatic mutation profiles of 2,433 breast cancers refine their genomic and transcriptomic landscapes. *Nat Commun*, **7**: 11908.
- Perou, C.M., Sørlie, T., Eisen, M.B., van de Rijn, M., Jeffrey, S.S., Rees, C.A., Pollack, J.R., Ross, D.T., Johnsen, H., Akslen, L.A., et al. (2000) Molecular portraits of human breast tumours. *Nature*, **406**(6797): 747–752.
- Pleasance, E.D., Cheetham, R.K., Stephens, P.J., McBride, D.J., Humphray, S.J., Greenman, C.D., Varela, I., Lin, M.L., Ordonez, G.R., Bignell, G.R., et al. (2010) A comprehensive catalogue of somatic mutations from a human cancer genome. *Nature*, **463**(7278): 191–196.
- Polyak, K. and Weinberg, R.A. (2009) Transitions between epithelial and mesenchymal states: acquisition of malignant and stem cell traits. *Nat Rev Cancer*, **9**(4): 265–73.
- Prahallas, A., Sun, C., Huang, S., Di Nicolantonio, F., Salazar, R., Zecchin, D., Beijersbergen, R.L., Bardelli, A., and Bernards, R. (2012) Unresponsiveness of colon cancer to *BRAF*(v600e) inhibition through feedback activation of egfr. *Nature*, **483**(7387): 100–3.
- R Core Team (2016) *R: A Language and Environment for Statistical Computing*. R Foundation for Statistical Computing, Vienna, Austria. R version 3.3.2.

- Ravnan, M.C. and Matalka, M.S. (2012) Vemurafenib in patients with *BRAF* v600e mutation-positive advanced melanoma. *Clin Ther*, **34**(7): 1474–86.
- Ritchie, M.E., Phipson, B., Wu, D., Hu, Y., Law, C.W., Shi, W., and Smyth, G.K. (2015) limma powers differential expression analyses for RNA-sequencing and microarray studies. *Nucleic Acids Research*, **43**(7): e47.
- Robin, J.D., Ludlow, A.T., LaRanger, R., Wright, W.E., and Shay, J.W. (2016) Comparison of DNA Quantification Methods for Next Generation Sequencing. *Sci Rep*, **6**: 24067.
- Robinson, M.D. and Oshlack, A. (2010) A scaling normalization method for differential expression analysis of RNA-seq data. *Genome Biol*, **11**(3): R25.
- Roguev, A., Bandyopadhyay, S., Zofall, M., Zhang, K., Fischer, T., Collins, S.R., Qu, H., Shales, M., Park, H.O., Hayles, J., *et al.* (2008) Conservation and rewiring of functional modules revealed by an epistasis map in fission yeast. *Science*, **322**(5900): 405–10.
- Rung, J. and Brazma, A. (2013) Reuse of public genome-wide gene expression data. *Nat Rev Genet*, **14**(2): 89–99.
- Rustici, G., Kolesnikov, N., Brandizi, M., Burdett, T., Dylag, M., Emam, I., Farne, A., Hastings, E., Ison, J., Keays, M., *et al.* (2013) ArrayExpress update—trends in database growth and links to data analysis tools. *Nucleic Acids Res*, **41**(Database issue): D987–990.
- Ryan, C., Lord, C., and Ashworth, A. (2014) Daisy: Picking synthetic lethals from cancer genomes. *Cancer Cell*, **26**(3): 306–308.
- Sander, J.D. and Joung, J.K. (2014) Crispr-cas systems for editing, regulating and targeting genomes. *Nat Biotechnol*, **32**(4): 347–55.
- Sanger, F. and Coulson, A. (1975) A rapid method for determining sequences in dna by primed synthesis with dna polymerase. *Journal of Molecular Biology*, **94**(3): 441 – 448.
- Scheuer, L., Kauff, N., Robson, M., Kelly, B., Barakat, R., Satagopan, J., Ellis, N., Hensley, M., Boyd, J., Borgen, P., *et al.* (2002) Outcome of preventive surgery and screening for breast and ovarian cancer in BRCA mutation carriers. *J Clin Oncol*, **20**(5): 1260–1268.

- Semb, H. and Christofori, G. (1998) The tumor-suppressor function of E-cadherin. *Am J Hum Genet*, **63**(6): 1588–93.
- Sing, T., Sander, O., Beerenwinkel, N., and Lengauer, T. (2005) Rocr: visualizing classifier performance in r. *Bioinformatics*, **21**(20): 7881.
- Slurm development team (Slurm) (2017) Slurm workload manager. <https://slurm.schedmd.com/>. Accessed: 25/03/2017.
- Sørlie, T., Perou, C.M., Tibshirani, R., Aas, T., Geisler, S., Johnsen, H., Hastie, T., Eisen, M.B., van de Rijn, M., Jeffrey, S.S., et al. (2001) Gene expression patterns of breast carcinomas distinguish tumor subclasses with clinical implications. *Proc Natl Acad Sci USA*, **98**(19): 10869–10874.
- Stajich, J.E. and Lapp, H. (2006) Open source tools and toolkits for bioinformatics: significance, and where are we? *Brief Bioinformatics*, **7**(3): 287–296.
- Stratton, M.R., Campbell, P.J., and Futreal, P.A. (2009) The cancer genome. *Nature*, **458**(7239): 719–724.
- Ström, C. and Helleday, T. (2012) Strategies for the use of poly(adenosine diphosphate ribose) polymerase (parp) inhibitors in cancer therapy. *Biomolecules*, **2**(4): 635–649.
- Sun, C., Wang, L., Huang, S., Heynen, G.J.J.E., Prahallad, A., Robert, C., Haanen, J., Blank, C., Wesseling, J., Willems, S.M., et al. (2014) Reversible and adaptive resistance to *BRAF*(v600e) inhibition in melanoma. *Nature*, **508**(7494): 118–122.
- Taylor, I.W., Linding, R., Warde-Farley, D., Liu, Y., Pesquita, C., Faria, D., Bull, S., Pawson, T., Morris, Q., and Wrana, J.L. (2009) Dynamic modularity in protein interaction networks predicts breast cancer outcome. *Nat Biotechnol*, **27**(2): 199–204.
- Telford, B.J., Chen, A., Beetham, H., Frick, J., Brew, T.P., Gould, C.M., Single, A., Godwin, T., Simpson, K.J., and Guilford, P. (2015) Synthetic lethal screens identify vulnerabilities in gpcr signalling and cytoskeletal organization in E-cadherin-deficient cells. *Mol Cancer Ther*, **14**(5): 1213–1223.
- The 1000 Genomes Project Consortium (1000 Genomes) (2010) A map of human genome variation from population-scale sequencing. *Nature*, **467**(7319): 1061–1073.

- The Cancer Genome Atlas Research Network (TCGA) (2012) Comprehensive molecular portraits of human breast tumours. *Nature*, **490**(7418): 61–70.
- The Cancer Genome Atlas Research Network (TCGA) (2017a) The Cancer Genome Atlas Project. <https://cancergenome.nih.gov/>. Accessed: 26/03/2017.
- The Cancer Genome Atlas Research Network (TCGA) (2017b) The Cancer Genome Atlas Project Data Portal. <https://tcga-data.nci.nih.gov/>. Accessed: 06/02/2017 (via cBioPortal).
- The Cancer Society of New Zealand (Cancer Society of NZ) (2017) What is cancer? <https://otago-southland.cancernz.org.nz/en/cancer-information/other-links/what-is-cancer-3/>. Accessed: 22/03/2017.
- The Catalogue Of Somatic Mutations In Cancer (COSMIC) (2016) Cosmic: The catalogue of somatic mutations in cancer. <http://cancer.sanger.ac.uk/cosmic>. Release 79 (23/08/2016), Accessed: 05/02/2017.
- The Comprehensive R Archive Network (CRAN) (2017) Cran. <https://cran.r-project.org/>. Accessed: 24/03/2017.
- The ENCODE Project Consortium (ENCODE) (2004) The ENCODE (ENCyclopedia Of DNA Elements) Project. *Science*, **306**(5696): 636–640.
- The Internation Cancer Genome Consortium (ICGC) (2017) ICGC Data Portal. <https://dcc.icgc.org/>. Accessed: 06/02/2017.
- The National Cancer Institute (NCI) (2015) The genetics of cancer. <https://www.cancer.gov/about-cancer/causes-prevention/genetics>. Published: 22/04/2015, Accessed: 22/03/2017.
- The New Zealand eScience Infrastructure (NeSI) (2017) NeSI. <https://www.nesi.org.nz/>. Accessed: 25/03/2017.
- The Pharmaceutical Management Agency (PHARMAC) (2016) Approval of multi-product funding proposal with roche.
- Tierney, L., Rossini, A.J., Li, N., and Sevcikova, H. (2015) *snow: Simple Network of Workstations*. R package version 0.4-2.

- Tiong, K.L., Chang, K.C., Yeh, K.T., Liu, T.Y., Wu, J.H., Hsieh, P.H., Lin, S.H., Lai, W.Y., Hsu, Y.C., Chen, J.Y., *et al.* (2014) Csnk1e/ctnnb1 are synthetic lethal to tp53 in colorectal cancer and are markers for prognosis. *Neoplasia*, **16**(5): 441–50.
- Tischler, J., Lehner, B., and Fraser, A.G. (2008) Evolutionary plasticity of genetic interaction networks. *Nat Genet*, **40**(4): 390–391.
- Tomasetti, C. and Vogelstein, B. (2015) Cancer etiology. Variation in cancer risk among tissues can be explained by the number of stem cell divisions. *Science*, **347**(6217): 78–81.
- Tong, A.H., Evangelista, M., Parsons, A.B., Xu, H., Bader, G.D., Page, N., Robinson, M., Raghibizadeh, S., Hogue, C.W., Bussey, H., *et al.* (2001) Systematic genetic analysis with ordered arrays of yeast deletion mutants. *Science*, **294**(5550): 2364–8.
- Tong, A.H., Lesage, G., Bader, G.D., Ding, H., Xu, H., Xin, X., Young, J., Berriz, G.F., Brost, R.L., Chang, M., *et al.* (2004) Global mapping of the yeast genetic interaction network. *Science*, **303**(5659): 808–13.
- Travers, J. and Milgram, S. (1969) An experimental study of the small world problem. *Sociometry*, **32**(4): 425–443.
- Tsai, H.C., Li, H., Van Neste, L., Cai, Y., Robert, C., Rassool, F.V., Shin, J.J., Harbom, K.M., Beaty, R., Pappou, E., *et al.* (2012) Transient low doses of dna-demethylating agents exert durable antitumor effects on hematological and epithelial tumor cells. *Cancer Cell*, **21**(3): 430–46.
- Tutt, A., Robson, M., Garber, J.E., Domchek, S.M., Audeh, M.W., Weitzel, J.N., Friedlander, M., Arun, B., Loman, N., Schmutzler, R.K., *et al.* (2010) Oral poly(adt-ribose) polymerase inhibitor olaparib in patients with *BRCA1* or *BRCA2* mutations and advanced breast cancer: a proof-of-concept trial. *Lancet*, **376**(9737): 235–44.
- van der Meer, R., Song, H.Y., Park, S.H., Abdulkadir, S.A., and Roh, M. (2014) RNAi screen identifies a synthetic lethal interaction between PIM1 overexpression and PLK1 inhibition. *Clinical Cancer Research*, **20**(12): 3211–3221.
- van Steen, K. (2012) Travelling the world of genegene interactions. *Briefings in Bioinformatics*, **13**(1): 1–19.
- van Steen, M. (2010) *Graph Theory and Complex Networks: An Introduction*. Maarten van Steen, VU Amsterdam.

- Vapnik, V.N. (1995) *The nature of statistical learning theory*. Springer-Verlag New York, Inc.
- Vargas, J.J., Gusella, G., Najfeld, V., Klotman, M., and Cara, A. (2004) Novel integrase-defective lentiviral episomal vectors for gene transfer. *Hum Gene Ther*, **15**: 361–372.
- Vizeacoumar, F.J., Arnold, R., Vizeacoumar, F.S., Chandrashekhar, M., Buzina, A., Young, J.T., Kwan, J.H., Sayad, A., Mero, P., Lawo, S., *et al.* (2013) A negative genetic interaction map in isogenic cancer cell lines reveals cancer cell vulnerabilities. *Mol Syst Biol*, **9**: 696.
- Vogelstein, B., Papadopoulos, N., Velculescu, V.E., Zhou, S., Diaz, L.A., and Kinzler, K.W. (2013) Cancer genome landscapes. *Science*, **339**(6127): 1546–1558.
- Vos, C.B., Cleton-Jansen, A.M., Berx, G., de Leeuw, W.J., ter Haar, N.T., van Roy, F., Cornelisse, C.J., Peterse, J.L., and van de Vijver, M.J. (1997) E-cadherin inactivation in lobular carcinoma in situ of the breast: an early event in tumorigenesis. *Br J Cancer*, **76**(9): 1131–3.
- Wang, K., Singh, D., Zeng, Z., Coleman, S.J., Huang, Y., Savich, G.L., He, X., Mieczkowski, P., Grimm, S.A., Perou, C.M., *et al.* (2010) MapSplice: accurate mapping of RNA-seq reads for splice junction discovery. *Nucleic Acids Res*, **38**(18): e178.
- Wang, K., Yuen, S.T., Xu, J., Lee, S.P., Yan, H.H., Shi, S.T., Siu, H.C., Deng, S., Chu, K.M., Law, S., *et al.* (2014) Whole-genome sequencing and comprehensive molecular profiling identify new driver mutations in gastric cancer. *Nat Genet*, **46**(6): 573–582.
- Wang, X. and Simon, R. (2013) Identification of potential synthetic lethal genes to p53 using a computational biology approach. *BMC Medical Genomics*, **6**(1): 30.
- Wappett, M. (2014) Bisep: Toolkit to identify candidate synthetic lethality. r package version 2.0.
- Wappett, M., Dulak, A., Yang, Z.R., Al-Watban, A., Bradford, J.R., and Dry, J.R. (2016) Multi-omic measurement of mutually exclusive loss-of-function enriches for candidate synthetic lethal gene pairs. *BMC Genomics*, **17**: 65.

- Warnes, G.R., Bolker, B., Bonebakker, L., Gentleman, R., Liaw, W.H.A., Lumley, T., Maechler, M., Magnusson, A., Moeller, S., Schwartz, M., *et al.* (2015) *gplots: Various R Programming Tools for Plotting Data*. R package version 2.17.0.
- Watts, D.J. and Strogatz, S.H. (1998) Collective dynamics of 'small-world' networks. *Nature*, **393**(6684): 440–2.
- Weinstein, I.B. (2000) Disorders in cell circuitry during multistage carcinogenesis: the role of homeostasis. *Carcinogenesis*, **21**(5): 857–864.
- Weinstein, J.N., Akbani, R., Broom, B.M., Wang, W., Verhaak, R.G., McConkey, D., Lerner, S., Morgan, M., Creighton, C.J., Smith, C., *et al.* (2014) Comprehensive molecular characterization of urothelial bladder carcinoma. *Nature*, **507**(7492): 315–322.
- Weinstein, J.N., Collisson, E.A., Mills, G.B., Shaw, K.R., Ozenberger, B.A., Ellrott, K., Shmulevich, I., Sander, C., Stuart, J.M., Chang, K., *et al.* (2013) The Cancer Genome Atlas Pan-Cancer analysis project. *Nat Genet*, **45**(10): 1113–1120.
- Wickham, H. and Chang, W. (2016) *devtools: Tools to Make Developing R Packages Easier*. R package version 1.12.0.
- Wickham, H., Danenberg, P., and Eugster, M. (2017) *roxygen2: In-Line Documentation for R*. R package version 6.0.1.
- Wong, S.L., Zhang, L.V., Tong, A.H.Y., Li, Z., Goldberg, D.S., King, O.D., Lesage, G., Vidal, M., Andrews, B., Bussey, H., *et al.* (2004) Combining biological networks to predict genetic interactions. *Proceedings of the National Academy of Sciences of the United States of America*, **101**(44): 15682–15687.
- World Health Organization (WHO) (2017) Fact sheet: Cancer. <http://www.who.int/mediacentre/factsheets/fs297/en/>. Updated February 2017, Accessed: 22/03/2017.
- Wu, M., Li, X., Zhang, F., Li, X., Kwoh, C.K., and Zheng, J. (2014) In silico prediction of synthetic lethality by meta-analysis of genetic interactions, functions, and pathways in yeast and human cancer. *Cancer Inform*, **13**(Suppl 3): 71–80.
- Yu, H. (2002) Rmpi: Parallel statistical computing in r. *R News*, **2**(2): 10–14.

- Zhang, F., Wu, M., Li, X.J., Li, X.L., Kwoh, C.K., and Zheng, J. (2015) Predicting essential genes and synthetic lethality via influence propagation in signaling pathways of cancer cell fates. *J Bioinform Comput Biol*, **13**(3): 1541002.
- Zhang, J., Baran, J., Cros, A., Guberman, J.M., Haider, S., Hsu, J., Liang, Y., Rivkin, E., Wang, J., Whitty, B., et al. (2011) International cancer genome consortium data portal a one-stop shop for cancer genomics data. *Database: The Journal of Biological Databases and Curation*, **2011**: bar026.
- Zhong, W. and Sternberg, P.W. (2006) Genome-wide prediction of *C. elegans* genetic interactions. *Science*, **311**(5766): 1481–1484.
- Zweig, M.H. and Campbell, G. (1993) Receiver-operating characteristic (roc) plots: a fundamental evaluation tool in clinical medicine. *Clinical Chemistry*, **39**(4): 561–577.

Appendix A

Sample Quality

A.1 Sample Correlation

Samples were excluded from expression analysis based on sample correlations and the clustering analysis presented below, as described in Section 2.2.2.

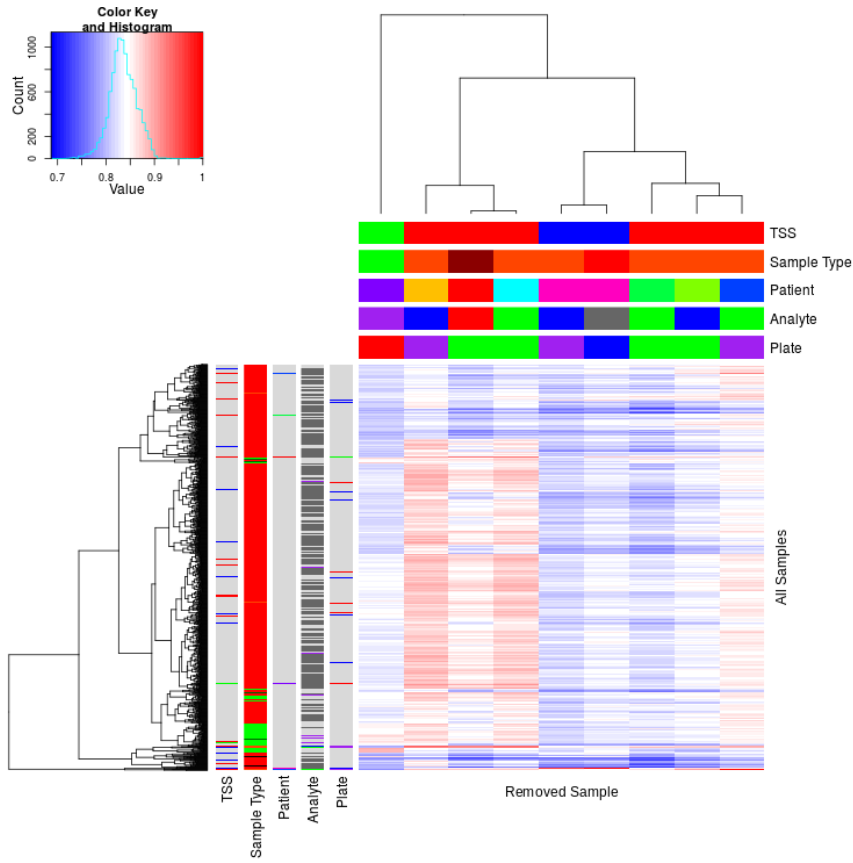


Figure A.1: Correlation profiles of removed samples. Correlation matrix heatmap (Euclidean distance) of all samples in TCGA breast cancer dataset (left) clustered for all samples against removed samples (top): tissue source site (TSS), sample type with reds for tumour and greens for normal, patient (A2QH in pink), with varied analyte and plate (corresponding to batch in Table 2.1). Excluded samples cluster at the bottom and annotation (left) show shared properties between samples in the dataset.

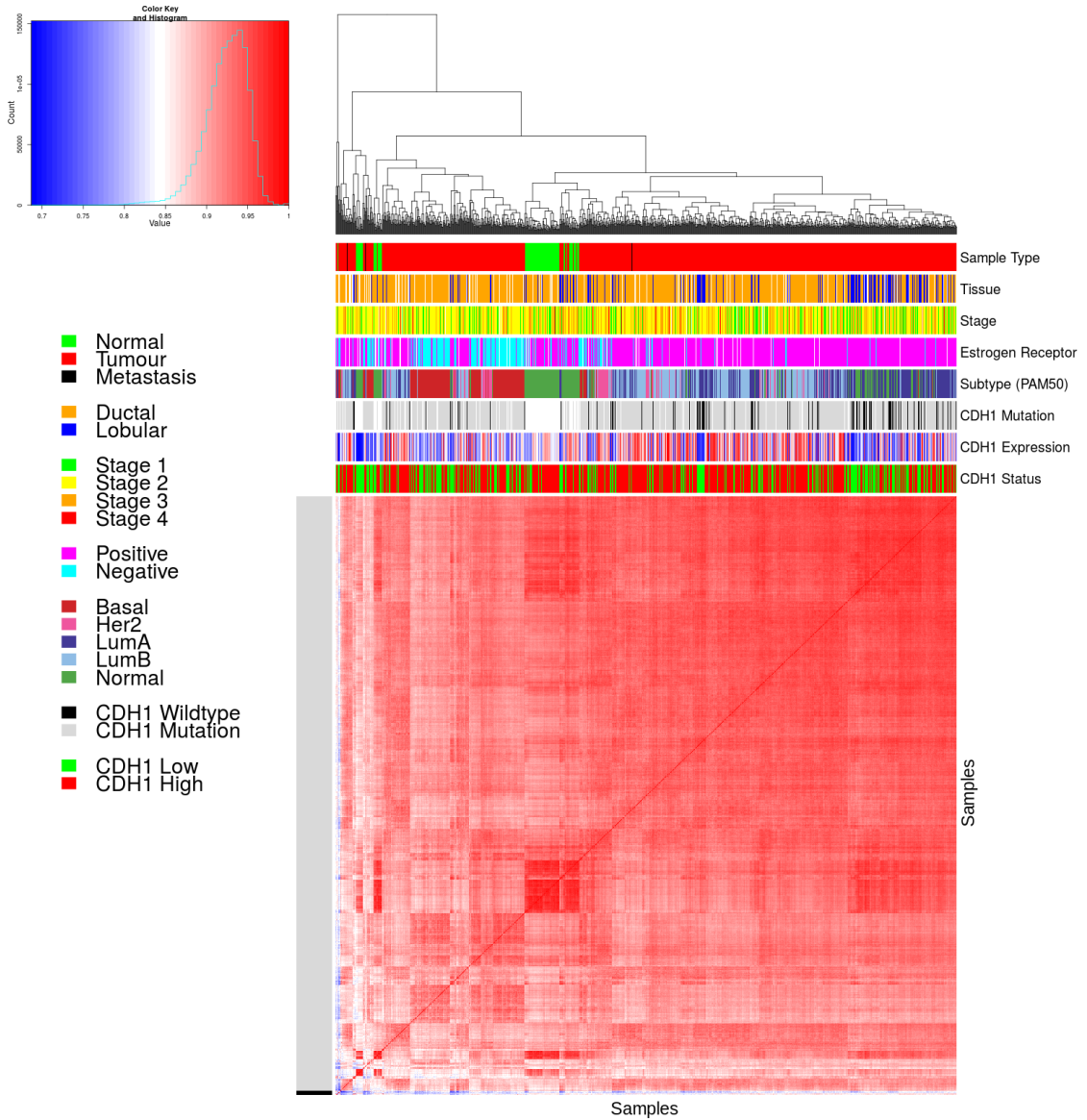


Figure A.2: Correlation analysis and sample removal. Correlation matrix heatmap (Euclidean distance) of all samples in TCGA breast cancer dataset against each other annotated for sample clinical data: sample type, tissue type, tumour stage, Estrogen receptor (IHC) and intrinsic subtype (from the PAM50 method). CDH1 somatic mutation, gene expression, and status for SLIPT prediction are also annotated. Discrete variables are coloured as displayed in the legend and continuous variables on a blue-red scale as shown in the colour key. Trimmed samples cluster at the bottom of the heatmap and the colour bars of the left show which were removed for quality concerns.

A.2 Replicate Samples in TCGA Breast

Replicate samples were picked where possible from the TCGA breast cancer gene expression data to examine for sample quality. Independent samples of the same tumour are expected to have very high Pearson's correlation between their expression profiles unless there were issues with sample collection or preparation and are thus an indicator of sample quality. The log-transformed raw read counts for replicate samples were examined in Figures A.3–A.5. These were examined before normalisation which would be expected to increase sample concordance.

Another consideration are the samples which were removed for quality concerns (in Section 2.2.2). While these were selected by unbiased hierarchical clustering (See Figure A.2), it is notable that many of the excluded (tumour) samples were performed in replicate despite relatively few replicate samples in the overall dataset. These samples correlate poorly with the rest of the dataset, in addition to with replicate samples.

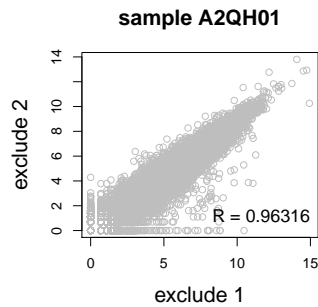


Figure A.3: **Replicate excluded samples.** Both tumour samples of patient A2QH were excluded as they were poorly correlated with other samples, although they are highly similar to each other as shown by Pearson's correlation of log-raw counts.

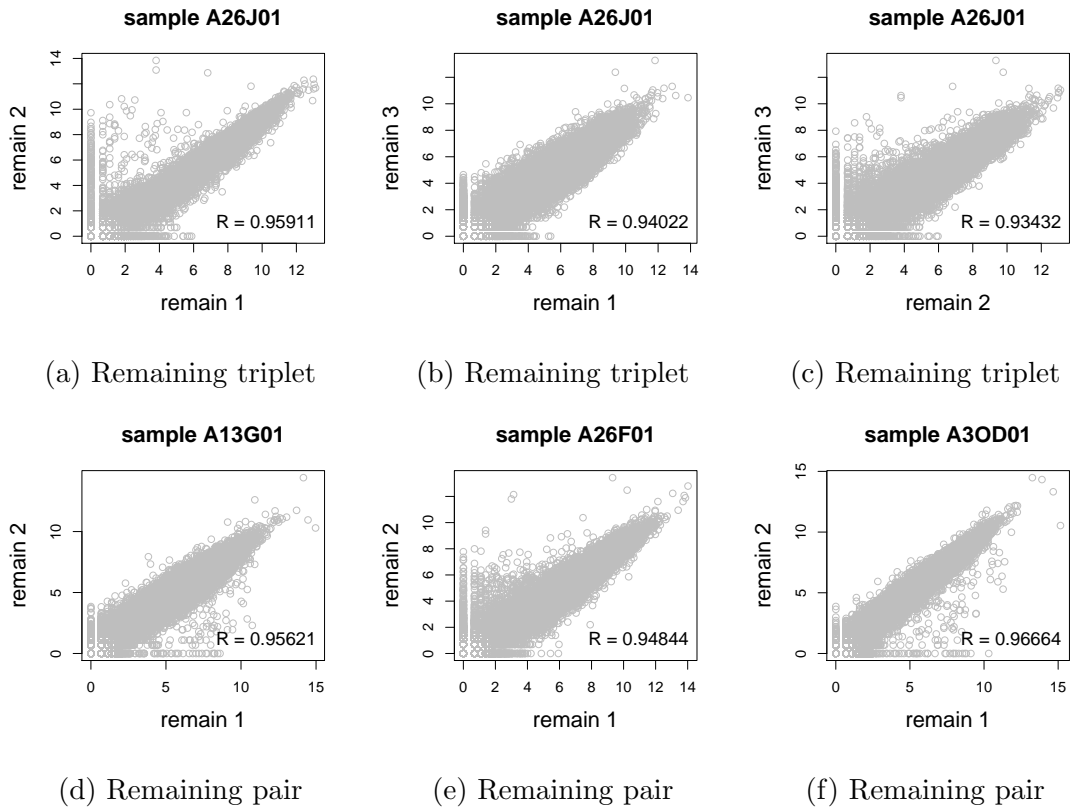


Figure A.4: **Replicate samples with all remaining.** Patient A26J was sampled 3 times and compared pairwise. Pairs of samples were also compared for other patients with replicate samples. In all cases, replicate samples remaining in the dataset were highly concordant as shown by Pearson's correlation of log-raw counts.

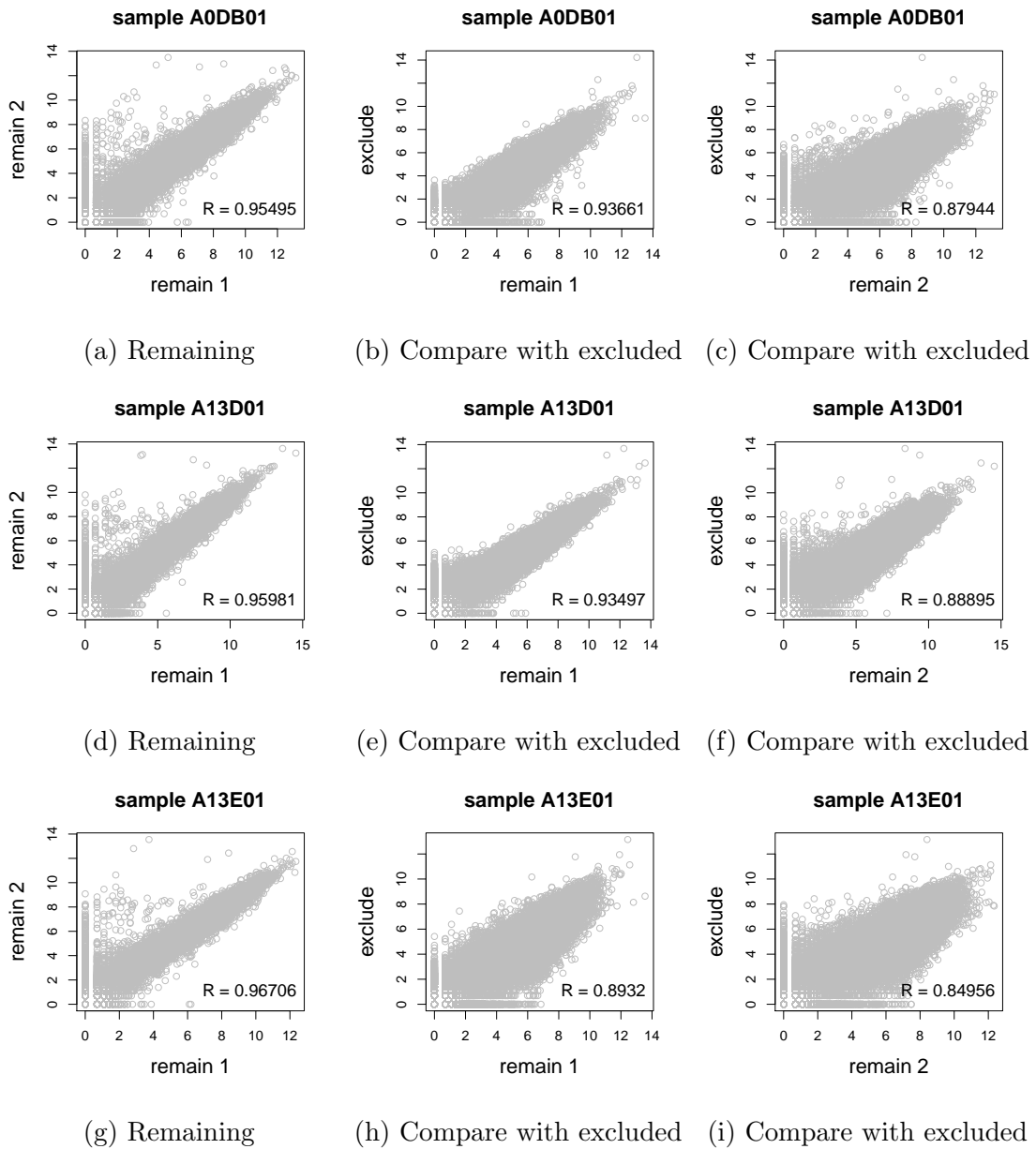


Figure A.5: Replicate samples with some excluded. (continued on next page)

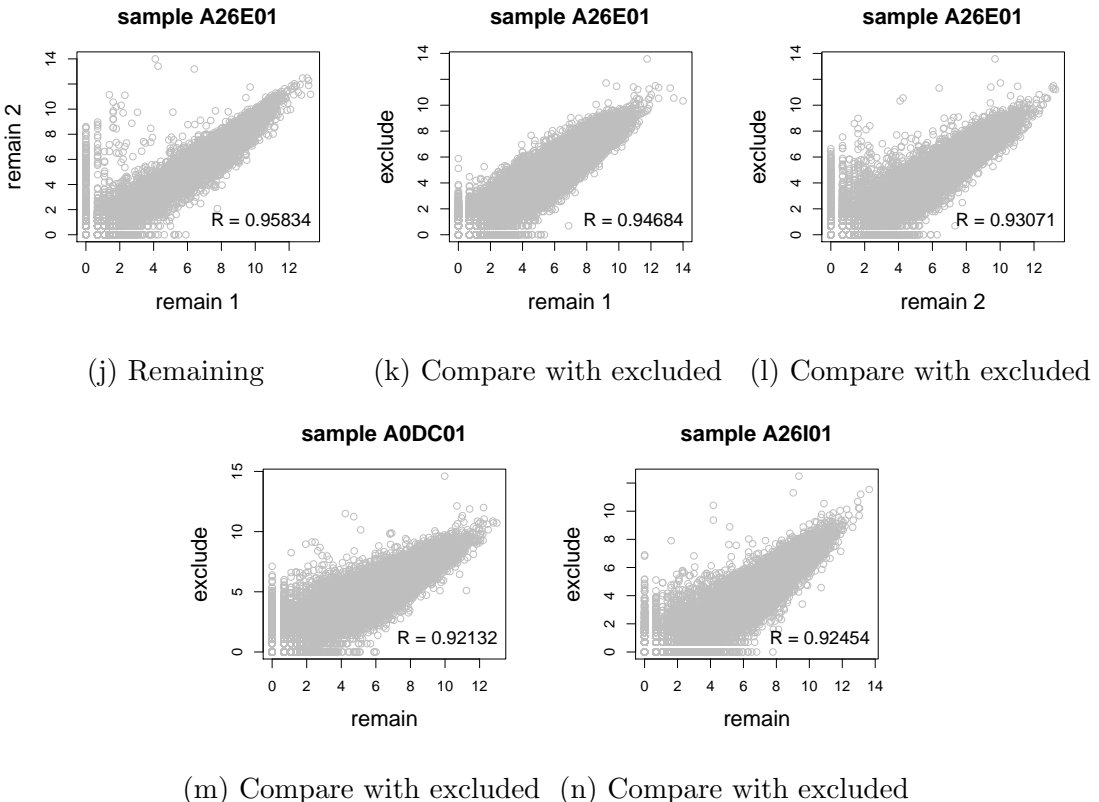


Figure A.5: **Replicate samples with some excluded.** Patients A0DB, A13D, A13E, and A26E were each sampled 3 times and compared pairwise. Pairs of samples were also compared for other patients with replicate samples. In all cases, the replicate samples remaining in the dataset more were highly concordant (as shown by Pearson's correlation of log-raw counts) than those excluded from the analysis.

Appendix B

Software Used for Thesis

Table B.1: R Packages used during Thesis

Package	Repository	Laptop	Lab	Server	NeSI
base	base	3.3.2	3.3.2	3.3.1	3.3.0
abind	CRAN		1.4-5		1.4-3
acepack	CRAN		1.4.1		1.3-3.3
ade4	CRAN		1.7-5		
annaffy	Bioconductor		1.46.0		
AnnotationDbi	Bioconductor		1.36.0	1.36.0	1.34.4
apComplex	CRAN		2.40.0		
ape	CRAN		4		3.4
arm	CRAN		1.9-3		
assertthat	CRAN	0.1	0.1	0.1	0.1
backports	CRAN	1.0.5	1.0.4	1.0.5	1.0.2
base64	CRAN			2	2
base64enc	CRAN		0.1-3		0.1-3
beanplot	CRAN		1.2	1.2	1.2
BH	CRAN	1.60.0-2	1.62.0-1	1.62.0-1	1.60.0-2
Biobase	Bioconductor		2.34.0	2.34.0	2.32.0
BiocGenerics	Bioconductor		0.20.0	0.20.0	0.18.0
BiocInstaller	Bioconductor		1.24.0	1.20.3	1.22.3
BiocParallel	Bioconductor		1.8.1	1.8.1	
Biostrings	Bioconductor		2.42.1	2.42.0	
BiSEp	Bioconductor		2.0.1	2.0.1	2.0.1

bitops	CRAN	1.0-6	1.0-6	1.0-6	1.0-6
boot	base	1.3-18	1.3-18	1.3-18	1.3-18
brew	CRAN	1.0-6	1.0-6	1.0-6	1.0-6
broom	CRAN	0.4.1			
caTools	CRAN	1.17.1	1.17.1	1.17.1	1.17.1
cgdssr	CRAN		1.2.5		
checkmate	CRAN		1.8.2		1.7.4
chron	CRAN	2.3-47	2.3-48	2.3-50	2.3-47
class	base	7.3-14	7.3-14	7.3-14	7.3-14
cluster	base	2.0.5	2.0.5	2.0.5	2.0.4
coda	CRAN		0.19-1		0.18-1
codetools	base	0.2-15	0.2-15	0.2-15	0.2-14
colorRamps	CRAN		2.3		
colorspace	CRAN	1.2-6	1.3-2	1.3-2	1.2-6
commonmark	CRAN	1.1		1.2	
compiler	base	3.3.2	3.3.2	3.3.1	3.3.0
corpcor	CRAN		1.6.8	1.6.8	1.6.8
Cprob	CRAN		1.2.4		
crayon	CRAN	1.3.2	1.3.2	1.3.2	1.3.2
crop	CRAN		0.0-2	0.0-2	
curl	CRAN	1.2	2.3	2.3	0.9.7
d3Network	CRAN		0.5.2.1		
data.table	CRAN	1.9.6	1.10.0	1.10.1	1.9.6
data.tree	CRAN		0.7.0	0.7.0	
datasets	base	3.3.2	3.3.2	3.3.1	3.3.0
DBI	CRAN	0.5-1	0.5-1	0.5-1	0.5-1
dendextend	CRAN	1.4.0	1.4.0	1.4.0	
DEoptimR	CRAN	1.0-8	1.0-8	1.0-8	1.0-4
desc	CRAN	1.1.0		1.1.0	
devtools	CRAN	1.12.0	1.12.0	1.12.0	1.12.0
DiagrammeR	CRAN		0.9.0	0.9.0	
dichromat	CRAN	2.0-0	2.0-0	2.0-0	2.0-0
digest	CRAN	0.6.10	0.6.11	0.6.12	0.6.9
diptest	CRAN	0.75-7	0.75-7	0.75-7	
doParallel	CRAN	1.0.10	1.0.10	1.0.10	1.0.10

dplyr	CRAN	0.5.0	0.5.0	0.5.0	0.5.0
ellipse	CRAN		0.3-8	0.3-8	0.3-8
evaluate	CRAN		0.1	0.1	0.9
fdrtool	CRAN		1.2.15		
fields	CRAN		8.1		
flexmix	CRAN	2.3-13	2.3-13	2.3-13	
forcats	CRAN	0.2.0			
foreach	CRAN	1.4.3	1.4.3	1.4.3	1.4.3
foreign	base	0.8-67	0.8-67	0.8-67	0.8-66
formatR	CRAN		1.4	1.4	1.4
Formula	CRAN		1.2-1		1.2-1
fpc	CRAN	2.1-10	2.1-10	2.1-10	
futile.logger	CRAN		1.4.3	1.4.3	1.4.1
futile.options	CRAN		1.0.0	1.0.0	1.0.0
gdata	CRAN	2.17.0	2.17.0	2.17.0	2.17.0
geepack	CRAN		1.2-1		
GenomeInfoDb	Bioconductor		1.10.2	1.10.1	
GenomicAlignments	Bioconductor		1.10.0	1.10.0	
GenomicRanges	Bioconductor		1.26.2	1.26.1	
ggm	CRAN		2.3		
ggplot2	CRAN	2.1.0	2.2.1	2.2.1	2.1.0
git2r	CRAN	0.15.0	0.18.0	0.16.0	0.15.0
glasso	CRAN		1.8		
GO.db	Bioconductor		3.4.0	3.2.2	3.3.0
GOSemSim	Bioconductor		2.0.3	1.28.2	1.30.3
gplots	CRAN	3.0.1	3.0.1	3.0.1	3.0.1
graph	Bioconductor		1.52.0		
graphics	base	3.3.2	3.3.2	3.3.1	3.3.0
graphsim	GitHub TomKellyGenetics	0.1.0	0.1.0	0.1.0	0.1.0
grDevices	base	3.3.2	3.3.2	3.3.1	3.3.0
grid	base	3.3.2	3.3.2	3.3.1	3.3.0
gridBase	CRAN	0.4-7	0.4-7	0.4-7	0.4-7
gridExtra	CRAN	2.2.1	2.2.1	2.2.1	2.2.1
gridGraphics	CRAN		0.1-5		

gtable	CRAN	0.2.0	0.2.0	0.2.0	0.2.0
gtools	CRAN	3.5.0	3.5.0	3.5.0	3.5.0
haven	CRAN	1.0.0			
heatmap.2x	GitHub		0.0.0.9000	0.0.0.9000	0.0.0.9000
	TomKellyGenetics				0.0.0.9000
hgu133plus2.db	Bioconductor		3.2.3		
highr	CRAN		0.6	0.6	0.6
Hmisc	CRAN		4.0-2	4.0-2	3.17-4
hms	CRAN	0.2	0.3		
htmlTable	CRAN		1.8	1.9	
htmltools	CRAN	0.3.5	0.3.5	0.3.5	0.3.5
htmlwidgets	CRAN		0.8	0.8	
httpuv	CRAN	1.3.3		1.3.3	
httr	CRAN	1.2.1	1.2.1	1.2.1	1.1.0
huge	CRAN		1.2.7		
hunspell	CRAN		2.3		2
hypergraph	CRAN		1.46.0		
igraph	CRAN	1.0.1	1.0.1	1.0.1	1.0.1
igraph.extensions	GitHub				
	TomKellyGenetics	0.1.0.9001	0.1.0.9001	0.1.0.9001	0.1.0.9001
influenceR	CRAN		0.1.0	0.1.0	
info.centrality	GitHub				
	TomKellyGenetics	0.1.0	0.1.0	0.1.0	0.1.0
IRanges	Bioconductor		2.8.1	2.8.1	2.6.1
irlba	CRAN	2.1.1	2.1.2	2.1.2	2.0.0
iterators	CRAN	1.0.8	1.0.8	1.0.8	1.0.8
jpeg	CRAN		0.1-8		
jsonlite	CRAN	1.1	1.2	1.3	0.9.20
KEGG.db	Bioconductor		3.2.3		
kernlab	CRAN	0.9-25	0.9-25	0.9-25	
KernSmooth	base	2.23-15	2.23-15	2.23-15	2.23-15
knitr	CRAN		1.15.1	1.15.1	1.14
labeling	CRAN	0.3	0.3	0.3	0.3
lambda.r	CRAN		1.1.9	1.1.9	1.1.7
lattice	base	0.20-34	0.20-34	0.20-34	0.20-33

latticeExtra	CRAN		0.6-28		0.6-28
lava	CRAN		1.4.6		
lavaan	CRAN		0.5-22		
lazyeval	CRAN	0.2.0	0.2.0	0.2.0	0.2.0
les	CRAN		1.24.0		
lgtdl	CRAN		1.1.3		
limma	Bioconductor		3.30.7	3.30.3	
lme4	CRAN		1.1-12		1.1-12
lubridate	CRAN	1.6.0			
magrittr	CRAN	1.5	1.5	1.5	1.5
maps	CRAN		3.1.1		
markdown	CRAN		0.7.7	0.7.7	0.7.7
MASS	base	7.3-45	7.3-45	7.3-45	7.3-45
Matrix	base	1.2-7.1	1.2-7.1	1.2-8	1.2-6
matrixcalc	CRAN	1.0-3	1.0-3	1.0-3	1.0-3
mclust	CRAN	5.2	5.2.1	5.2.2	5.2
memoise	CRAN	1.0.0	1.0.0	1.0.0	1.0.0
methods	base	3.3.2	3.3.2	3.3.1	3.3.0
mgcv	base	1.8-16	1.8-16	1.8-17	1.8-12
mi	CRAN		1		
mime	CRAN	0.5	0.5	0.5	0.4
minqa	CRAN		1.2.4		1.2.4
mnormt	CRAN	1.5-5	1.5-5		1.5-4
modelr	CRAN	0.1.0			
modeltools	CRAN	0.2-21	0.2-21	0.2-21	
multtest	Bioconductor		2.30.0	2.30.0	
munsell	CRAN	0.4.3	0.4.3	0.4.3	0.4.3
mvtnorm	CRAN	1.0-5	1.0-5	1.0-6	1.0-5
network	CRAN		1.13.0		
nlme	base	3.1-128	3.1-128	3.1-131	3.1-128
nloptr	CRAN		1.0.4		1.0.4
NMF	CRAN	0.20.6	0.20.6	0.20.6	0.20.6
nnet	base	7.3-12	7.3-12	7.3-12	7.3-12
numDeriv	CRAN		2016.8-1		2014.2-1
openssl	CRAN	0.9.4	0.9.6	0.9.6	0.9.4

org.Hs.eg.db	Bioconductor		3.1.2		3.3.0
org.Sc.sgd.db	Bioconductor		3.4.0		
parallel	base	3.3.2	3.3.2	3.3.1	3.3.0
pathway.structure	GitHub	0.1.0	0.1.0	0.1.0	0.1.0
.permutation	TomKellyGenetics				
pbivnorm	CRAN		0.6.0		
PGSEA	Bioconductor		1.48.0		
pkgmaker	CRAN	0.22	0.22	0.22	0.22
PKI	CRAN		0.1-3		
plogr	CRAN		0.1-1	0.1-1	
plot.igraph	GitHub	0.0.0.9001	0.0.0.9001	0.0.0.9001	0.0.0.9001
	TomKellyGenetics				
plotrix	CRAN		3.6-4		
plyr	CRAN	1.8.4	1.8.4	1.8.4	1.8.3
png	CRAN		0.1-7		0.1-7
prabclus	CRAN	2.2-6	2.2-6	2.2-6	
praise	CRAN	1.0.0	1.0.0		1.0.0
pROC	CRAN		1.8	1.9.1	
prodlim	CRAN		1.5.7		
prof.tree	CRAN		0.1.0		
protools	CRAN		0.99-2		
progress	CRAN			1.1.2	
psych	CRAN	1.6.12	1.6.12		
purrr	CRAN	0.2.2	0.2.2	0.2.2	0.2.2
qgraph	CRAN		1.4.1		
quadprog	CRAN		1.5-5	1.5-5	1.5-5
R.methodsS3	CRAN		1.7.1		1.7.1
R.oo	CRAN		1.21.0		1.20.0
R.utils	CRAN		2.5.0		
R6	CRAN	2.1.3	2.2.0	2.2.0	2.1.3
RBGL	CRAN		1.50.0		
RColorBrewer	CRAN	1.1-2	1.1-2	1.1-2	1.1-2
Rcpp	CRAN	0.12.7	0.12.9	0.12.9	0.12.7
RcppArmadillo	CRAN			0.7.700.0.0	0.6.700.6.0
RcppEigen	CRAN		0.3.2.9.0		0.3.2.8.1

RCurl	CRAN		1.95-4.8	1.95-4.8	1.95-4.8
reactome.db	Bioconductor		1.52.1	1.52.1	
reactometree	GitHub		0.1		
	TomKellyGenetics				
readr	CRAN	1.0.0	1.0.0		
readxl	CRAN	0.1.1			
registry	CRAN	0.3	0.3	0.3	0.3
reshape2	CRAN	1.4.1	1.4.2	1.4.2	1.4.1
rgeff	CRAN		0.15.3	0.15.3	
rgl	CRAN			0.97.0	0.95.1441
Rgraphviz	CRAN		2.18.0		
rjson	CRAN		0.2.15		
RJSONIO	CRAN		1.3-0		
rmarkdown	CRAN		1.3	1.3	1
Rmpi	CRAN		0.6-6		0.6-5
rngtools	CRAN	1.2.4	1.2.4	1.2.4	1.2.4
robustbase	CRAN	0.92-7	0.92-7	0.92-7	0.92-5
ROCR	CRAN	1.0-7	1.0-7	1.0-7	1.0-7
Rook	CRAN		1.1-1	1.1-1	
roxygen2	CRAN	6.0.1	5.0.1	6.0.1	5.0.1
rpart	base	4.1-10	4.1-10	4.1-10	4.1-10
rprojroot	CRAN	1.2	1.1	1.2	
Rsamtools	Bioconductor		1.26.1	1.26.1	
rsconnect	CRAN		0.7		
RSQLite	CRAN		1.1-2	1.1-2	1.0.0
rstudioapi	CRAN	0.6	0.6	0.6	0.6
rvest	CRAN	0.3.2			
S4Vectors	Bioconductor		0.12.1	0.12.0	0.10.3
safe	Bioconductor		3.14.0	3.10.0	
scales	CRAN	0.4.0	0.4.1	0.4.1	0.4.0
selectr	CRAN	0.3-1			
sem	CRAN		3.1-8		
shiny	CRAN	0.14		1.0.0	
slipt	GitHub		0.1.0	0.1.0	0.1.0
	TomKellyGenetics				

sm	CRAN	2.2-5.4	2.2-5.4		
sna	CRAN		2.4		
snow	CRAN	0.4-1	0.4-2	0.4-2	0.3-13
sourcetools	CRAN	0.1.5		0.1.5	
SparseM	CRAN		1.74		1.7
spatial	base	7.3-11	7.3-11	7.3-11	7.3-11
splines	base	3.3.2	3.3.2	3.3.1	3.3.0
statnet.common	CRAN		3.3.0		
stats	base	3.3.2	3.3.2	3.3.1	3.3.0
stats4	base	3.3.2	3.3.2	3.3.1	3.3.0
stringi	CRAN	1.1.1	1.1.2	1.1.2	1.0-1
stringr	CRAN	1.1.0	1.1.0	1.2.0	1.0.0
Summarized Experiment	Bioconductor		1.4.0	1.4.0	
survival	base	2.39-4	2.40-1	2.40-1	2.39-4
tcltk	base	3.3.2	3.3.2	3.3.1	3.3.0
testthat	CRAN	1.0.2	1.0.2		1.0.2
tibble	CRAN	1.2	1.2	1.2	1.2
tidyverse	GitHub hadley	1.1.1			
timeline	CRAN		0.9		
tools	base	3.3.2	3.3.2	3.3.1	3.3.0
tpr	CRAN		0.3-1		
trimcluster	CRAN	0.1-2	0.1-2	0.1-2	
Unicode	CRAN	9.0.0-1	9.0.0-1	9.0.0-1	
utils	base	3.3.2	3.3.2	3.3.1	3.3.0
vioplot	CRAN		0.2		
vioplotx	GitHub TomKellyGenetics	0.0.0.9000	0.0.0.9000		
viridis	CRAN	0.3.4	0.3.4	0.3.4	
visNetwork	CRAN		1.0.3	1.0.3	
whisker	CRAN	0.3-2	0.3-2	0.3-2	0.3-2
withr	CRAN	1.0.2	1.0.2	1.0.2	1.0.2
XML	base	3.98-1.3	3.98-1.1	3.98-1.5	3.98-1.4

xml2	CRAN	1.1.1	1.1.1	1.0.0
xtable	CRAN	1.8-2	1.8-2	1.8-2
XVector	Bioconductor		0.14.0	0.14.0
yaml	CRAN		2.1.14	2.1.14
zlibbioc	CRAN		1.20.0	1.20.0
zoo	CRAN	1.7-13	1.7-14	1.7-13

Appendix C

Secondary Screen Data

A series of experimental genome-wide siRNA screens have been performed on synthetic lethal partners of *CDH1* (Telford *et al.*, 2015). The strongest candidates from a primary screen were subject to a further secondary screen for validation by independent replication with 4 gene knockdowns with different targeting siRNA. As shown in Table C.1, there is significant ($p = 7.49 \times 10^{-3}$ by Fisher’s exact test) association between SLIPT candidates and stronger validations of siRNA candidates. Since there were more SLIPT– genes among those not validated and more SLIPT+ genes among those validated with several siRNAs, this supports the use of SLIPT as a synthetic lethal discovery procedure which may augment such screening experiments.

Table C.1: Comparing SLIPT genes against Secondary siRNA Screen in breast cancer

		Secondary Screen					Total	
		0/4	1/4	2/4	3/4	4/4		
SLIPT+	Observed	70	46	31	8	2	157	
	Expected	85	44	10	4	2		
SLIPT–	Observed	190	90	31	10	4	325	
	Expected	175	91	42	12	4		
		Total	280	136	52	18	6	482

Similar analysis with mtSLIPT, comparing SLIPT against *CDH1* somatic mutation with siRNA validation results was not significant ($p = 7.02 \times 10^{-1}$ by Fisher’s exact test). However, as shown in Table C.2, the observed and expected values were in a direction consistent with that observed above for SLIPT against low *CDH1* expression.

It is not unexpected that this result does not have comparable statistical support due to the lower sample size for mutation data.

Table C.2: Comparing mtSLIPT genes against Secondary siRNA Screen in breast cancer

		Secondary Screen					Total
		0/4	1/4	2/4	3/4	4/4	
mtSLIPT+	Observed	54	35	17	4	6	111
	Expected	60	31	14	4	1	
mtSLIPT-	Observed	206	101	45	14	5	371
	Expected	200	105	48	14	4	
Total		269	143	63	19	6	482

This analysis was replicated on a (smaller) stomach cancer dataset but it was less conclusive ($p = 2.36 \times 10^{-1}$ by Fisher's exact test). As shown in Table C.3, fewer SLIPT candidates were validated than expected statistically. However, these results in stomach cancer may not be directly comparable to experiments in a breast cell line. Genes validated by 0 or 1 siRNA behave consistently with the results above.

Table C.3: Comparing SLIPT genes against Secondary siRNA Screen in stomach cancer

		Secondary Screen					Total
		0/4	1/4	2/4	3/4	4/4	
SLIPT+	Observed	67	47	13	4	1	132
	Expected	71	37	17	5	2	
SLIPT-	Observed	195	90	50	14	5	354
	Expected	190	100	46	13	4	
Total		262	137	63	19	6	486

Appendix D

Mutation Analysis in Breast Cancer

D.1 Synthetic Lethal Genes and Pathways

SLIPT expression analysis (described in Section 3.1) on TCGA breast cancer data ($n = 969$) found the following genes and pathways, described in sections 4.1 and 4.1.1.

Table D.1: Candidate synthetic lethal gene partners of *CDH1* from mtSLIPT

Gene	Observed	Expected	χ^2 value	p-value	p-value (FDR)
<i>TFAP2B</i>	8	36.7	89.5	3.60×10^{-20}	8.37×10^{-17}
<i>ZNF423</i>	15	36.7	78.8	7.89×10^{-18}	1.22×10^{-14}
<i>CALCOCO1</i>	11	36.7	76.8	2.09×10^{-17}	2.59×10^{-14}
<i>RBM5</i>	13	36.7	75.7	3.65×10^{-17}	4.00×10^{-14}
<i>BTG2</i>	7	36.7	71.7	2.72×10^{-16}	1.81×10^{-13}
<i>RXRA</i>	6	36.7	70.5	5.00×10^{-16}	2.97×10^{-13}
<i>SLC27A1</i>	11	36.7	70.3	5.42×10^{-16}	2.97×10^{-13}
<i>MEF2D</i>	12	36.7	69.6	7.86×10^{-16}	3.95×10^{-13}
<i>NISCH</i>	12	36.7	69.6	7.86×10^{-16}	3.95×10^{-13}
<i>AVPR2</i>	9	36.7	69.2	9.36×10^{-16}	4.58×10^{-13}
<i>CRY2</i>	13	36.7	68.9	1.07×10^{-15}	4.98×10^{-13}
<i>RAPGEF3</i>	13	36.7	68.9	1.07×10^{-15}	4.98×10^{-13}
<i>NRIP2</i>	10	36.7	68.2	1.58×10^{-15}	7.18×10^{-13}
<i>DARC</i>	12	36.7	66.4	3.76×10^{-15}	1.54×10^{-12}
<i>SFRS5</i>	12	36.7	66.4	3.76×10^{-15}	1.54×10^{-12}
<i>NOSTRIN</i>	5	36.7	65.1	7.40×10^{-15}	2.70×10^{-12}
<i>KIF13B</i>	12	36.7	63.4	1.69×10^{-14}	5.16×10^{-12}
<i>TENC1</i>	10	36.7	62.5	2.67×10^{-14}	7.40×10^{-12}
<i>MFAP4</i>	12	36.7	60.5	7.17×10^{-14}	1.67×10^{-11}
<i>ELN</i>	13	36.7	59.7	1.07×10^{-13}	2.32×10^{-11}
<i>SGK223</i>	14	36.7	59	1.51×10^{-13}	3.05×10^{-11}
<i>KIF12</i>	11	36.7	58.8	1.74×10^{-13}	3.34×10^{-11}
<i>SELP</i>	11	36.7	58.8	1.74×10^{-13}	3.34×10^{-11}
<i>CIRBP</i>	9	36.7	58.7	1.83×10^{-13}	3.41×10^{-11}
<i>CTDSP1</i>	9	36.7	58.7	1.83×10^{-13}	3.41×10^{-11}

Strongest candidate SL partners for *CDH1* by mtSLIPT with observed and expected numbers of *CDH1* mutant The Cancer Genome Atlas (TCGA) breast tumours with low expression of partner genes.

Table D.2: Pathways for *CDH1* partners from mtSLIPT

Pathways Over-represented	Pathway Size	SL Genes	p-value (FDR)
Eukaryotic Translation Elongation	86	60	2.0×10^{-128}
Peptide chain elongation	83	59	2.0×10^{-128}
Eukaryotic Translation Termination	83	58	2.3×10^{-125}
Viral mRNA Translation	81	57	2.5×10^{-124}
Nonsense Mediated Decay independent of the Exon Junction Complex	88	59	8.6×10^{-124}
Nonsense-Mediated Decay	103	61	5.2×10^{-117}
Nonsense Mediated Decay enhanced by the Exon Junction Complex	103	61	5.2×10^{-117}
Formation of a pool of free 40S subunits	93	58	1.6×10^{-116}
L13a-mediated translational silencing of Ceruloplasmin expression	103	59	1.3×10^{-111}
3' -UTR-mediated translational regulation	103	59	1.3×10^{-111}
GTP hydrolysis and joining of the 60S ribosomal subunit	104	59	6.2×10^{-111}
SRP-dependent cotranslational protein targeting to membrane	104	58	2.9×10^{-108}
Eukaryotic Translation Initiation	111	59	3.0×10^{-106}
Cap-dependent Translation Initiation	111	59	3.0×10^{-106}
Influenza Viral RNA Transcription and Replication	108	57	5.1×10^{-103}
Influenza Infection	117	59	1.5×10^{-102}
Translation	141	64	3.7×10^{-101}
Influenza Life Cycle	112	57	1.4×10^{-100}
GPCR downstream signalling	472	116	1.0×10^{-80}
Hemostasis	422	105	1.4×10^{-78}

Gene set over-representation analysis (hypergeometric test) for Reactome pathways in mtSLIPT partners for *CDH1*.

The genes and pathways identified in Tables D.1 and D.2 were derived from comparing the expression profiles of potential partners to the mutation status of *CDH1* (as shown in Figure 3.2). Thus the following analysis is only limited the samples for which TCGA provides both expression and somatic mutation data.

D.2 Synthetic Lethal Expression Profiles

Similar to the analysis of synthetic lethal partners against low *CDH1* expression in 4.1.2, the partners detected from *CDH1* mutation were also examined for their expression profiles and the pathway composition of gene clusters. Hierarchical clustering was performed on mtSLIPT partners for *CDH1* as showing in Figure D.1. Overrepresentation for Reactome pathways for each of the gene clusters identified is given in Table D.3.

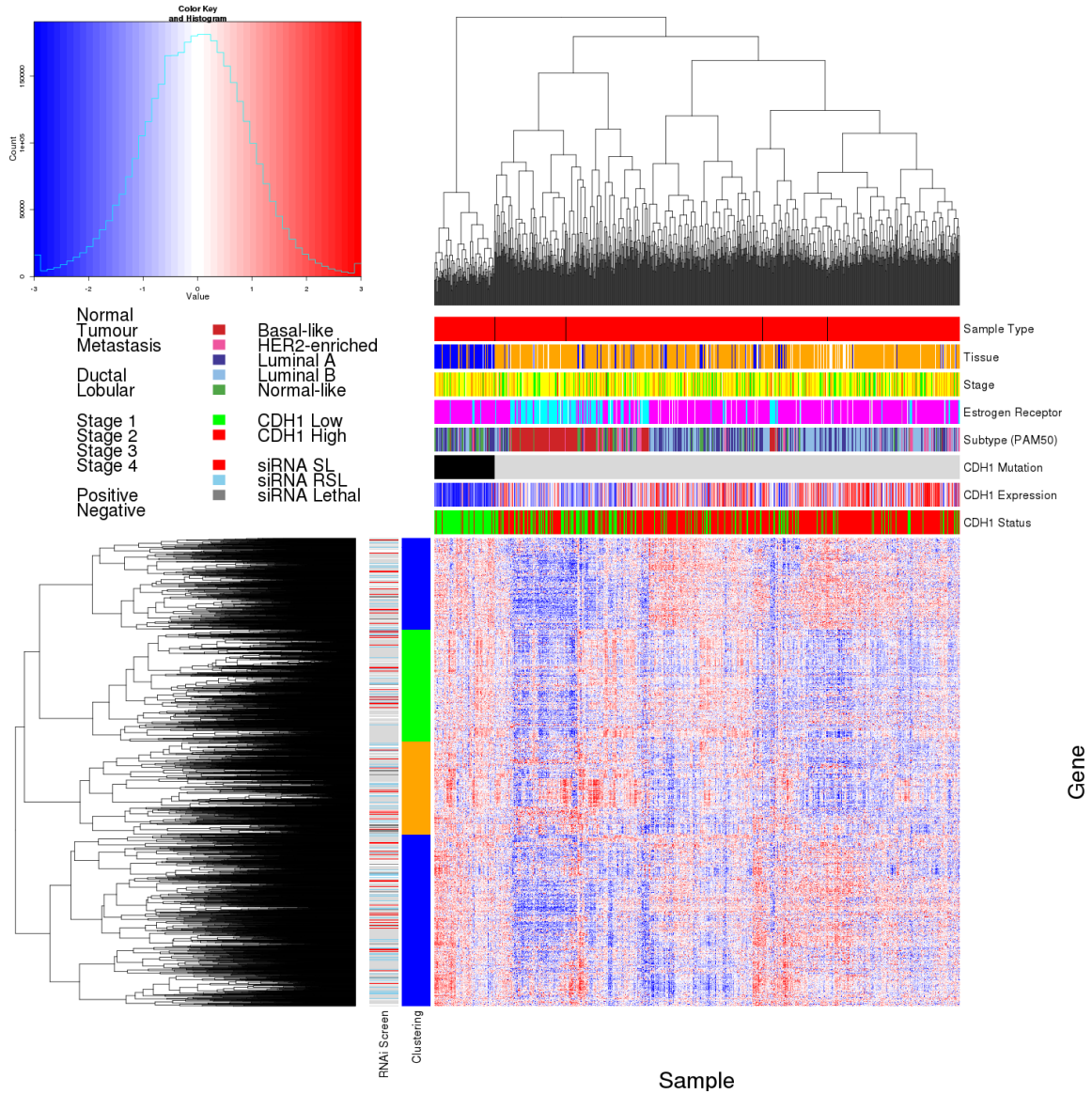


Figure D.1: Synthetic lethal expression profiles of analysed samples. Gene expression profile heatmap (correlation distance) of all samples (separated by *CDH1* somatic mutation status) analysed in TCGA breast cancer dataset for gene expression of 3,743 candidate partners of E-cadherin (*CDH1*) from mtSLIPT prediction (with significant FDR adjusted $p < 0.05$). Deeply clustered, inter-correlated genes form several main groups, each containing genes that were SL candidates or toxic in an siRNA screen Telford *et al.* (2015). Clusters had different sample groups highly expressing the synthetic lethal candidates in *CDH1* mutant samples and often lowly expressing *CDH1* wildtype samples (which were not tested for), although many of the *CDH1* mutant samples had among the lowest *CDH1* expression. In contrast to the expression analysis the (predominantly *CDH1* wildtype) basal subtype and estrogen receptor negative samples have depleted expression among most candidate synthetic lethal partners.

Table D.3: Pathway composition for clusters of *CDH1* partners from mtSLIPT

Pathways Over-represented in Cluster 1	Pathway Size	Cluster Genes	p-value (FDR)
Olfactory Signalling Pathway	57	8	7.1×10^{-9}
Assembly of the primary cilium	149	14	8.0×10^{-9}
Sphingolipid metabolism	62	8	9.6×10^{-9}
Signalling by ERBB4	133	12	5.1×10^{-8}
PI3K Cascade	65	7	4.9×10^{-7}
Circadian Clock	33	5	4.9×10^{-7}
Nuclear signalling by ERBB4	34	5	4.9×10^{-7}
Intraflagellar transport	35	5	4.9×10^{-7}
PI3K events in ERBB4 signalling	87	8	4.9×10^{-7}
PIP3 activates AKT signalling	87	8	4.9×10^{-7}
PI3K events in ERBB2 signalling	87	8	4.9×10^{-7}
PI-3K cascade:FGFR1	87	8	4.9×10^{-7}
PI-3K cascade:FGFR2	87	8	4.9×10^{-7}
PI-3K cascade:FGFR3	87	8	4.9×10^{-7}
PI-3K cascade:FGFR4	87	8	4.9×10^{-7}
Deadenylation of mRNA	22	4	5.6×10^{-7}
PI3K/AKT activation	90	8	5.6×10^{-7}
Cargo trafficking to the periciliary membrane	38	5	5.6×10^{-7}
Pathways Over-represented in Cluster 2	Pathway Size	Cluster Genes	p-value (FDR)
G _{αs} signalling events	83	19	5.1×10^{-25}
Extracellular matrix organization	238	30	1.4×10^{-18}
Hemostasis	422	46	2.7×10^{-16}
Aquaporin-mediated transport	32	9	2.7×10^{-16}
Transcriptional regulation of white adipocyte differentiation	56	11	1.7×10^{-15}
Degradation of the extracellular matrix	102	15	1.7×10^{-15}
Integration of energy metabolism	84	13	8.8×10^{-15}
GPCR downstream signalling	472	48	2.8×10^{-14}
G _{αz} signalling events	15	6	5.0×10^{-14}
Molecules associated with elastic fibres	33	8	5.4×10^{-14}
Phase 1 - Functionalization of compounds	67	11	5.6×10^{-14}
Platelet activation, signalling and aggregation	179	20	5.6×10^{-14}
Vasopressin regulates renal water homeostasis via Aquaporins	24	7	6.1×10^{-14}
Elastic fibre formation	37	8	$.03 \times 10^{-13}$
Calmodulin induced events	27	7	3.3×10^{-13}
CaM pathway	27	7	3.3×10^{-13}
cGMP effects	18	6	3.6×10^{-13}
G _{αi} signalling events	167	18	6.3×10^{-13}
Pathways Over-represented in Cluster 3	Pathway Size	Cluster Genes	p-value (FDR)
Eukaryotic Translation Elongation	86	55	1.1×10^{-112}
Peptide chain elongation	83	54	1.3×10^{-112}
Viral mRNA Translation	81	53	1.6×10^{-111}
Eukaryotic Translation Termination	83	53	7.1×10^{-110}
Nonsense Mediated Decay independent of the Exon Junction Complex	88	54	1.0×10^{-108}
Formation of a pool of free 40S subunits	93	53	4.1×10^{-102}
Nonsense-Mediated Decay	103	54	3.9×10^{-98}
Nonsense Mediated Decay enhanced by the Exon Junction Complex	103	54	3.9×10^{-98}
L13a-mediated translational silencing of Ceruloplasmin expression	103	53	1.2×10^{-95}
3' -UTR-mediated translational regulation	103	53	1.2×10^{-95}
SRP-dependent cotranslational protein targeting to membrane	104	53	4.3×10^{-95}
GTP hydrolysis and joining of the 60S ribosomal subunit	104	53	4.3×10^{-95}
Influenza Viral RNA Transcription and Replication	108	53	9.6×10^{-93}
Eukaryotic Translation Initiation	111	53	4.2×10^{-91}
Cap-dependent Translation Initiation	111	53	4.2×10^{-91}
Influenza Life Cycle	112	53	1.4×10^{-90}
Influenza Infection	117	53	6.2×10^{-88}
Translation	141	55	3×10^{-81}
Pathways Over-represented in Cluster 4	Pathway Size	Cluster Genes	p-value (FDR)
ECM proteoglycans	66	10	2.9×10^{-11}
deactivation of the beta-catenin transactivating complex	38	7	5.1×10^{-10}
Arachidonic acid metabolism	41	7	1.1×10^{-9}
G _{αq} signalling events	149	14	4.0×10^{-9}
HS-GAG degradation	21	5	4.5×10^{-9}
Uptake and actions of bacterial toxins	22	5	6.1×10^{-9}
Gastrin-CREB signalling pathway via PKC and MAPK	170	15	6.1×10^{-9}
RNA Polymerase I, RNA Polymerase III, and Mitochondrial Transcription	64	8	6.1×10^{-9}
Non-integrin membrane-ECM interactions	53	7	1.5×10^{-8}
Syndecan interactions	25	5	1.5×10^{-8}
NOTCH1 Intracellular Domain Regulates Transcription	40	6	2.3×10^{-8}
Synthesis of Leukotrienes and Eoxins	15	4	3.2×10^{-8}
Signalling by NOTCH1	59	7	5.3×10^{-8}
Regulation of insulin secretion	44	6	6.0×10^{-8}
Metabolism of lipids and lipoproteins	471	37	8.2×10^{-8}
Signalling by NOTCH1	80	8	1.2×10^{-7}
Platelet activation, signalling and aggregation	179	14	1.2×10^{-7}
Recruitment of mitotic centrosome proteins and complexes	64	7	1.2×10^{-7}

Pathway over-representation analysis for Reactome pathways with the number of genes in each pathway (Pathway Size), number of genes within the pathway identified (Cluster Genes), and the pathway over-representation p-value (adjusted by FDR) from the hypergeometric test.

D.3 Comparison to Primary Screen

The mutation synthetic lethal partners with *CDH1* were also compared to siRNA primary screen data (Telford *et al.*, 2015), as performed in Section 4.2.1. These are expected to be more concordant with the experimental results performed on a null mutant, however this is not the case at the gene level: less genes overlapped with experimental candidates in Figure D.2. This may be affected by lower sample size for mutations in TCGA data or lower frequency (expected value) of *CDH1* mutations compared to low expression.

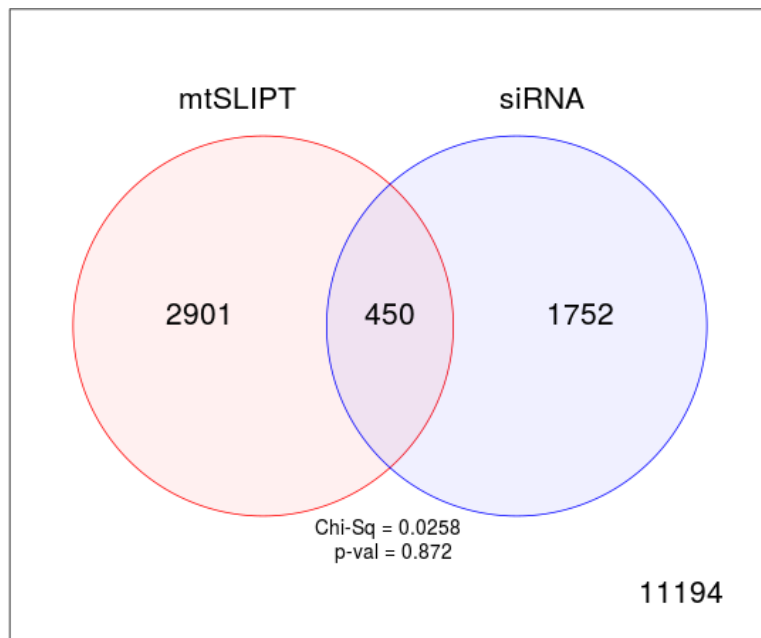


Figure D.2: **Comparison of mtSLIPT to siRNA.** Testing the overlap of gene candidates for E-cadherin synthetic lethal partners between computational (SLIPT) and experimental screening (siRNA) approaches. The χ^2 test suggests that the overlap is no more than would be expected by chance ($p = 0.281$).

Despite a lower sample size (and low number of predicted partners) for mutation analysis, the pathway composition (Tables D.2 and D.4) is similar to expression analysis, as described in Section 4.2.5. In particular, the resampling analysis (Section D.3.1) supported many of the results of expression analysis (Section 4.2.5.1) with Tables D.5 and D.6 detecting many of the same or functionally-related pathways.

Table D.4: Pathway composition for *CDH1* partners from mtSLIPT and siRNA

Predicted only by SLIPT (2901 genes)	Pathway Size	Genes Identified	p-value (FDR)
Eukaryotic Translation Elongation	87	57	2.8×10^{-120}
Peptide chain elongation	84	56	3.1×10^{-120}
Eukaryotic Translation Termination	84	55	2.8×10^{-117}
Viral mRNA Translation	82	54	4.1×10^{-116}
Nonsense Mediated Decay independent of the Exon Junction Complex	89	55	3.7×10^{-113}
Formation of a pool of free 40S subunits	94	55	2.8×10^{-109}
Nonsense-Mediated Decay	104	57	8.4×10^{-108}
Nonsense Mediated Decay enhanced by the Exon Junction Complex	104	57	8.4×10^{-108}
L13a-mediated translational silencing of Ceruloplasmin expression	104	56	3.4×10^{-105}
3' -UTR-mediated translational regulation	104	56	3.4×10^{-105}
GTP hydrolysis and joining of the 60S ribosomal subunit	105	56	1.4×10^{-104}
Eukaryotic Translation Initiation	112	56	2.8×10^{-100}
Cap-dependent Translation Initiation	112	56	2.8×10^{-100}
SRP-dependent cotranslational protein targeting to membrane	105	54	2.2×10^{-99}
Influenza Viral RNA Transcription and Replication	109	54	5.3×10^{-97}
Influenza Life Cycle	113	54	9.6×10^{-95}
Influenza Infection	118	55	1.7×10^{-94}
Translation	142	60	3.5×10^{-94}
Infectious disease	349	77	5.9×10^{-62}
Extracellular matrix organization	241	54	3.0×10^{-52}

Detected only by siRNA screen (1752 genes)	Pathway Size	Genes Identified	p-value (FDR)
Class A/1 (Rhodopsin-like receptors)	282	69	1.9×10^{-59}
GPCR ligand binding	363	78	2.7×10^{-54}
Peptide ligand-binding receptors	175	41	1.5×10^{-42}
$G_{\alpha i}$ signalling events	184	41	1.1×10^{-40}
Gastrin-CREB signalling pathway via PKC and MAPK	180	37	1.5×10^{-35}
$G_{\alpha q}$ signalling events	159	34	3.7×10^{-35}
DAP12 interactions	159	27	1.1×10^{-24}
VEGFA-VEGFR2 Pathway	91	19	1.0×10^{-23}
Downstream signal transduction	146	24	1.9×10^{-22}
Signalling by VEGF	99	19	2.6×10^{-22}
DAP12 signalling	149	24	4.2×10^{-22}
Organelle biogenesis and maintenance	264	34	4.3×10^{-20}
Downstream signalling of activated FGFR1	134	21	4.3×10^{-20}
Downstream signalling of activated FGFR2	134	21	4.3×10^{-20}
Downstream signalling of activated FGFR3	134	21	4.3×10^{-20}
Downstream signalling of activated FGFR4	134	21	4.3×10^{-20}
Signalling by ERBB2	146	22	5.3×10^{-20}
Signalling by FGFR	146	22	5.3×10^{-20}
Signalling by FGFR1	146	22	5.3×10^{-20}
Signalling by FGFR2	146	22	5.3×10^{-20}

Intersection of SLIPT and siRNA screen (450 genes)	Pathway Size	Genes Identified	p-value (FDR)
HS-GAG degradation	21	4	4.9×10^{-6}
Retinoid metabolism and transport	39	5	4.9×10^{-6}
Platelet activation, signalling and aggregation	186	13	4.9×10^{-6}
Signalling by NOTCH4	11	3	4.9×10^{-6}
$G_{\alpha s}$ signalling events	100	8	5.0×10^{-6}
Defective EXT2 causes exostoses 2	12	3	5.0×10^{-6}
Defective EXT1 causes exostoses 1, TRPS2 and CHDS	12	3	5.0×10^{-6}
Class A/1 (Rhodopsin-like receptors)	289	18	2.2×10^{-5}
Signalling by PDGF	173	11	2.9×10^{-5}
Circadian Clock	34	4	2.9×10^{-5}
Signalling by ERBB4	139	9	4.3×10^{-5}
Role of LAT2/NTAL/LAB on calcium mobilization	99	7	4.4×10^{-5}
Peptide ligand-binding receptors	181	11	4.5×10^{-5}
Defective B4GALT7 causes EDS, progeroid type	19	3	4.5×10^{-5}
Defective B3GAT3 causes JDSSDHD	19	3	4.5×10^{-5}
Signalling by NOTCH	80	6	4.5×10^{-5}
$G_{\alpha q}$ signalling events	164	10	5.1×10^{-5}
Response to elevated platelet cytosolic Ca^{2+}	84	6	7.1×10^{-5}
Signalling by ERBB2	148	9	7.1×10^{-5}
Signalling by SCF-KIT	129	8	8.3×10^{-5}

D.3.1 Resampling Analysis

Table D.5: Pathways for *CDH1* partners from mtSLIPT

Reactome Pathway	Over-representation	Permutation
Eukaryotic Translation Elongation	3.2×10^{-128}	$< 7.035 \times 10^{-4}$
Peptide chain elongation	3.2×10^{-128}	$< 7.035 \times 10^{-4}$
Eukaryotic Translation Termination	3.7×10^{-125}	$< 7.035 \times 10^{-4}$
Viral mRNA Translation	4.1×10^{-124}	$< 7.035 \times 10^{-4}$
Nonsense Mediated Decay independent of the Exon Junction Complex	1.4×10^{-123}	$< 7.035 \times 10^{-4}$
Nonsense-Mediated Decay	8.4×10^{-117}	$< 7.035 \times 10^{-4}$
Nonsense Mediated Decay enhanced by the Exon Junction Complex	8.4×10^{-117}	$< 7.035 \times 10^{-4}$
Formation of a pool of free 40S subunits	2.6×10^{-116}	$< 7.035 \times 10^{-4}$
L13a-mediated translational silencing of Ceruloplasmin expression	2.0×10^{-111}	$< 7.035 \times 10^{-4}$
3' -UTR-mediated translational regulation	2.0×10^{-111}	$< 7.035 \times 10^{-4}$
GTP hydrolysis and joining of the 60S ribosomal subunit	9.9×10^{-111}	$< 7.035 \times 10^{-4}$
SRP-dependent cotranslational protein targeting to membrane	4.7×10^{-108}	$< 7.035 \times 10^{-4}$
Eukaryotic Translation Initiation	4.8×10^{-106}	$< 7.035 \times 10^{-4}$
Cap-dependent Translation Initiation	4.8×10^{-106}	$< 7.035 \times 10^{-4}$
Influenza Viral RNA Transcription and Replication	8.1×10^{-103}	$< 7.035 \times 10^{-4}$
Influenza Infection	2.4×10^{-102}	$< 7.035 \times 10^{-4}$
Translation	6.0×10^{-101}	$< 7.035 \times 10^{-4}$
Influenza Life Cycle	2.2×10^{-100}	$< 7.035 \times 10^{-4}$
Disease	2.1×10^{-90}	0.013347
GPCR downstream signalling	1.6×10^{-80}	0.095478
Hemostasis	2.1×10^{-78}	0.2671
Signalling by GPCR	1.2×10^{-73}	0.44939
<i>Extracellular matrix organization</i>	2.2×10^{-67}	0.054008
Metabolism of proteins	1.4×10^{-66}	0.9607
Signal Transduction	2.1×10^{-66}	0.48184
Developmental Biology	2.5×10^{-66}	0.54075
Innate Immune System	5.3×10^{-66}	0.9589
Infectious disease	9.6×10^{-66}	0.21075
Signalling by NGF	1.1×10^{-62}	0.43356
Immune System	2.8×10^{-62}	0.23052

Over-representation (hypergeometric test) and Permutation p-values adjusted for multiple tests across pathways (FDR). Significant pathways are marked in bold (FDR < 0.05) and italics (FDR < 0.1).

Table D.6: Pathways for *CDH1* partners from mtSLIPT and siRNA primary screen

Reactome Pathway	Over-representation	Permutation
Visual phototransduction	1.2×10^{-9}	0.86279
G_{αs} signalling events	2.9×10^{-7}	0.023066
Retinoid metabolism and transport	2.9×10^{-7}	0.299
Acylic chain remodelling of PS	1.1×10^{-5}	0.42584
Transcriptional regulation of white adipocyte differentiation	1.1×10^{-5}	0.53928
Chemokine receptors bind chemokines	1.1×10^{-5}	0.95259
<i>Signalling by NOTCH4</i>	1.2×10^{-5}	0.079229
Defective EXT2 causes exostoses 2	1.2×10^{-5}	0.22292
Defective EXT1 causes exostoses 1, TRPS2 and CHDS	1.2×10^{-5}	0.22292
Platelet activation, signalling and aggregation	1.2×10^{-5}	0.48853
Serotonin receptors	1.4×10^{-5}	0.34596
Nicotinamide salvaging	1.4×10^{-5}	0.70881
Phase 1 - Functionalization of compounds	2×10^{-5}	0.31142
Amine ligand-binding receptors	2.5×10^{-5}	0.34934
Acylic chain remodelling of PE	3.8×10^{-5}	0.42615
Signalling by GPCR	3.8×10^{-5}	0.93888
Molecules associated with elastic fibres	3.9×10^{-5}	0.017982
DAP12 interactions	3.9×10^{-5}	0.71983
Beta defensins	3.9×10^{-5}	0.91458
Cytochrome P ₄₅₀ - arranged by substrate type	4.7×10^{-5}	0.83493
GPCR ligand binding	5.7×10^{-5}	0.95258
Acylic chain remodelling of PC	6.1×10^{-5}	0.42584
Response to elevated platelet cytosolic Ca ²⁺	6.4×10^{-5}	0.54046
Arachidonic acid metabolism	6.7×10^{-5}	0.026696
Defective B4GALT7 causes EDS, progeroid type	7.3×10^{-5}	0.24921
Defective B3GAT3 causes JDSSDHD	7.3×10^{-5}	0.24921
Hydrolysis of LPC	7.3×10^{-5}	0.80663
Elastic fibre formation	7.4×10^{-5}	0.0058768
HS-GAG degradation	9.4×10^{-5}	0.0083179
<i>Bile acid and bile salt metabolism</i>	9.4×10^{-5}	0.079905
Netrin-1 signalling	0.00011	0.92216
Integration of energy metabolism	0.00011	0.011152
Dectin-2 family	0.00012	0.10385
Platelet sensitization by LDL	0.00012	0.34596
DAP12 signalling	0.00012	0.62787
Defensins	0.00012	0.77542
GPCR downstream signalling	0.00012	0.79454
<i>Diseases associated with glycosaminoglycan metabolism</i>	0.00013	0.065927
<i>Diseases of glycosylation</i>	0.00013	0.065927
Signalling by Retinoic Acid	0.00013	0.22292
Signalling by Leptin	0.00013	0.34596
Signalling by SCF-KIT	0.00013	0.70881
Opioid Signalling	0.00013	0.96053
Signalling by NOTCH	0.00015	0.26884
Platelet homeostasis	0.00015	0.4878
Signalling by NOTCH1	0.00016	0.13043
Class B/2 (Secretin family receptors)	0.00016	0.13994
<i>Diseases of Immune System</i>	0.0002	0.0795
<i>Diseases associated with the TLR signalling cascade</i>	0.0002	0.0795
A tetrasaccharide linker sequence is required for GAG synthesis	0.0002	0.42615

Over-representation (hypergeometric test) and Permutation p-values adjusted for multiple tests across pathways (FDR). Significant pathways are marked in bold (FDR < 0.05) and italics (FDR < 0.1).

D.4 Compare SLIPT genes

The mutation synthetic lethal partners with *CDH1* were also compared to siRNA primary screen data (Telford *et al.*, 2015), by correlation and siRNA viability as described in sections 4.2.2 and 4.2.3.

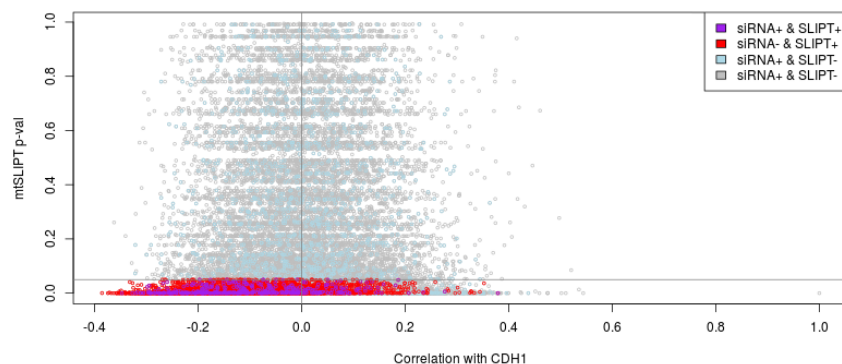


Figure D.3: Compare mtSLIPT and siRNA genes with correlation. The mtSLIPT p-values were compared against Pearson's correlation of expression with *CDH1*. Genes detected by SLIPT or siRNA are coloured according to the legend.

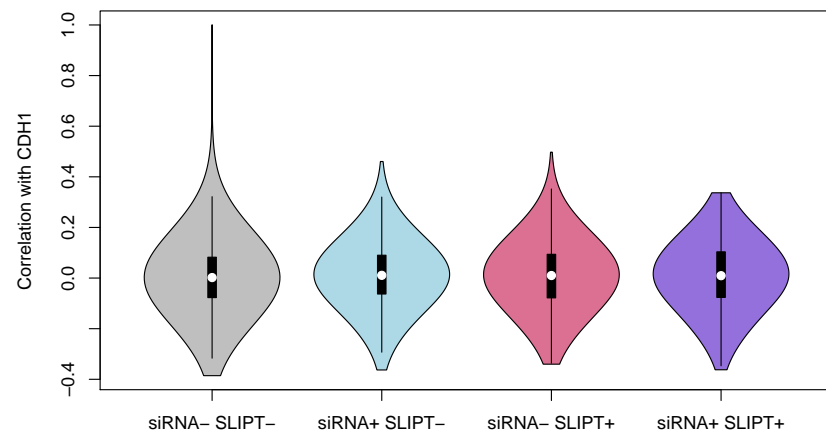


Figure D.4: Compare mtSLIPT and siRNA genes with correlation. Genes detected by mtSLIPT against *CDH1* mutation and siRNA screening were compared against Pearson's correlation of expression with *CDH1*. There were no differences in correlation between the gene groups.

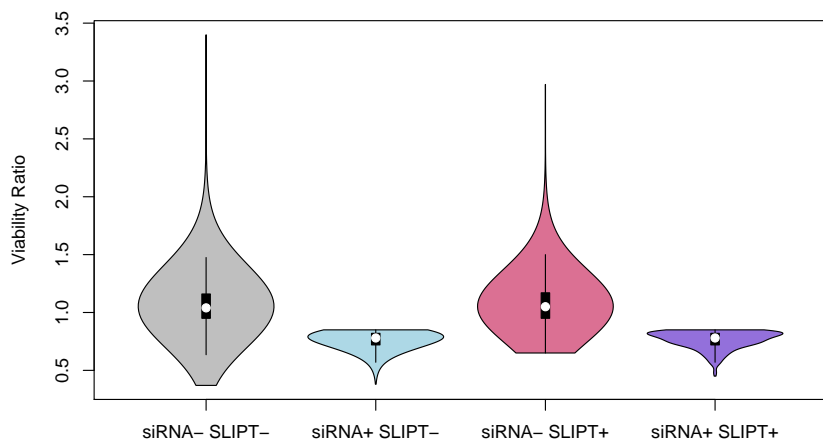


Figure D.5: Compare mtSLIPT and siRNA genes with siRNA viability. Genes detected as candidate synthetic lethal partners by mtSLIPT (in TCGA breast cancer) expression analysis against *CDH1* mutation and experimental screening (with siRNA) were compared against the viability ratio of *CDH1* mutant and wildtype cells in the primary siRNA screen. There were clear no differences in viability between genes detected by mtSLIPT and those not with the differences being primarily due to viability thresholds being used to detect synthetic lethality by Telford *et al.* (2015).

D.5 Metagene Analysis

Metagene analysis was also performed for synthetic lethal candidates for *CDH1* mutation. These are described and compared to expression analysis in Section 4.3.3.

Table D.7: Candidate synthetic lethal metagenes against *CDH1* from mtSLIPT

Pathway	ID	Observed	Expected	χ^2 value	p-value	p-value (FDR)
Neurotoxicity of clostridium toxins	168799	8	36.7	79.4	5.71×10^{-18}	3.14×10^{-15}
Aquaporin-mediated transport	445717	8	36.7	76.3	2.73×10^{-17}	9.01×10^{-15}
Toxicity of botulinum toxin type G (BoNT/G)	5250989	8	36.7	76.3	2.73×10^{-17}	9.01×10^{-15}
ABC-family proteins mediated transport	382556	10	36.7	68.2	1.58×10^{-15}	1.86×10^{-13}
G _{αz} signalling events	418597	10	36.7	59.9	9.97×10^{-14}	5.48×10^{-12}
Regulation of IGF transport and uptake by IGFBPs	381426	9	36.7	56.3	5.88×10^{-13}	2.11×10^{-11}
GP1b-IX-V activation signalling	430116	8	36.7	55.7	8.20×10^{-13}	2.76×10^{-11}
GABA receptor activation	977443	12	36.7	55.1	1.07×10^{-12}	3.26×10^{-11}
Vasopressin regulates renal water homeostasis via Aquaporins	432040	9	36.7	54.1	1.77×10^{-12}	4.88×10^{-11}
Toxicity of botulinum toxin type D (BoNT/D)	5250955	14	36.7	53.4	2.54×10^{-12}	6.64×10^{-11}
Toxicity of botulinum toxin type F (BoNT/F)	5250981	14	36.7	53.4	2.54×10^{-12}	6.64×10^{-11}
STAT6-mediated induction of chemokines	3249367	16	36.7	52.2	4.72×10^{-12}	1.13×10^{-10}
Toxicity of botulinum toxin type B (BoNT/B)	5250958	14	36.7	50.8	9.5×10^{-12}	1.98×10^{-10}
S6K1 signalling	165720	12	36.7	50.2	1.24×10^{-11}	2.5×10^{-10}
G _{αs} signalling events	418555	11	36.7	49.2	2.08×10^{-11}	3.85×10^{-10}
RHO GTPases activate CIT	5625900	14	36.7	48.2	3.34×10^{-11}	5.9×10^{-10}
NADE modulates death signalling	205025	15	36.7	47.4	5.00×10^{-11}	8.32×10^{-10}
Keratan sulfate degradation	2022857	10	36.7	46.6	7.5×10^{-11}	1.15×10^{-9}
Signalling by Retinoic Acid	5362517	10	36.7	46.6	7.5×10^{-11}	1.15×10^{-9}
Adenylate cyclase inhibitory pathway	170670	14	36.7	45.9	1.11×10^{-10}	1.59×10^{-9}
Inhibition of adenylate cyclase pathway	997269	14	36.7	45.9	1.11×10^{-10}	1.59×10^{-9}
Fatty acids	211935	6	36.7	45.7	1.21×10^{-10}	1.72×10^{-9}
Ionotropic activity of Kainate Receptors	451306	13	36.7	44.6	2.03×10^{-10}	2.58×10^{-9}
Activation of Ca-permeable Kainate Receptor	451308	13	36.7	44.6	2.03×10^{-10}	2.58×10^{-9}
RA biosynthesis pathway	5365859	13	36.7	44.6	2.03×10^{-10}	2.58×10^{-9}

Strongest candidate SL partners for *CDH1* by mtSLIPT with observed and expected numbers of mutant *CDH1* TCGA breast cancer tumours with low expression of partner metagenes.

D.6 Mutation Variation

Mutations have different effects as shown by the following examples in cancer genes.

D.6.1 Mutation Frequency

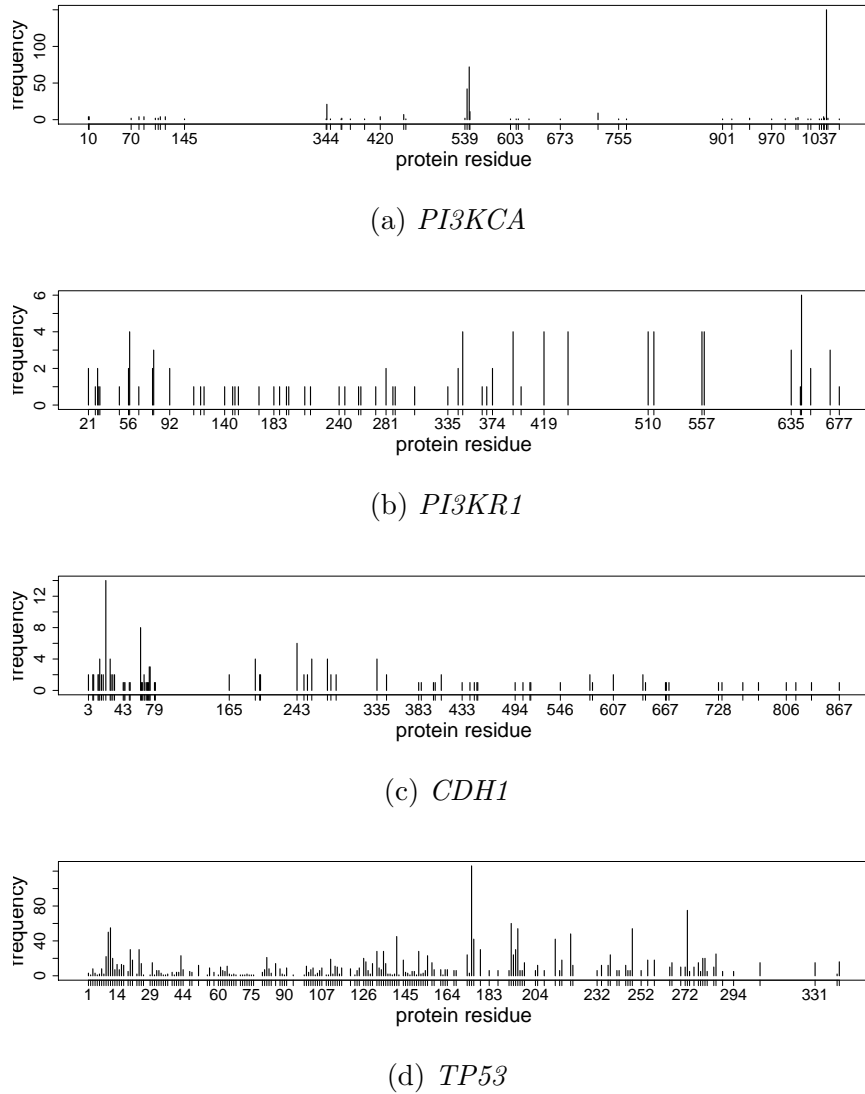


Figure D.6: **Somatic mutation locus.** Mutation frequency at each locus in TCGA breast cancer. *PIK3CA* shows clear recurrent E545K and H1047R oncogene mutations consistent with it being an oncogene. *PIK3R1* and *CDH1* are tumour suppressors with inactivating mutations distributed throughout the gene, whereas *TP53* exhibits both of these properties and a very high mutation frequency compared to other genes.

D.6.2 PI3K Mutation Expression

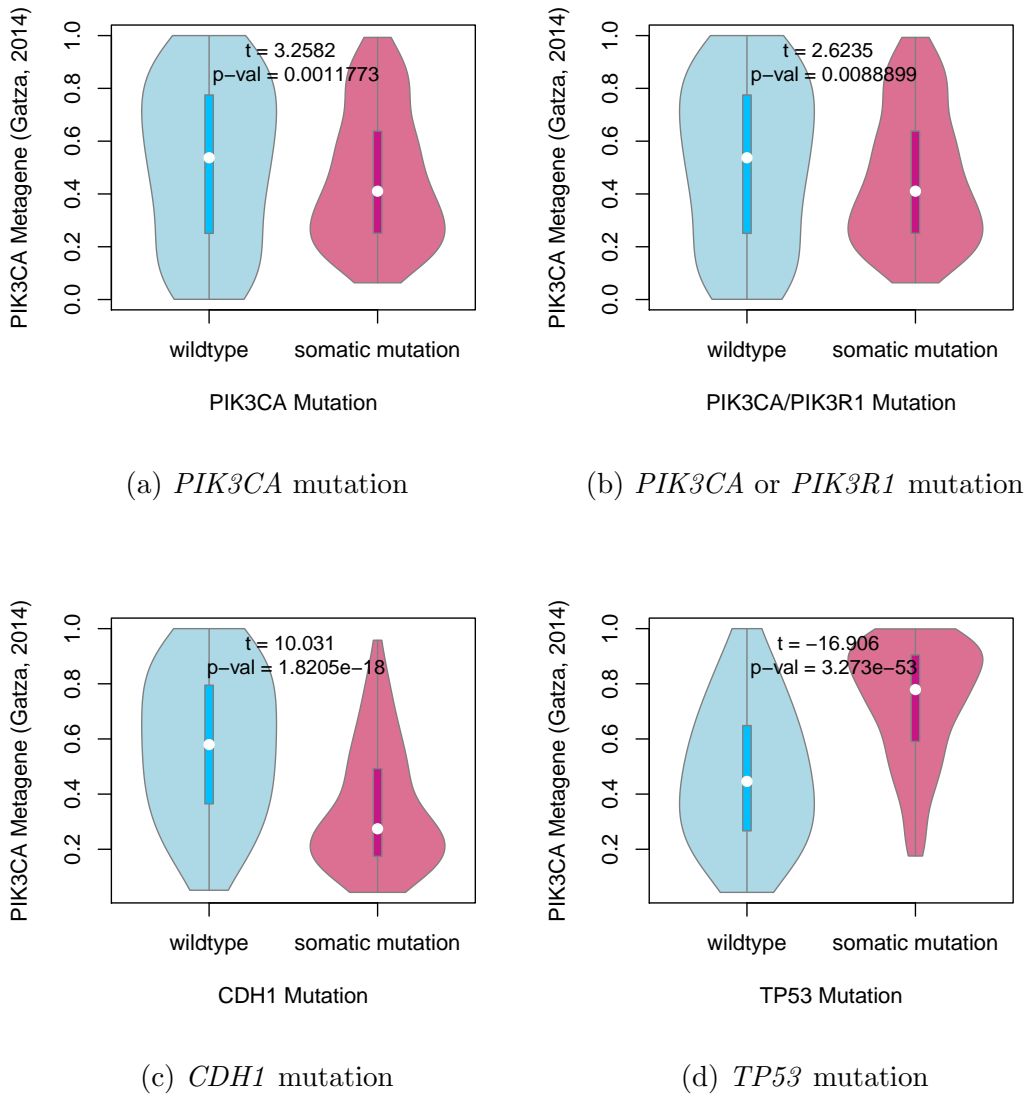


Figure D.7: Somatic mutation against PIK3CA metagene. Mutations in *PIK3CA*, *PIK3R1*, *CDH1*, and *TP53* were examined in TCGA breast cancer for their effect on the PIK3CA (Gatza *et al.*, 2014) pathway metagene. The tumour suppressors *CDH1* and *TP53* showed an increase and decrease in the metagene respectively, whereas *PIK3CA* and *PIK3R1* mutations weaker evidence of decrease in metagene levels.

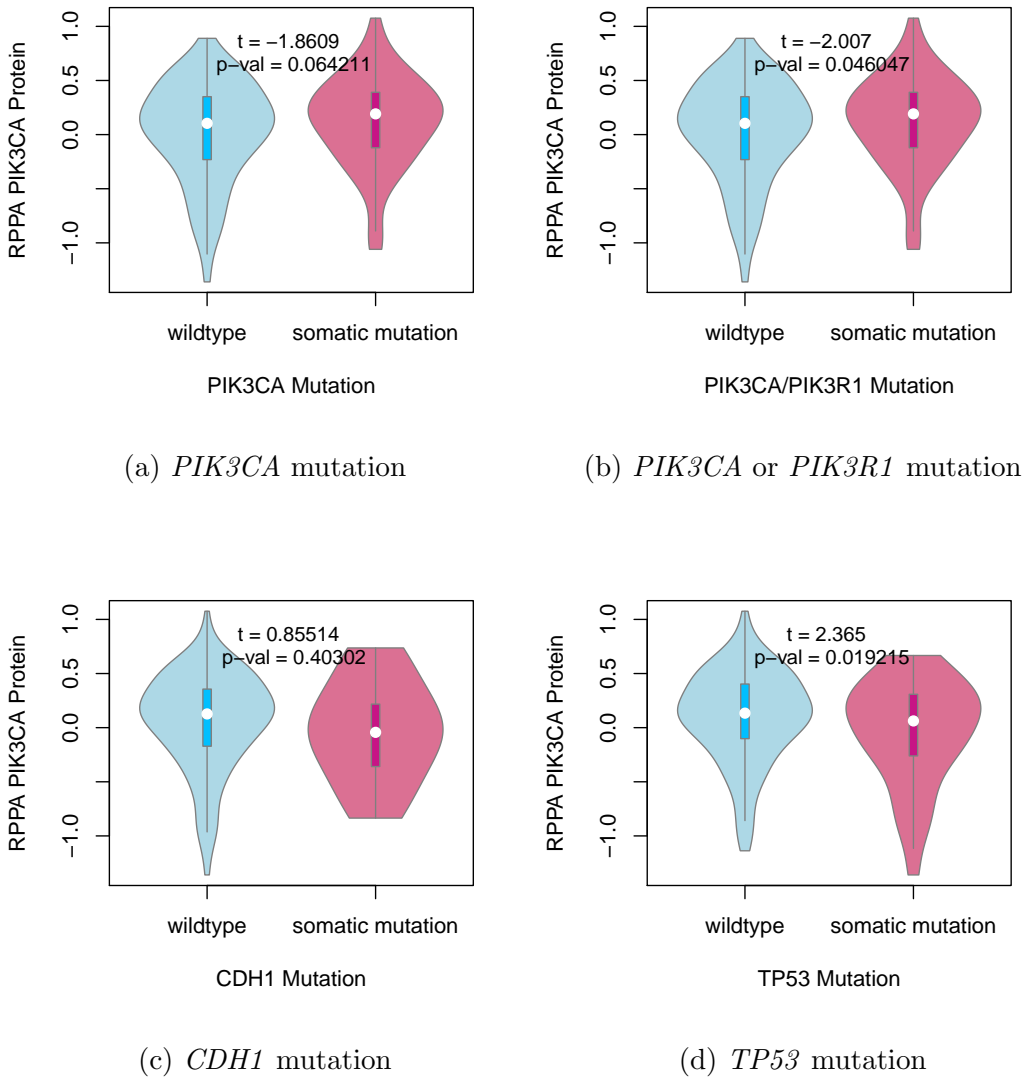


Figure D.8: Somatic mutation against PI3K protein. Mutations in *PIK3CA*, *PIK3R1*, *CDH1*, and *TP53* were examined in TCGA breast cancer for their effect on the expression of the p110 α protein (encoded by *PIK3CA*). Protein levels were significantly elevated in samples with *PIK3CA* or *PIK3R1* mutations and lower in samples with *TP53* mutations.

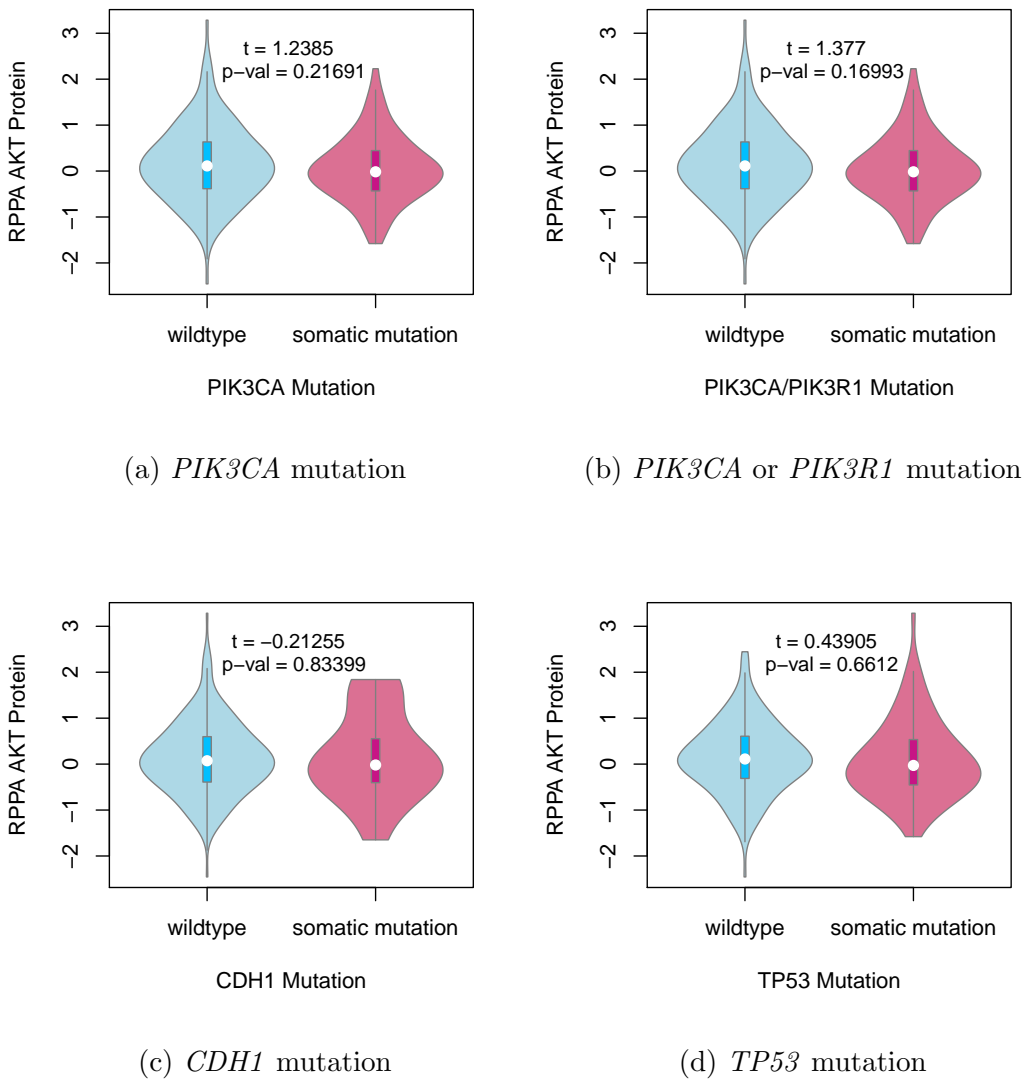


Figure D.9: Somatic mutation against AKT protein. Mutations in *PIK3CA*, *PIK3R1*, *CDH1*, and *TP53* were examined in TCGA breast cancer for their effect on the expression of the AKT protein (a downstream target of *PIK3CA*). Protein levels were not significantly different in samples mutations in any of these cancer genes.

Appendix E

Metagene Expression Profiles

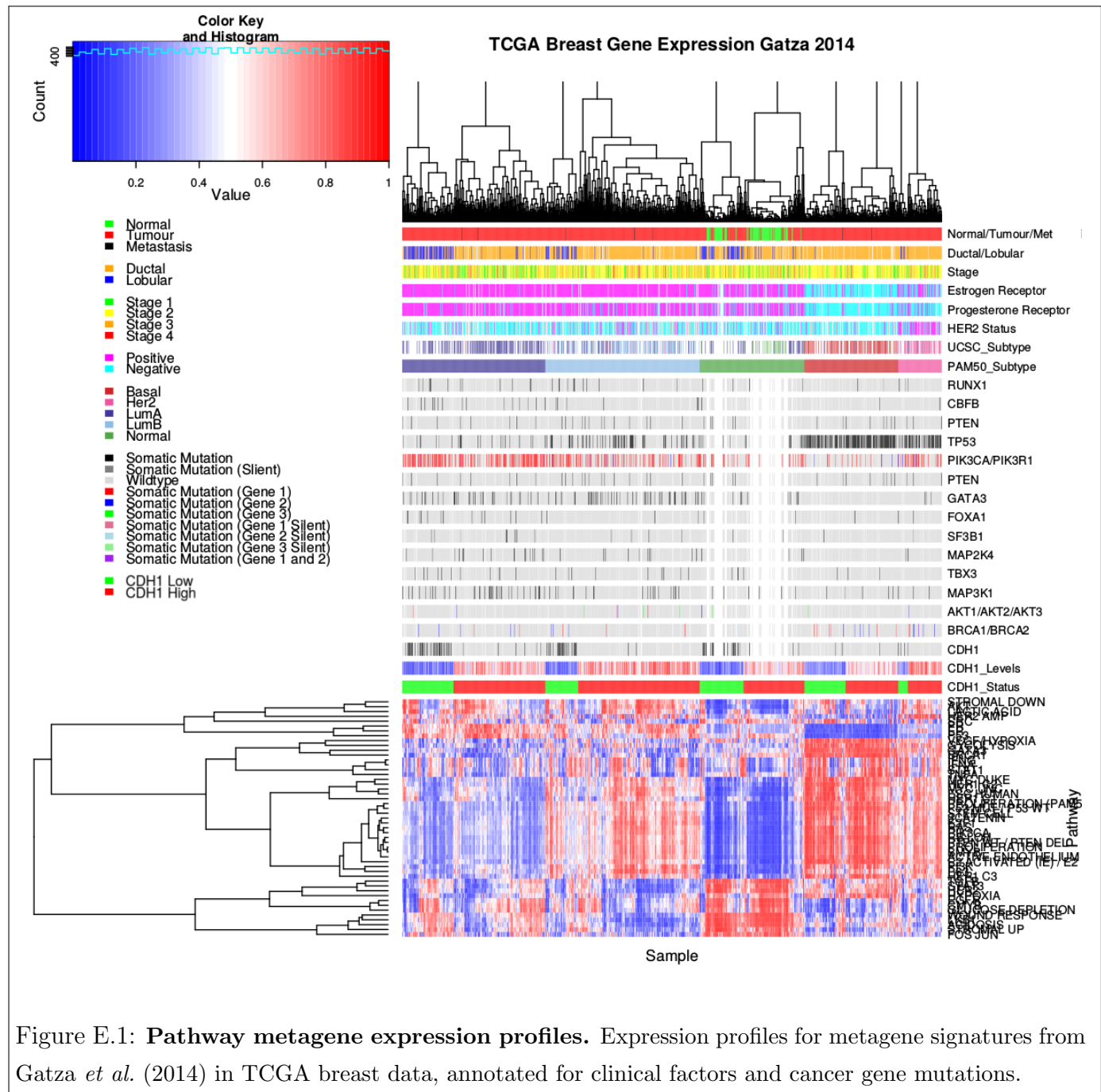


Figure E.1: **Pathway metagene expression profiles.** Expression profiles for metagene signatures from Gatza *et al.* (2014) in TCGA breast data, annotated for clinical factors and cancer gene mutations.

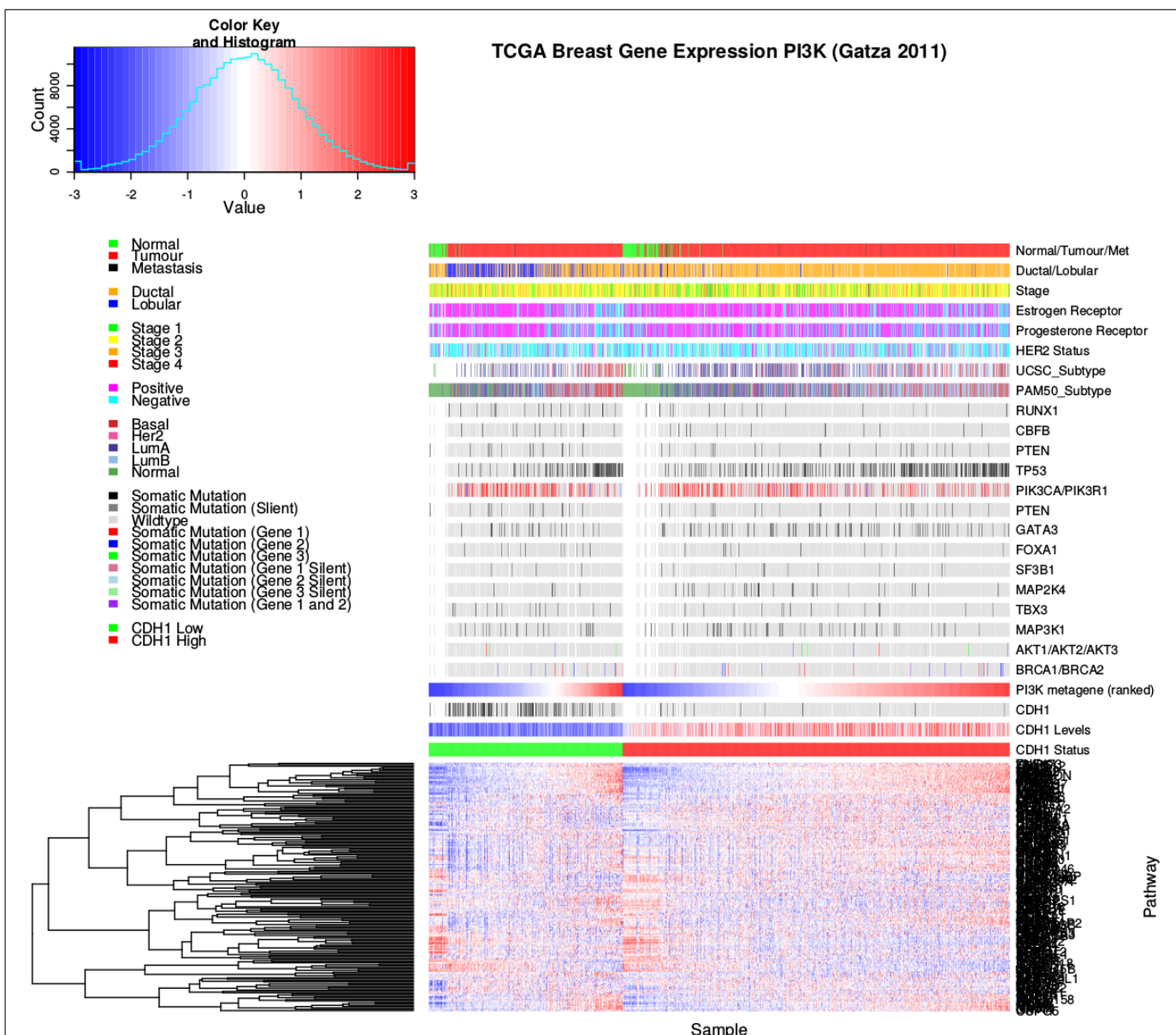
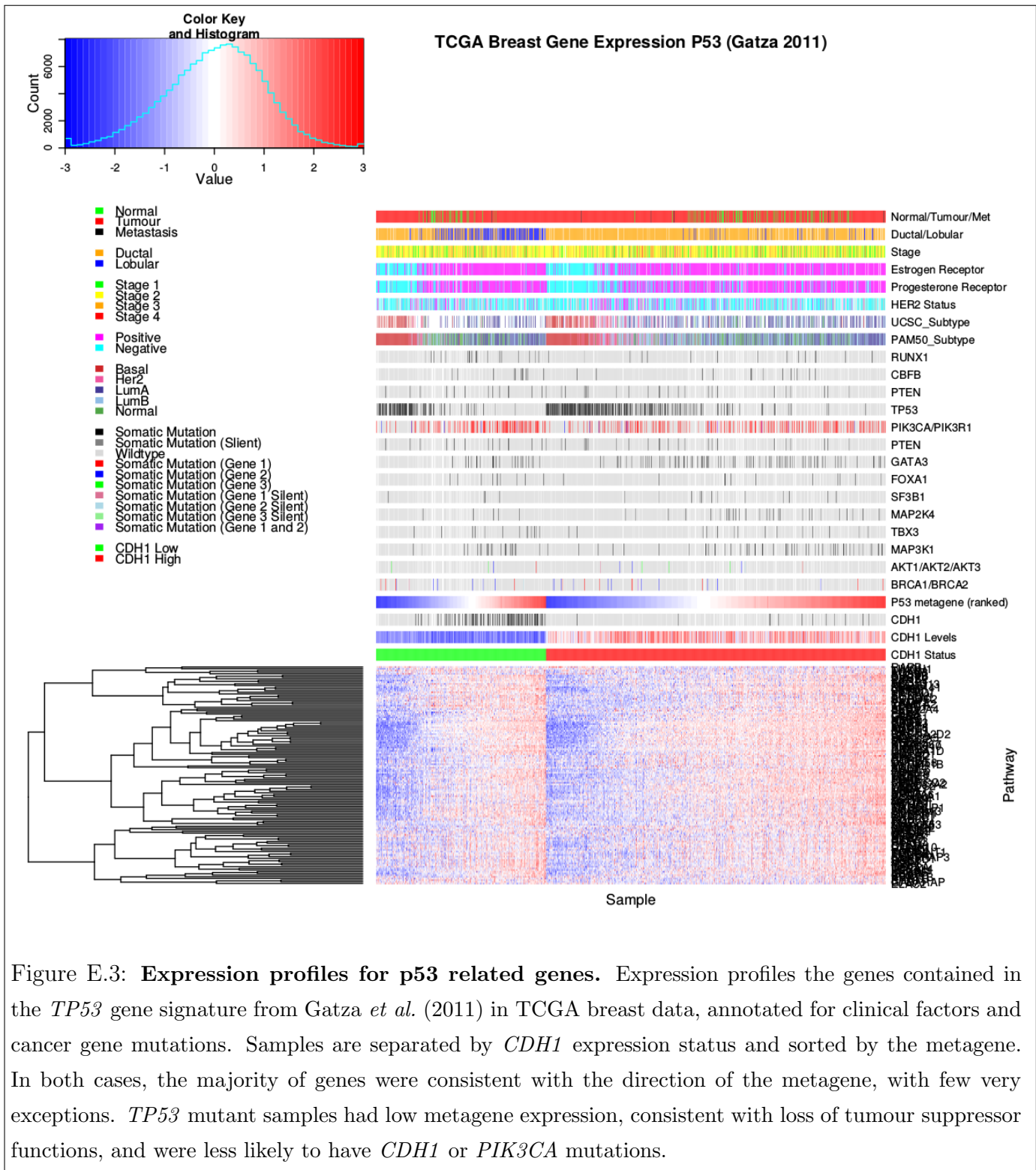


Figure E.2: Expression profiles for constituent genes of PI3K. Expression profiles the genes contained in the PI3K gene signature from Gatza *et al.* (2011) in TCGA breast data, annotated for clinical factors and cancer gene mutations. Samples are separated by *CDH1* expression status and sorted by the metagene. In both cases, the majority of genes were consistent with the direction of the PI3K metagene, although considerable proportion were inversely correlated with the metagene. Normal samples had low PI3K metagene expression and *TP53* mutant samples had high PI3K expression. Although, oncogenic *PIK3CA* and tumour suppressor *PIK3R1* mutations across samples including those with low metagene response.



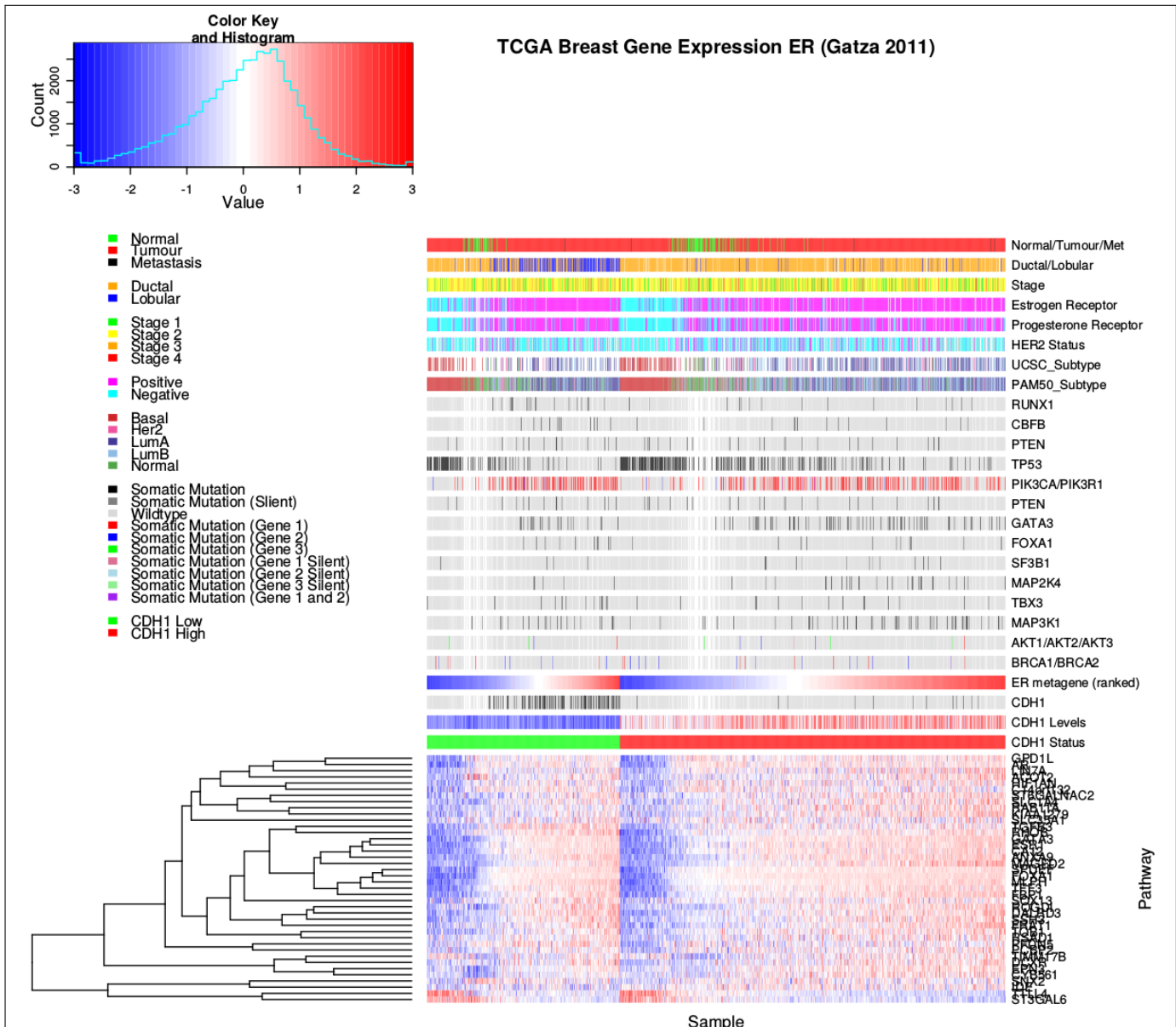
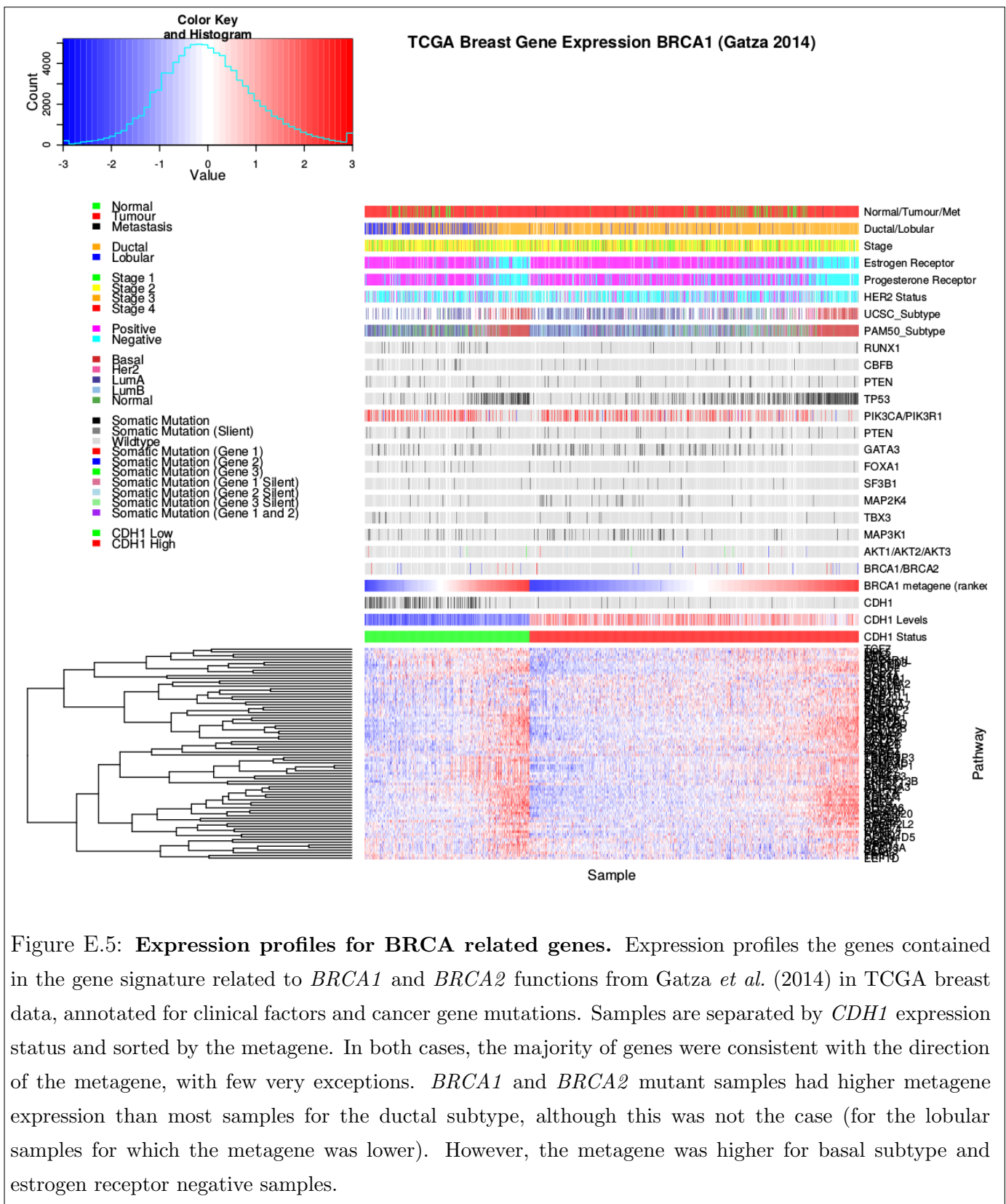


Figure E.4: Expression profiles for estrogen receptor related genes. Expression profiles for the genes contained in the estrogen receptor (ER) gene signature from Gatza *et al.* (2011) in TCGA breast data, annotated for clinical factors and cancer gene mutations. Samples are separated by *CDH1* expression status and sorted by the metagene. In both cases, the majority of genes were consistent with the direction of the metagene, with very few exceptions being inversely correlated. Estrogen receptor (by antibody staining) negative samples had low metagene expression, as expected. These were more likely to be ductal and basal subtypes, lacking *CDH1* or *PIK3CA* mutations.



Appendix F

Stomach Expression Analysis

The following results are a replication of the TCGA results (in Chapter 4) with stomach cancer data, using synthetic lethality (SLIPT) against *CDH1* mutation.

F.1 Synthetic Lethal Genes and Pathways

Table F.1: Synthetic lethal gene partners of *CDH1* from SLIPT in stomach cancer

Gene	Observed	Expected	χ^2 value	p-value	p-value (FDR)
<i>PRAF2</i>	17	50.4	121	3.54×10^{-25}	1.45×10^{-21}
<i>EMP3</i>	17	50.4	115	5.06×10^{-24}	1.48×10^{-20}
<i>PLEKHO1</i>	22	50.4	112	2.14×10^{-23}	4.75×10^{-20}
<i>SELM</i>	20	50.4	111	5.13×10^{-23}	8.09×10^{-20}
<i>GYPC</i>	20	50.4	110	5.77×10^{-23}	8.45×10^{-20}
<i>COX7A1</i>	18	50.4	109	1.15×10^{-22}	1.39×10^{-19}
<i>TNFSF12</i>	20	50.4	106	4.06×10^{-22}	4.38×10^{-19}
<i>SEPT4</i>	17	50.4	106	6.58×10^{-22}	5.91×10^{-19}
<i>LGALS1</i>	19	50.4	105	6.64×10^{-22}	5.91×10^{-19}
<i>RARRES2</i>	27	50.4	105	8.02×10^{-22}	6.85×10^{-19}
<i>VEGFB</i>	16	50.4	104	1.19×10^{-21}	9.74×10^{-19}
<i>PRR24</i>	22	50.4	102	2.96×10^{-21}	2.02×10^{-18}
<i>SYNC</i>	19	50.4	102	3.73×10^{-21}	2.39×10^{-18}
<i>MAGEH1</i>	17	50.4	100	9.52×10^{-21}	5.01×10^{-18}
<i>HSPB2</i>	23	50.4	99.6	1.19×10^{-20}	5.82×10^{-18}
<i>SMARCD3</i>	19	50.4	99	1.59×10^{-20}	7.57×10^{-18}
<i>CREM</i>	13	50.4	98.1	2.48×10^{-20}	1.13×10^{-17}
<i>GNG11</i>	20	50.4	97.3	3.68×10^{-20}	1.59×10^{-17}
<i>GNAI2</i>	17	50.4	96.4	5.75×10^{-20}	2.36×10^{-17}
<i>FUNDC2</i>	22	50.4	95.9	7.39×10^{-20}	2.91×10^{-17}
<i>CNRIP1</i>	21	50.4	95.3	1.0×10^{-19}	3.66×10^{-17}
<i>CALHM2</i>	22	50.4	93.1	2.94×10^{-19}	1.06×10^{-16}
<i>ARID5A</i>	18	50.4	92.7	3.47×10^{-19}	1.22×10^{-16}
<i>ST3GAL3</i>	27	50.4	92.2	4.49×10^{-19}	1.56×10^{-16}
<i>LOC339524</i>	21	50.4	92.1	4.8×10^{-19}	1.59×10^{-16}

SLIPT partners of *CDH1* with observed and expected numbers of TCGA stomach cancer samples with low expression of both genes.

Table F.2: Pathway composition for clusters of *CDH1* partners in stomach SLIPT

Pathways Over-represented in Cluster 1	Pathway Size	Cluster Genes	p-value (FDR)
Viral mRNA Translation	82	48	1.3×10^{-97}
Formation of a pool of free 40S subunits	94	51	1.3×10^{-97}
Eukaryotic Translation Elongation	87	49	4.8×10^{-97}
Peptide chain elongation	84	48	1.4×10^{-96}
Eukaryotic Translation Termination	84	48	1.4×10^{-96}
GTP hydrolysis and joining of the 60S ribosomal subunit	105	52	7.9×10^{-94}
Nonsense Mediated Decay independent of the Exon Junction Complex	89	48	3.1×10^{-93}
L13a-mediated translational silencing of Ceruloplasmin expression	104	51	5.1×10^{-92}
3' -UTR-mediated translational regulation	104	51	5.1×10^{-92}
SRP-dependent cotranslational protein targeting to membrane	105	51	1.7×10^{-91}
Eukaryotic Translation Initiation	112	52	3.3×10^{-90}
Cap-dependent Translation Initiation	112	52	3.3×10^{-90}
Translation	142	56	3.6×10^{-85}
Nonsense-Mediated Decay	104	48	1.2×10^{-84}
Nonsense Mediated Decay enhanced by the Exon Junction Complex	104	48	1.2×10^{-84}
Influenza Viral RNA Transcription and Replication	109	48	4.1×10^{-82}
Influenza Life Cycle	113	48	3.4×10^{-80}
Influenza Infection	118	48	6.4×10^{-78}
Pathways Over-represented in Cluster 2	Pathway Size	Cluster Genes	p-value (FDR)
Immunoregulatory interactions between a Lymphoid and a non-Lymphoid cell	65	12	1.3×10^{-15}
Phosphorylation of CD3 and TCR zeta chains	18	6	1.7×10^{-12}
Generation of second messenger molecules	29	7	2.7×10^{-12}
PD-1 signalling	21	6	7.4×10^{-12}
TCR signalling	62	9	4.3×10^{-11}
Translocation of ZAP-70 to Immunological synapse	16	5	1.1×10^{-10}
Interferon alpha/beta signalling	68	9	1.6×10^{-10}
Initial triggering of complement	17	5	1.6×10^{-10}
IKK complex recruitment mediated by RIP1	19	5	5.1×10^{-10}
TRIF-mediated programmed cell death	10	4	6.2×10^{-10}
Creation of C4 and C2 activators	11	4	1.3×10^{-9}
RHO GTPases Activate NADPH Oxidases	11	4	1.3×10^{-9}
Interferon Signalling	175	15	2.3×10^{-9}
Chemokine receptors bind chemokines	52	7	4.0×10^{-9}
Interferon gamma signalling	74	8	1.6×10^{-8}
TRAF6 mediated induction of TAK1 complex	15	4	1.6×10^{-8}
Activation of IRF3/IRF7 mediated by TBK1/IKK epsilon	16	4	2.7×10^{-8}
Downstream TCR signalling	45	6	3.5×10^{-8}
Pathways Over-represented in Cluster 3	Pathway Size	Cluster Genes	p-value (FDR)
Uptake and actions of bacterial toxins	22	4	3.5×10^{-6}
Neurotoxicity of clostridium toxins	10	3	3.5×10^{-6}
Activation of PPARGC1A (PGC-1alpha) by phosphorylation	10	3	3.5×10^{-6}
SMAD2/SMAD3:SMAD4 heterotrimer regulates transcription	28	4	1.4×10^{-5}
Assembly of the primary cilium	149	10	2.5×10^{-5}
Serotonin Neurotransmitter Release Cycle	15	3	2.5×10^{-5}
Glycosaminoglycan metabolism	114	8	3.3×10^{-5}
Platelet homeostasis	54	5	3.3×10^{-5}
Norepinephrine Neurotransmitter Release Cycle	17	3	3.3×10^{-5}
Acetylcholine Neurotransmitter Release Cycle	17	3	3.3×10^{-5}
G _{αs} signalling events	100	7	5.5×10^{-5}
GABA synthesis, release, reuptake and degradation	19	3	5.6×10^{-5}
deactivation of the beta-catenin transactivating complex	39	4	6.7×10^{-5}
Dopamine Neurotransmitter Release Cycle	20	3	6.7×10^{-5}
IRS-related events triggered by IGF1R	83	6	7.1×10^{-5}
Generic Transcription Pathway	186	11	7.1×10^{-5}
Termination of O-glycan biosynthesis	21	3	7.4×10^{-5}
Kinesins	22	3	8.5×10^{-5}
Pathways Over-represented in Cluster 4	Pathway Size	Cluster Genes	p-value (FDR)
Extracellular matrix organization	241	97	8.8×10^{-126}
Axon guidance	289	75	8.3×10^{-72}
Hemostasis	445	101	8.3×10^{-72}
Developmental Biology	432	95	3.0×10^{-67}
Response to elevated platelet cytosolic Ca ²⁺	84	37	5.8×10^{-67}
Platelet degranulation	79	36	5.8×10^{-67}
Degradation of the extracellular matrix	104	39	6.7×10^{-63}
Platelet activation, signalling and aggregation	186	52	6.6×10^{-62}
ECM proteoglycans	66	31	8.1×10^{-61}
Neuronal System	272	64	5.1×10^{-60}
Signalling by PDGF	173	47	9.7×10^{-57}
Integrin cell surface interactions	82	31	1.9×10^{-53}
Collagen biosynthesis and modifying enzymes	56	26	1.1×10^{-52}
Collagen formation	67	28	1.4×10^{-52}
Class A/1 (Rhodopsin-like receptors)	289	61	2.3×10^{-52}
GPCR ligand binding	373	73	2.8×10^{-52}
Elastic fibre formation	38	22	4.7×10^{-52}
Non-integrin membrane-ECM interactions	53	24	7.0×10^{-49}

Pathway over-representation analysis for Reactome pathways with the number of genes in each pathway (Pathway Size), number of genes within the pathway identified (Cluster Genes), and the pathway over-representation p-value (adjusted by FDR) from the hypergeometric test.

F.2 Comparison to Primary Screen

The synthetic lethal partners with *CDH1* expression in stomach cancers were also compared to siRNA primary screen data (Telford *et al.*, 2015), as performed in Section 4.2.1. These are expected to be more concordant with the experimental results performed on a null mutant, however this is not the case at the gene level: less genes overlapped with experimental candidates in Figure F.1. This may be affected by lower sample size for mutations in TCGA data or lower frequency (expected value) of *CDH1* mutations compared to low expression.

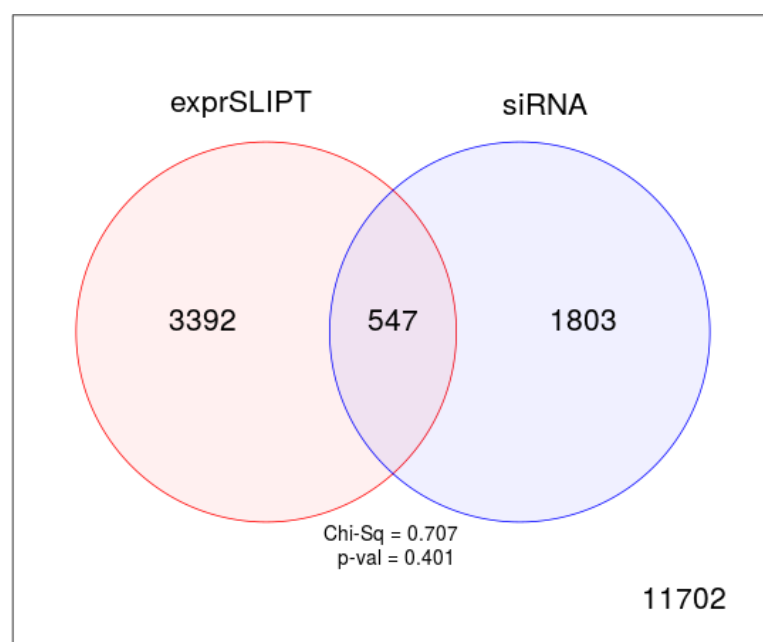


Figure F.1: **Comparison of SLIPT in stomach to siRNA.** Testing the overlap of gene candidates for E-cadherin synthetic lethal partners between computational (SLIPT) and experimental screening (siRNA) approaches. The χ^2 test suggests that the overlap is no more than would be expected by chance ($p = 0.281$).

Table F.3: Pathway composition for *CDH1* partners from SLIPT and siRNA screening

Predicted only by SLIPT (3392 genes)	Pathway	Size	Genes Identified	p-value (FDR)
Extracellular matrix organization		238	90	3.4×10^{-107}
Eukaryotic Translation Termination		79	46	7.6×10^{-91}
Viral mRNA Translation		77	45	1.2×10^{-89}
Eukaryotic Translation Elongation		82	46	5.8×10^{-89}
Peptide chain elongation		79	45	2.1×10^{-88}
Nonsense Mediated Decay independent of the Exon Junction Complex		84	46	9.4×10^{-88}
Formation of a pool of free 40S subunits		89	47	3.3×10^{-87}
GTP hydrolysis and joining of the 60S ribosomal subunit		100	48	3.2×10^{-83}
Axon guidance		284	84	3.9×10^{-82}
Developmental Biology		426	111	4.2×10^{-82}
L13a-mediated translational silencing of Ceruloplasmin expression		99	47	1.4×10^{-81}
3' -UTR-mediated translational regulation		99	47	1.4×10^{-81}
SRP-dependent cotranslational protein targeting to membrane		99	47	1.4×10^{-81}
Nonsense-Mediated Decay		99	47	1.4×10^{-81}
Nonsense Mediated Decay enhanced by the Exon Junction Complex		99	47	1.4×10^{-81}
Hemostasis		438	112	1.2×10^{-80}
Eukaryotic Translation Initiation		107	48	8.0×10^{-80}
Cap-dependent Translation Initiation		107	48	8.0×10^{-80}
Infectious disease		338	90	1.6×10^{-76}
Neuronal System		267	77	1.6×10^{-76}

Detected only by siRNA screen (1803 genes)	Pathway	Size	Genes Identified	p-value (FDR)
Class A/1 (Rhodopsin-like receptors)		282	62	8.1×10^{-50}
GPCR ligand binding		363	71	4.9×10^{-46}
Peptide ligand-binding receptors		175	38	7.9×10^{-38}
G _{αi} signalling events		184	37	1.1×10^{-34}
Gastrin-CREB signalling pathway via PKC and MAPK		180	35	1.4×10^{-32}
G _{αq} signalling events		159	32	4.8×10^{-32}
DAP12 interactions		159	29	1.4×10^{-27}
Downstream signal transduction		146	26	2.4×10^{-25}
DAP12 signalling		149	26	6.4×10^{-25}
VEGFA-VEGFR2 Pathway		91	19	8.1×10^{-24}
Signalling by PDGF		172	27	5.7×10^{-23}
Signalling by ERBB2		146	24	1.4×10^{-22}
Signalling by VEGF		99	19	2.0×10^{-22}
Visual phototransduction		85	17	1.3×10^{-21}
Downstream signalling of activated FGFR1		134	22	1.3×10^{-21}
Downstream signalling of activated FGFR2		134	22	1.3×10^{-21}
Downstream signalling of activated FGFR3		134	22	1.3×10^{-21}
Downstream signalling of activated FGFR4		134	22	1.3×10^{-21}
Signalling by FGFR		146	23	2.0×10^{-21}
Signalling by FGFR1		146	23	2.0×10^{-21}

Intersection of SLIPT and siRNA screen (547 genes)	Pathway	Size	Genes Identified	p-value (FDR)
Class A/1 (Rhodopsin-like receptors)		282	25	3.9×10^{-9}
Platelet activation, signalling and aggregation		182	17	3.9×10^{-9}
Response to elevated platelet cytosolic Ca ²⁺		82	9	5.5×10^{-8}
Platelet homeostasis		53	7	5.7×10^{-8}
Nucleotide-like (purinergic) receptors		16	4	1.8×10^{-7}
Platelet degranulation		77	8	2.8×10^{-7}
Peptide ligand-binding receptors		175	14	3.8×10^{-7}
Molecules associated with elastic fibres		34	5	7.1×10^{-7}
Amine ligand-binding receptors		35	5	8.6×10^{-7}
G _{αi} signalling events		184	14	9.8×10^{-7}
GPCR ligand binding		363	27	1.1×10^{-6}
Elastic fibre formation		38	5	1.5×10^{-6}
G _{αq} signalling events		159	12	1.9×10^{-6}
Serotonin receptors		12	3	3.8×10^{-6}
P2Y receptors		12	3	3.8×10^{-6}
Signal amplification		16	3	2.3×10^{-5}
Gastrin-CREB signalling pathway via PKC and MAPK		180	12	2.3×10^{-5}
Complement cascade		33	4	2.4×10^{-5}
Glycosaminoglycan metabolism		110	8	2.5×10^{-5}
Glycogen breakdown (glycogenolysis)		17	3	2.7×10^{-5}

F.2.1 Resampling Analysis

Table F.4: Pathways for *CDH1* partners from SLIPT in stomach cancer

Reactome Pathway	Over-representation	Permutation
<i>Extracellular matrix organization</i>	7.5×10^{-140}	0.070215
Hemostasis	1.8×10^{-121}	0.25804
Developmental Biology	9.2×10^{-107}	0.53032
Axon guidance	1.5×10^{-102}	0.6704
Eukaryotic Translation Termination	1.9×10^{-99}	$> 1.031 \times 10^{-5}$
GPCR ligand binding	3.8×10^{-99}	0.54914
Viral mRNA Translation	3.3×10^{-98}	$> 1.031 \times 10^{-5}$
Formation of a pool of free 40S subunits	3.3×10^{-98}	$> 1.031 \times 10^{-5}$
Eukaryotic Translation Elongation	1.6×10^{-97}	$> 1.031 \times 10^{-5}$
Peptide chain elongation	7.2×10^{-97}	$> 1.031 \times 10^{-5}$
Class A/1 (Rhodopsin-like receptors)	2.7×10^{-96}	0.58174
Nonsense Mediated Decay independent of the Exon Junction Complex	3×10^{-96}	$> 1.031 \times 10^{-5}$
Infectious disease	2.6×10^{-94}	0.25484
GTP hydrolysis and joining of the 60S ribosomal subunit	3.4×10^{-94}	$> 1.031 \times 10^{-5}$
L13a-mediated translational silencing of Ceruloplasmin expression	2.8×10^{-92}	$> 1.031 \times 10^{-5}$
3' -UTR-mediated translational regulation	2.8×10^{-92}	$> 1.031 \times 10^{-5}$
Neuronal System	8.4×10^{-92}	0.53433
SRP-dependent cotranslational protein targeting to membrane	9.5×10^{-92}	$> 1.031 \times 10^{-5}$
Eukaryotic Translation Initiation	2.0×10^{-90}	$> 1.031 \times 10^{-5}$
Cap-dependent Translation Initiation	2.0×10^{-90}	$> 1.031 \times 10^{-5}$
Nonsense-Mediated Decay	7.4×10^{-90}	$> 1.031 \times 10^{-5}$
Nonsense Mediated Decay enhanced by the Exon Junction Complex	7.4×10^{-90}	$> 1.031 \times 10^{-5}$
Adaptive Immune System	8.1×10^{-88}	0.14116
Translation	1.3×10^{-87}	$> 1.031 \times 10^{-5}$
Platelet activation, signalling and aggregation	1.3×10^{-86}	0.28959
Influenza Infection	1×10^{-82}	$> 1.031 \times 10^{-5}$
Influenza Viral RNA Transcription and Replication	2.4×10^{-82}	$> 1.031 \times 10^{-5}$
Influenza Life Cycle	2×10^{-80}	$> 1.031 \times 10^{-5}$
Response to elevated platelet cytosolic Ca ²⁺	4.9×10^{-78}	0.50817
Signalling by NGF	1.6×10^{-75}	0.38518
Rho GTPase cycle	5.1×10^{-75}	0.14864
Signalling by PDGF	7.4×10^{-74}	0.40493
<i>Signalling by Rho GTPases</i>	5.1×10^{-73}	0.077217
Glycosaminoglycan metabolism	1.4×10^{-68}	0.52984
<i>G_{ai} signalling events</i>	1.8×10^{-66}	0.9254
Metabolism of carbohydrates	1.1×10^{-65}	0.39501
G_{as} signalling events	2.7×10^{-65}	0.0050293
Potassium Channels	2.7×10^{-65}	0.53359
Transmission across Chemical Synapses	1.8×10^{-64}	0.81833
ECM proteoglycans	3.4×10^{-64}	0.083482
Peptide ligand-binding receptors	4.8×10^{-64}	0.62817
Degradation of the extracellular matrix	1.1×10^{-63}	0.80879
Platelet homeostasis	5.3×10^{-63}	0.53134
NGF signalling via TRKA from the plasma membrane	6.1×10^{-63}	0.57117
Integration of energy metabolism	4.5×10^{-61}	0.10889
Collagen formation	5.4×10^{-61}	0.29896
Integrin cell surface interactions	7×10^{-59}	0.18167
Collagen biosynthesis and modifying enzymes	7×10^{-59}	0.30208
Neurotransmitter Receptor Binding And Downstream Transmission	8.7×10^{-57}	0.82522
In The Postsynaptic Cell		
Signalling by Wnt	8.7×10^{-57}	0.25468

Over-representation (hypergeometric test) and Permutation p-values adjusted for multiple tests across pathways (FDR). Significant pathways are marked in bold (FDR < 0.05) and italics (FDR < 0.1).

Table F.5: Pathways for *CDH1* partners from SLIPT in stomach and siRNA screen

Reactome Pathway	Over-representation	Permutation
Platelet activation, signalling and aggregation	3.9×10^{-9}	0.49557
Class A/1 (Rhodopsin-like receptors)	3.9×10^{-9}	0.98432
Response to elevated platelet cytosolic Ca ²⁺	5.5×10^{-8}	0.54349
Platelet homeostasis	5.7×10^{-8}	0.45017
Nucleotide-like (purinergic) receptors	1.8×10^{-7}	0.36966
Peptide ligand-binding receptors	3.8×10^{-7}	0.91294
Molecules associated with elastic fibres	7.1×10^{-7}	0.0025868
Amine ligand-binding receptors	8.6×10^{-7}	0.43303
G _{ai} signalling events	9.8×10^{-7}	0.99626
GPCR ligand binding	1.1×10^{-6}	0.97733
Elastic fibre formation	1.5×10^{-6}	0.0025868
G _{aq} signalling events	1.9×10^{-6}	0.86089
P2Y receptors	3.8×10^{-6}	0.18795
Serotonin receptors	3.8×10^{-6}	0.37853
Signal amplification	2.3×10^{-5}	0.47856
Gastrin-CREB signalling pathway via PKC and MAPK	2.3×10^{-5}	0.98567
Complement cascade	2.4×10^{-5}	$> 3.4628 \times 10^{-6}$
Glycosaminoglycan metabolism	2.5×10^{-5}	0.38953
Glycogen breakdown (glycogenolysis)	2.7×10^{-5}	0.83772
Defective B4GALT7 causes EDS, progeroid type	4.9×10^{-5}	0.10792
Defective B3GAT3 causes JDSSDHD	4.9×10^{-5}	0.10792
Role of LAT2/NTAL/LAB on calcium mobilization	5.6×10^{-5}	0.35373
Cell surface interactions at the vascular wall	5.6×10^{-5}	0.47642
G_{as} signalling events	6×10^{-5}	0.019858
Signalling by NOTCH	6×10^{-5}	0.19008
A tetrasaccharide linker sequence is required for GAG synthesis	0.00017	0.47642
Extracellular matrix organization	0.00018	0.0047308
Collagen formation	0.00018	0.19245
Effects of PIP2 hydrolysis	0.0002	0.37779
Syndecan interactions	0.0002	0.37779
Diseases associated with glycosaminoglycan metabolism	0.00023	0.01028
Diseases of glycosylation	0.00023	0.01028
<i>Chondroitin sulfate/dermatan sulfate metabolism</i>	0.00023	0.085541
Integrin alphaIIb beta3 signalling	0.00028	0.76936
Keratan sulfate biosynthesis	0.00034	0.68744
Rho GTPase cycle	0.00034	0.15675
Creation of C4 and C2 activators	0.00035	0.12275
Abacavir transport and metabolism	0.00035	0.12443
Amine compound SLC transporters	0.00037	0.69773
FCER1 mediated NF-κB activation	0.00037	0.69846
Fc epsilon receptor (FCER1) signalling	0.00056	0.43303
Defective EXT2 causes exostoses 2	0.00067	0.16053
Defective EXT1 causes exostoses 1, TRPS2 and CHDS	0.00067	0.16053
<i>Collagen biosynthesis and modifying enzymes</i>	0.00071	0.052911
Keratan sulfate/keratin metabolism	0.00073	0.46533
G alpha (12/13) signalling events	0.00078	0.59164
SEMA3A-Plexin repulsion signalling by inhibiting Integrin adhesion	0.00084	0.038504
Signal attenuation	0.00084	0.37779
Eicosanoid ligand-binding receptors	0.0011	0.11117
SOS-mediated signalling	0.0011	0.25387

Over-representation (hypergeometric test) and Permutation p-values adjusted for multiple tests across pathways (FDR). Significant pathways are marked in bold (FDR < 0.05) and italicics (FDR < 0.1).

F.3 Metagene Analysis

Metagene analysis was also performed for synthetic lethal candidates for *CDH1* expression in stomach cancer. These are described and compared to mutation analysis in Section G.4.

Table F.6: Candidate synthetic lethal metagenes against *CDH1* from SLIPT in stomach cancer

Pathway	ID	Observed	Expected	χ^2 value	p-value	p-value (FDR)
Cell-Cell communication	1500931	18	50.4	110	7.43×10^{-23}	1.53×10^{-20}
VEGFR2 mediated vascular permeability	5218920	19	50.4	109	1.36×10^{-22}	2.49×10^{-20}
Sema4D in semaphorin signalling	400685	20	50.4	104	1.62×10^{-21}	2.12×10^{-19}
Ion transport by P-type ATPases	936837	17	50.4	100	8.29×10^{-21}	8.06×10^{-19}
Sialic acid metabolism	4085001	19	50.4	95.3	9.95×10^{-20}	7.82×10^{-18}
Synthesis of pyrophosphates in the cytosol	1855167	26	50.4	94	1.86×10^{-19}	1.23×10^{-17}
Keratan sulfate/keratin metabolism	1638074	25	50.4	93.5	2.36×10^{-19}	1.44×10^{-17}
Ion channel transport	983712	19	50.4	92.8	3.37×10^{-19}	1.99×10^{-17}
Keratan sulfate biosynthesis	2022854	26	50.4	91.4	6.79×10^{-19}	3.62×10^{-17}
Arachidonic acid metabolism	2142753	22	50.4	90.6	9.81×10^{-19}	5.07×10^{-17}
RHO GTPases activate CIT	5625900	22	50.4	87	5.80×10^{-18}	2.66×10^{-16}
Stimuli-sensing channels	2672351	25	50.4	85.8	1.03×10^{-17}	4.58×10^{-16}
Synthesis of PI	1483226	19	50.4	85.6	1.15×10^{-17}	4.89×10^{-16}
G-protein activation	202040	19	50.4	85.3	1.34×10^{-17}	5.53×10^{-16}
NrCAM interactions	447038	22	50.4	84.3	2.1×10^{-17}	8.27×10^{-16}
Inwardly rectifying K^+ channels	1296065	24	50.4	83.5	3.19×10^{-17}	1.22×10^{-15}
Calcitonin-like ligand receptors	419812	20	50.4	82.2	6.07×10^{-17}	2.13×10^{-15}
Prostacyclin signalling through prostacyclin receptor	392851	24	50.4	81.8	7.27×10^{-17}	2.5×10^{-15}
Presynaptic function of Kainate receptors	500657	26	50.4	79.7	2.00×10^{-16}	6.34×10^{-15}
ADP signalling through P2Y purinoceptor 12	392170	23	50.4	79.2	2.57×10^{-16}	7.71×10^{-15}
regulation of FZD by ubiquitination	4641263	22	50.4	78.8	3.15×10^{-16}	9.3×10^{-15}
Toxicity of tetanus toxin (TeNT)	5250982	27	50.4	78.7	3.36×10^{-16}	9.75×10^{-15}
Gap junction degradation	190873	21	50.4	78.5	3.66×10^{-16}	1.04×10^{-14}
Nephrin interactions	373753	25	50.4	78.2	4.21×10^{-16}	1.14×10^{-14}
GABA synthesis, release, reuptake and degradation	888590	26	50.4	77	7.69×10^{-16}	1.95×10^{-14}

Strongest candidate SL partners for *CDH1* by SLIPT with observed and expected numbers of TCGA stomach cancer samples with low expression of both genes.

Appendix G

Stomach Mutation Analysis

The following results are a replication of the TCGA results (in Appendix D) with stomach cancer data, using synthetic lethality (mtSLIPT) against *CDH1* mutation.

G.1 Synthetic Lethal Genes and Pathways

Table G.1: Synthetic lethal gene partners of *CDH1* from mtSLIPT in stomach cancer

Gene	Observed	Expected	χ^2 value	p-value	p-value (FDR)
<i>OLFML1</i>	5	10.1	29.2	4.53×10^{-7}	0.0031
<i>NRIP2</i>	6	10.1	25.4	3.11×10^{-6}	0.00706
<i>VIM</i>	3	10.1	24.7	4.29×10^{-6}	0.00706
<i>TCF4</i>	5	10.1	24.7	4.33×10^{-6}	0.00706
<i>ZEB2</i>	5	10.1	24.7	4.33×10^{-6}	0.00706
<i>BCL2</i>	2	10.1	22	1.66×10^{-5}	0.0155
<i>SMARCA2</i>	2	10.1	22	1.66×10^{-5}	0.0155
<i>CCND2</i>	3	10.1	21.1	2.61×10^{-5}	0.0155
<i>MMP19</i>	3	10.1	21.1	2.61×10^{-5}	0.0155
<i>NEURL1B</i>	3	10.1	21.1	2.61×10^{-5}	0.0155
<i>IGFBP6</i>	6	10.1	21.1	2.65×10^{-5}	0.0155
<i>OGN</i>	6	10.1	21.1	2.65×10^{-5}	0.0155
<i>THY1</i>	6	10.2	21	2.7×10^{-5}	0.0155
<i>DZIP1</i>	4	10.1	20.6	3.29×10^{-5}	0.0155
<i>LOC650368</i>	4	10.1	20.6	3.29×10^{-5}	0.0155
<i>PCOLCE</i>	4	10.1	20.6	3.29×10^{-5}	0.0155
<i>PTGFR</i>	4	10.1	20.6	3.29×10^{-5}	0.0155
<i>RUNX1T1</i>	4	10.1	20.6	3.29×10^{-5}	0.0155
<i>CLEC2B</i>	5	10.1	20.6	3.3×10^{-5}	0.0155
<i>MSC</i>	5	10.1	20.6	3.3×10^{-5}	0.0155
<i>NISCH</i>	5	10.1	20.6	3.3×10^{-5}	0.0155
<i>TSPAN11</i>	5	10.1	20.6	3.3×10^{-5}	0.0155
<i>KCTD12</i>	2	10.1	19.1	7.19×10^{-5}	0.0246
<i>LRRC55</i>	2	10.1	19.1	7.19×10^{-5}	0.0246
<i>PCBP3</i>	2	10.1	19.1	7.19×10^{-5}	0.0246

mtSLIPT partners with observed and expected numbers of *CDH1* mutant TCGA stomach cancer samples with low expression of partner genes.

Table G.2: Pathways for *CDH1* partners from mtSLIPT in stomach cancer

Pathways Over-represented	Pathway Size	SL Genes	p-value (FDR)
Extracellular matrix organization	241	20	9.6×10^{-9}
Elastic fibre formation	38	6	3.7×10^{-8}
Diseases associated with glycosaminoglycan metabolism	26	5	3.7×10^{-8}
Diseases of glycosylation	26	5	3.7×10^{-8}
Nitric oxide stimulates guanylate cyclase	24	4	3.1×10^{-6}
Molecules associated with elastic fibres	34	4	3.7×10^{-5}
Platelet homeostasis	54	5	3.7×10^{-5}
Initial triggering of complement	17	3	3.7×10^{-5}
Regulation of IGF transport and uptake by IGFBPs	17	3	3.7×10^{-5}
Collagen degradation	58	5	5.6×10^{-5}
Defective B4GALT7 causes EDS, progeroid type	19	3	5.6×10^{-5}
Defective B3GAT3 causes JDSSDHD	19	3	5.6×10^{-5}
Degradation of the extracellular matrix	104	7	8.0×10^{-5}
ECM proteoglycans	66	5	0.00017
A tetrasaccharide linker sequence is required for GAG synthesis	25	3	0.00025
RHO GTPases Activate WASPs and WAVEs	29	3	0.00059
Non-integrin membrane-ECM interactions	53	4	0.00065
Creation of C4 and C2 activators	11	2	0.00079
Dermatan sulfate biosynthesis	11	2	0.00079
Integrin cell surface interactions	82	5	0.00098

Gene set over-representation analysis (hypergeometric test) for Reactome pathways in mtSLIPT partners for *CDH1*.

G.2 Synthetic Lethal Expression Profiles

Similar to the analysis of synthetic lethal partners against low *CDH1* expression in F.1, the partners detected from *CDH1* mutation were also examined for their expression profiles and the pathway composition of gene clusters. Hierarchical clustering was performed on mtSLIPT partners for *CDH1* as showing in Figure G.1. Over-representation for Reactome pathways for each of the gene clusters identified is given in Table G.3.

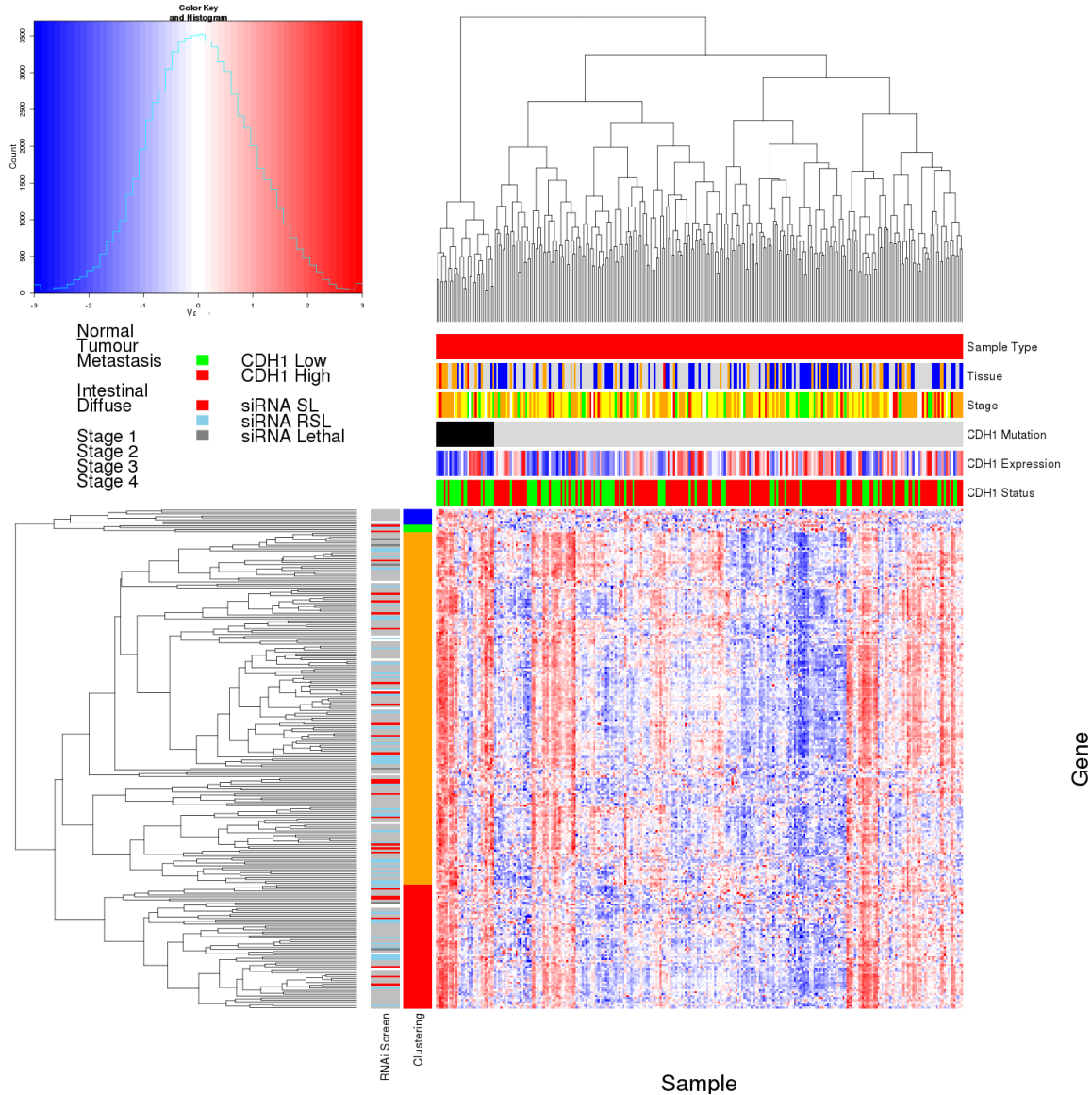


Figure G.1: Synthetic lethal expression profiles of analysed samples. Gene expression profile heatmap (correlation distance) of all samples (separated by the 1/3 quantile of *CDH1* expression) analysed in TCGA stomach cancer dataset for gene expression of 257 candidate partners of E-cadherin (*CDH1*) from SLIPT prediction (with significant FDR adjusted $p < 0.05$). Deeply clustered, inter-correlated genes form several main groups, each containing genes that were SL candidates or toxic in an siRNA screen (Telford *et al.*, 2015). Clusters had different sample groups highly expressing the synthetic lethal candidates in *CDH1* low samples, notably diffuse and *CDH1* mutant samples have elevated expression in one or more distinct clusters, although there was less complexity and variation among candidate synthetic lethal partners than in breast data. *CDH1* low samples also contained most of samples with *CDH1* mutations.

Table G.3: Pathway composition for clusters of *CDH1* partners in stomach mtSLIPT

Pathways Over-represented in Cluster 1	Pathway Size	Cluster Genes	p-value (FDR)
CD28 dependent PI3K/Akt signalling	15	1	1
Hormone-sensitive lipase (HSL)-mediated triacylglycerol hydrolysis	19	1	1
CD28 co-stimulation	26	1	1
Lipid digestion, mobilization, and transport	48	1	1
Costimulation by the CD28 family	51	1	1
Dectin-1 mediated noncanonical NF- κ B signalling	58	1	1
CLEC7A (Dectin-1) signalling	99	1	1
C-type lectin receptors (CLRs)	123	1	1
Adaptive Immune System	418	1	1
Metabolism of lipids and lipoproteins	494	1	1
Interleukin-6 signalling	10	0	1
Apoptosis	150	0	1
Hemostasis	445	0	1
Intrinsic Pathway for Apoptosis	36	0	1
Cleavage of Growing Transcript in the Termination Region	33	0	1
PKB-mediated events	28	0	1
PI3K Cascade	68	0	1
RAF/MAP kinase cascade	10	0	1
Pathways Over-represented in Cluster 2	Pathway Size	Cluster Genes	p-value (FDR)
Kinesins	22	1	1
O-linked glycosylation of mucins	49	1	1
O-linked glycosylation	59	1	1
MHC class II antigen presentation	85	1	1
Factors involved in megakaryocyte development and platelet production	120	1	1
Post-translational protein modification	303	1	1
Adaptive Immune System	418	1	1
Hemostasis	445	1	1
Interleukin-6 signalling	10	0	1
Apoptosis	150	0	1
Intrinsic Pathway for Apoptosis	36	0	1
Cleavage of Growing Transcript in the Termination Region	33	0	1
PKB-mediated events	28	0	1
PI3K Cascade	68	0	1
RAF/MAP kinase cascade	10	0	1
Global Genomic NER (GG-NER)	35	0	1
Repair synthesis for gap-filling by DNA polymerase in TC-NER	15	0	1
Gap-filling DNA repair synthesis and ligation in TC-NER	17	0	1
Pathways Over-represented in Cluster 3	Pathway Size	Cluster Genes	p-value (FDR)
Extracellular matrix organization	241	20	9.6×10^{-9}
Elastic fibre formation	38	6	3.7×10^{-8}
Diseases associated with glycosaminoglycan metabolism	26	5	3.7×10^{-8}
Diseases of glycosylation	26	5	3.7×10^{-8}
Molecules associated with elastic fibres	34	4	4.8×10^{-5}
Initial triggering of complement	17	3	4.8×10^{-5}
Regulation of IGF transport and uptake by IGFBPs	17	3	4.8×10^{-5}
Collagen degradation	58	5	6.7×10^{-5}
Defective B4GALT7 causes EDS, progeroid type	19	3	6.7×10^{-5}
Defective B3GAT3 causes JDSSDHD	19	3	6.7×10^{-5}
Degradation of the extracellular matrix	104	7	9.5×10^{-5}
ECM proteoglycans	66	5	0.0002
A tetrasaccharide linker sequence is required for GAG synthesis	25	5	0.00029
Non-integrin membrane-ECM interactions	53	4	0.00079
Creation of C4 and C2 activators	11	2	0.00093
Dermatan sulfate biosynthesis	11	2	0.00093
Integrin cell surface interactions	82	5	0.0012
Keratan sulfate degradation	12	2	0.0012
Pathways Over-represented in Cluster 4	Pathway Size	Cluster Genes	p-value (FDR)
cGMP effects	18	2	0.11
Nitric oxide stimulates guanylate cyclase	24	2	0.19
Neurotoxicity of clostridium toxins	10	1	1
Platelet homeostasis	54	2	1
Eicosanoid ligand-binding receptors	14	1	1
Prolactin receptor signalling	15	1	1
Acyl chain remodelling of PI	15	1	1
Signalling by FGFR1 fusion mutants	15	1	1
PKA activation	16	1	1
PKA-mediated phosphorylation of CREB	17	1	1
Synthesis of glycosylphosphatidylinositol (GPI)	17	1	1
PKA activation in glucagon signalling	17	1	1
Butyrate Response Factor 1 (BRF1) destabilizes mRNA	17	1	1
Other semaphorin interactions	19	1	1
Acyl chain remodelling of PE	21	1	1
Signalling by Leptin	21	1	1
DARPP-32 events	22	1	1
Glucagon-like Peptide-1 (GLP1) regulates insulin secretion	22	1	1

Pathway over-representation analysis for Reactome pathways with the number of genes in each pathway (Pathway Size), number of genes within the pathway identified (Cluster Genes), and the pathway over-representation p-value (adjusted by FDR) from the hypergeometric test.

G.3 Comparison to Primary Screen

The mutation synthetic lethal partners with *CDH1* were also compared to siRNA primary screen data (Telford *et al.*, 2015), as performed in Section 4.2.1. These are expected to be more concordant with the experimental results performed on a null mutant, however this is not the case at the gene level: less genes overlapped with experimental candidates in Figure G.2. This may be affected by lower sample size for mutations in TCGA data or lower frequency (expected value) of *CDH1* mutations compared to low expression.

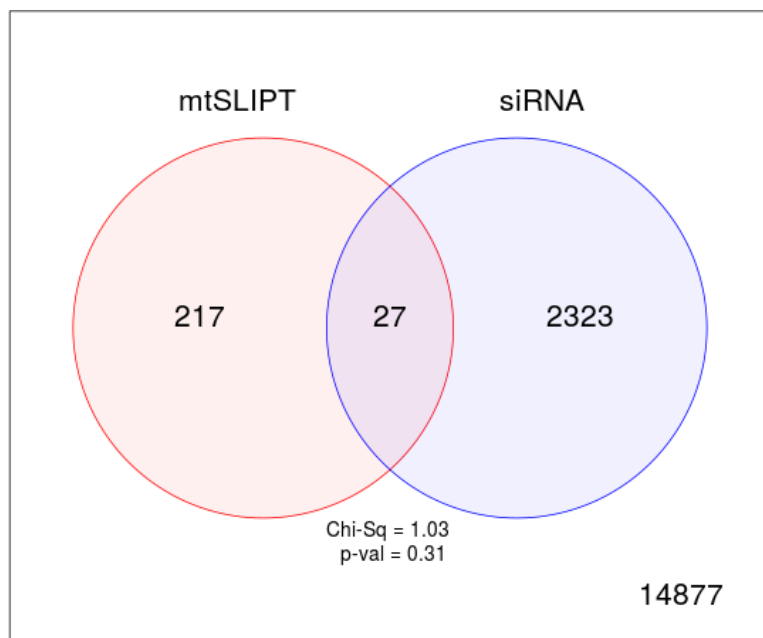


Figure G.2: **Comparison of mtSLIPT in stomach to siRNA.** Testing the overlap of gene candidates for E-cadherin synthetic lethal partners between computational (mtSLIPT) and experimental screening (siRNA) approaches. The χ^2 test suggests that the overlap is no more than would be expected by chance ($p = 0.872$).

Table G.4: Pathway composition for *CDH1* partners from mtSLIPT and siRNA

Predicted only by SLIPT (217 genes)	Pathway Size	Genes Identified	p-value (FDR)
Diseases associated with glycosaminoglycan metabolism	26	5	1.6×10^{-7}
Diseases of glycosylation	26	5	1.6×10^{-7}
Extracellular matrix organization	238	18	1.7×10^{-6}
Elastic fibre formation	38	5	4.6×10^{-6}
Initial triggering of complement	16	3	7.3×10^{-5}
Regulation of IGF transport and uptake by IGFBPs	17	3	8.9×10^{-5}
Defective B4GALT7 causes EDS, progeroid type	19	3	0.00013
Defective B3GAT3 causes JDSSDHD	19	3	0.00013
Collagen degradation	57	5	0.00013
ECM proteoglycans	65	5	0.00039
A tetrasaccharide linker sequence is required for GAG synthesis	24	3	0.00039
Nitric oxide stimulates guanylate cyclase	24	3	0.00039
RHO GTPases Activate WASPs and WAVEs	28	3	0.00094
Creation of C4 and C2 activators	10	2	0.00098
Non-integrin membrane-ECM interactions	52	4	0.0012
Dermatan sulfate biosynthesis	11	2	0.0013
Degradation of the extracellular matrix	101	6	0.0016
Keratan sulfate degradation	12	2	0.0016
Complement cascade	33	3	0.0018
Molecules associated with elastic fibres	34	3	0.002

Detected only by siRNA screen (2323 genes)	Pathway Size	Genes Identified	p-value (FDR)
Class A/1 (Rhodopsin-like receptors)	282	86	6.5×10^{-85}
GPCR ligand binding	363	97	9.2×10^{-79}
Peptide ligand-binding receptors	175	52	4.5×10^{-61}
G _{αi} signalling events	184	49	1.6×10^{-53}
G _{αq} signalling events	159	43	5.2×10^{-50}
Gastrin-CREB signalling pathway via PKC and MAPK	180	46	9.4×10^{-50}
DAP12 interactions	159	35	8.3×10^{-37}
Platelet activation, signalling and aggregation	182	37	2.3×10^{-35}
Hemostasis	438	71	3.3×10^{-35}
Downstream signal transduction	146	32	7.7×10^{-35}
Signalling by PDGF	172	35	2.1×10^{-34}
DAP12 signalling	149	32	2.7×10^{-34}
Signalling by ERBB2	146	31	2.5×10^{-33}
Signalling by NGF	266	44	5.3×10^{-31}
Downstream signalling of activated FGFR1	134	28	5.3×10^{-31}
Downstream signalling of activated FGFR2	134	28	5.3×10^{-31}
Downstream signalling of activated FGFR3	134	28	5.3×10^{-31}
Downstream signalling of activated FGFR4	134	28	5.3×10^{-31}
Signalling by FGFR	146	29	2.0×10^{-30}
Signalling by FGFR1	146	29	2.0×10^{-30}

Intersection of SLIPT and siRNA screen (23 genes)	Pathway Size	Genes Identified	p-value (FDR)
ADP signalling through P2Y purinoceptor 1	10	1	1
G-protein beta:gamma signalling	11	1	1
G-protein activation	12	1	1
Eicosanoid ligand-binding receptors	14	1	1
Platelet homeostasis	53	2	1
G _{αz} signalling events	15	1	1
Signal amplification	16	1	1
Activation of Kainate Receptors upon glutamate binding	17	1	1
Thrombin signalling through protease activated receptors (PARs)	17	1	1
Nitric oxide stimulates guanylate cyclase	24	1	1
Activation of G protein gated Potassium channels	25	1	1
G protein gated Potassium channels	25	1	1
Inhibition of voltage gated Ca ²⁺ channels via Gbeta/gamma subunits	25	1	1
Laminin interactions	29	1	1
Inwardly rectifying K ⁺ channels	31	1	1
Glucagon signalling in metabolic regulation	33	1	1
Molecules associated with elastic fibres	34	1	1
Ca ²⁺ pathway	36	1	1
Elastic fibre formation	38	1	1
GABA B receptor activation	38	1	1

G.3.1 Resampling Analysis

Table G.5: Pathways for *CDH1* partners from mtSLIPT in stomach cancer

Reactome Pathway	Over-representation	Permutation
<i>Extracellular matrix organization</i>	9.6×10^{-9}	0.057678
Elastic fibre formation	3.7×10^{-8}	0.033817
<i>Diseases associated with glycosaminoglycan metabolism</i>	3.7×10^{-8}	0.049336
<i>Diseases of glycosylation</i>	3.7×10^{-8}	0.049336
<i>Nitric oxide stimulates guanylate cyclase</i>	3.1×10^{-6}	0.037904
Initial triggering of complement	3.7×10^{-5}	0.020828
Molecules associated with elastic fibres	3.7×10^{-5}	0.027865
<i>Regulation of IGF transport and uptake by IGFBPs</i>	3.7×10^{-5}	0.069102
<i>Platelet homeostasis</i>	3.7×10^{-5}	0.097294
<i>Defective B4GALT7 causes EDS, progeroid type</i>	5.6×10^{-5}	0.081505
<i>Defective B3GAT3 causes JDSSDHD</i>	5.6×10^{-5}	0.081505
Collagen degradation	5.6×10^{-5}	0.1104
<i>Degradation of the extracellular matrix</i>	8×10^{-5}	0.43477
<i>ECM proteoglycans</i>	0.00017	0.06469
<i>A tetrasaccharide linker sequence is required for GAG synthesis</i>	0.00025	0.10536
<i>RHO GTPases Activate WASPs and WAVES</i>	0.00059	0.053929
<i>Non-integrin membrane-ECM interactions</i>	0.00065	0.10424
<i>Creation of C4 and C2 activators</i>	0.00079	0.05461
<i>Dermatan sulfate biosynthesis</i>	0.00079	0.21163
<i>Integrin cell surface interactions</i>	0.00098	0.092405
<i>Glucagon signalling in metabolic regulation</i>	0.00098	0.13425
<i>Keratan sulfate degradation</i>	0.00098	0.22137
Complement cascade	0.0011	0.01552
<i>CS/DS degradation</i>	0.0012	0.065012
<i>Eicosanoid ligand-binding receptors</i>	0.0016	0.066128
<i>Nuclear signalling by ERBB4</i>	0.0016	0.15511
<i>Collagen formation</i>	0.0026	0.13447
cGMP effects	0.0041	0.020195
<i>Voltage gated Potassium channels</i>	0.0041	0.068923
Chondroitin sulfate biosynthesis	0.0059	$> 1.5862 \times 10^{-5}$
<i>Chondroitin sulfate/dermatan sulfate metabolism</i>	0.0065	0.087745
<i>Heparan sulfate/heparin (HS-GAG) metabolism</i>	0.0071	0.085622
<i>Synthesis of substrates in N-glycan biosynthesis</i>	0.0085	0.09456
<i>Regulation of actin dynamics for phagocytic cup formation</i>	0.0085	0.096227
<i>CDO in myogenesis</i>	0.01	0.32599
<i>Myogenesis</i>	0.01	0.32599
<i>Syndecan interactions</i>	0.012	0.10975
<i>Activation of Matrix Metalloproteinases</i>	0.012	0.33499
<i>Glycosaminoglycan metabolism</i>	0.012	0.29716
<i>Collagen biosynthesis and modifying enzymes</i>	0.013	0.10774
<i>Keratan sulfate biosynthesis</i>	0.016	0.12644
<i>O-linked glycosylation</i>	0.016	0.65101
<i>Laminin interactions</i>	0.021	0.12766
<i>Biosynthesis of the N-glycan precursor (dolichol lipid-linked oligosaccharide) and transfer to a nascent protein</i>	0.027	0.065782
<i>Sialic acid metabolism</i>	0.027	0.13413
<i>Keratan sulfate/keratin metabolism</i>	0.029	0.15708
<i>Potassium Channels</i>	0.032	0.43477
<i>Fcgamma receptor (FCGR) dependent phagocytosis</i>	0.042	0.15851
<i>Ion transport by P-type ATPases</i>	0.048	0.66686
<i>Retinoid metabolism and transport</i>	0.051	0.058715

Over-representation (hypergeometric test) and Permutation p-values adjusted for multiple tests across pathways (FDR).

Significant pathways are marked in bold (FDR < 0.05) and italics (FDR < 0.1).

Table G.6: Pathways for *CDH1* partners from mtSLIPT in stomach and siRNA screen

Reactome Pathway	Over-representation	Permutation
SLBP independent Processing of Histone Pre-mRNAs	1	$> 1.2349 \times 10^{-5}$
Mitochondrial protein import	1	$> 1.2349 \times 10^{-5}$
Voltage gated Potassium channels	1	$> 1.2349 \times 10^{-5}$
Tandem pore domain potassium channels	1	$> 1.2349 \times 10^{-5}$
L13a-mediated translational silencing of Ceruloplasmin expression	1	$> 1.2349 \times 10^{-5}$
Eukaryotic Translation Elongation	1	$> 1.2349 \times 10^{-5}$
Peptide chain elongation	1	$> 1.2349 \times 10^{-5}$
3' -UTR-mediated translational regulation	1	$> 1.2349 \times 10^{-5}$
Activation of Matrix Metalloproteinases	1	$> 1.2349 \times 10^{-5}$
HIV Infection	1	$> 1.2349 \times 10^{-5}$
Cell Cycle	1	$> 1.2349 \times 10^{-5}$
Influenza Infection	1	$> 1.2349 \times 10^{-5}$
Influenza Life Cycle	1	$> 1.2349 \times 10^{-5}$
Influenza Viral RNA Transcription and Replication	1	$> 1.2349 \times 10^{-5}$
Neurotoxicity of clostridium toxins	1	$> 1.2349 \times 10^{-5}$
p38MAPK events	1	$> 1.2349 \times 10^{-5}$
SCF-beta-TrCP mediated degradation of Emi1	1	$> 1.2349 \times 10^{-5}$
SRP-dependent cotranslational protein targeting to membrane	1	$> 1.2349 \times 10^{-5}$
Vpu mediated degradation of CD4	1	$> 1.2349 \times 10^{-5}$
Serotonin Neurotransmitter Release Cycle	1	$> 1.2349 \times 10^{-5}$
Acetylcholine Binding And Downstream Events	1	$> 1.2349 \times 10^{-5}$
Viral mRNA Translation	1	$> 1.2349 \times 10^{-5}$
Cobalamin (Cbl, vitamin B12) transport and metabolism	1	$> 1.2349 \times 10^{-5}$
ERK/MAPK targets	1	$> 1.2349 \times 10^{-5}$
Vitamin B5 (pantothenate) metabolism	1	$> 1.2349 \times 10^{-5}$
Signalling by BMP	1	$> 1.2349 \times 10^{-5}$
Synthesis of Leukotrienes (LT) and Eoxins (EX)	1	$> 1.2349 \times 10^{-5}$
Separation of Sister Chromatids	1	$> 1.2349 \times 10^{-5}$
Mitotic Metaphase and Anaphase	1	$> 1.2349 \times 10^{-5}$
TRP channels	1	$> 1.2349 \times 10^{-5}$
Defects in cobalamin (B12) metabolism	1	$> 1.2349 \times 10^{-5}$
Regulation by c-FLIP	1	$> 1.2349 \times 10^{-5}$
Attenuation phase	1	$> 1.2349 \times 10^{-5}$
Autodegradation of the E3 ubiquitin ligase COP1	1	$> 1.2349 \times 10^{-5}$
Apoptotic cleavage of cell adhesion proteins	1	$> 1.2349 \times 10^{-5}$
Negative regulation of TCF-dependent signalling by WNT ligand antagonists	1	$> 1.2349 \times 10^{-5}$
PERK regulates gene expression	1	$> 1.2349 \times 10^{-5}$
Regulation of the Fanconi anemia pathway	1	$> 1.2349 \times 10^{-5}$
Passive transport by Aquaporins	1	$> 1.2349 \times 10^{-5}$
Lysosome Vesicle Biogenesis	1	$> 1.2349 \times 10^{-5}$
Zinc transporters	1	$> 1.2349 \times 10^{-5}$
Zinc influx into cells by the SLC39 gene family	1	$> 1.2349 \times 10^{-5}$
Asparagine N-linked glycosylation	1	$> 1.2349 \times 10^{-5}$
AUF1 (hnRNP D0) destabilizes mRNA	1	$> 1.2349 \times 10^{-5}$
Asymmetric localization of PCP proteins	1	$> 1.2349 \times 10^{-5}$
degradation of DVL	1	$> 1.2349 \times 10^{-5}$
CASP8 activity is inhibited	1	$> 1.2349 \times 10^{-5}$
Degradation of GLI1 by the proteasome	1	$> 1.2349 \times 10^{-5}$
BBSome-mediated cargo-targeting to cilium	1	$> 1.2349 \times 10^{-5}$
Regulation of necroptotic cell death	1	$> 1.2349 \times 10^{-5}$

G.4 Metagene Analysis

Metagene analysis was also performed for synthetic lethal candidates for *CDH1* mutation in stomach cancer. These are described and compared to expression analysis in Section F.3.

Table G.7: Candidate synthetic lethal metagenes against *CDH1* from mtSLIPT in stomach cancer

Pathway	ID	Observed	Expected	χ^2 value	p-value	p-value (FDR)
Prostacyclin signalling through prostacyclin receptor	392851	1	10.1	26.5	1.73×10^{-6}	0.00286
Cell surface interactions at the vascular wall	202733	3	10.1	21.1	2.61×10^{-5}	0.00642
The NLRP1 inflammasome	844455	3	10.1	21.1	2.61×10^{-5}	0.00642
Innate Immune System	168249	6	10.1	21.1	2.65×10^{-5}	0.00642
Keratan sulfate/keratin metabolism	1638074	4	10.1	20.6	3.29×10^{-5}	0.00642
Keratan sulfate biosynthesis	2022854	4	10.1	20.6	3.29×10^{-5}	0.00642
Signalling by SCF-KIT	1433557	5	10.1	20.6	3.30×10^{-5}	0.00642
VEGFA-VEGFR2 Pathway	4420097	5	10.1	20.6	3.30×10^{-5}	0.00642
p130Cas linkage to MAPK signalling for integrins	372708	2	10.1	19.1	7.19×10^{-5}	0.00651
cGMP effects	418457	8	10.1	19	7.46×10^{-5}	0.00651
Regulation of cytoskeletal remodeling and cell spreading by IPP complex components	446388	8	10.1	19	7.46×10^{-5}	0.00651
Fcgamma receptor (FCGR) dependent phagocytosis	2029480	3	10.1	17.9	0.000127	0.00651
A third proteolytic cleavage releases NICD	157212	7	10.1	17.9	0.00013	0.00651
Signalling by NGF	166520	7	10.1	17.9	0.00013	0.00651
Signalling by VEGF	194138	7	10.1	17.9	0.00013	0.00651
Regulation of thyroid hormone activity	350864	7	10.1	17.9	0.00013	0.00651
Nitric oxide stimulates guanylate cyclase	392154	7	10.1	17.9	0.00013	0.00651
Platelet homeostasis	418346	7	10.1	17.9	0.00013	0.00651
PI3K events in ERBB4 signalling	1250342	4	10.1	17.3	0.000179	0.00651
PIP3 activates AKT signalling	1257604	4	10.1	17.3	0.000179	0.00651
GAB1 signalosome	180292	4	10.1	17.3	0.000179	0.00651
PI3K events in ERBB2 signalling	1963642	4	10.1	17.3	0.000179	0.00651
PI3K/AKT Signalling in Cancer	2219528	4	10.1	17.3	0.000179	0.00651
Rap1 signalling	392517	4	10.1	17.3	0.000179	0.00651
Lysosphingolipid and LPA receptors	419408	4	10.1	17.3	0.000179	0.00651

Strongest candidate SL partners for *CDH1* by mtSLIPT with observed and expected numbers of *CDH1* mutant TCGA stomach cancer samples with low expression of partner metagenes.

Appendix H

Global Synthetic Lethality in Stomach Cancer

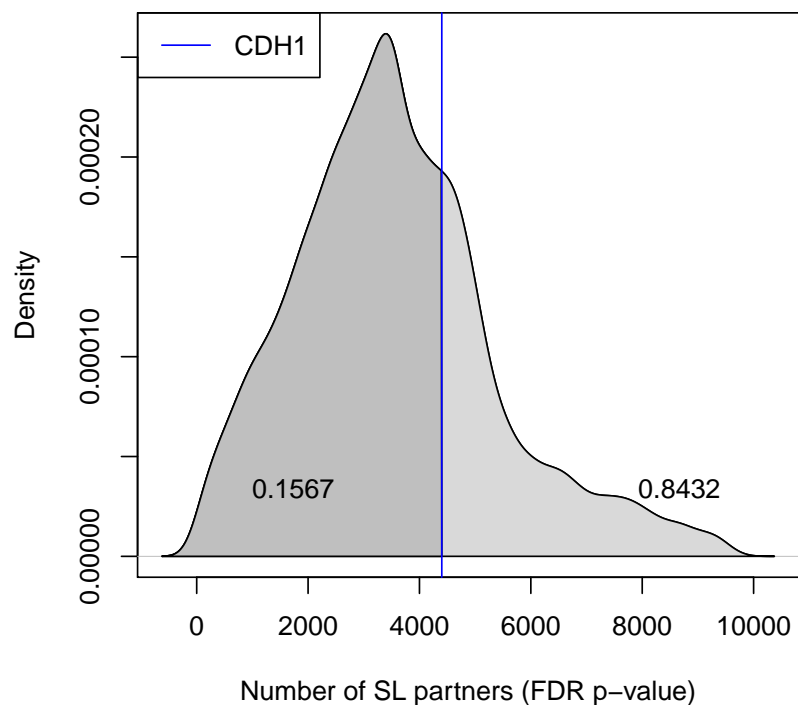


Figure H.1: **Synthetic lethal partners across query genes.** Global synthetic lethal pairs were examined across the genome in TCGA stomach expression data by applying SLIPT across query genes. The high number of predicted partners for *CDH1* was typical for a human gene and lower than many other genes.

H.1 Hub Genes

Table H.1: Query synthetic lethal genes with the most SLIPT partners

Gene	Direction	raw p-value	p-value (FDR)	SLIPT raw p-value	SLIPT (FDR)
<i>HEG1</i>	10719	16956	16724	9616	9532
<i>SYNE1</i>	10755	17210	16984	9749	9676
<i>A2M</i>	10743	16650	16378	9529	9433
<i>ANK2</i>	11008	16616	16355	9764	9653
<i>TTC28</i>	10757	16523	16248	9530	9429
<i>FAT4</i>	10451	16286	15978	9225	9115
<i>MRVI1</i>	10904	16967	16718	9775	9686
<i>PAPLN</i>	10483	16405	16104	9305	9193
<i>NFASC</i>	10773	16575	16307	9578	9475
<i>MACF1</i>	9697	16378	16058	8620	8540
<i>HMCN1</i>	10475	16101	15733	9156	9008
<i>MPDZ</i>	10878	16550	16299	9599	9491
<i>FLRT2</i>	10776	16760	16473	9590	9464
<i>SETBP1</i>	10869	16632	16349	9615	9489
<i>LAMA4</i>	10463	16447	16121	9273	9151
<i>IL1R1</i>	10611	16185	15803	9299	9174
<i>ABCA6</i>	10499	16573	16318	9260	9158
<i>LAMC1</i>	10238	15777	15392	8837	8691
<i>TNS1</i>	10920	17038	16806	9836	9751
<i>AMOTL1</i>	10612	16458	16178	9367	9250

Genes with the most candidate SL partners SLIPT in TCGA stomach expression data with the number of partner genes predicted by direction criteria and χ^2 testing separately and combined as a SLIPT analysis. Where specified, the p-values for the χ^2 test were adjusted for multiple tests (FDR).

H.2 Hub Pathways

Table H.2: Pathways for genes with the most SLIPT partners

Pathways Over-represented	Pathway Size	SL Genes	p-value	p-value (FDR)
Molecules associated with elastic fibres	34	10	4.6×10^{-21}	2.7×10^{-18}
Extracellular matrix organization	241	29	5.3×10^{-21}	2.7×10^{-18}
Smooth Muscle Contraction	29	9	5.6×10^{-20}	1.6×10^{-17}
Elastic fibre formation	38	10	6×10^{-20}	1.6×10^{-17}
Nitric oxide stimulates guanylate cyclase	24	8	6.9×10^{-19}	1.4×10^{-16}
Muscle contraction	64	12	8.3×10^{-19}	1.4×10^{-16}
Platelet homeostasis	54	11	1.3×10^{-18}	1.9×10^{-16}
cGMP effects	18	6	3.3×10^{-15}	4.3×10^{-13}
Laminin interactions	30	7	1.3×10^{-14}	1.6×10^{-12}
Axon guidance	289	25	5×10^{-13}	5.2×10^{-11}
Signalling by BMP	23	5	3.7×10^{-11}	3.2×10^{-9}
RHO GTPases activate PAKs	23	5	3.7×10^{-11}	3.2×10^{-9}
Non-integrin membrane-ECM interactions	53	7	7.2×10^{-11}	5.8×10^{-9}
Rho GTPase cycle	120	11	1.2×10^{-10}	8.7×10^{-9}
Degradation of the extracellular matrix	104	10	1.3×10^{-10}	8.8×10^{-9}
Netrin-1 signalling	42	6	2.5×10^{-10}	1.6×10^{-8}
Developmental Biology	432	32	8.3×10^{-10}	5×10^{-8}
L1CAM interactions	80	8	8.7×10^{-10}	5×10^{-8}
Semaphorin interactions	64	7	1.1×10^{-9}	6.1×10^{-8}
Cell-extracellular matrix interactions	18	4	1.3×10^{-9}	6.6×10^{-8}

Gene set over-representation analysis (hypergeometric test) for Reactome pathways in the top 500 “hub” genes with the most candidate synthetic lethal partners by SLIPT analysis of TCGA stomach expression data.

Appendix I

Replication in cell line encyclopaedia

Table I.1: Candidate synthetic lethal gene partners of *CDH1* from SLIPT in CCLE

Gene	Observed	Expected	χ^2 value	p-value	p-value (FDR)
<i>ZEB1</i>	24	115	555	7.84×10^{-119}	3.62×10^{-116}
<i>RP11-620J15.3</i>	17	115	471	1.54×10^{-100}	3.68×10^{-98}
<i>AP1S2</i>	20	115	462	1.38×10^{-98}	3.07×10^{-96}
<i>VIM</i>	24	115	424	1.73×10^{-90}	3.06×10^{-88}
<i>CCDC88A</i>	24	115	418	3.94×10^{-89}	6.86×10^{-87}
<i>RECK</i>	28	115	416	8.23×10^{-89}	1.42×10^{-86}
<i>AP1M1</i>	16	115	414	2.42×10^{-88}	4.06×10^{-86}
<i>ZEB2</i>	23	115	396	2.32×10^{-84}	3.4×10^{-82}
<i>WIPF1</i>	25	115	390	4.9×10^{-83}	6.74×10^{-81}
<i>SLC35B4</i>	29	115	386	3.2×10^{-82}	4.38×10^{-80}
<i>SACS</i>	28	115	373	2.13×10^{-79}	2.7×10^{-77}
<i>ST3GAL2</i>	25	115	351	9.7×10^{-75}	1.08×10^{-72}
<i>ATP8B2</i>	38	115	341	1.53×10^{-72}	1.61×10^{-70}
<i>IFFO1</i>	39	115	332	1.66×10^{-70}	1.65×10^{-68}
<i>EMP3</i>	38	115	329	5.04×10^{-70}	4.95×10^{-68}
<i>LEPRE1</i>	40	115	325	5.4×10^{-69}	5.22×10^{-67}
<i>STARD9</i>	39	115	311	4.52×10^{-66}	3.96×10^{-64}
<i>DENND5A</i>	48	115	304	1.89×10^{-64}	1.59×10^{-62}
<i>SYT11</i>	38	115	300	1.21×10^{-63}	9.89×10^{-62}
<i>EID2B</i>	38	115	299	1.99×10^{-63}	1.61×10^{-61}
<i>NXPE3</i>	35	115	294	1.71×10^{-62}	1.35×10^{-60}
<i>STX2</i>	49	115	293	3.83×10^{-62}	3×10^{-60}
<i>ARHGEF6</i>	43	115	289	2.2×10^{-61}	1.71×10^{-59}
<i>KATNAL1</i>	50	115	283	4.45×10^{-60}	3.38×10^{-58}
<i>ANXA6</i>	37	115	282	8.92×10^{-60}	6.67×10^{-58}

Strongest candidate SL partners for *CDH1* by SLIPT with observed and expected numbers of Cancer Cell Line Encyclopaedia (CCLE) samples with low expression of both genes.

Table I.2: Candidate synthetic lethal gene partners of *CDH1* from SLIPT in breast CCLE

Gene	Observed	Expected	χ^2 value	p-value	p-value (FDR)
<i>MIR155HG</i>	1	6.78	31.5	2.41×10^{-6}	0.00371
<i>ENPP2</i>	1	6.78	30.7	3.47×10^{-6}	0.00383
<i>DCLK2</i>	3	6.78	28.3	1.08×10^{-5}	0.0071
<i>PID1</i>	1	6.78	27.8	1.34×10^{-5}	0.00791
<i>SCFD2</i>	5	6.78	27.7	1.42×10^{-5}	0.00791
<i>FAT4</i>	4	6.78	27.3	1.69×10^{-5}	0.00865
<i>ILK</i>	1	6.78	26.9	2.04×10^{-5}	0.00884
<i>RWDD1</i>	0	6.78	26.8	2.15×10^{-5}	0.00884
<i>RIC8A</i>	2	6.78	26.8	2.2×10^{-5}	0.00884
<i>F2RL2</i>	1	6.78	26.6	2.34×10^{-5}	0.00901
<i>SDCBP</i>	5	6.78	25.9	3.26×10^{-5}	0.0108
<i>PPM1F</i>	4	6.78	25.8	3.41×10^{-5}	0.0108
<i>IKBIP</i>	5	6.78	25.8	3.49×10^{-5}	0.0108
<i>SPRED1</i>	3	6.78	25.5	3.97×10^{-5}	0.0108
<i>RNH1</i>	1	6.78	25.4	4.22×10^{-5}	0.0108
<i>SYDE1</i>	3	6.78	25.4	4.22×10^{-5}	0.0108
<i>LINC00968</i>	1	6.78	25.2	4.63×10^{-5}	0.0109
<i>ARHGEF10</i>	5	6.78	24.5	6.22×10^{-5}	0.0116
<i>P4HA1</i>	0	6.78	24.5	6.34×10^{-5}	0.0116
<i>AZI2</i>	2	6.78	24.5	6.34×10^{-5}	0.0116
<i>TNFAIP6</i>	2	6.78	24.5	6.34×10^{-5}	0.0116
<i>CD200</i>	4	6.78	24.5	6.37×10^{-5}	0.0116
<i>SMPD1</i>	1	6.78	24.4	6.67×10^{-5}	0.0116
<i>ATP6V1G2</i>	3	6.78	24.2	7.33×10^{-5}	0.0123
<i>FGF2</i>	4	6.78	24.1	7.49×10^{-5}	0.0123

Strongest candidate SL partners for *CDH1* by SLIPT with observed and expected numbers of CCLE breast samples with low expression of both genes.

Table I.3: Candidate synthetic lethal gene partners of *CDH1* from SLIPT in stomach CCLE

Gene	Observed	Expected	χ^2 value	p-value	p-value (FDR)
<i>ZEB1</i>	1	4.45	36	2.84×10^{-7}	0.00175
<i>WDR47</i>	0	4.45	26.7	2.3×10^{-5}	0.013
<i>KANK2</i>	1	4.45	25.1	4.81×10^{-5}	0.0222
<i>LEPRE1</i>	0	4.45	24.5	6.26×10^{-5}	0.0228
<i>KATNAL1</i>	0	4.45	24.3	6.88×10^{-5}	0.0231
<i>TET1</i>	0	4.45	23.9	8.23×10^{-5}	0.0249
<i>AP1S2</i>	1	4.45	23.1	0.00012	0.0273
<i>CDKN2C</i>	1	4.45	22.8	0.000136	0.0292
<i>ARMC4</i>	1	4.45	22.4	0.000164	0.0315
<i>CSTF3</i>	1	4.45	22.4	0.000166	0.0315
<i>FAM216A</i>	1	4.45	22.4	0.000166	0.0315
<i>ANKRD32</i>	1	4.45	22.4	0.000166	0.0315
<i>WDR35</i>	1	4.45	22.4	0.000169	0.0315
<i>ECI2</i>	0	4.45	21.7	0.000232	0.0378
<i>SAMD8</i>	0	4.45	21.7	0.000232	0.0378
<i>CHST12</i>	0	4.45	21.7	0.000232	0.0378
<i>RPL23AP32</i>	0	4.45	21.7	0.000232	0.0378
<i>STARD9</i>	1	4.45	21.7	0.000232	0.0378
<i>MCM8</i>	0	4.45	21.5	0.000255	0.0379

Strongest candidate SL partners for *CDH1* by SLIPT with observed and expected numbers of CCLE stomach samples with low expression of both genes.

Table I.4: Pathways for *CDH1* partners from SLIPT in stomach CCLE

Pathways Over-represented	Pathway Size	SL Genes	p-value (FDR)
Nef mediated downregulation of MHC class I complex cell surface expression	10	1	1
Unwinding of DNA	11	1	1
Processing of Intronless Pre-mRNAs	13	1	1
E2F mediated regulation of DNA replication	20	1	1
Chondroitin sulfate biosynthesis	20	1	1
Post-Elongation Processing of Intronless pre-mRNA	21	1	1
Nef-mediates down modulation of cell surface receptors by recruiting them to clathrin adapters	21	1	1
Processing of Capped Intronless Pre-mRNA	21	1	1
Post-Elongation Processing of Intron-Containing pre-mRNA	23	1	1
Activation of the pre-replicative complex	23	1	1
mRNA 3'-end processing	23	1	1
Golgi Associated Vesicle Biogenesis	24	1	1
Lysosome Vesicle Biogenesis	25	1	1
Oncogene Induced Senescence	27	1	1
The role of Nef in HIV-1 replication and disease pathogenesis	28	1	1
Cyclin D associated events in G1	29	1	1
G1 Phase	29	1	1
Cleavage of Growing Transcript in the Termination Region	31	1	1
Activation of ATR in response to replication stress	31	1	1
DNA strand elongation	31	1	1

Gene set over-representation analysis (hypergeometric test) for Reactome pathways in SLIPT partners for *CDH1*.

Table I.5: Pathways for *CDH1* partners from SLIPT in breast and stomach CCLE

Pathways Over-represented	Pathway Size	SL Genes	p-value (FDR)
Collagen formation	66	8	1.1×10^{-7}
Glycosaminoglycan metabolism	111	11	1.1×10^{-7}
Extracellular matrix organization	236	20	1.1×10^{-7}
Collagen biosynthesis and modifying enzymes	55	7	1.7×10^{-7}
Keratan sulfate biosynthesis	28	5	2.2×10^{-7}
Keratan sulfate/keratin metabolism	32	5	7.5×10^{-7}
ECM proteoglycans	65	7	1.1×10^{-6}
Non-integrin membrane-ECM interactions	52	6	2.0×10^{-6}
Cell junction organization	71	7	3.0×10^{-6}
Assembly of collagen fibrils and other multimeric structures	39	5	3.6×10^{-6}
Post-chaperonin tubulin folding pathway	14	3	1.7×10^{-5}
Adherens junctions interactions	29	4	1.7×10^{-5}
Cell-Cell communication	118	9	1.7×10^{-5}
Sialic acid metabolism	31	4	2.5×10^{-5}
Synthesis and interconversion of nucleotide di- and triphosphates	16	3	3.1×10^{-5}
Transport to the Golgi and subsequent modification	34	4	4.8×10^{-5}
Asparagine N-linked glycosylation	113	8	7.8×10^{-5}
Elastic fibre formation	37	4	8.5×10^{-5}
L1CAM interactions	77	6	9.5×10^{-5}
Signal transduction by L1	20	3	9.5×10^{-5}

Gene set over-representation analysis (hypergeometric test) for Reactome pathways in SLIPT partners for *CDH1*.

Appendix J

Synthetic Lethal Genes in Pathways

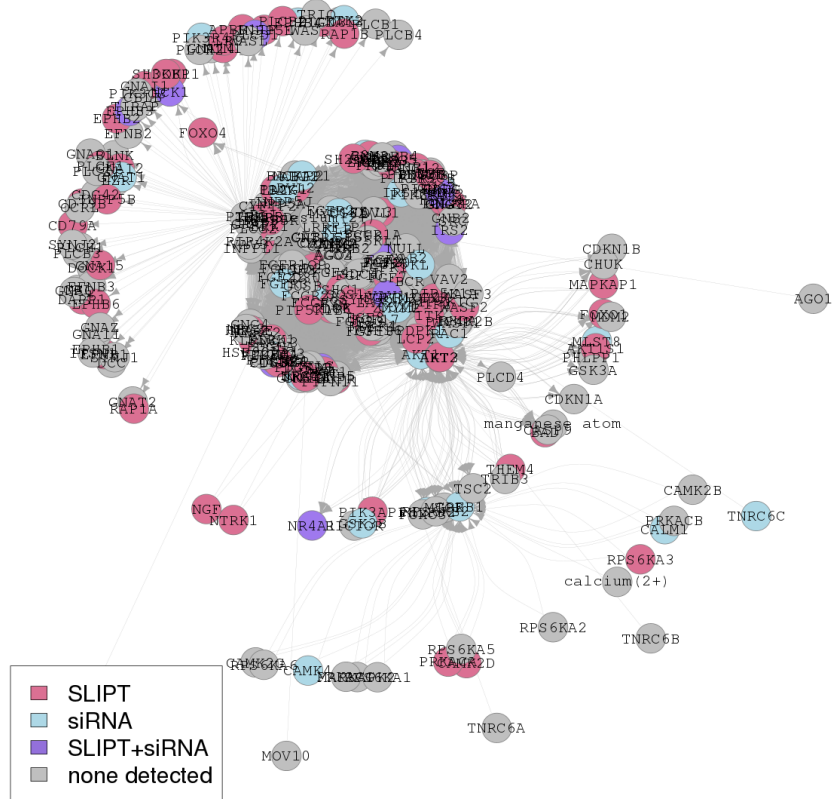


Figure J.1: **Synthetic Lethality in the PI3K/AKT Pathway.** The Reactome PI3K/AKT pathway with synthetic lethal candidates coloured as shown in the legend.

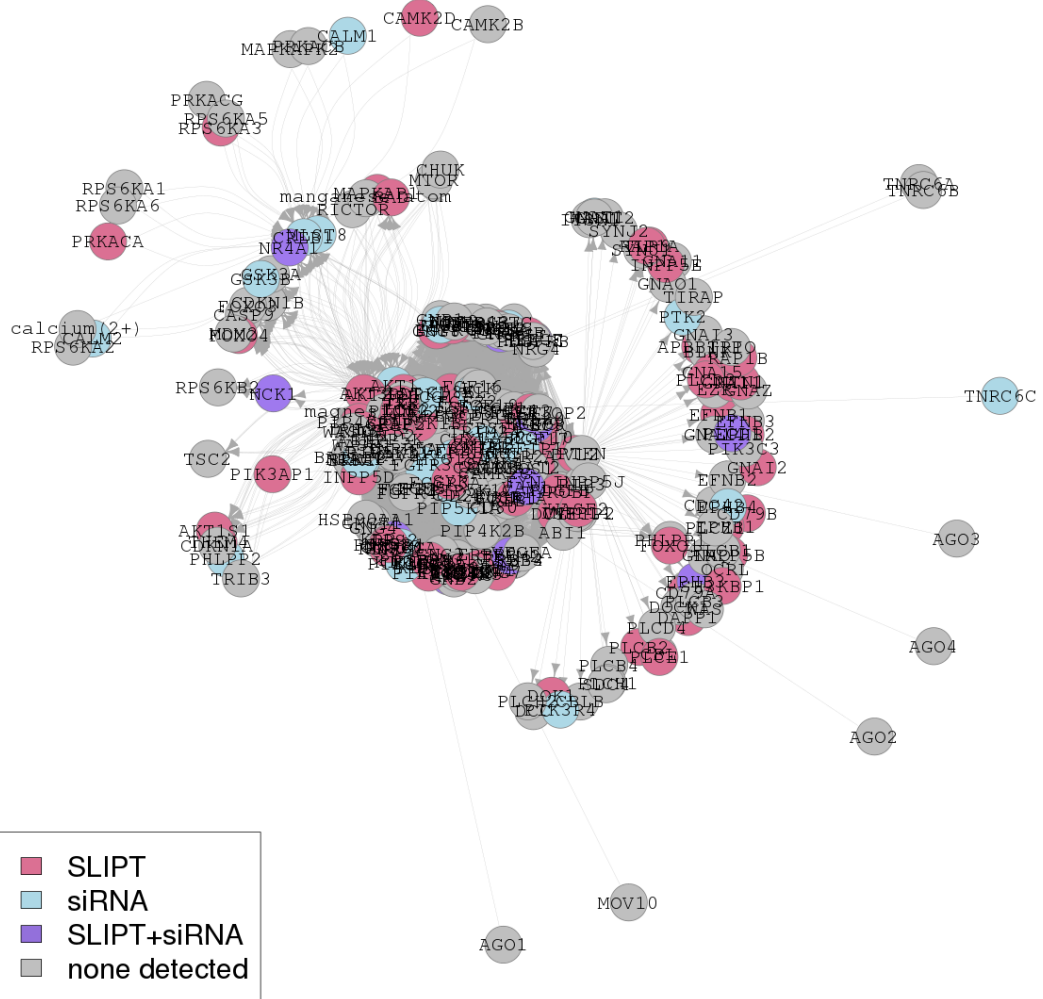


Figure J.2: Synthetic Lethality in the PI3K/AKT Pathway in Cancer. The Reactome PI3K/AKT Pathway in Cancer pathway with synthetic lethal candidates coloured as shown in the legend.

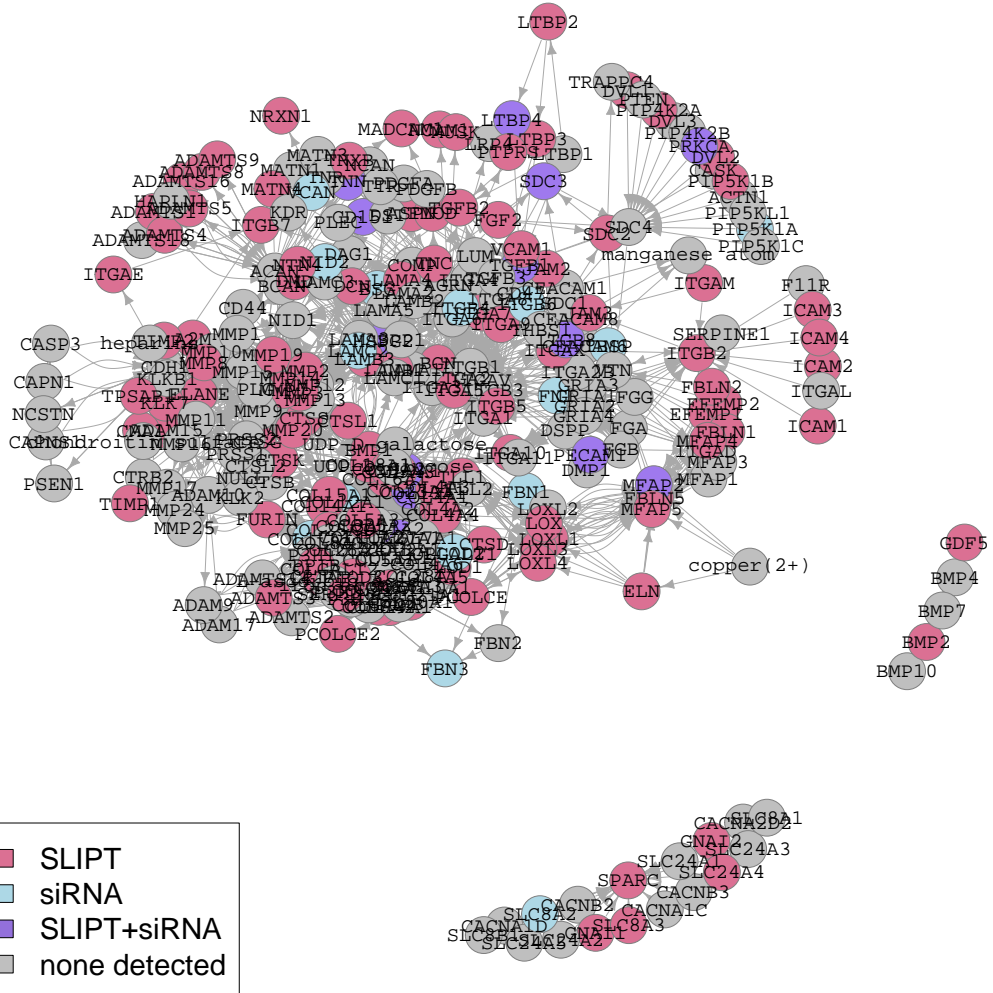


Figure J.3: **Synthetic Lethality in the Extracellular Matrix.** The Reactome Extracellular Matrix pathway with synthetic lethal candidates coloured as shown in the legend.

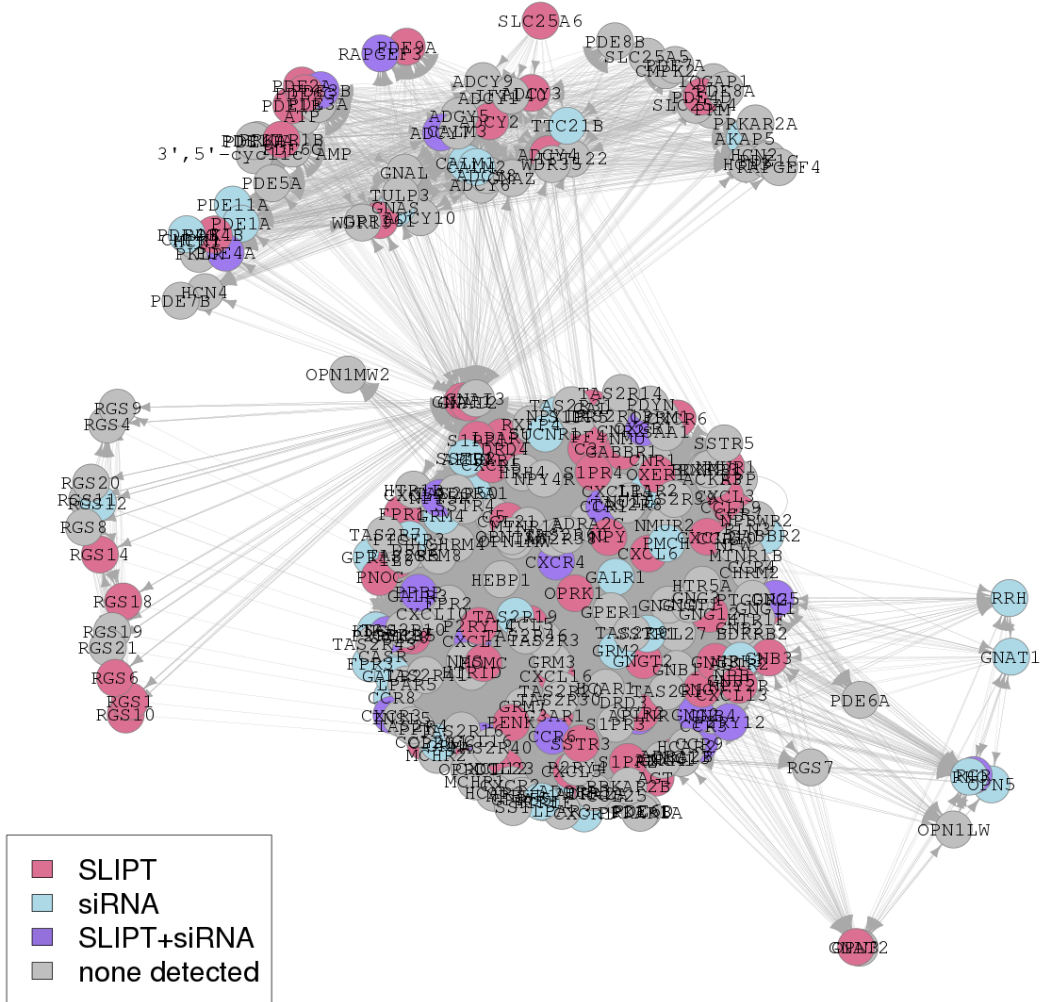


Figure J.4: Synthetic Lethality in the GPCRs. The Reactome $G_{\alpha i}$ pathway with synthetic lethal candidates coloured as shown in the legend.

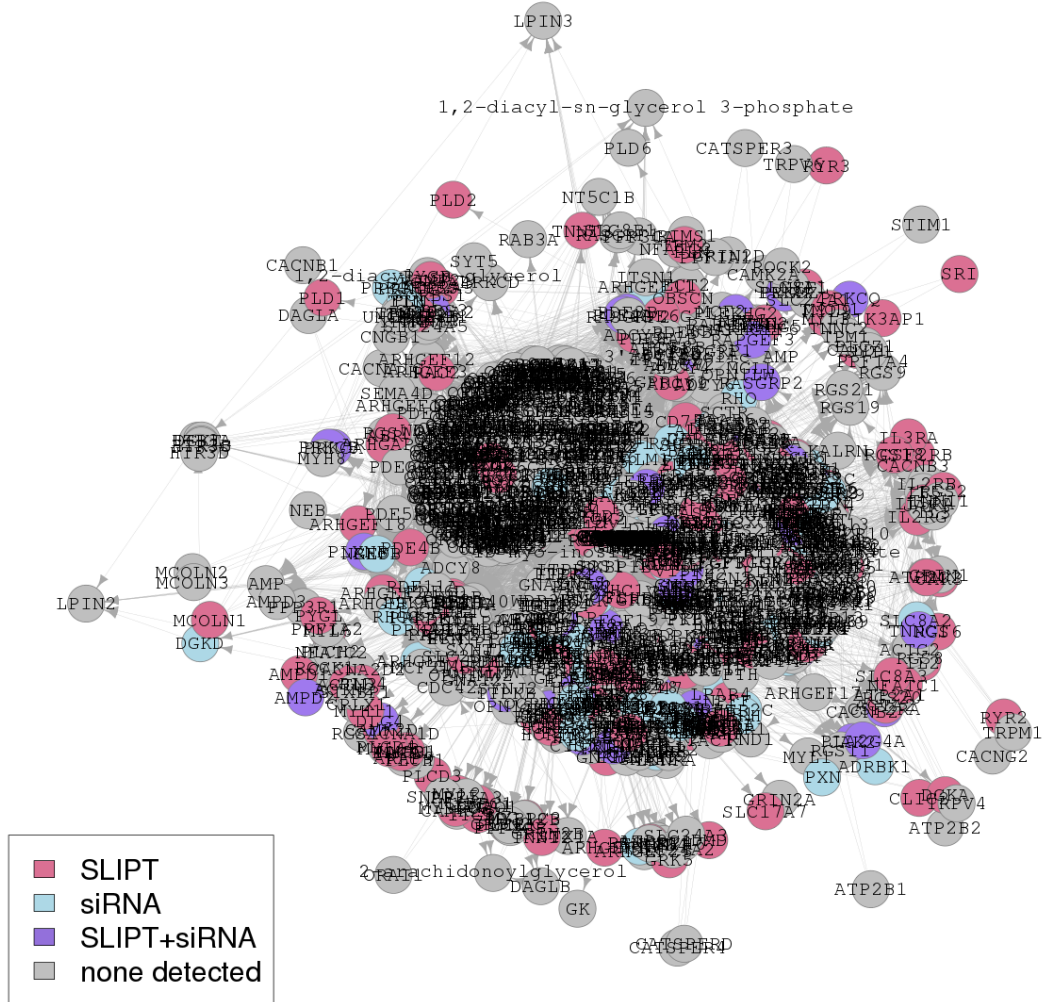


Figure J.5: **Synthetic Lethality in the GPCR Downstream.** The Reactome GPCR Downstream pathway with synthetic lethal candidates coloured as shown in the legend.

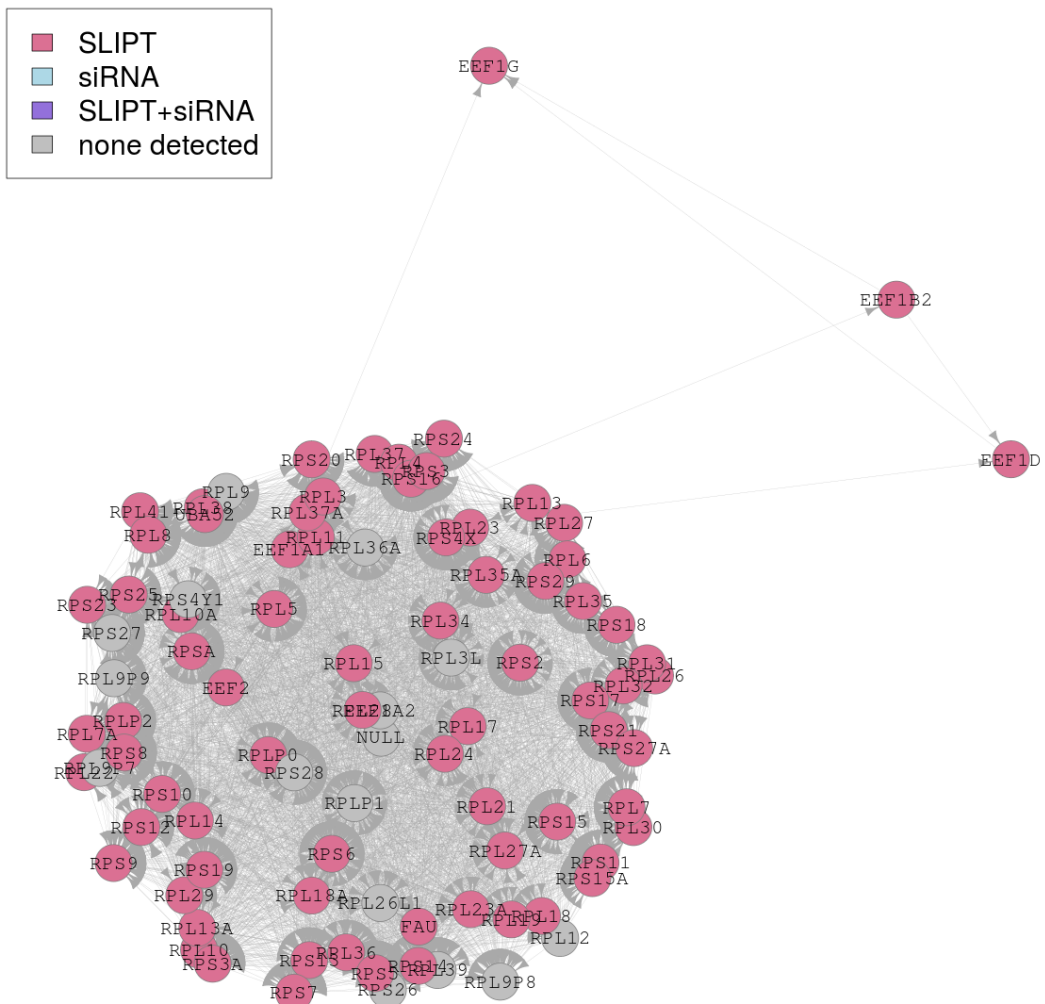


Figure J.6: **Synthetic Lethality in the Translation Elongation.** The Reactome Translation Elongation pathway with synthetic lethal candidates coloured as shown in the legend.

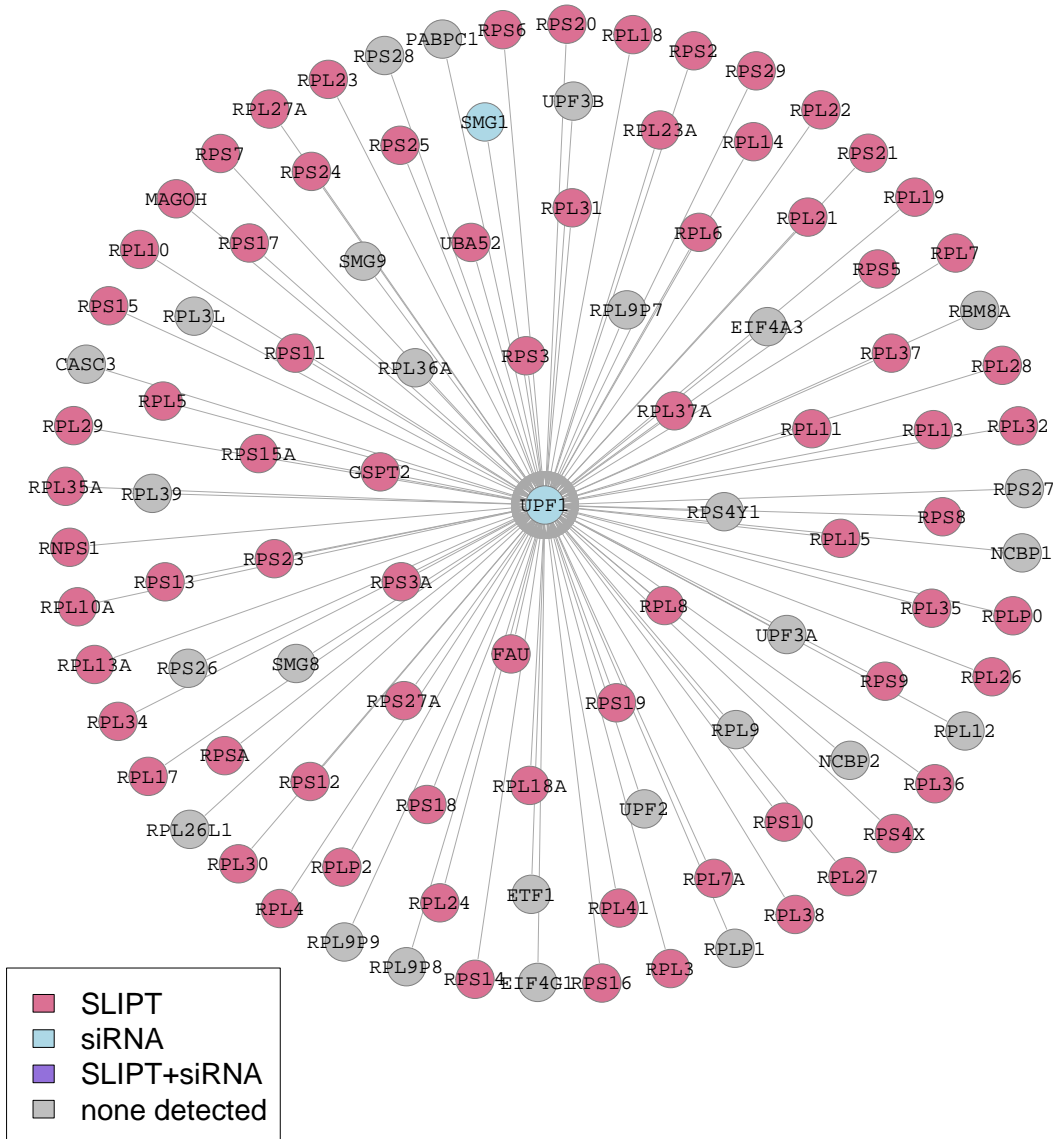


Figure J.7: Synthetic Lethality in the Nonsense-mediated Decay. The Reactome Nonsense-mediated Decay pathway with synthetic lethal candidates coloured as shown in the legend.

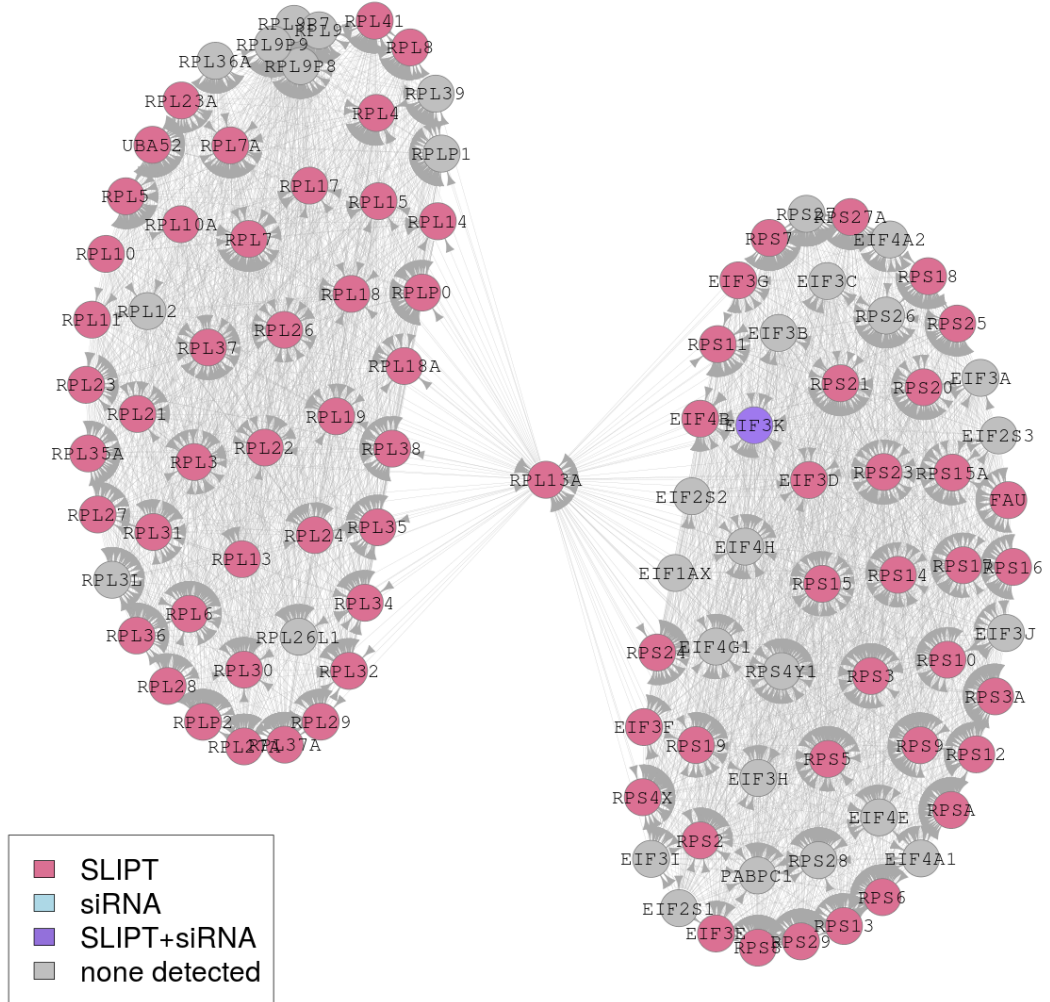


Figure J.8: **Synthetic Lethality in the 3' UTR.** The Reactome 3' UTR pathway with synthetic lethal candidates coloured as shown in the legend.

Appendix K

Pathway Connectivity for Mutation SLIPT

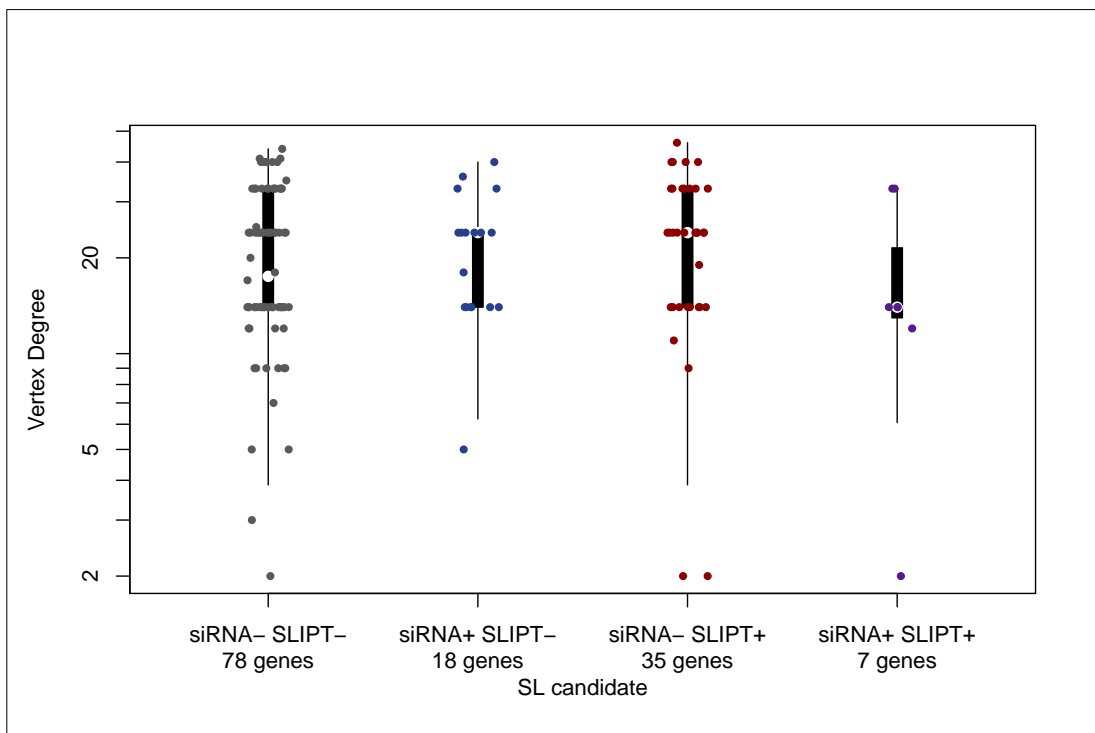


Figure K.1: **Synthetic Lethality and Vertex Degree.** The number of connected genes (vertex degree) was compared (on a log-scale across genes detected by mtSLIPT and short interfering ribonucleic acid (siRNA) screening in the Reactome PI3K cascade pathway. There were very few differences in vertex degree between the groups, although genes detected by siRNA included those with the fewest connections.

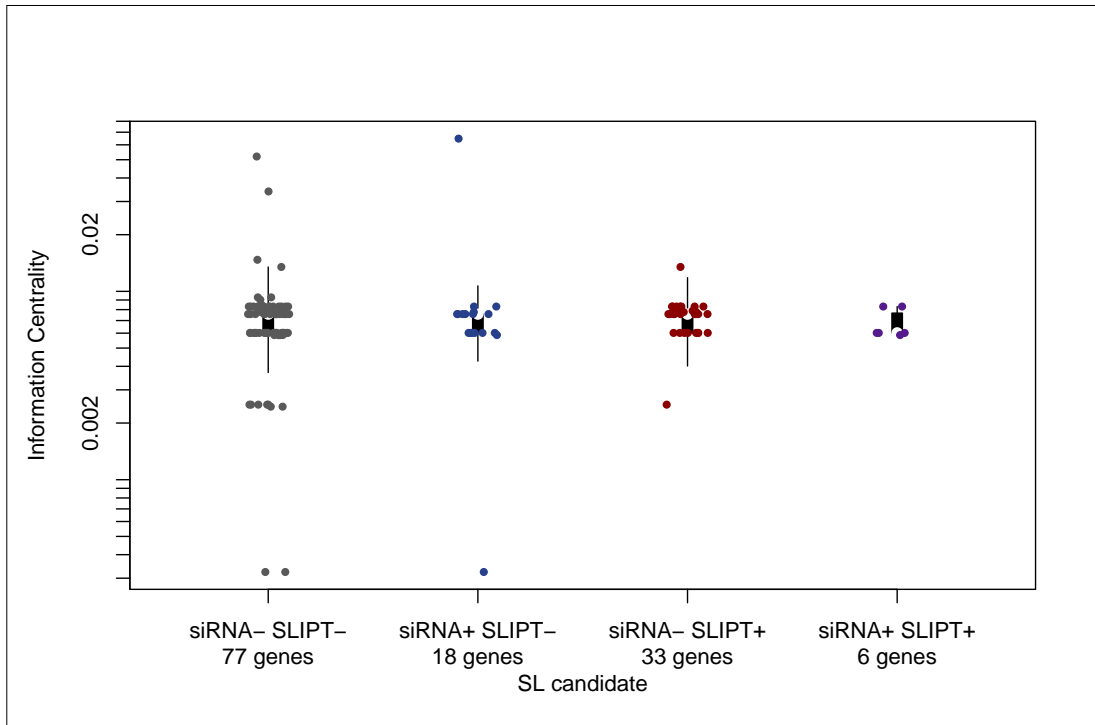


Figure K.2: Synthetic Lethality and Centrality. The information centrality was compared (on a log-scale across genes detected by mtSLIPT and siRNA screening in the Reactome PI3K cascade pathway. Genes detected by mtSLIPT or siRNA did not have higher connectivity than genes not detected by either approach. The gene with the highest centrality was detected by siRNA.

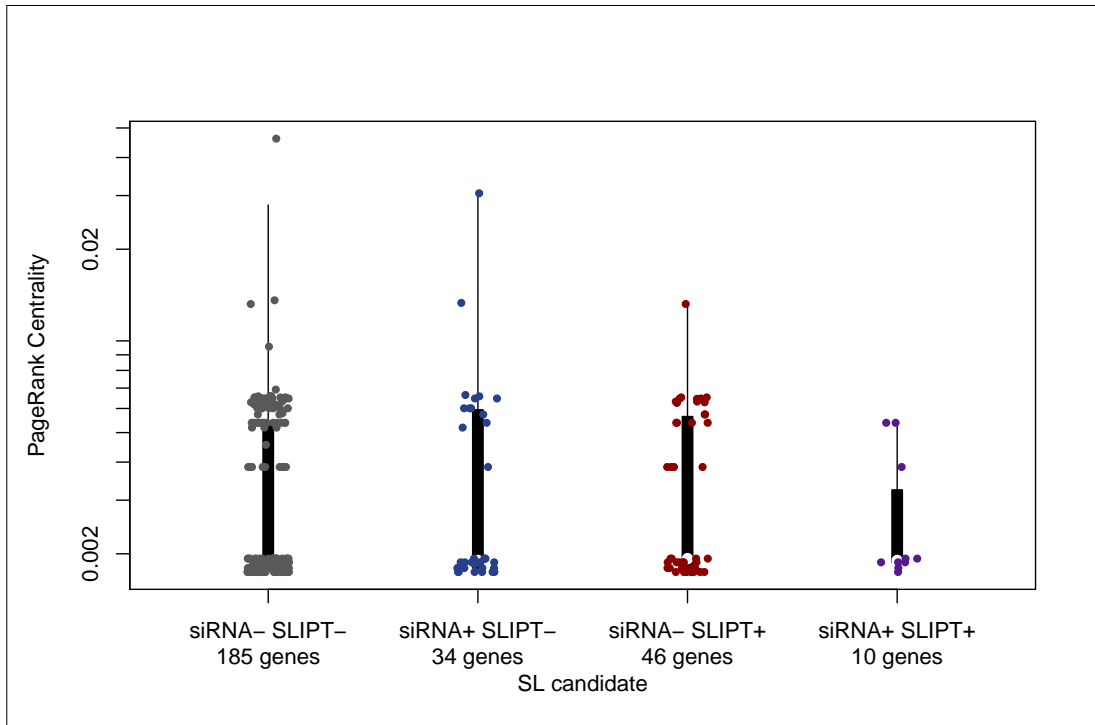


Figure K.3: Synthetic Lethality and PageRank. The PageRank centrality was compared (on a log-scale across genes detected by mtSLIPT and siRNA screening in the Reactome PI3K cascade pathway. Genes detected by siRNA had a more restricted range of centrality values than other genes not detected by either approach, although these groups also had fewer genes.

Table K.1: ANOVA for Synthetic Lethality and Vertex Degree

	DF	Sum Squares	Mean Squares	F-value	p-value
siRNA	1	15	15.50	0.0134	0.9084
mtSLIPT	1	196	195.94	0.1689	0.6825
siRNA×mtSLIPT	1	9	9.17	0.0079	0.9294

Analysis of variance for vertex degree against synthetic lethal detection approaches (with an interaction term)

Table K.2: ANOVA for Synthetic Lethality and Information Centrality

	DF	Sum Squares	Mean Squares	F-value	p-value
siRNA	1	0.000256	0.0002561	0.1851	0.6685
mtSLIPT	1	0.003225	0.0032247	2.3308	0.1318
siRNA×mtSLIPT	1	0.001238	0.0012385	0.8952	0.3476

Analysis of variance for information centrality against synthetic lethal detection approaches (with an interaction term)

Table K.3: ANOVA for Synthetic Lethality and PageRank Centrality

	DF	Sum Squares	Mean Squares	F-value	p-value
siRNA	1	0.0002038	2.0385×10^{-4}	1.1423	0.2892
mtSLIPT	1	0.0000208	2.0752×10^{-5}	0.1163	0.7342
siRNA×mtSLIPT	1	0.0000137	1.3743×10^{-5}	0.0770	0.7823

Analysis of variance for PageRank centrality against synthetic lethal detection approaches (with an interaction term)

Appendix L

Information Centrality for Gene Essentiality

Network structure is another useful strategy to analyse gene function and this has been used to investigate network properties of a network constructed from of Reactome pathways imported via Pathway Commons with Paxtools (Cerami *et al.*, 2011; Demir *et al.*, 2013). Most notably, information centrality which has been proposed as a measure of gene essentiality was calculated as performed by Kranthi *et al.* (2013) using the efficiency and shortest path between each pair of nodes in the network before and after a node of interest is removed to test the importance of a node to network connectivity. Reactome contains substrates and cofactors in addition to genes or proteins. In support of centrality as a measure of essentiality, a number of nodes with the highest centrality (shown in Table L.1) were essential nutrients including Mg²⁺, Ca²⁺, Zn²⁺, and Fe. In addition, there were genes important in development of epithelial tissues and breast cancer such as *IL8*, *GATA3*, and *CTNNB1* detected with relatively high information centrality.

Table L.1: Information centrality for genes and molecules in the Reactome network

Node	Centrality
<i>ZNF473</i>	0.0510
magnesium(2+)	0.0082
<i>XBP1</i>	0.0053
calcium(2+)	0.0050
zinc(2+)	0.0048
iron atom	0.0041
<i>FMN</i>	0.0040
<i>AGT</i>	0.0037
<i>HSP90AA1</i>	0.0029
phosphatidyl-L-serine	0.0029
<i>P2RX7</i>	0.0026
<i>PANX1</i>	0.0024
<i>NCAM1</i>	0.0022
<i>NUDT1</i>	0.0021
<i>PLAUR</i>	0.0020
<i>IL8</i>	0.0020
<i>HSPA8</i>	0.0019
<i>TYROBP</i>	0.0019
<i>CASP3</i>	0.0017
<i>GNAL</i>	0.0015
<i>CBLB</i>	0.0015
<i>HBB</i>	0.0014
<i>GATA4</i>	0.0013
<i>TGS1</i>	0.0013
<i>CTNNB1</i>	0.0012

Highest information centrality for genes (proteins), cofactors, and minerals in the Reactome network

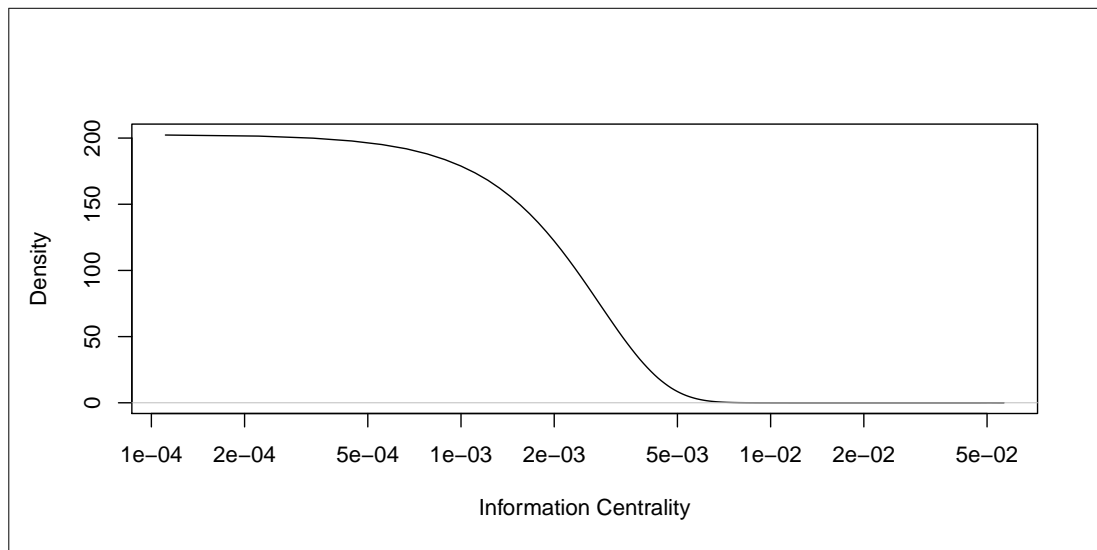


Figure L.1: **Information centrality distribution.** Information centrality in the Reactome network for nodes, including genes/proteins and other biomolecules.

Appendix M

Pathway Structure for Mutation SLIPT

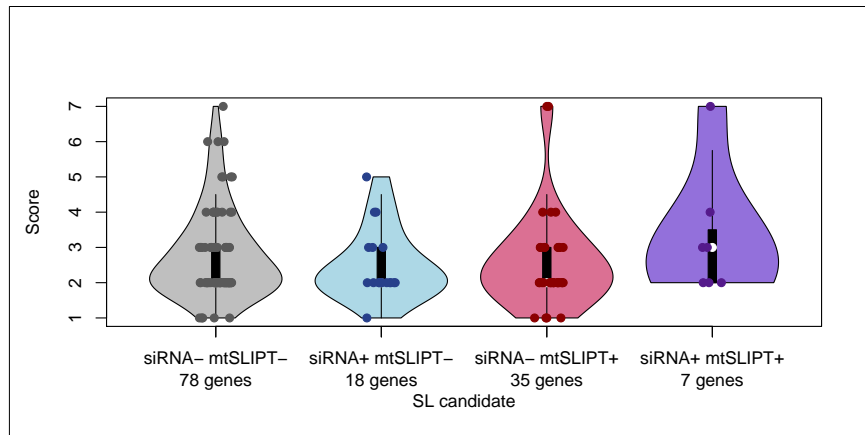


Figure M.1: **Synthetic Lethality and Heirarchy Score in PI3K.** The hierarchical distance scores were similarly distributed across mtSLIPT and siRNA genes. Genes detected by both methods had a higher (downstream) median than either group.

Table M.1: ANOVA for Synthetic Lethality and PI3K Hierarchy

	DF	Sum Squares	Mean Squares	F-value	p-value
siRNA	1	0.001	0.00070	0.0004	0.9841
mtSLIPT	1	0.007	0.0066	0.0040	0.9496
siRNA×mtSLIPT	1	3.906	3.9056	2.3829	0.1250

Analysis of variance for PI3K hierarchy score against synthetic lethal detection approaches (with an interaction term)

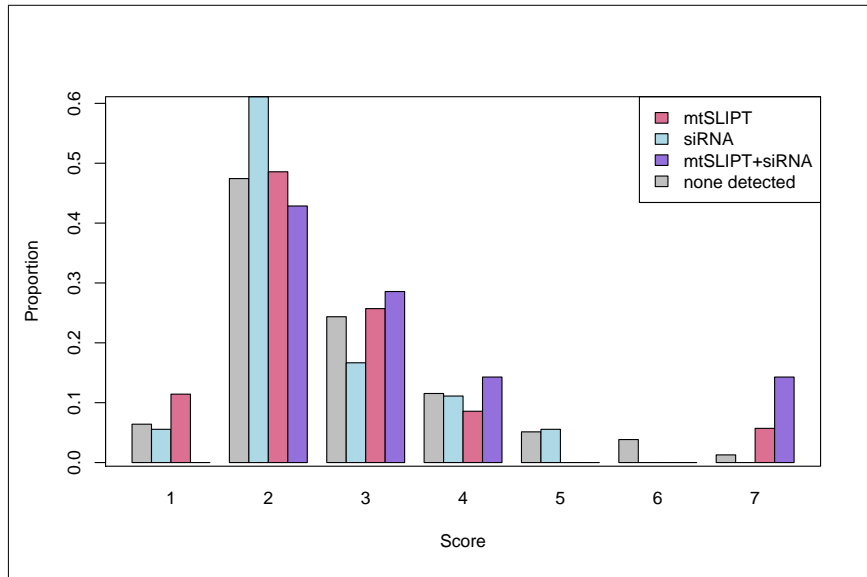


Figure M.2: **Hierarchy Score in PI3K against Synthetic Lethality in PI3K.** The number of mtSLIPT and siRNA genes against the hierarchical distance scores showing no significant tendency for either method to either of the pathway upstream or downstream extremities.

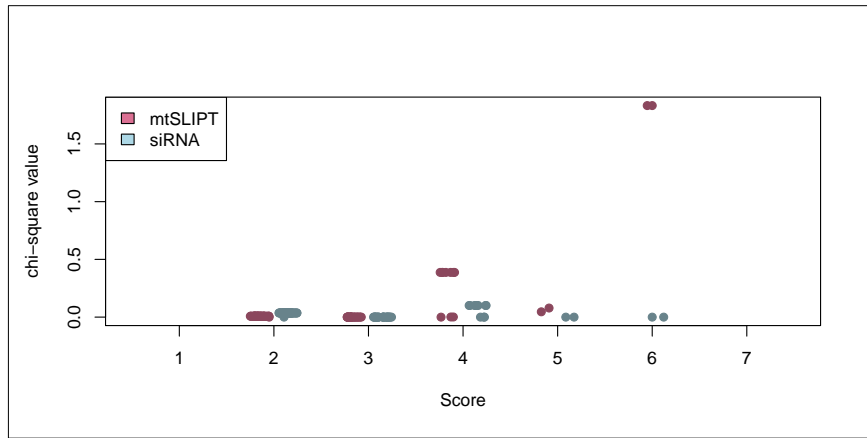


Figure M.3: **Structure of Synthetic Lethality in PI3K.** The number of mtSLIPT and siRNA genes against the hierarchical distance scores showing no significant tendency for either method to either of the pathway upstream or downstream extremities. The number of mtSLIPT and siRNA genes upstream or downstream of each gene in the Reactome PI3K pathway were tested (by the χ^2 -test). These are plotted as a split jitter stripchart against the hierarchical distance scores showing no significant tendency for either method to either of the pathway upstream or downstream extremities.

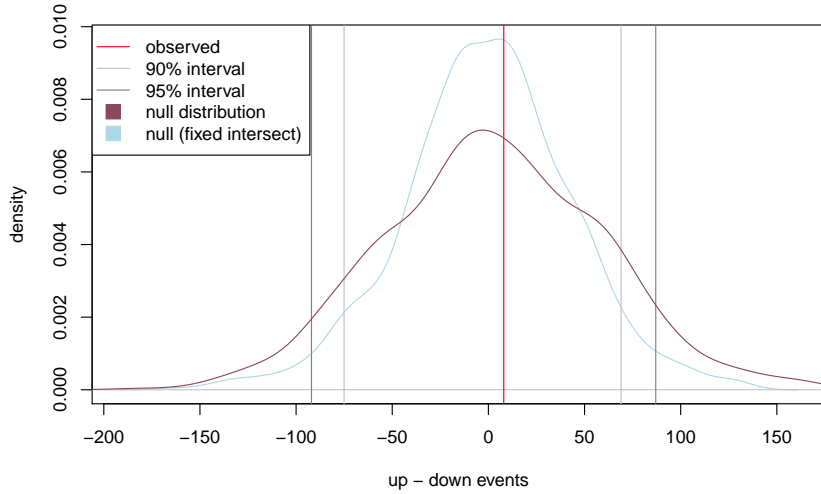


Figure M.4: Structure of Synthetic Lethality Resampling. A null distribution (10,000 iterations) of the siRNA genes upstream or downstream of mtSLIPT genes (shown by the difference) in the PI3K pathway. The observed events (red) were compared to the the distribution (violet) and were not significant. Genes detected by both methods were fixed for the distribution (blue). The genes detected by both approaches were used.

Table M.2: Resampling for pathway structure of synthetic lethal detection methods

Pathway	Graph		States		Observed				Permutation p-value	
	Nodes	Edges	mtSL	siRNA	Up	Down	Up-Down	Up/Down	Up-Down	Down-Up
PI3K Cascade	138	1495	42	25	131	123	8	1.065	0.4473	0.5466
PI3K/AKT Signalling in Cancer	275	12882	56	44	478	440	38	1.086	0.4163	0.5810
G_{αi} Signalling	292	22003	57	58	543	866	-323	0.627	0.9507	0.0488
GPCR downstream	1270	142071	218	160	7632	6500	1132	1.174	0.1707	0.8291
Elastic fibre formation	42	175	16	7	6	7	-1	0.857	0.5512	0.3681
Extracellular matrix	299	3677	81	29	313	347	-34	0.902	0.5762	0.4215
Formation of Fibrin	52	243	11	5	8	19	-11	0.421	0.7993	0.1800
Nonsense-Mediated Decay	103	102	56	2	0	0	0		0.197	0.1373
3'-UTR-mediated translational regulation	107	2860	56	1	52	1	51	52	0.1210	0.8751
Eukaryotic Translation Elongation	92	3746	57	0	0	0	0		0.4952	0.4892

Pathways in the Reactome network tested for structural relationships between mtSLIPT and siRNA genes by resampling. The raw p-value (computed without adjusting for multiple comparisons over pathways) is given for the difference in upstream and downstream paths from mtSLIPT to siRNA gene candidate partners of CDH1 with significant pathways highlighted in bold. Sampling was performed only in the target pathway and shortest paths were computed within it. Loops or paths in either direction that could not be resolved were excluded from the analysis. The gene detected by both mtSLIPT and siRNA (or resampling for them) were included in the analysis and the number of these were fixed to the number observed.

Appendix N

Performance of SLIPT and χ^2

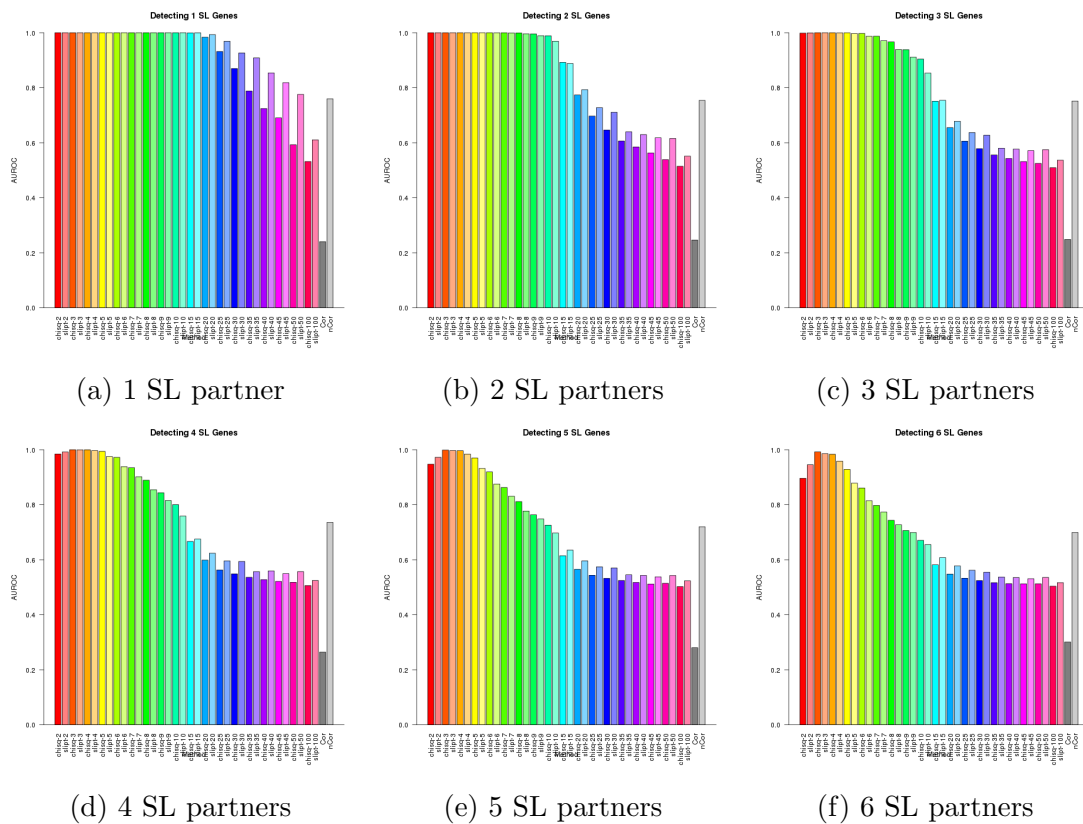


Figure N.1: Performance of χ^2 and SLIPT across quantiles. (continued on next page)

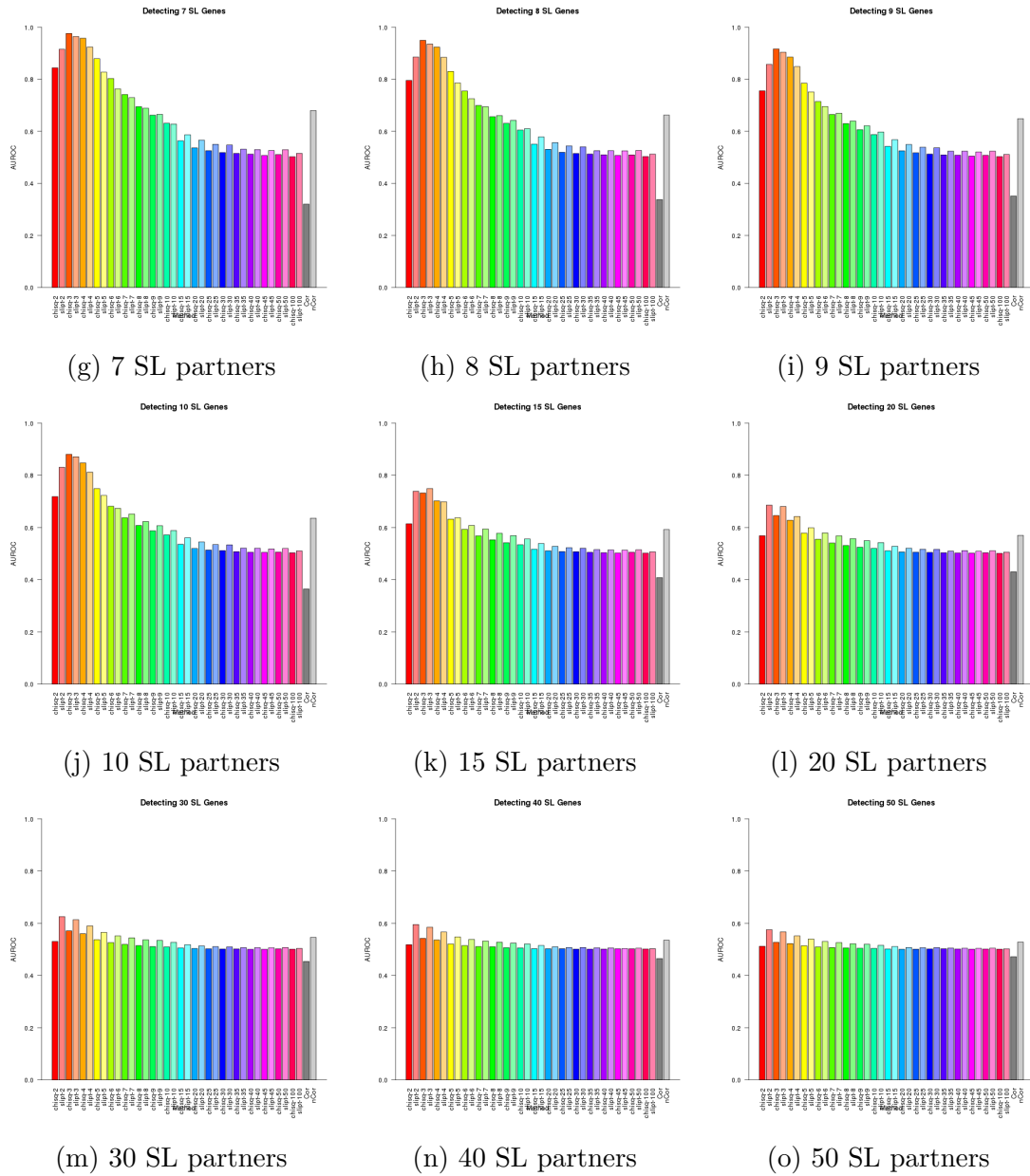


Figure N.1: Performance of χ^2 and SLIPT across quantiles. Synthetic lethal detection with quantiles as in axis labels. The barplot uses the same hues for each quantile (grey for correlation) and darker for χ^2 (and positive correlation). Synthetic Lethal Interaction Prediction Tool (SLIPT) and χ^2 perform similarly, peaking at $\frac{1}{3}$ -quantiles and converging to random (0.5). Negative correlation was higher than positive but not optimal quantiles for SLIPT or χ^2 . These findings are robust across different numbers of underlying synthetic lethal genes in 10,000 simulations of 100 genes and 1000 samples. SLIPT performs better than χ^2 for higher numbers of synthetic lethal genes and finer quantiles.

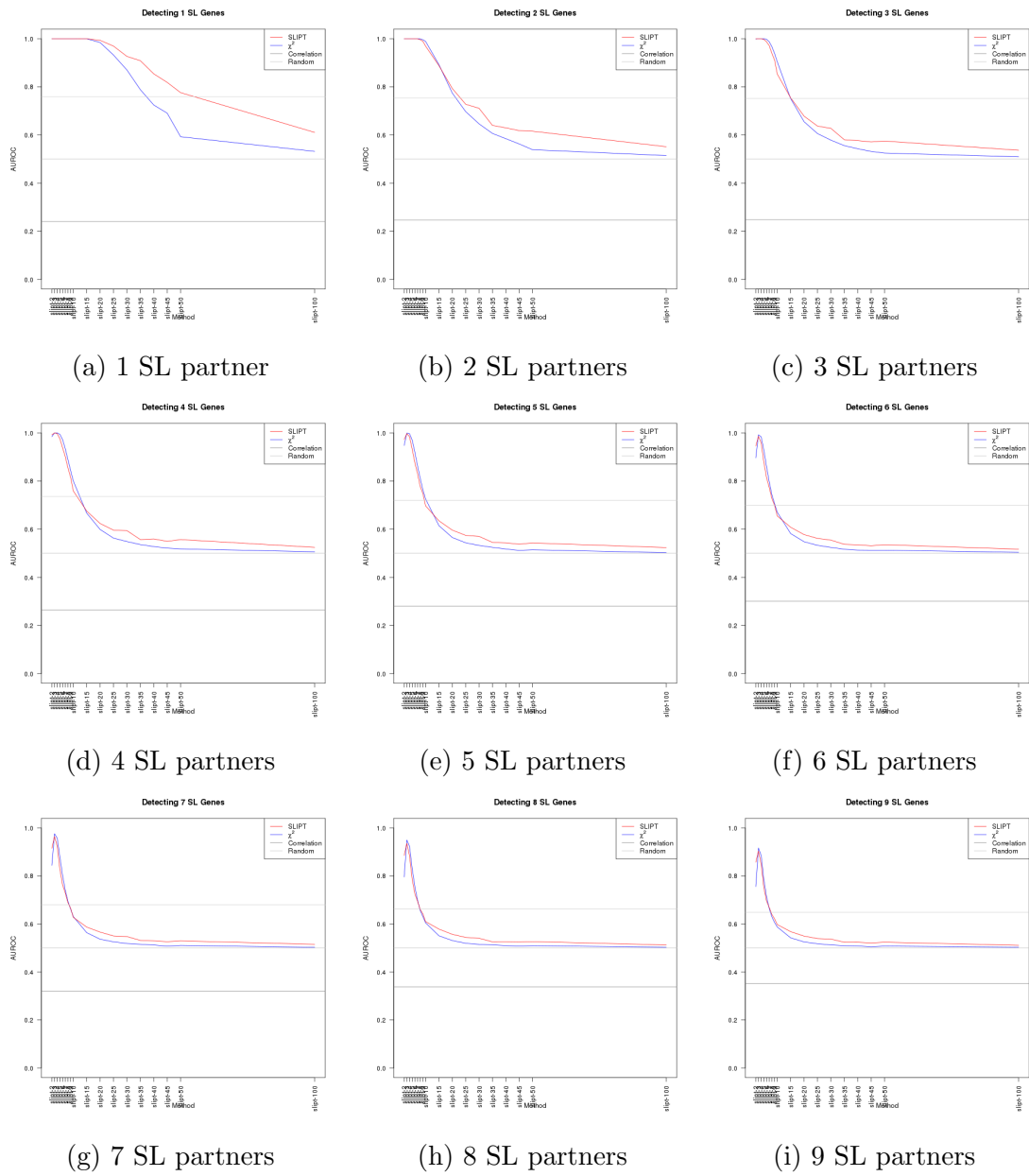


Figure N.2: **Performance of χ^2 and SLIPT across quantiles.** (continued on next page)

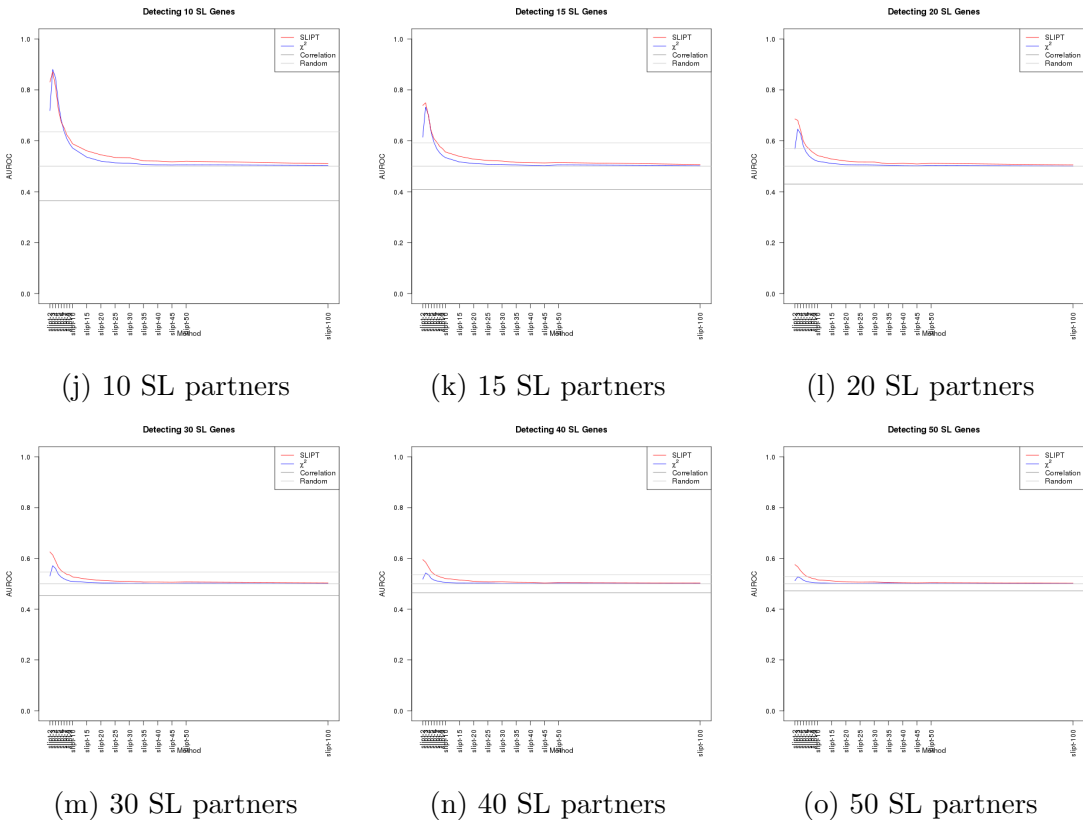


Figure N.2: Performance of χ^2 and SLIPT across quantiles. Synthetic lethal detection with quantiles as in axis labels. The line plots are coloured for SLIPT (red), χ^2 (blue) and correlation (grey) according to the legend. SLIPT and χ^2 perform similarly, peaking at $\frac{1}{3}$ -quantiles and converging to random (0.5). Negative correlation was higher than positive but not optimal quantiles for SLIPT or χ^2 . These findings are robust across different numbers of underlying synthetic lethal genes in 10,000 simulations of 100 genes and 1000 samples. SLIPT performs better than χ^2 for higher numbers of synthetic lethal genes and finer quantiles.

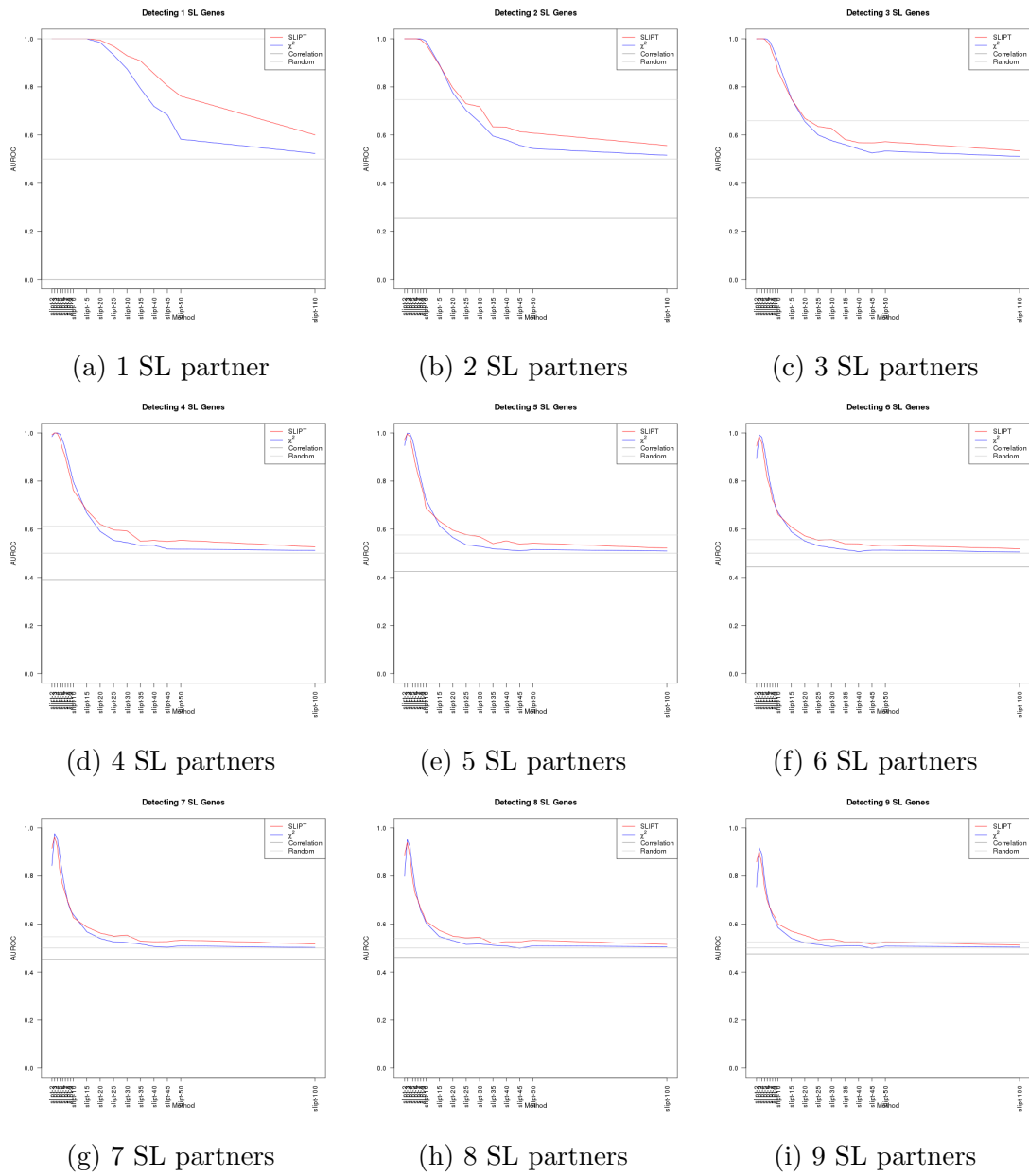


Figure N.3: **Performance of χ^2 and SLIPT across quantiles with more genes.**
 (continued on next page)

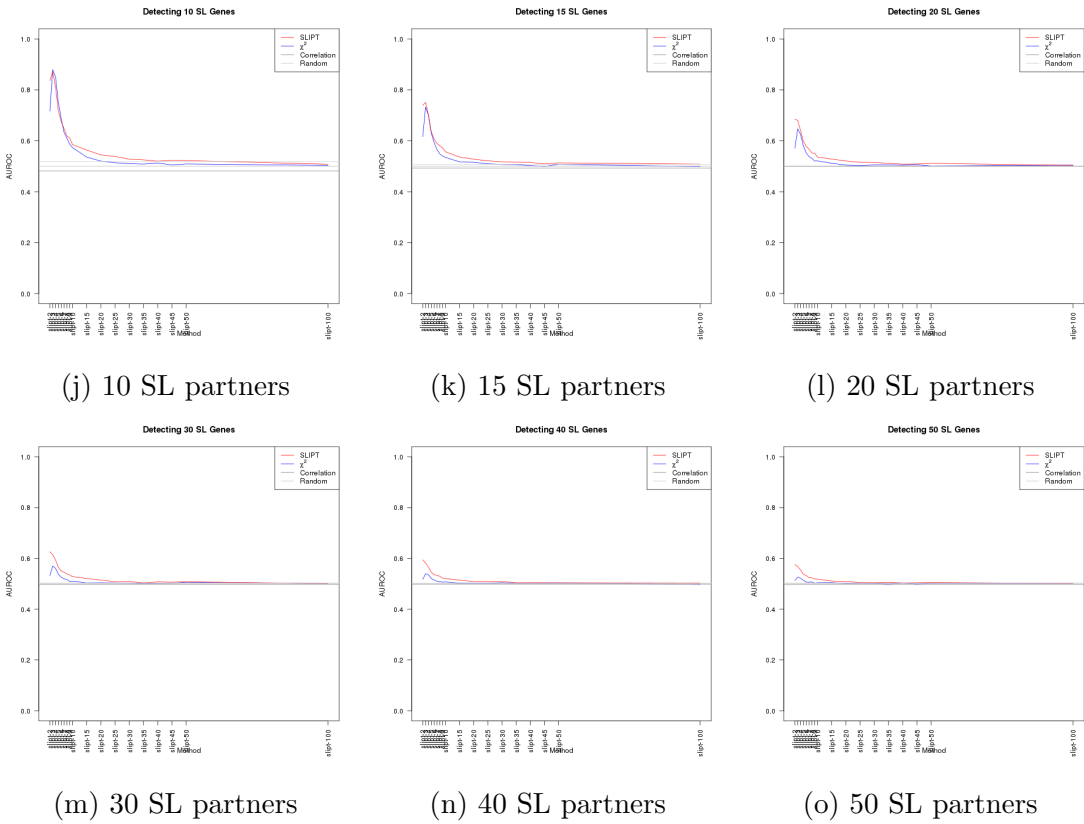


Figure N.3: Performance of χ^2 and SLIPT across quantiles with more genes.
 Synthetic lethal detection with quantiles as in axis labels. The line plots are coloured for SLIPT (red), χ^2 (blue) and correlation (grey) according to the legend. SLIPT and χ^2 perform similarly, peaking at $\frac{1}{3}$ -quantiles and converging to random (0.5). Negative correlation was higher than positive but not optimal quantiles for SLIPT or χ^2 . These findings are robust across different numbers of underlying synthetic lethal genes in 1000 simulations of 20,000 genes and 1000 samples. SLIPT performs better than χ^2 for higher numbers of synthetic lethal genes and finer quantiles.

N.0.1 Correlated Query Genes affects Specificity

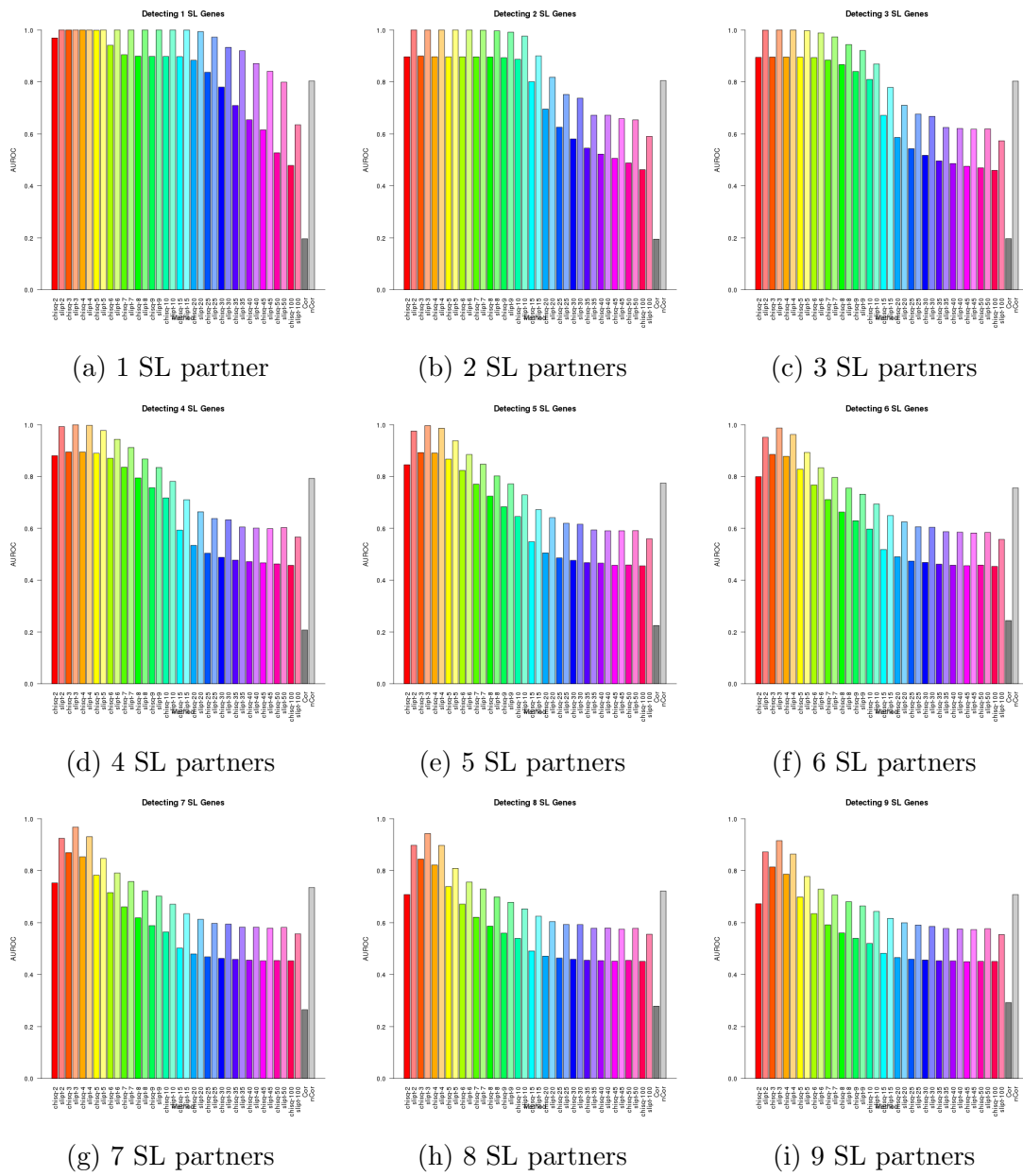


Figure N.4: **Performance of χ^2 and SLIPT across quantiles with query correlation.** (continued on next page)

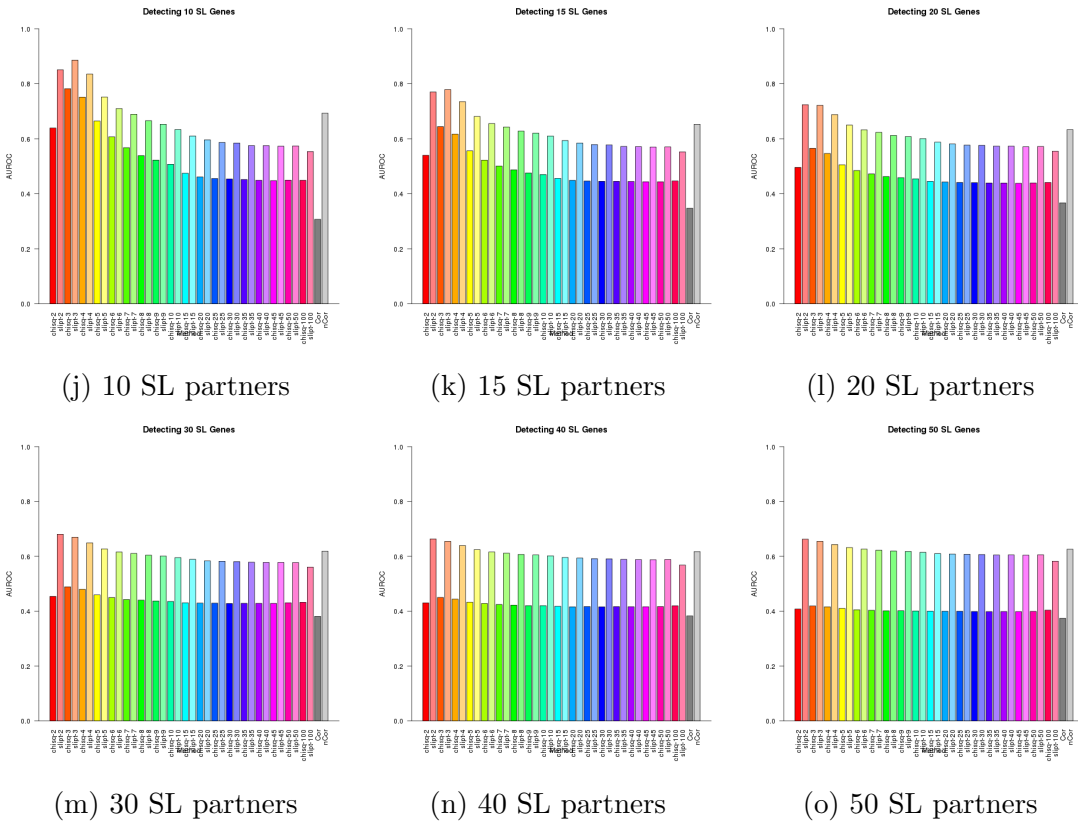


Figure N.4: Performance of χ^2 and SLIPT across quantiles with query correlation. Synthetic lethal detection with quantiles as in axis labels. The barplot uses the same hues for each quantile (grey for correlation) and darker for χ^2 (and positive correlation). SLIPT and χ^2 perform similarly, peaking at $\frac{1}{3}$ -quantiles and converging to random (0.5). Negative correlation was higher than positive but not optimal quantiles for SLIPT or χ^2 . These findings are robust across different numbers of underlying synthetic lethal genes in 10,000 simulations of 100 genes (including 10 correlated with the query) and 1000 samples. SLIPT performs consistently better than χ^2 with positively correlated genes.

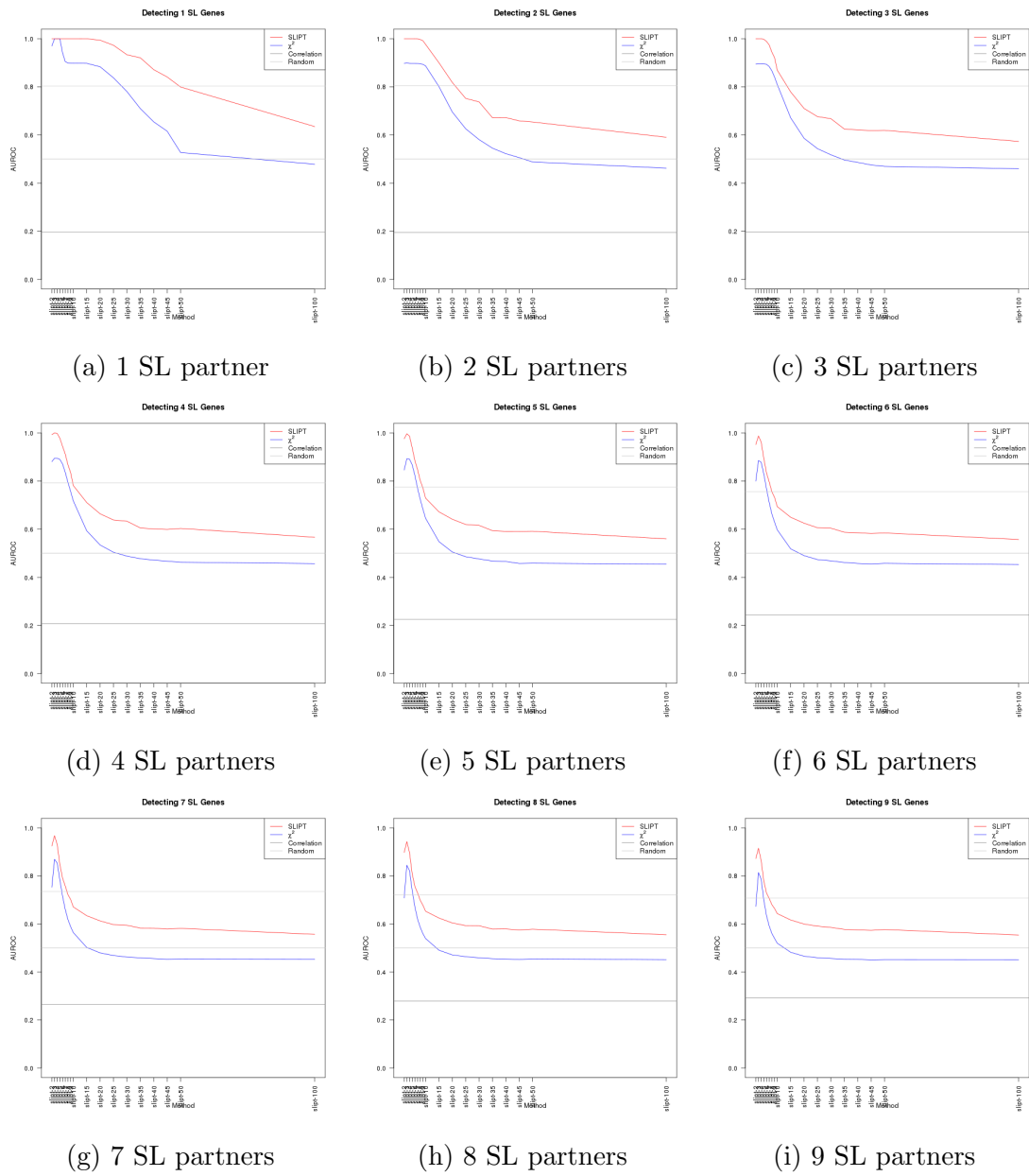


Figure N.5: **Performance of χ^2 and SLIPT across quantiles with query correlation.** (continued on next page)

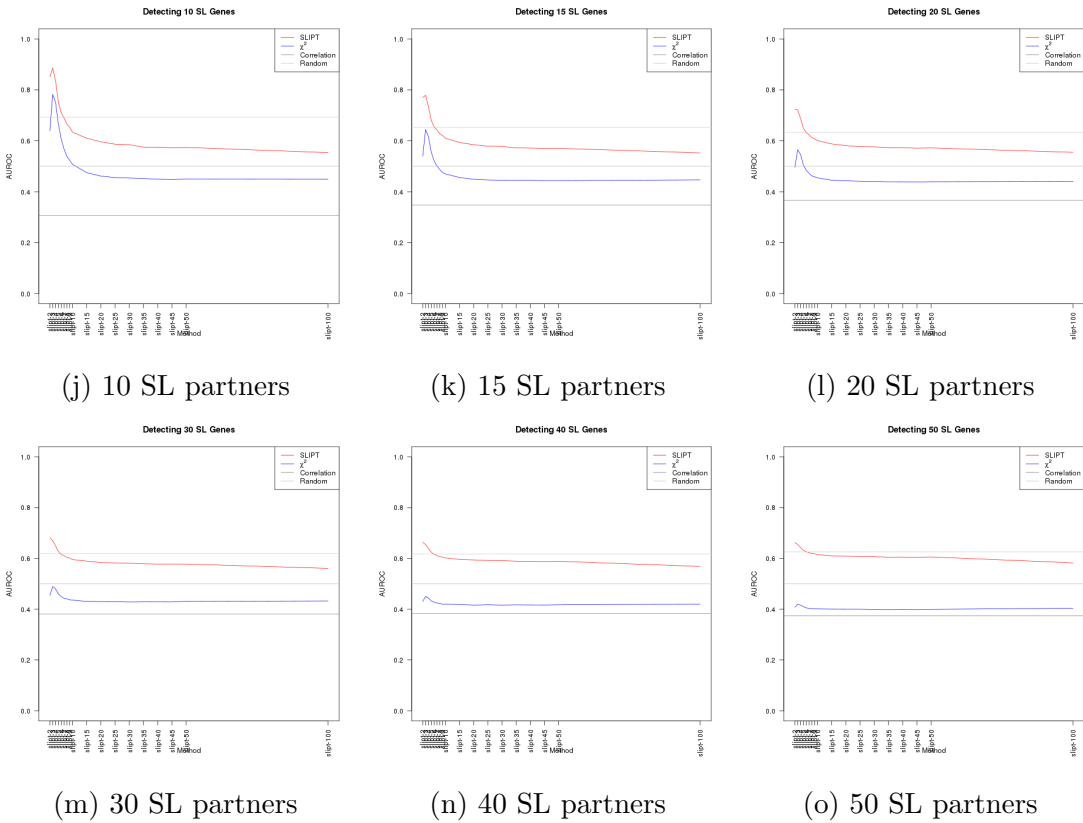


Figure N.5: Performance of χ^2 and SLIPT across quantiles with query correlation. Synthetic lethal detection with quantiles as in axis labels. The line plots are coloured for SLIPT (red), χ^2 (blue) and correlation (grey) according to the legend. SLIPT and χ^2 perform similarly, peaking at $\frac{1}{3}$ -quantiles and converging to random (0.5). Negative correlation was higher than positive but not optimal quantiles for SLIPT or χ^2 . These findings are robust across different numbers of underlying synthetic lethal genes in 10,000 simulations of 100 genes (including 10 correlated with the query) and 1000 samples. SLIPT performs consistently better than χ^2 with positively correlated genes.

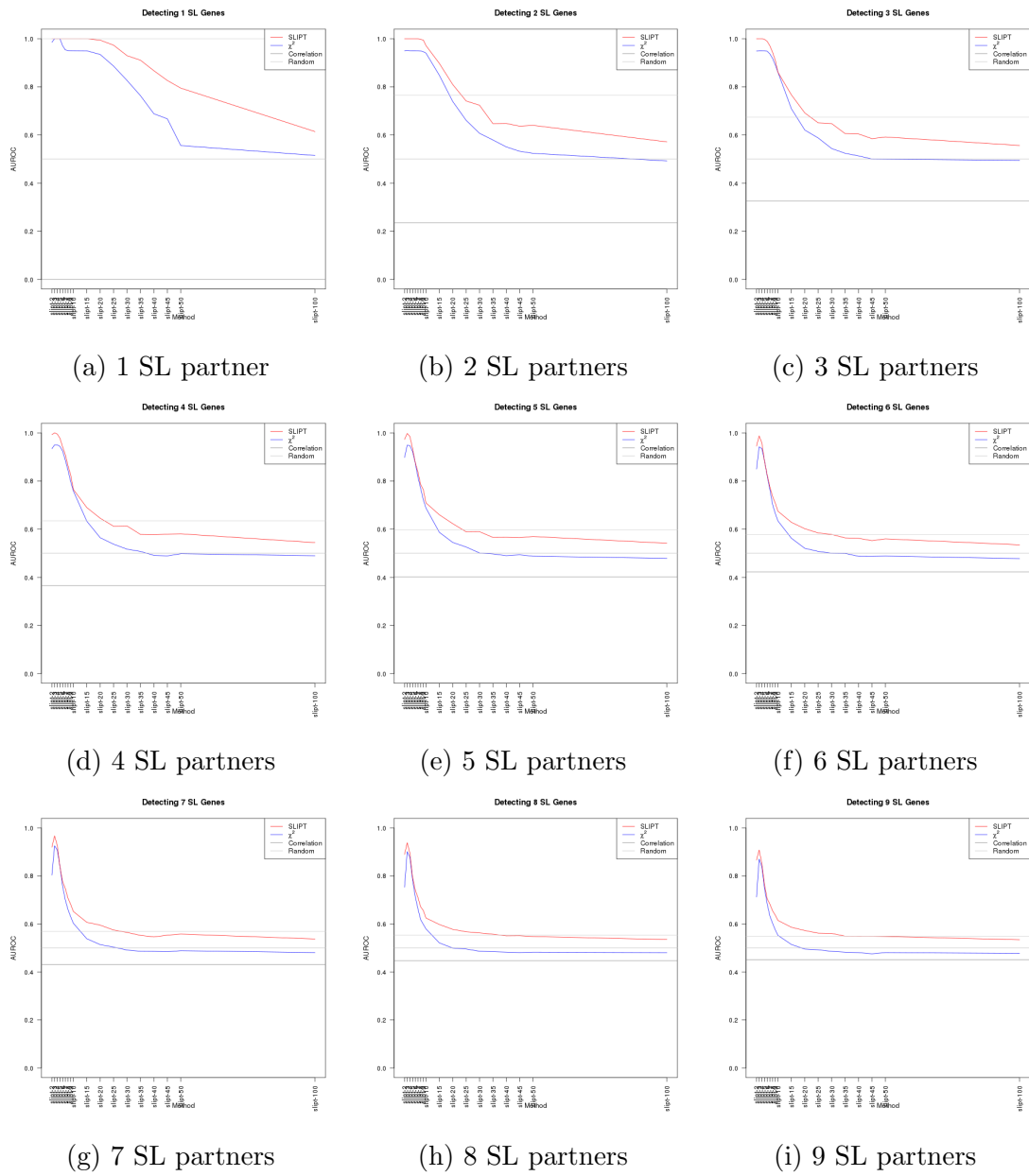


Figure N.6: **Performance of χ^2 and SLIPT across quantiles with query correlation and more genes.** (continued on next page)

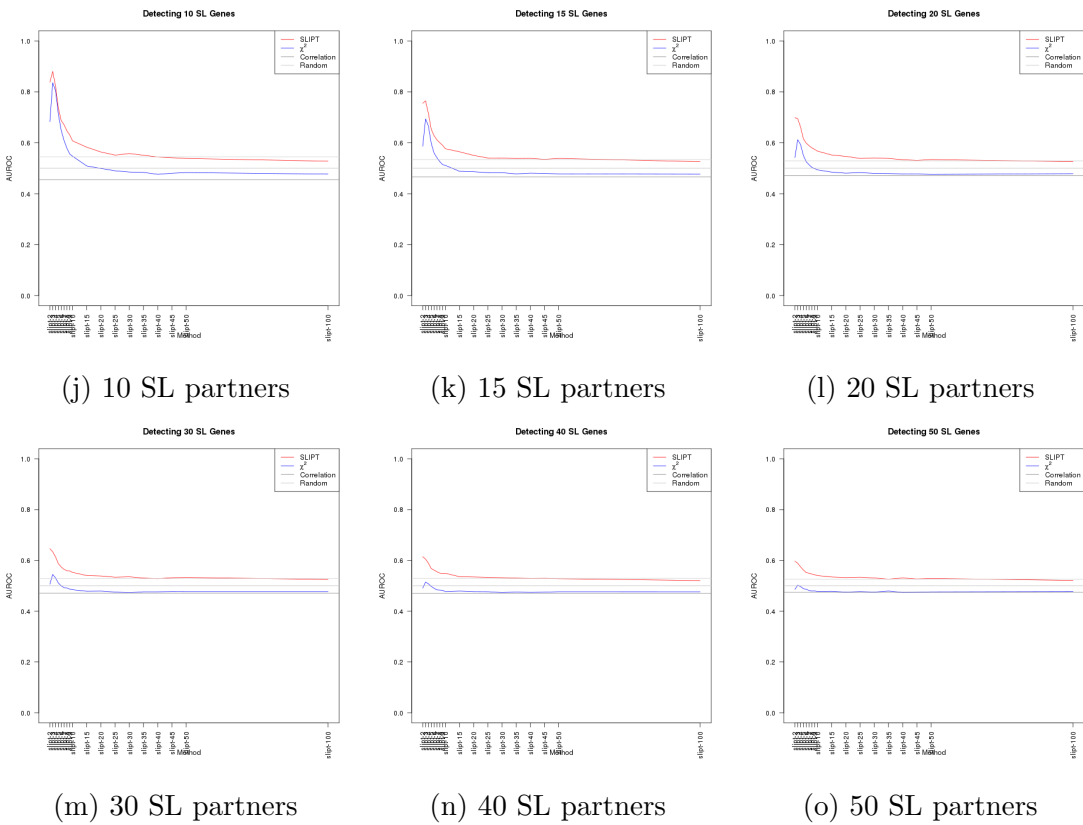


Figure N.6: Performance of χ^2 and SLIPT across quantiles with query correlation and more genes. Synthetic lethal detection with quantiles as in axis labels. The line plots are coloured for SLIPT (red), χ^2 (blue) and correlation (grey) according to the legend. SLIPT and χ^2 perform similarly, peaking at $\frac{1}{3}$ -quantiles and converging to random (0.5). Negative correlation was higher than positive but not optimal quantiles for SLIPT or χ^2 . These findings are robust across different numbers of underlying synthetic lethal genes in 1000 simulations of 20,000 genes (including 1000 correlated with the query) and 1000 samples. SLIPT performs consistently better than χ^2 with positively correlated genes.

Appendix O

Graph Structures

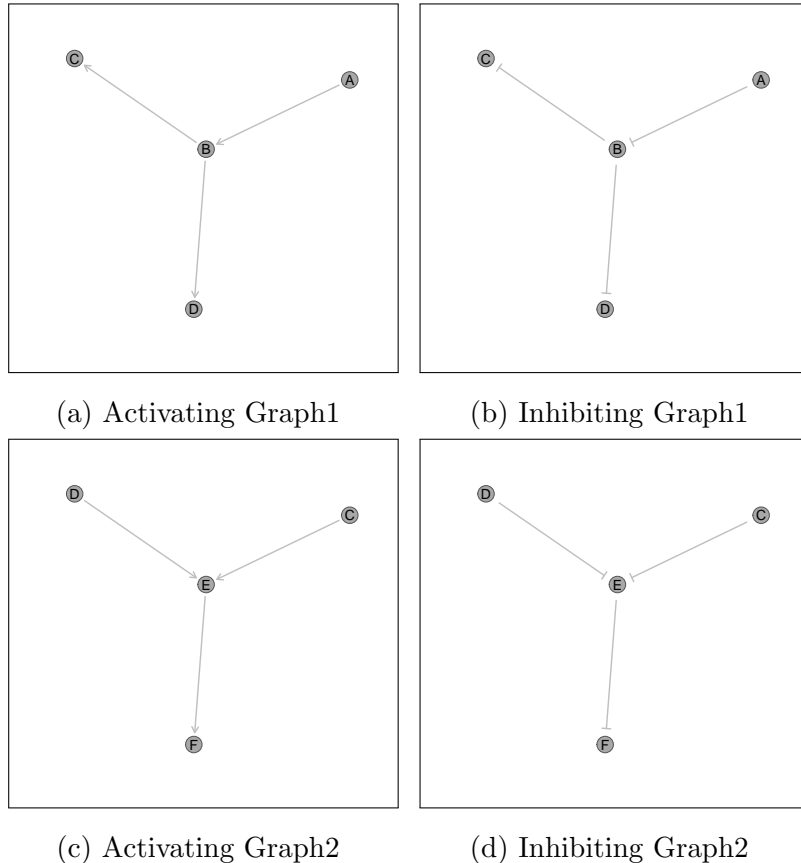
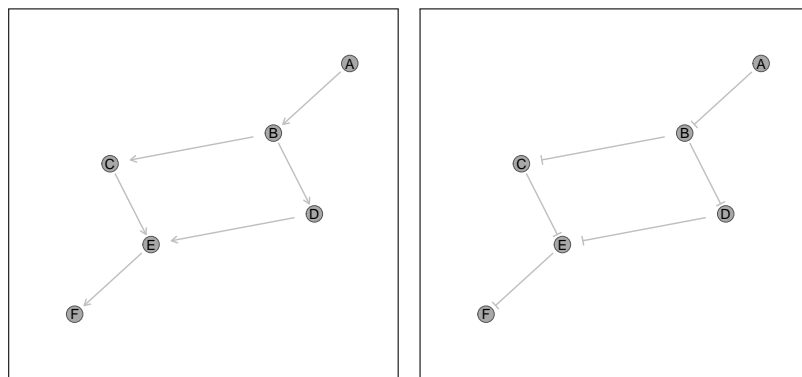


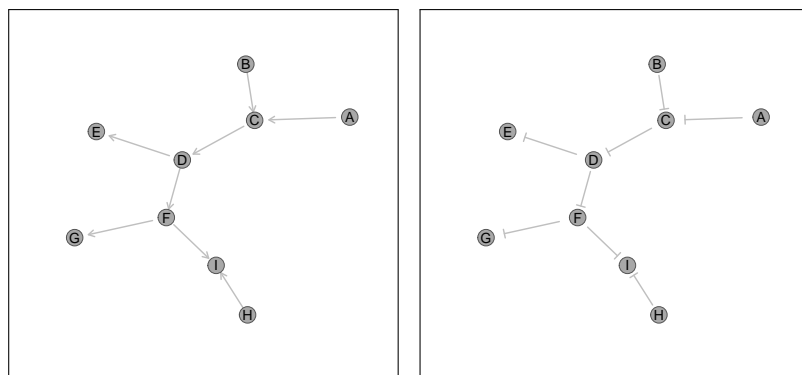
Figure O.1: **Simple graph structures.** A simple graph structures used to demonstrate the simulation procedure. Graph1 and Graph2 are examples of a pathway converging or diverging respectively which enables testing the importance of direction in pathway structures. These are used with both activating and inhibiting relationships as shown.



(a) Activating Graph3

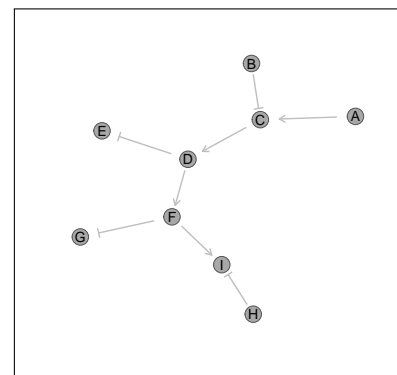
(b) Inhibiting Graph3

Figure O.2: **Simple graph structure.** A constructed graph structure used for the simulation procedure. Graph3 combines the converging and diverging paths of a pathway. These are used with both activating and inhibiting relationships as shown.



(a) Activating Graph4

(b) Inhibiting Graph4



(c) Mixed Graph4

Figure O.3: **Constructed graph structure.** A constructed graph structure used for the simulation procedure. Graph4 has a core cascade with branching signals. These are used with activating, inhibiting, and a combination of these relationships as shown.

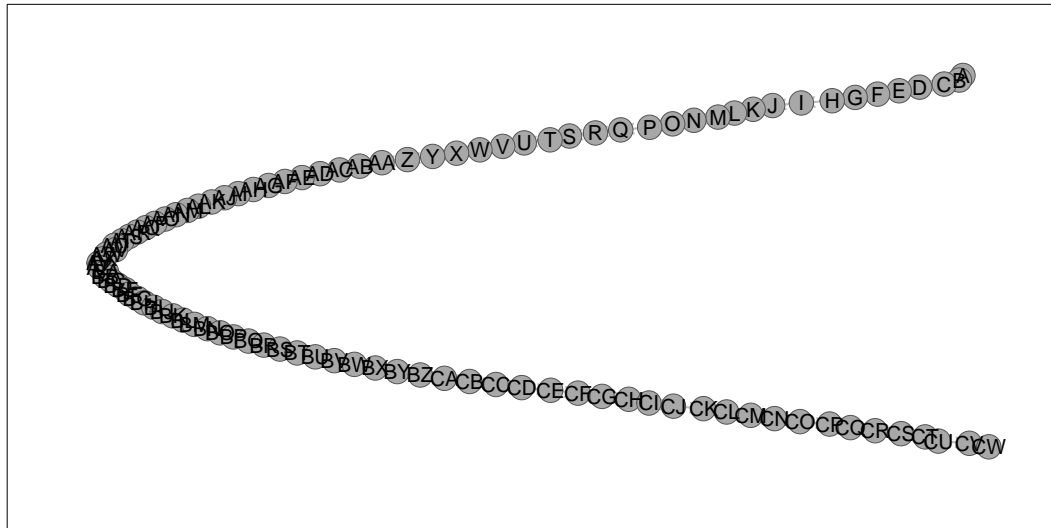
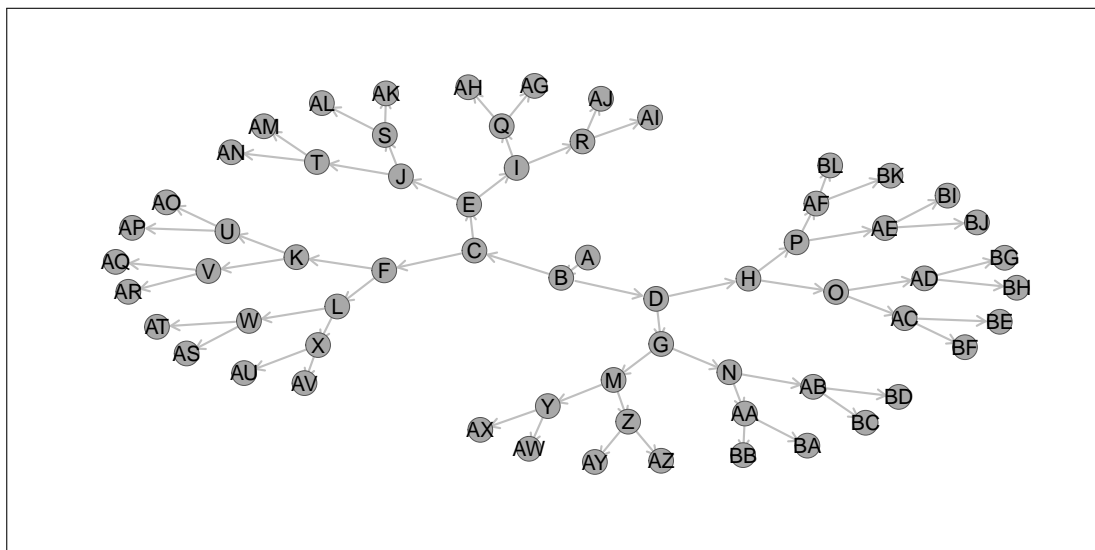
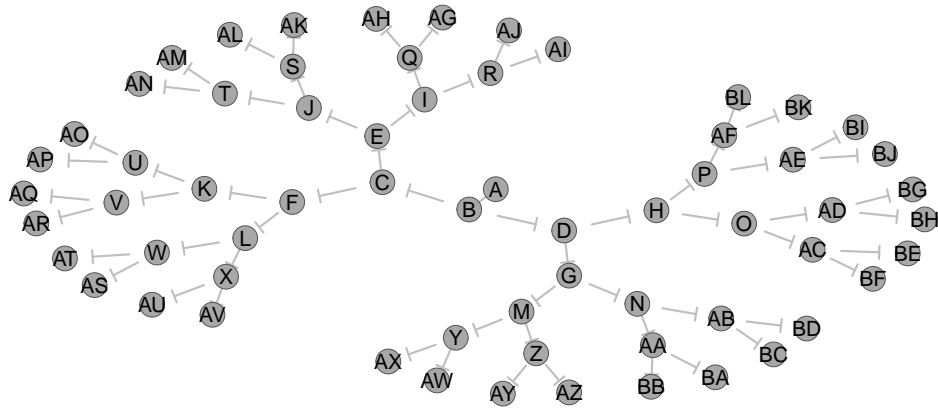


Figure O.4: **Large constructed graph structure.** A constructed graph structure used for the simulation procedure. Graph5 is an extended chain of 101 genes which are simulated with activating or inhibiting relations and these alternating along the chain.

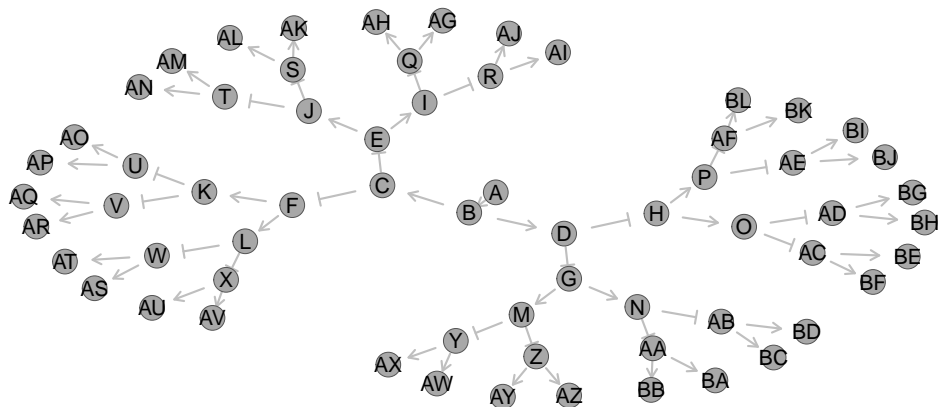


(a) Activating Graph6

Figure O.5: **Branching constructed graph structure.** (continued on next page)

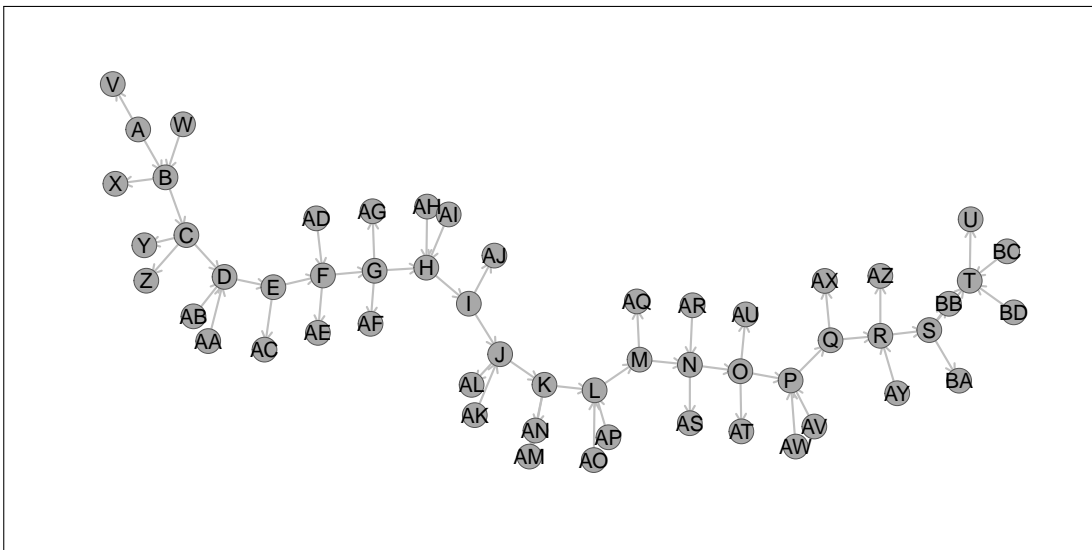


(b) Inhibiting Graph6

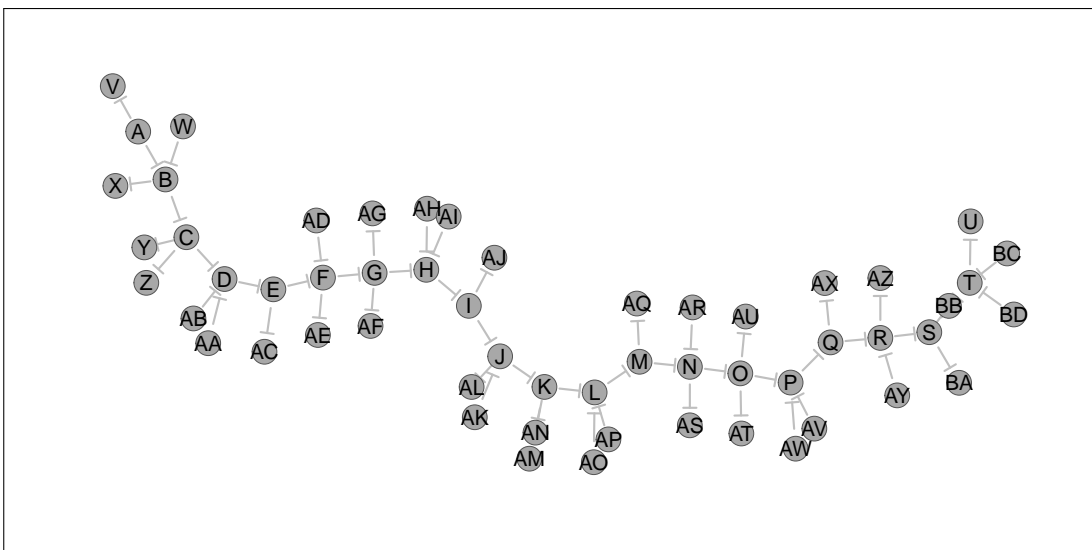


(c) Mixed Graph6

Figure O.5: Branching constructed graph structure. A constructed graph structure used for the simulation procedure. Graph6 is a branching signal cascade from a central hub. These are used with activating, inhibiting, and an alternating combination of these relationships as shown.

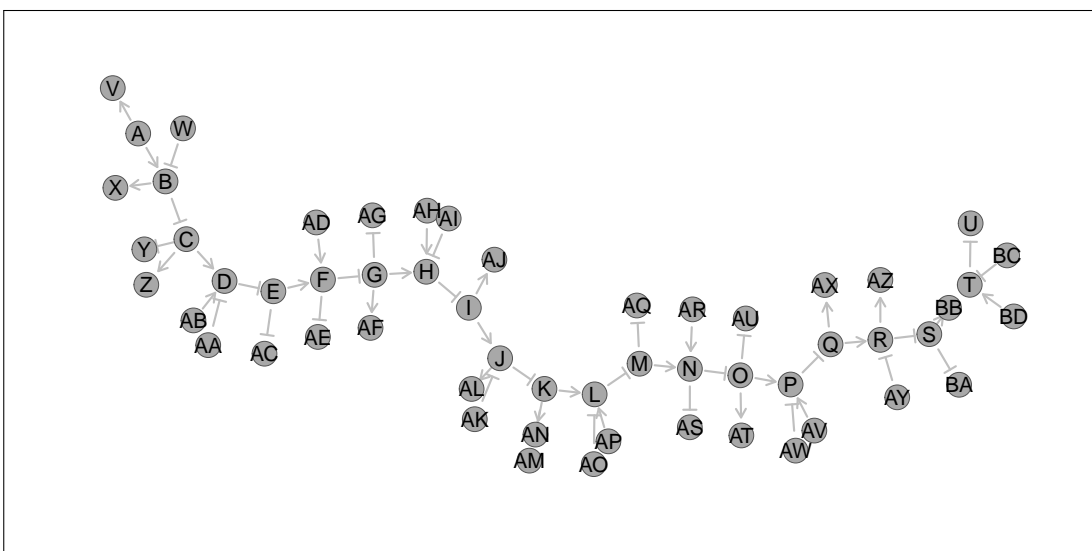


(a) Activating Graph7



(b) Inhibiting Graph7

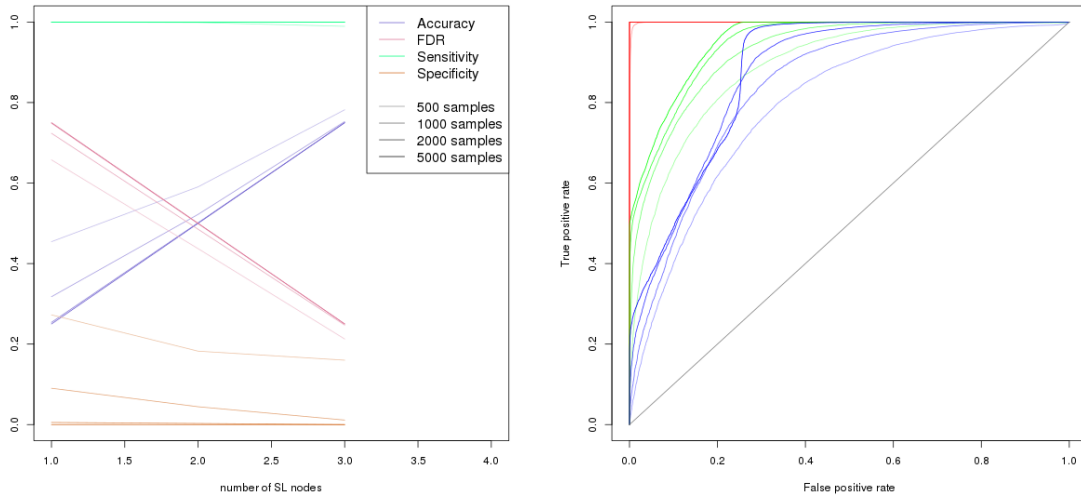
Figure O.6: **Complex constructed graph structure.** (continued on next page)



(c) Mixed Graph7

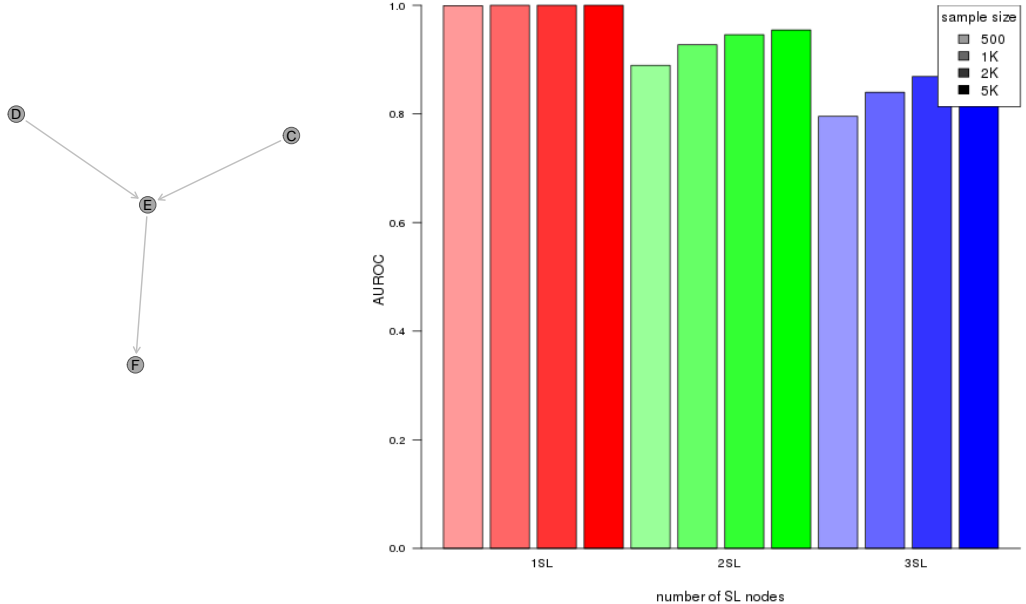
Figure O.6: **Complex constructed graph structure.** A constructed graph structure used for the simulation procedure. Graph7 has a core cascade with branching signals in and out of the pathway. These are used with activating, inhibiting, and a combination of these relationships as shown.

O.1 Simulations from Graph Structures



(a) Statistical evaluation

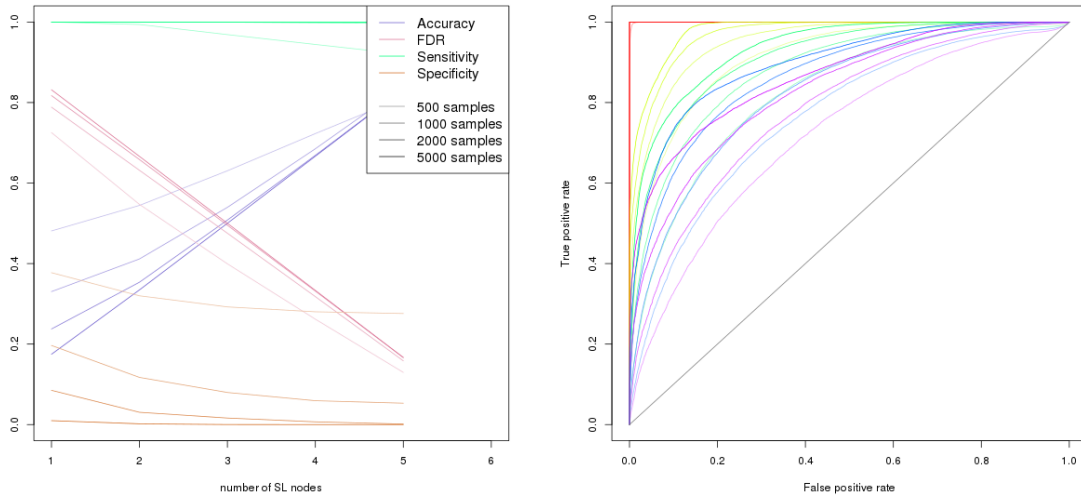
(b) Receiver operating characteristic



(c) Graph Structure

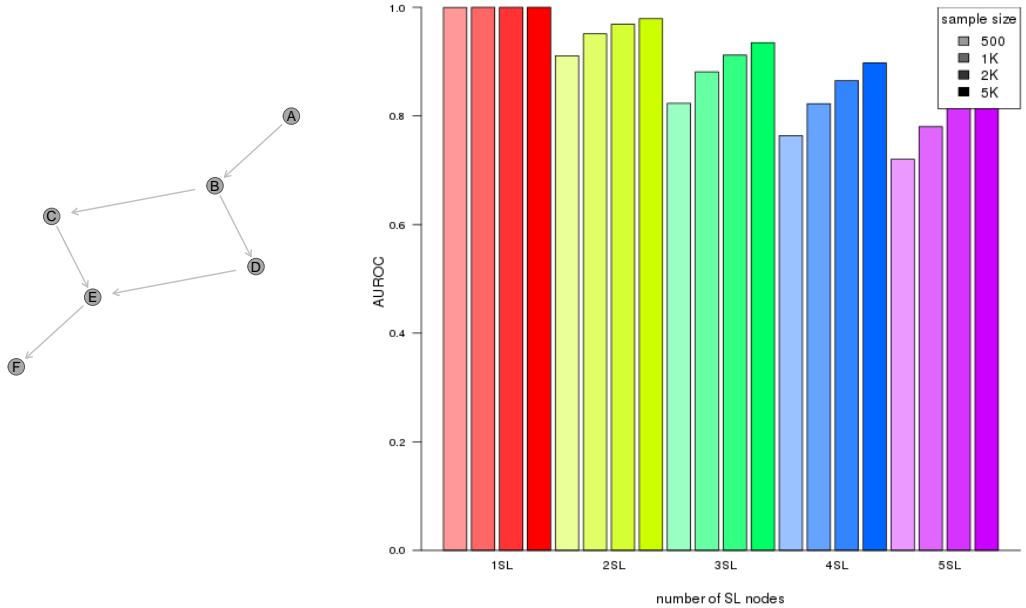
(d) Statistical performance

Figure O.7: Performance of simulations on a simple graph. Simulation of synthetic lethality was performed sampling from a multivariate normal distribution generated from Graph2. Performance of SLIPT declines for more synthetic partners and lower sample sizes. For each parameter value, 10,000 simulations were used.



(a) Statistical evaluation

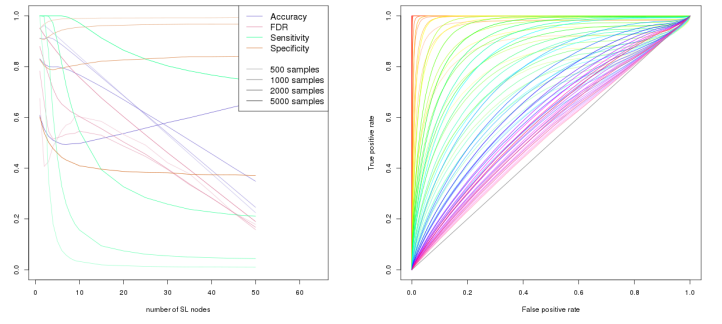
(b) Receiver operating characteristic



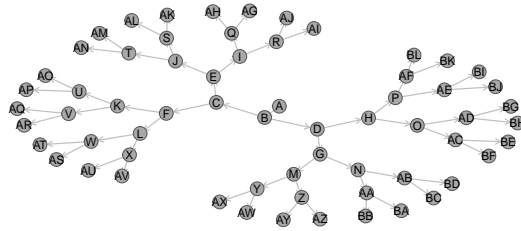
(c) Graph Structure

(d) Statistical performance

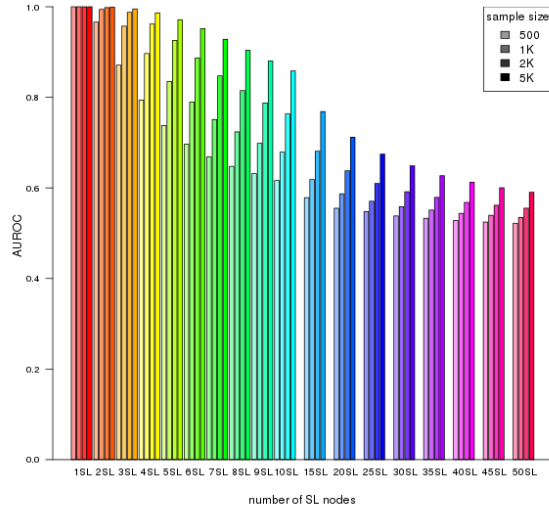
Figure O.8: **Performance of simulations on a constructed graph.** Simulation of synthetic lethality was performed sampling from a multivariate normal distribution generated from Graph3. Performance of SLIPT declines for more synthetic partners and lower sample sizes. For each parameter value, 10,000 simulations were used.



(a) Statistical evaluation (b) Receiver operating characteristic

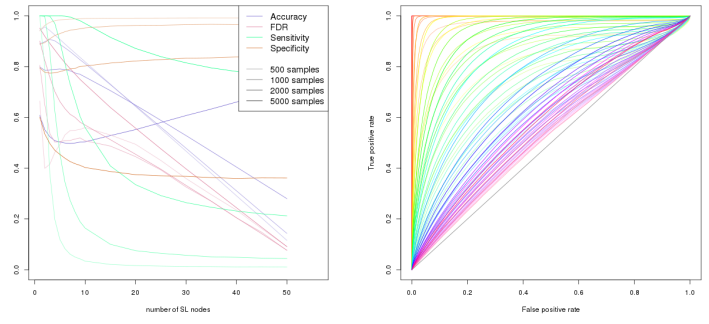


(c) Graph Structure

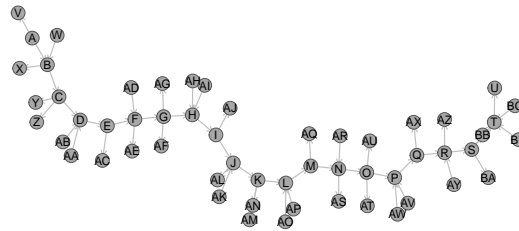


(d) Statistical performance

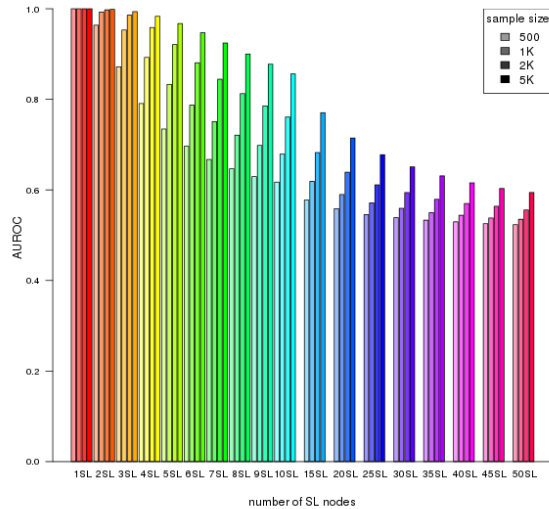
Figure O.9: Performance of simulations on a branching graph. Simulation of synthetic lethality was performed sampling from a multivariate normal distribution generated from Graph6. Performance of SLIPT declines for more synthetic partners and lower sample sizes. For each parameter value, 10,000 simulations were used.



(a) Statistical evaluation (b) Receiver operating characteristic



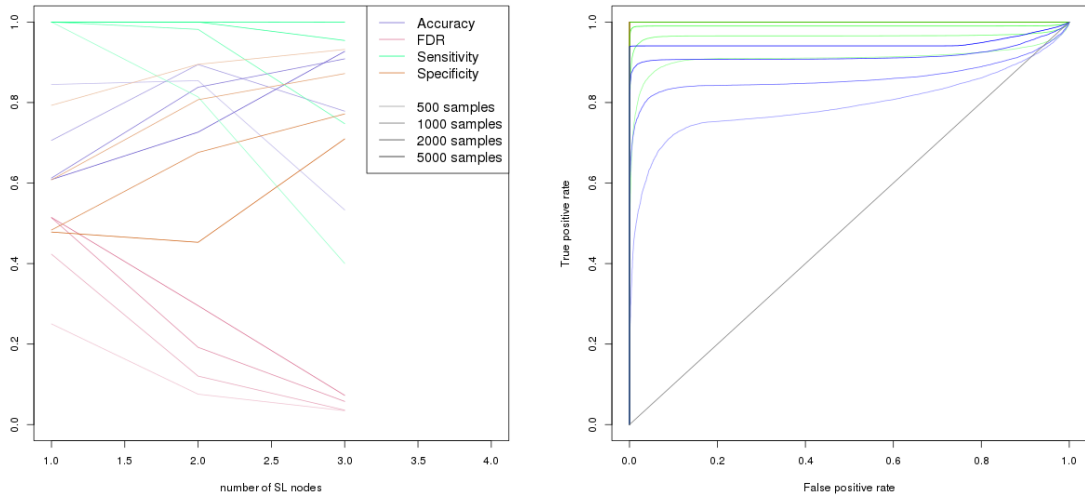
(c) Graph Structure



(d) Statistical performance

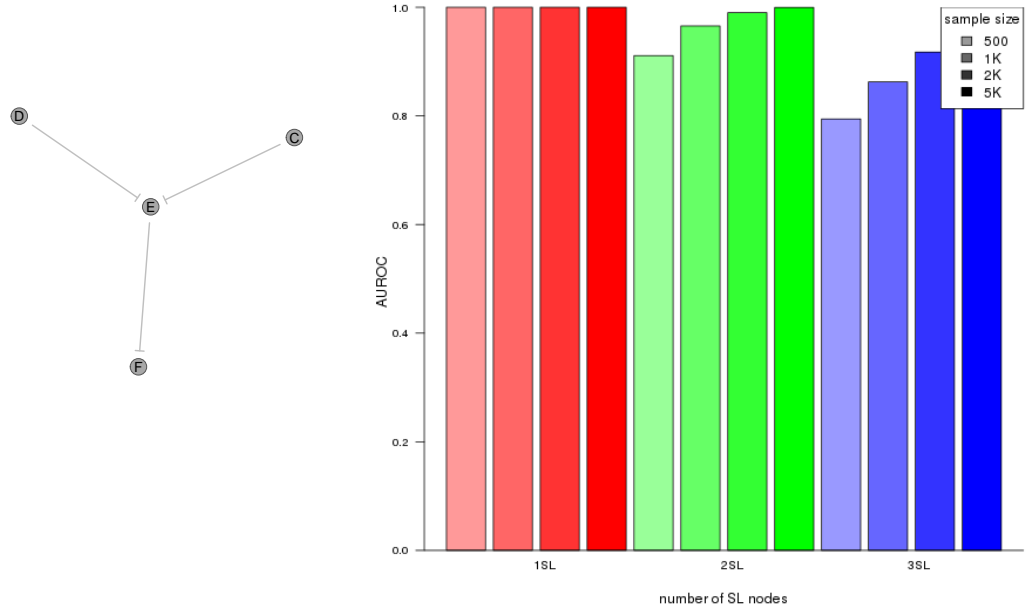
Figure O.10: Performance of simulations on a complex graph. Simulation of synthetic lethality was performed sampling from a multivariate normal distribution generated from Graph7. Performance of SLIPT declines for more synthetic partners and lower sample sizes. For each parameter value, 10,000 simulations were used.

O.2 Simulations from Inhibiting Graph Structures



(a) Statistical evaluation

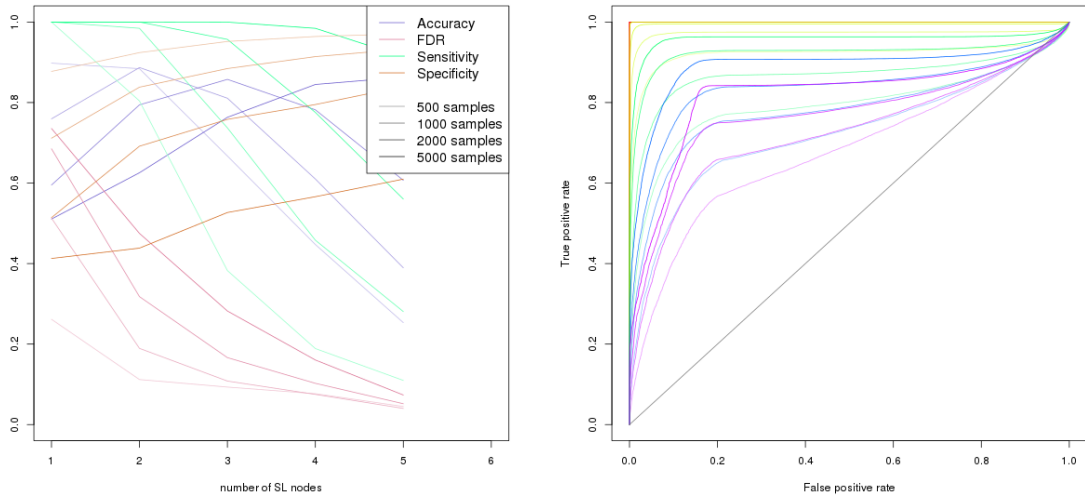
(b) Receiver operating characteristic



(c) Graph Structure

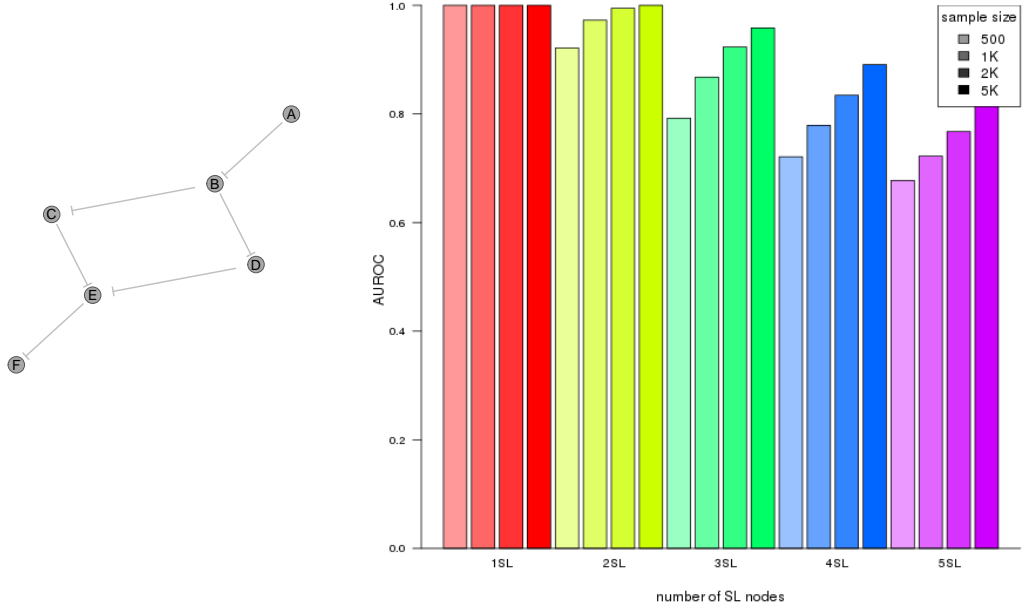
(d) Statistical performance

Figure O.11: **Performance of simulations on a simple graph with inhibition.** Simulation of synthetic lethality was performed sampling from a multivariate normal distribution generated from Graph2. Performance of SLIPT declines for more synthetic partners and lower sample sizes. For each parameter value, 10,000 simulations were used.



(a) Statistical evaluation

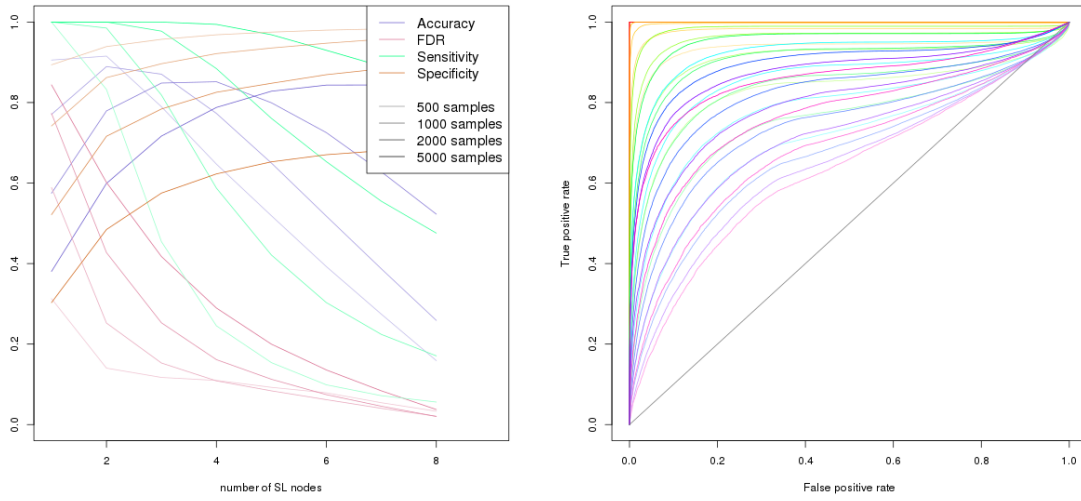
(b) Receiver operating characteristic



(c) Graph Structure

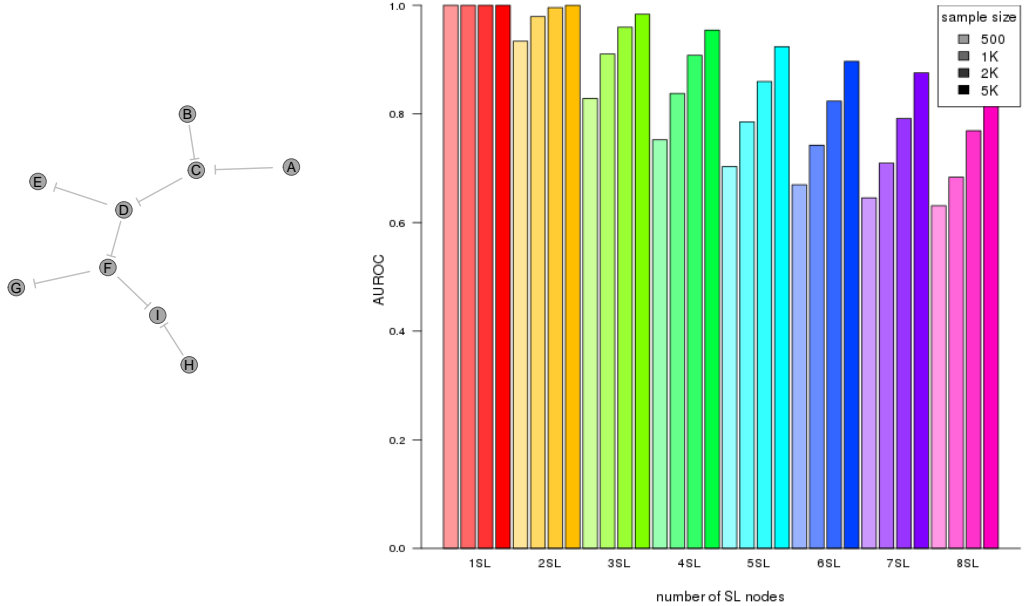
(d) Statistical performance

Figure O.12: **Performance of simulations on a simple graph with inhibition.** Simulation of synthetic lethality was performed sampling from a multivariate normal distribution generated from Graph3. Performance of SLIPT declines for more synthetic partners and lower sample sizes. For each parameter value, 10,000 simulations were used.



(a) Statistical evaluation

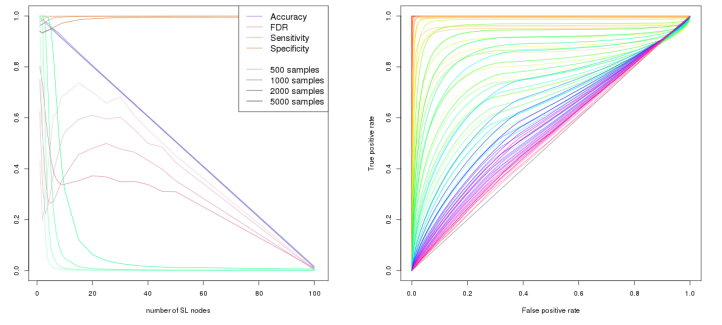
(b) Receiver operating characteristic



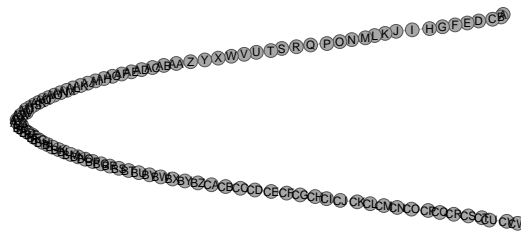
(c) Graph Structure

(d) Statistical performance

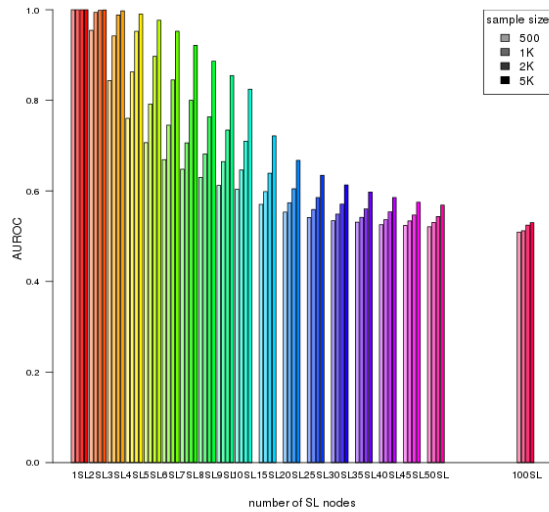
Figure O.13: Performance of simulations on a constructed graph with inhibition.
 Simulation of synthetic lethality was performed sampling from a multivariate normal distribution generated from Graph4 with only inhibitions. Performance of SLIPT declines for more synthetic partners and lower sample sizes. For each parameter value, 10,000 simulations were used.



(a) Statistical evaluation (b) Receiver operating characteristic

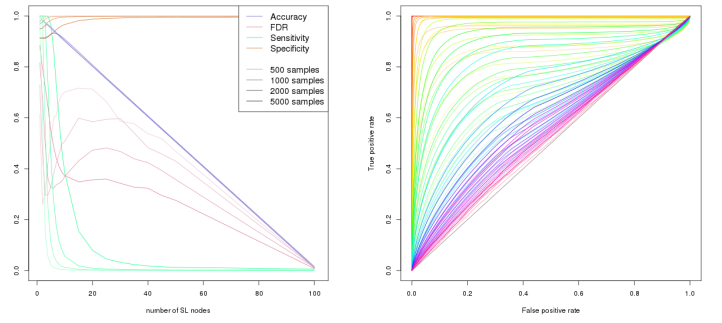


(c) Graph Structure



(d) Statistical performance

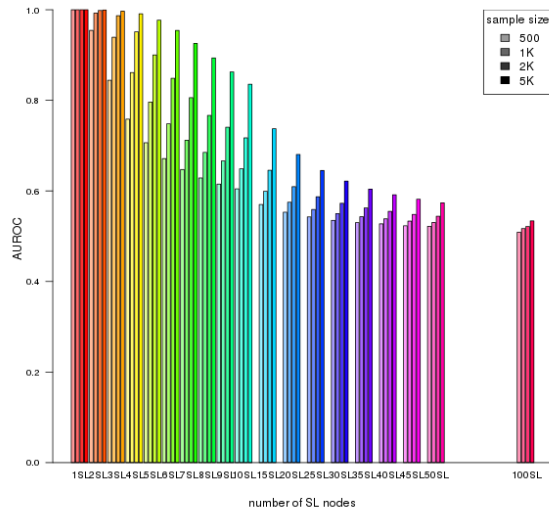
Figure O.14: Performance of simulations on a large constructed graph with inhibition. Simulation of synthetic lethality was performed sampling from a multivariate normal distribution generated from Graph5 with only inhibitions. Performance of SLIPT declines for more synthetic partners and lower sample sizes. For each parameter value, 10,000 simulations were used.



(a) Statistical evaluation (b) Receiver operating characteristic

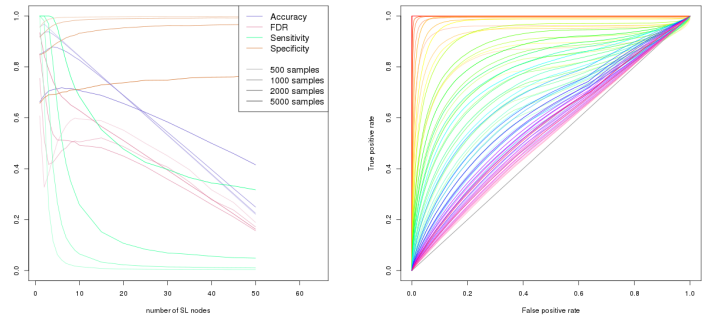


(c) Graph Structure

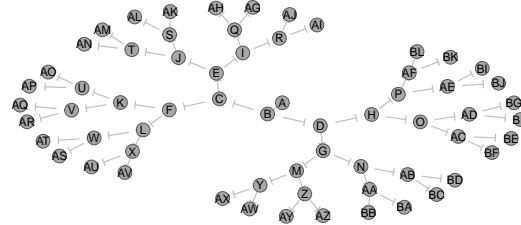


(d) Statistical performance

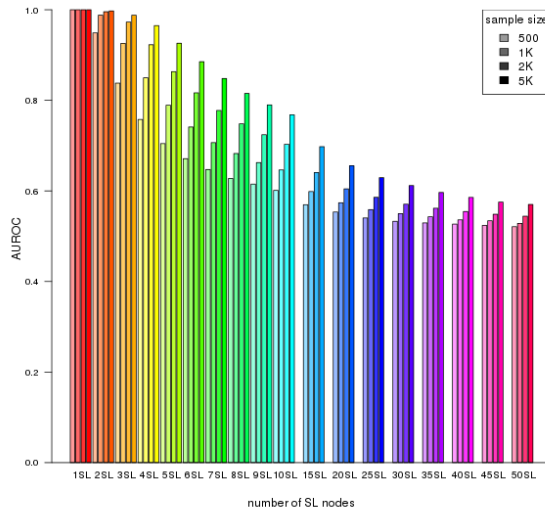
Figure O.15: Performance of simulations on a large constructed graph with inhibition. Simulation of synthetic lethality was performed sampling from a multivariate normal distribution generated from Graph5 with alternating inhibitions. Performance of SLIPT declines for more synthetic partners and lower sample sizes. For each parameter value, 10,000 simulations were used.



(a) Statistical evaluation (b) Receiver operating characteristic

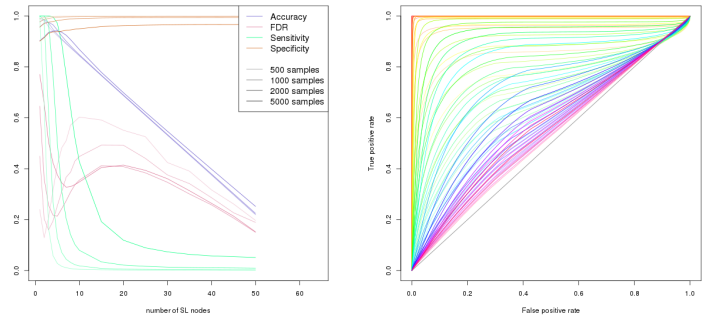


(c) Graph Structure

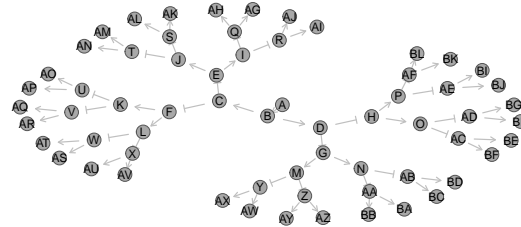


(d) Statistical performance

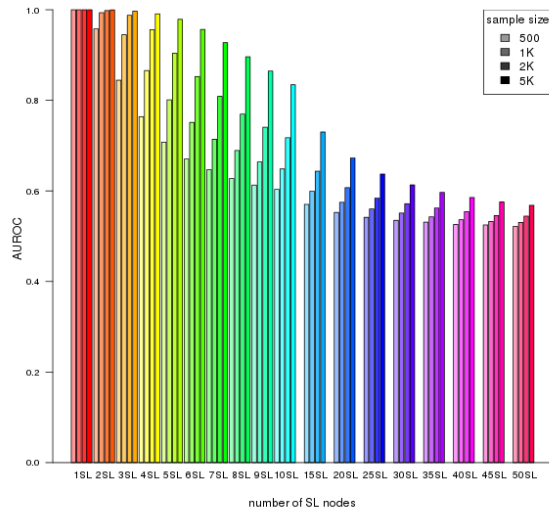
Figure O.16: **Performance of simulations on a branching graph with inhibition.** Simulation of synthetic lethality was performed sampling from a multivariate normal distribution generated from Graph6 with only inhibitions. Performance of SLIPT declines for more synthetic partners and lower sample sizes. For each parameter value, 10,000 simulations were used.



(a) Statistical evaluation (b) Receiver operating characteristic

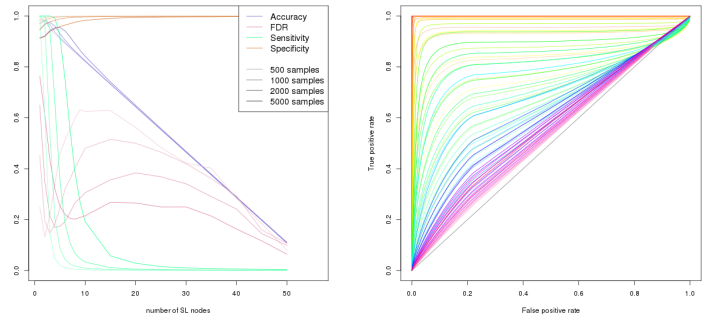


(c) Graph Structure

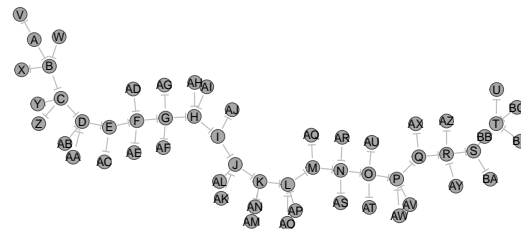


(d) Statistical performance

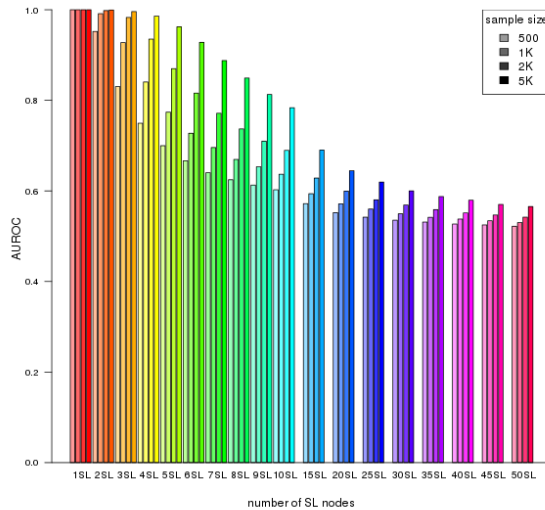
Figure O.17: Performance of simulations on a branching graph with inhibition.
 Simulation of synthetic lethality was performed sampling from a multivariate normal distribution generated from Graph6 with alternating inhibitions. Performance of SLIPT declines for more synthetic partners and lower sample sizes. For each parameter value, 10,000 simulations were used.



(a) Statistical evaluation (b) Receiver operating characteristic

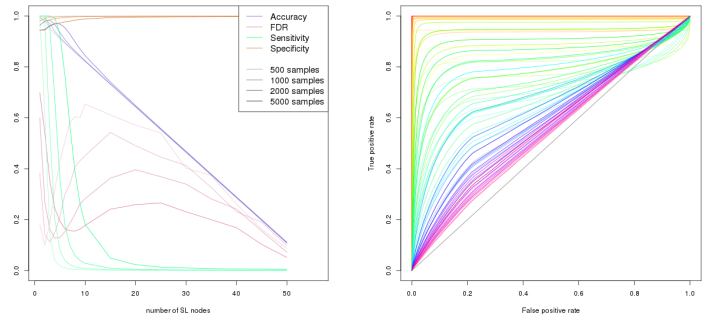


(c) Graph Structure

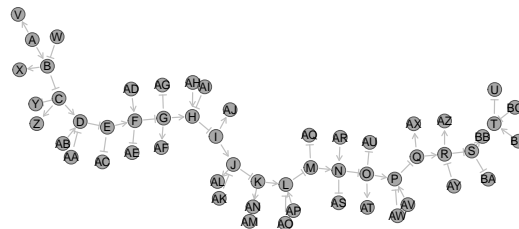


(d) Statistical performance

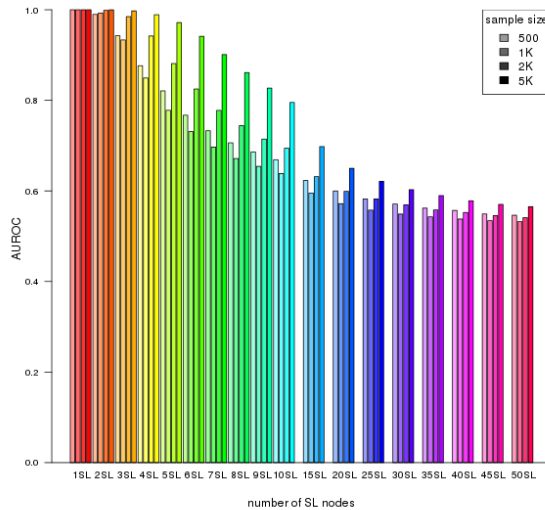
Figure O.18: Performance of simulations on a complex graph with inhibition. Simulation of synthetic lethality was performed sampling from a multivariate normal distribution generated from Graph7 with only inhibitions. Performance of SLIPT declines for more synthetic partners and lower sample sizes. For each parameter value, 10,000 simulations were used.



(a) Statistical evaluation (b) Receiver operating characteristic



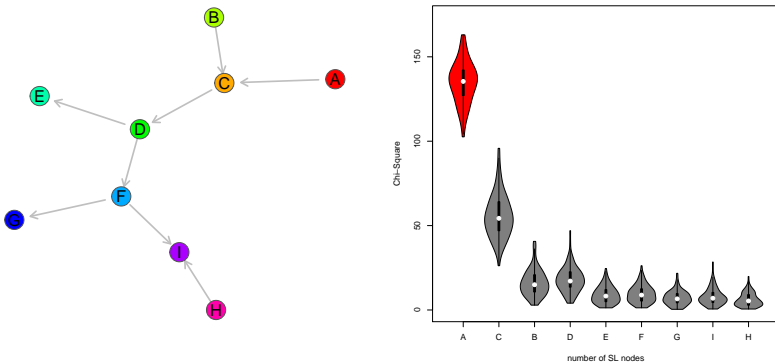
(c) Graph Structure



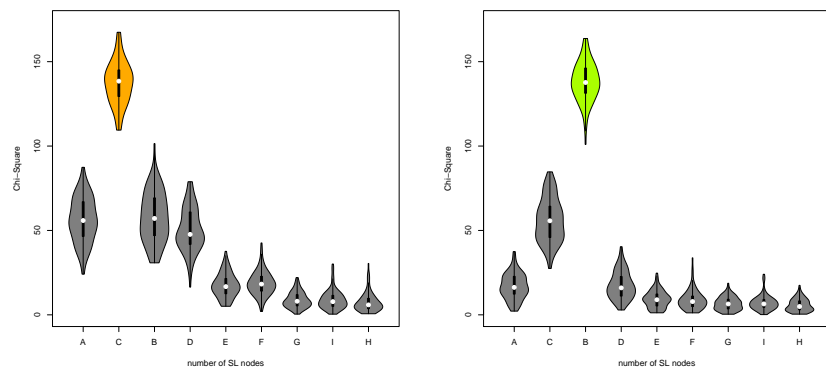
(d) Statistical performance

Figure O.19: Performance of simulations on a complex graph with inhibition.
 Simulation of synthetic lethality was performed sampling from a multivariate normal distribution generated from Graph7 with a combination of relationships. Performance of SLIPT declines for more synthetic partners and lower sample sizes. For each parameter value, 10,000 simulations were used.

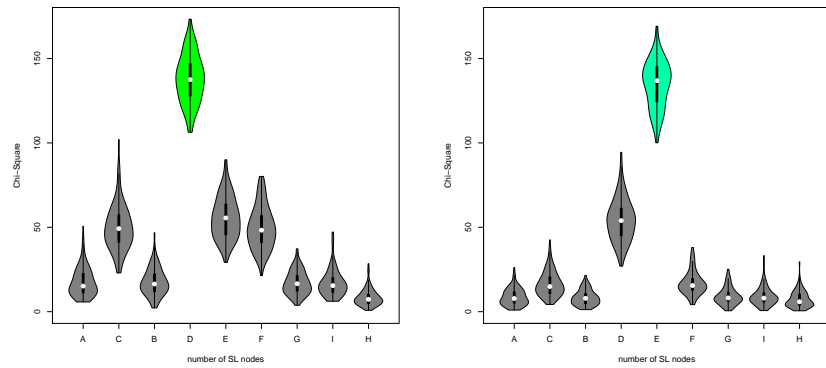
O.3 Simulation across Graph Structures



(a) Activating Graph Structure (b) χ^2 distribution for “A” SL



(c) Gene “B” SL (d) Gene “C” SL



(e) Gene “D” SL (f) Gene “E” SL

Figure O.20: **Detection of Synthetic Lethality within a Graph Structure.** (continued on next page)

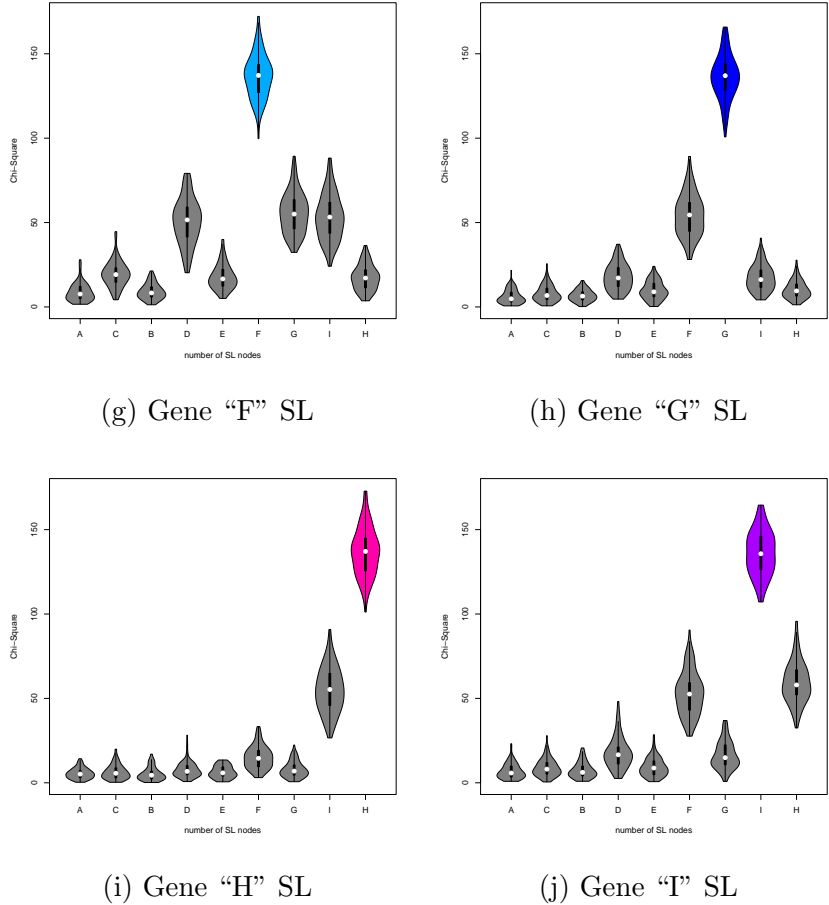
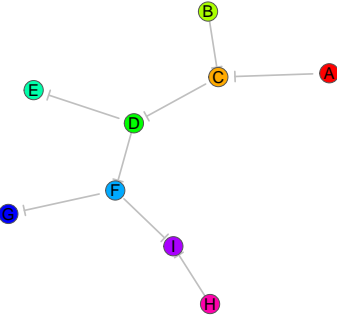
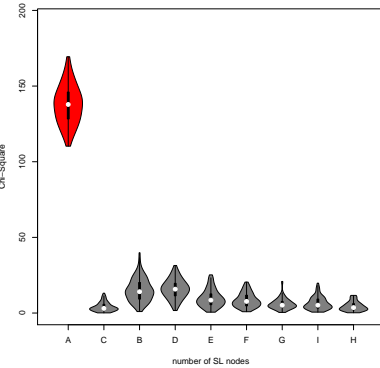


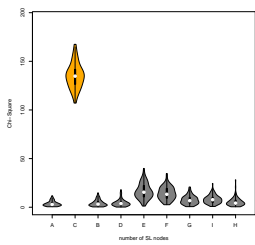
Figure O.20: Detection of Synthetic Lethality within a Graph Structure. Each gene was designated to be synthetic lethal separately and the χ^2 value from SLIPT was computed for each gene across the graph structure. For each synthetic lethal gene (highlighted in the respective colours), the χ^2 values were computed in 100 simulations of datasets of 20,000 genes including the graph structure and 1000 samples. For each synthetic lethal gene, the adjacent genes in the network also had elevated test statistics.



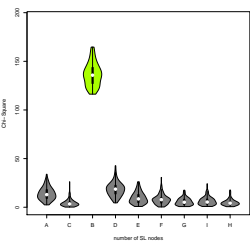
(a) Inhibiting Graph Structure



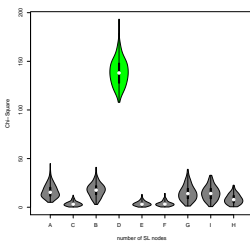
(b) χ^2 distribution for "A" SL



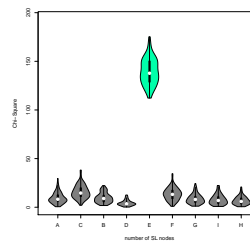
(c) Gene "B" SL



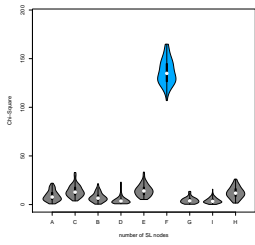
(d) Gene "C" SL



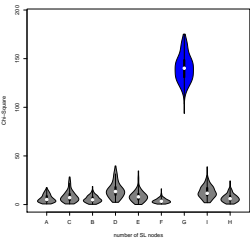
(e) Gene "D" SL



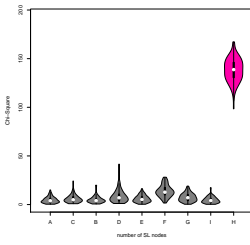
(f) Gene "E" SL



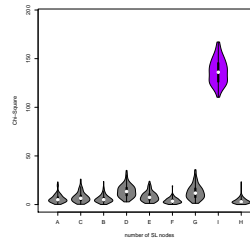
(g) Gene "F" SL



(h) Gene "G" SL

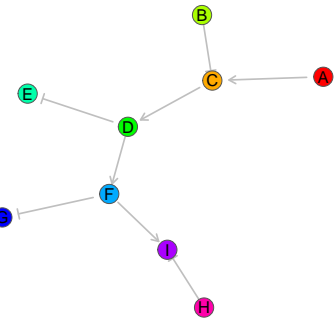


(i) Gene "H" SL

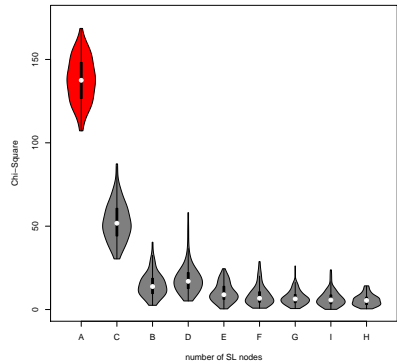


(j) Gene "I" SL

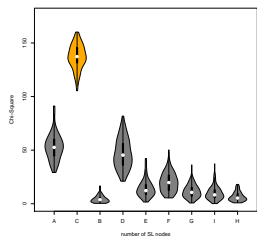
Figure O.21: Detection of Synthetic Lethality within an Inhibiting Graph Structure. Each gene was designated to be synthetic lethal separately and the χ^2 value from SLIPT was computed for each gene across the graph structure with inhibiting relationships. For each synthetic lethal gene (highlighted in the respective colours), the χ^2 values were computed in 100 simulations of datasets of 20,000 genes including the graph structure and 1000 samples. For each synthetic lethal gene, the adjacent genes exhibited lower χ^2 values with inhibiting relationships.



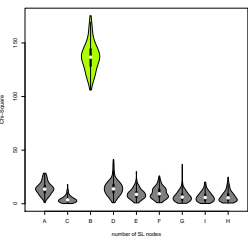
(a) Inhibiting Graph Structure



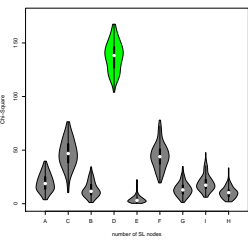
(b) χ^2 distribution for "A" SL



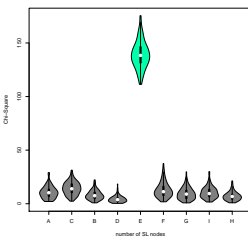
(c) Gene "B" SL



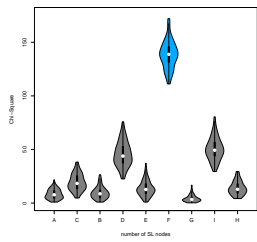
(d) Gene "C" SL



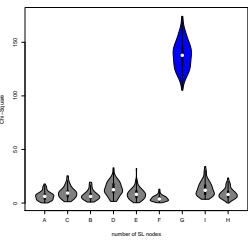
(e) Gene "D" SL



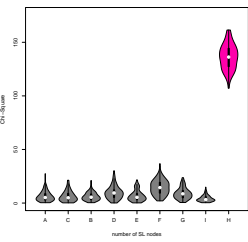
(f) Gene "E" SL



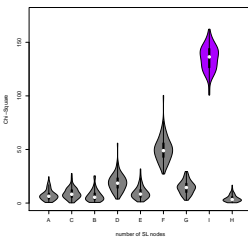
(g) Gene "F" SL



(h) Gene "G" SL



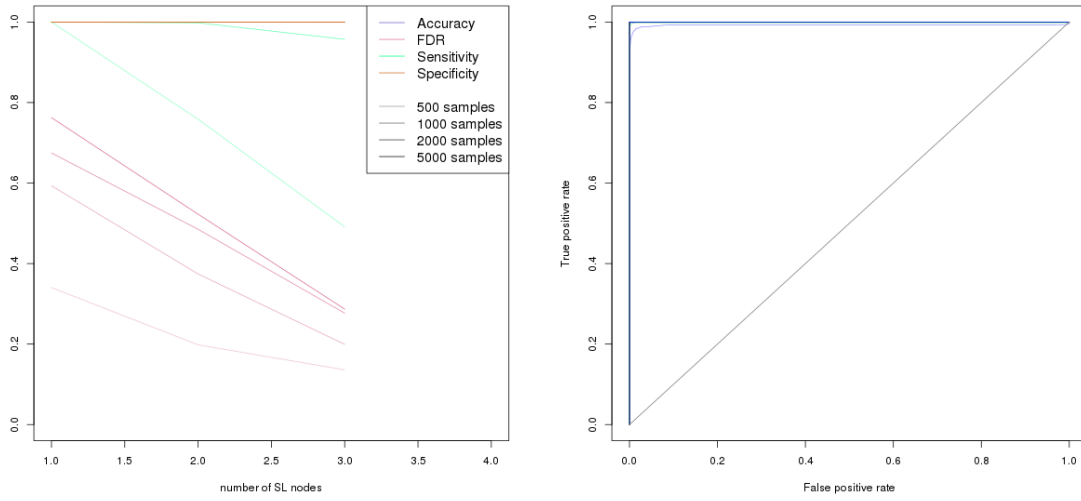
(i) Gene "H" SL



(j) Gene "I" SL

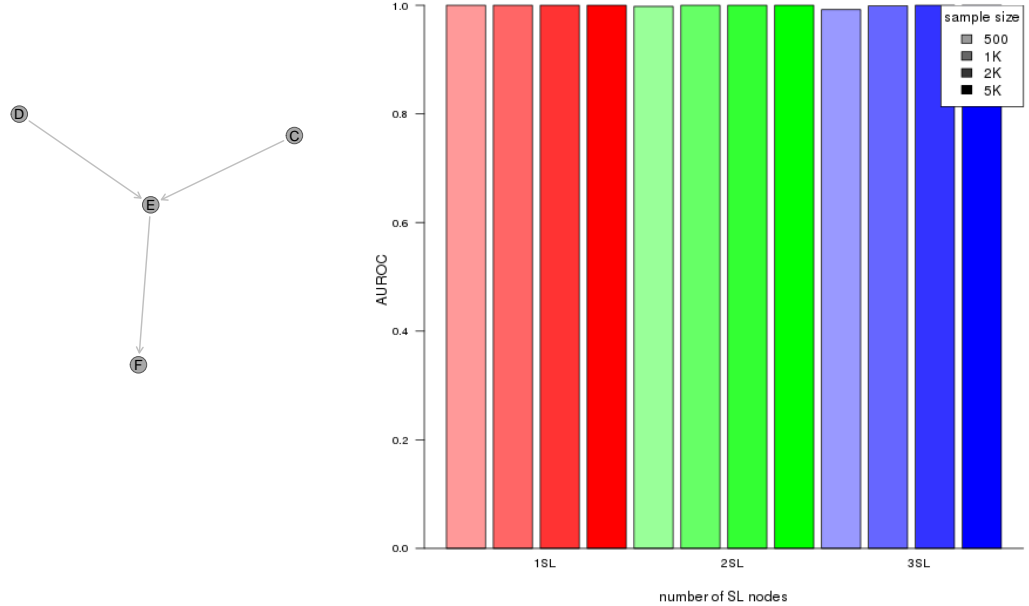
Figure O.22: Detection of Synthetic Lethality within an Inhibiting Graph Structure. Each gene was designated to be synthetic lethal separately and the χ^2 value from SLIPT was computed for each gene across the graph structure with inhibiting and relationships. For each synthetic lethal gene (highlighted in the respective colours), the χ^2 values were computed in 100 simulations of datasets of 20,000 genes including the graph structure and 1000 samples.

O.4 Graph Structure Simulations with 20K genes



(a) Statistical evaluation

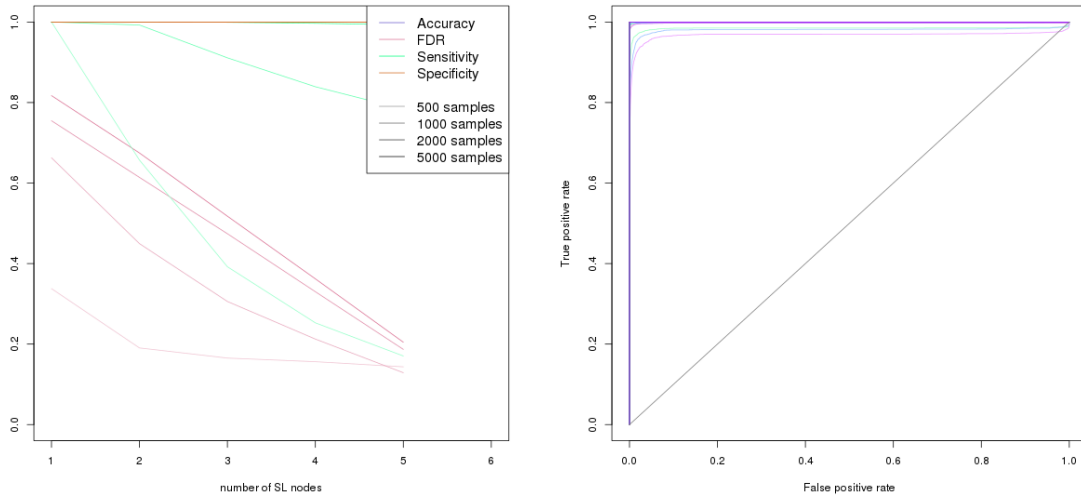
(b) Receiver operating characteristic



(c) Graph Structure

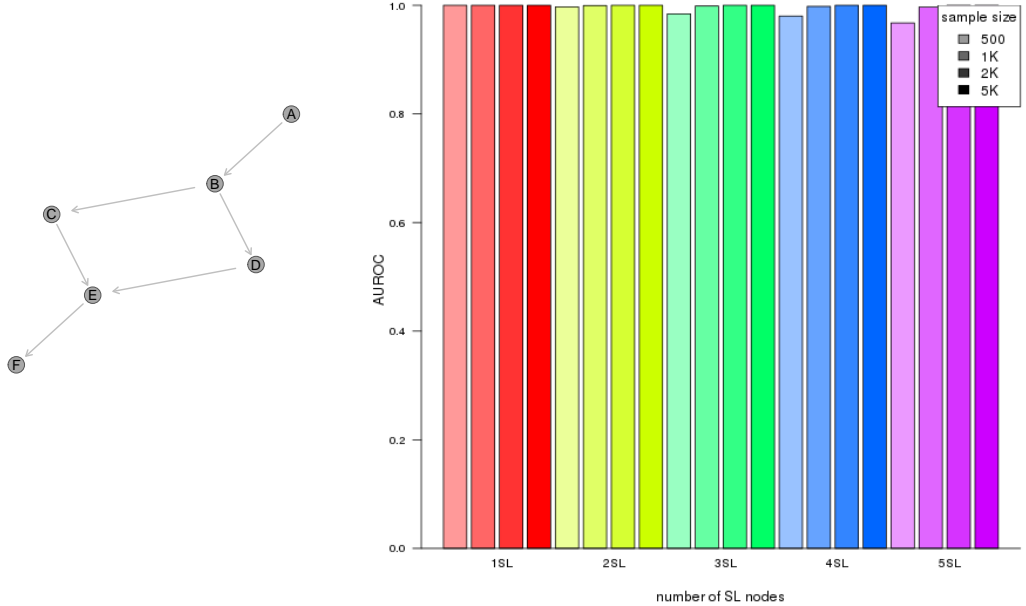
(d) Statistical performance

Figure O.23: Performance of simulations on a simple graph. Simulation of synthetic lethality was performed sampling from a multivariate normal distribution generated from Graph2 among 20,000 genes. Performance of SLIPT declines for more synthetic partners and lower sample sizes. For each parameter value, 1000 simulations were used.



(a) Statistical evaluation

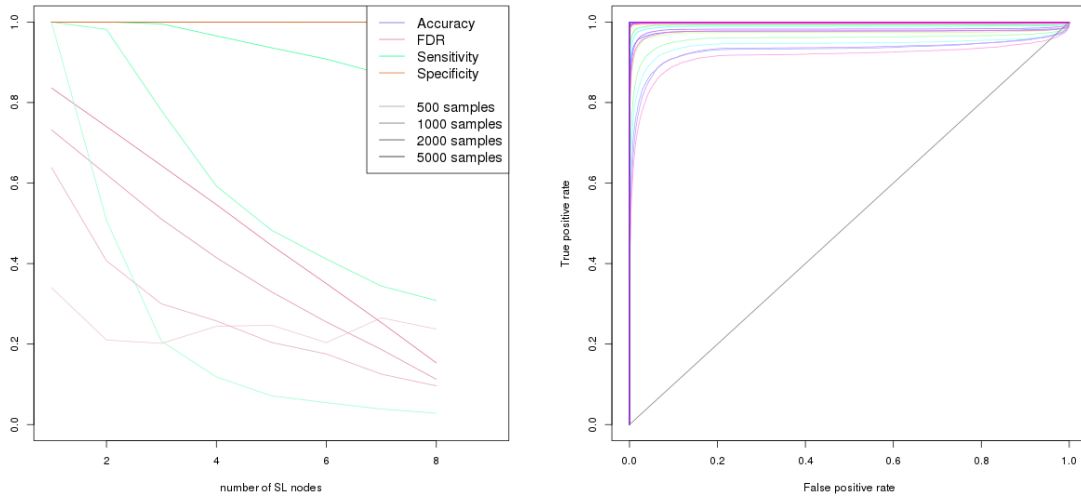
(b) Receiver operating characteristic



(c) Graph Structure

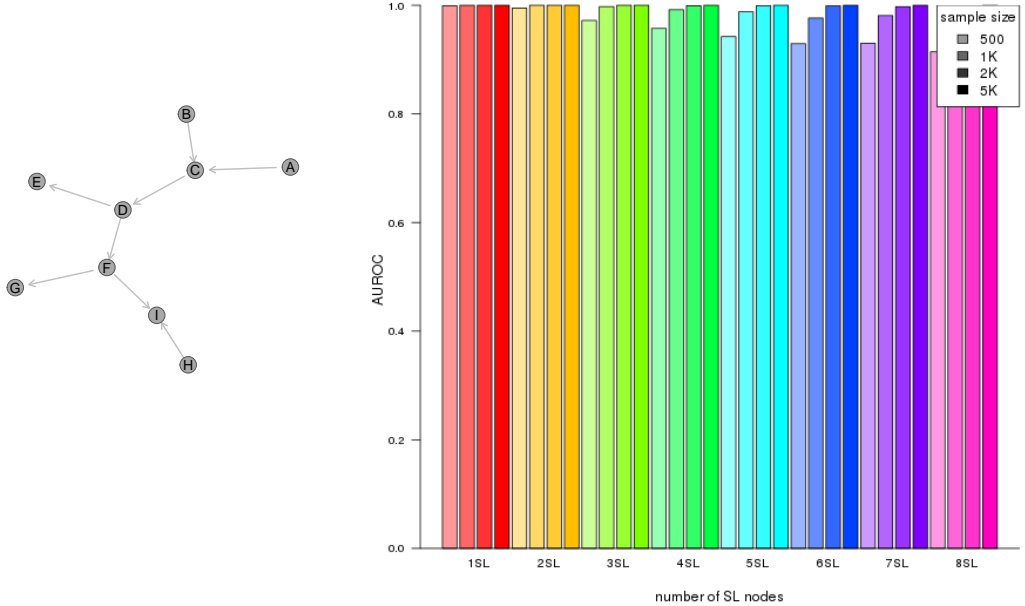
(d) Statistical performance

Figure O.24: **Performance of simulations including a simple graph.** Simulation of synthetic lethality was performed sampling from a multivariate normal distribution generated from Graph3 among 20,000 genes. Performance of SLIPT declines for more synthetic partners and lower sample sizes. For each parameter value, 1000 simulations were used.



(a) Statistical evaluation

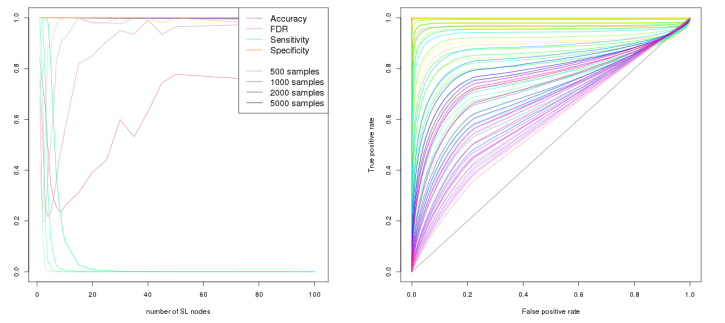
(b) Receiver operating characteristic



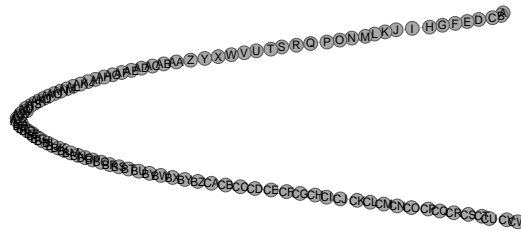
(c) Graph Structure

(d) Statistical performance

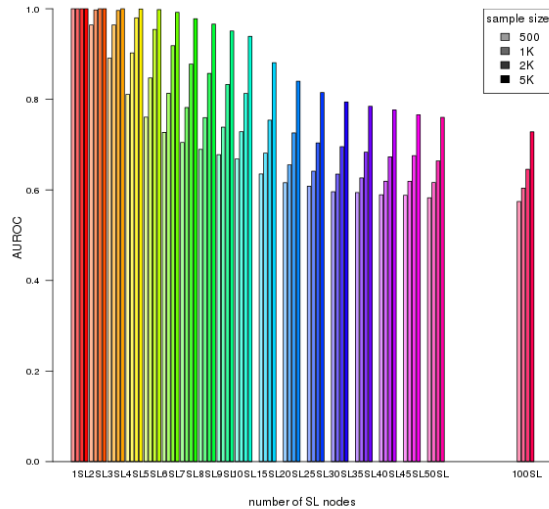
Figure O.25: **Performance of simulations including a constructed graph.** Simulation of synthetic lethality was performed sampling from a multivariate normal distribution generated from Graph4 among 20,000 genes. Performance of SLIPT declines for more synthetic partners and lower sample sizes. For each parameter value, 1000 simulations were used.



(a) Statistical evaluation (b) Receiver operating characteristic

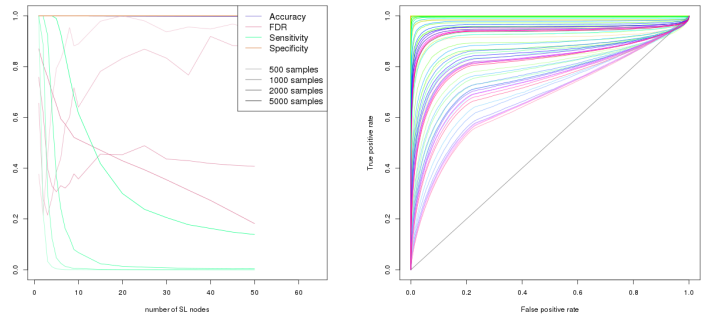


(c) Graph Structure

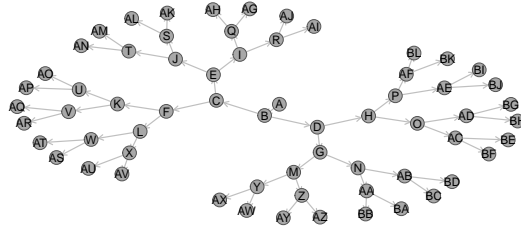


(d) Statistical performance

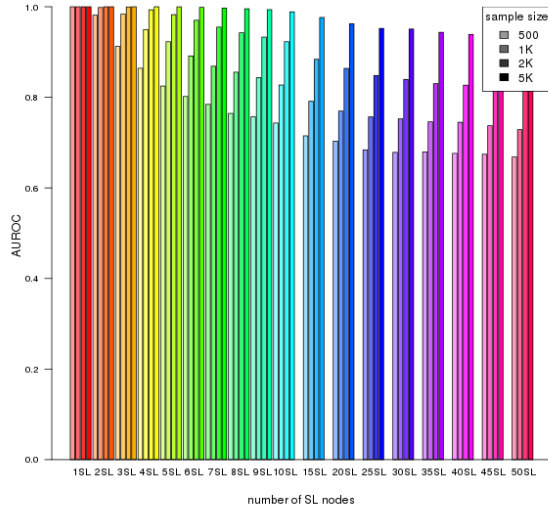
Figure O.26: Performance of simulations including a large graph. Simulation of synthetic lethality was performed sampling from a multivariate normal distribution generated from Graph5 among 20,000 genes. Performance of SLIPT declines for more synthetic partners and lower sample sizes. For each parameter value, 1000 simulations were used.



(a) Statistical evaluation (b) Receiver operating characteristic

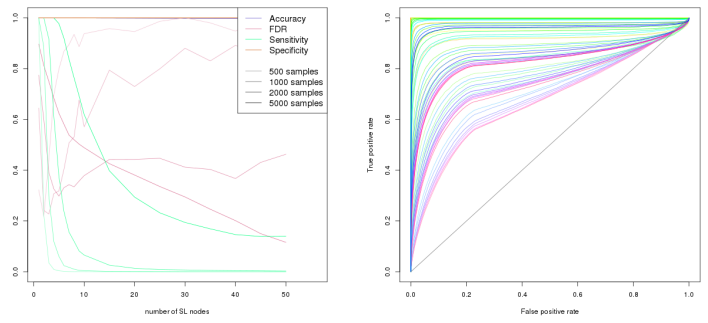


(c) Graph Structure

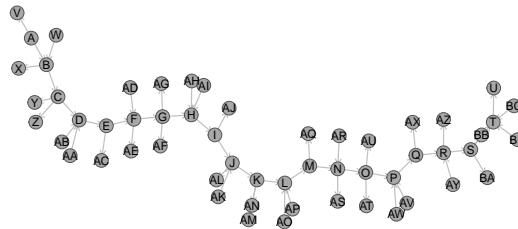


(d) Statistical performance

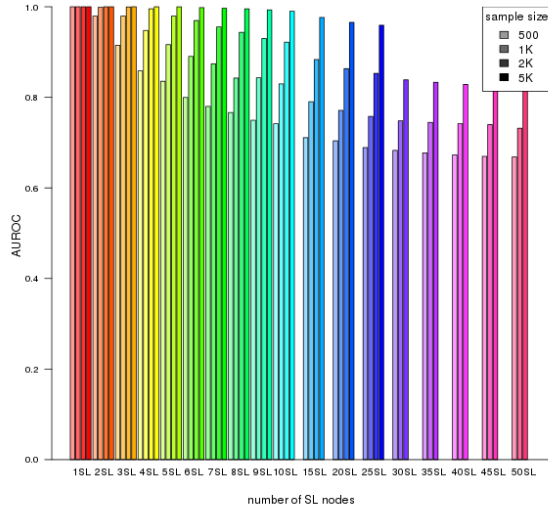
Figure O.27: Performance of simulations including a branching graph. Simulation of synthetic lethality was performed sampling from a multivariate normal distribution generated from Graph6 among 20,000 genes. Performance of SLIPT declines for more synthetic partners and lower sample sizes. For each parameter value, 1000 simulations were used.



(a) Statistical evaluation (b) Receiver operating characteristic



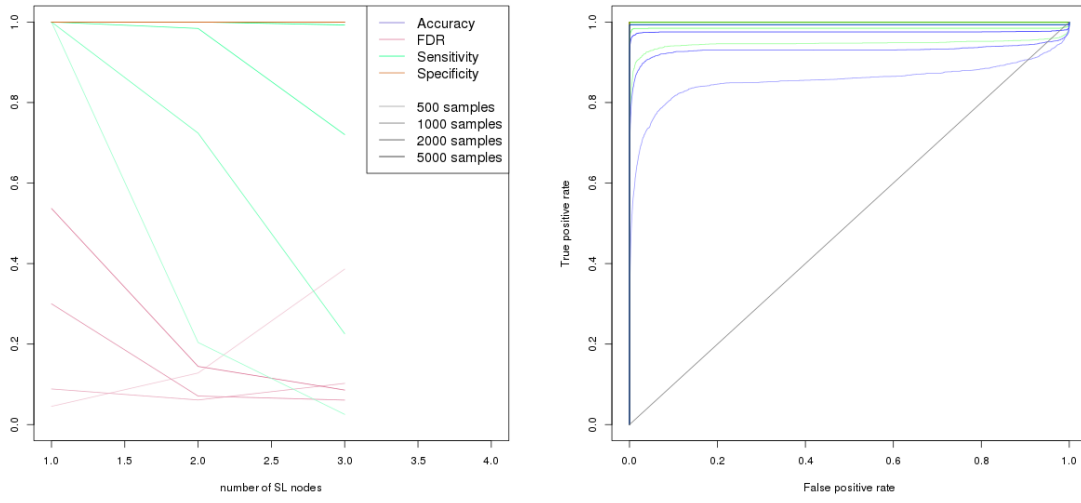
(c) Graph Structure



(d) Statistical performance

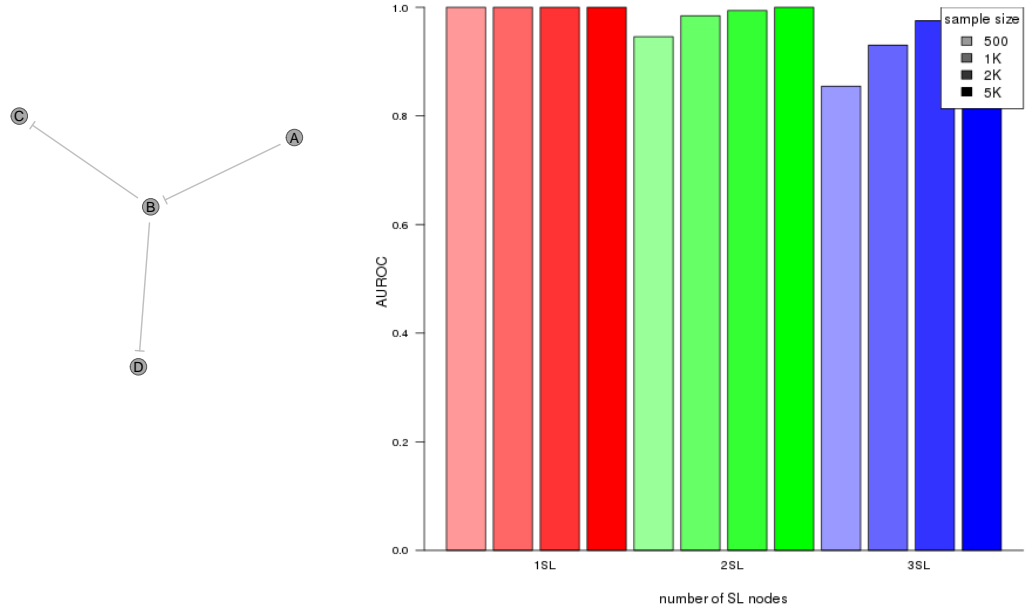
Figure O.28: Performance of simulations including a complex graph. Simulation of synthetic lethality was performed sampling from a multivariate normal distribution generated from Graph7 among 20,000 genes. Performance of SLIPT declines for more synthetic partners and lower sample sizes. For each parameter value, 1000 simulations were used.

O.4.1 Inhibiting Graph Structure Simulations with 20K genes



(a) Statistical evaluation

(b) Receiver operating characteristic



(c) Graph Structure

(d) Statistical performance

Figure O.29: Performance of simulations including a simple graph with inhibition.
 Simulation of synthetic lethality was performed sampling from a multivariate normal distribution generated from Graph1 with inhibitions among 20,000 genes. Performance of SLIPT declines for more synthetic partners and lower sample sizes. For each parameter value, 1000 simulations were used.

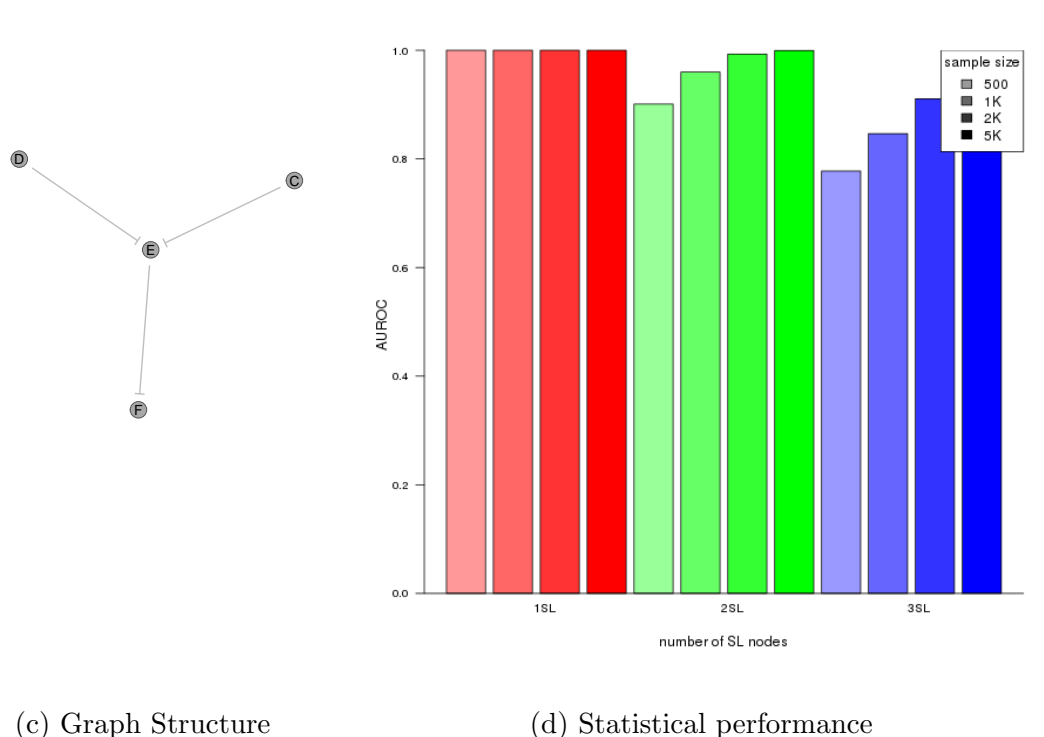
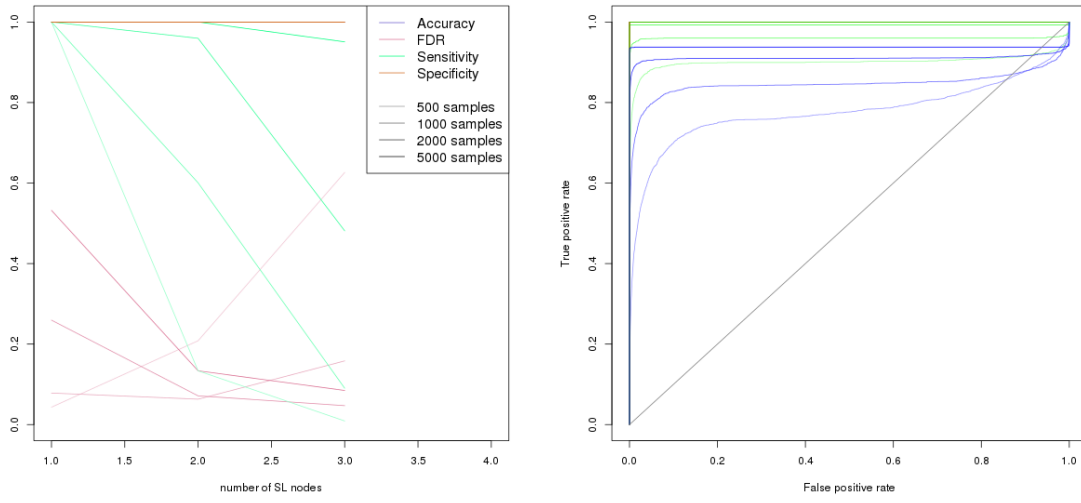
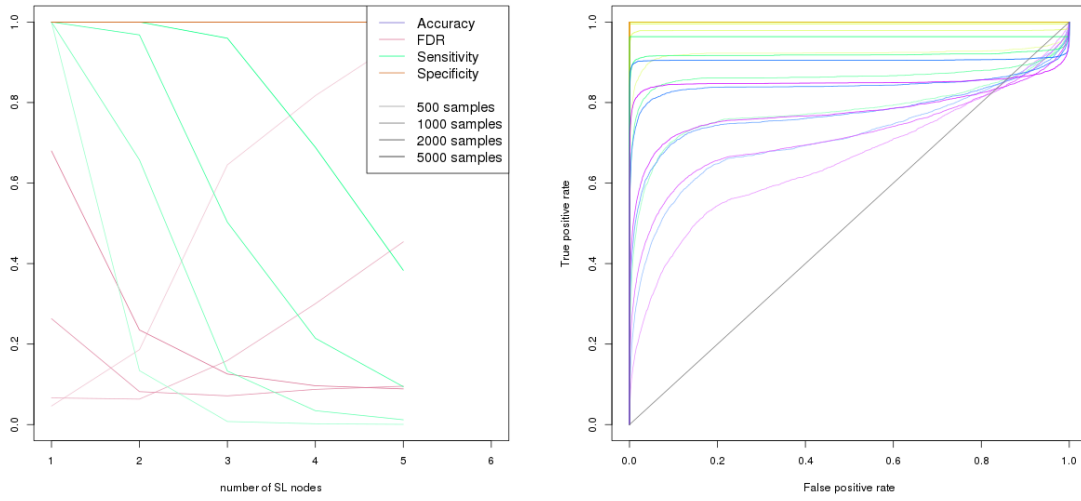
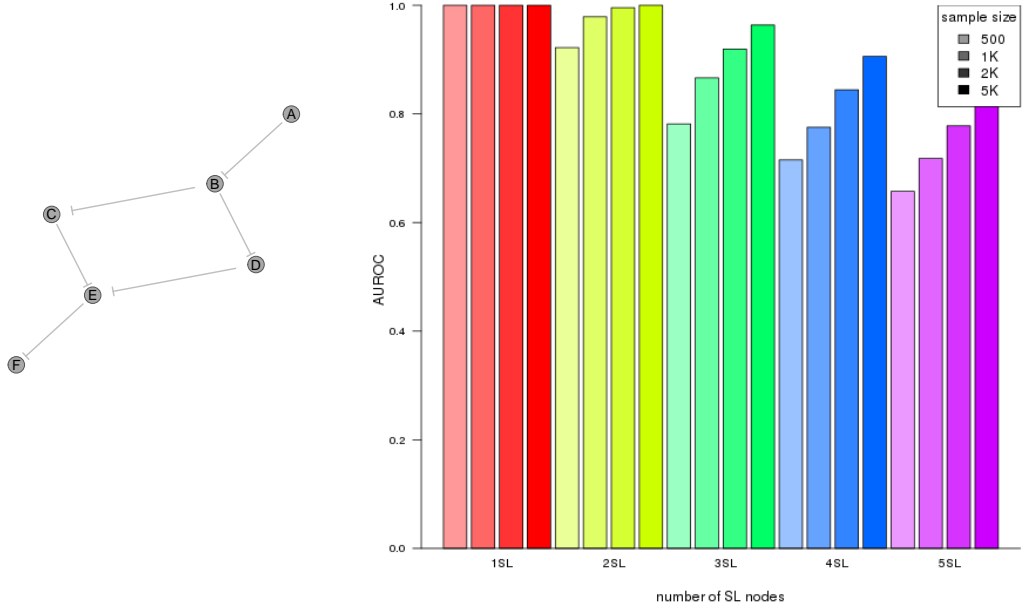


Figure O.30: Performance of simulations including a simple graph with inhibition.
 Simulation of synthetic lethality was performed sampling from a multivariate normal distribution generated from Graph2 with inhibitions among 20,000 genes. Performance of SLIPT declines for more synthetic partners and lower sample sizes. For each parameter value, 1000 simulations were used.



(a) Statistical evaluation

(b) Receiver operating characteristic



(c) Graph Structure

(d) Statistical performance

Figure O.31: Performance of simulations including a simple graph with inhibition.
 Simulation of synthetic lethality was performed sampling from a multivariate normal distribution generated from Graph3 with inhibitions among 20,000 genes. Performance of SLIPT declines for more synthetic partners and lower sample sizes. For each parameter value, 1000 simulations were used.

Simulations

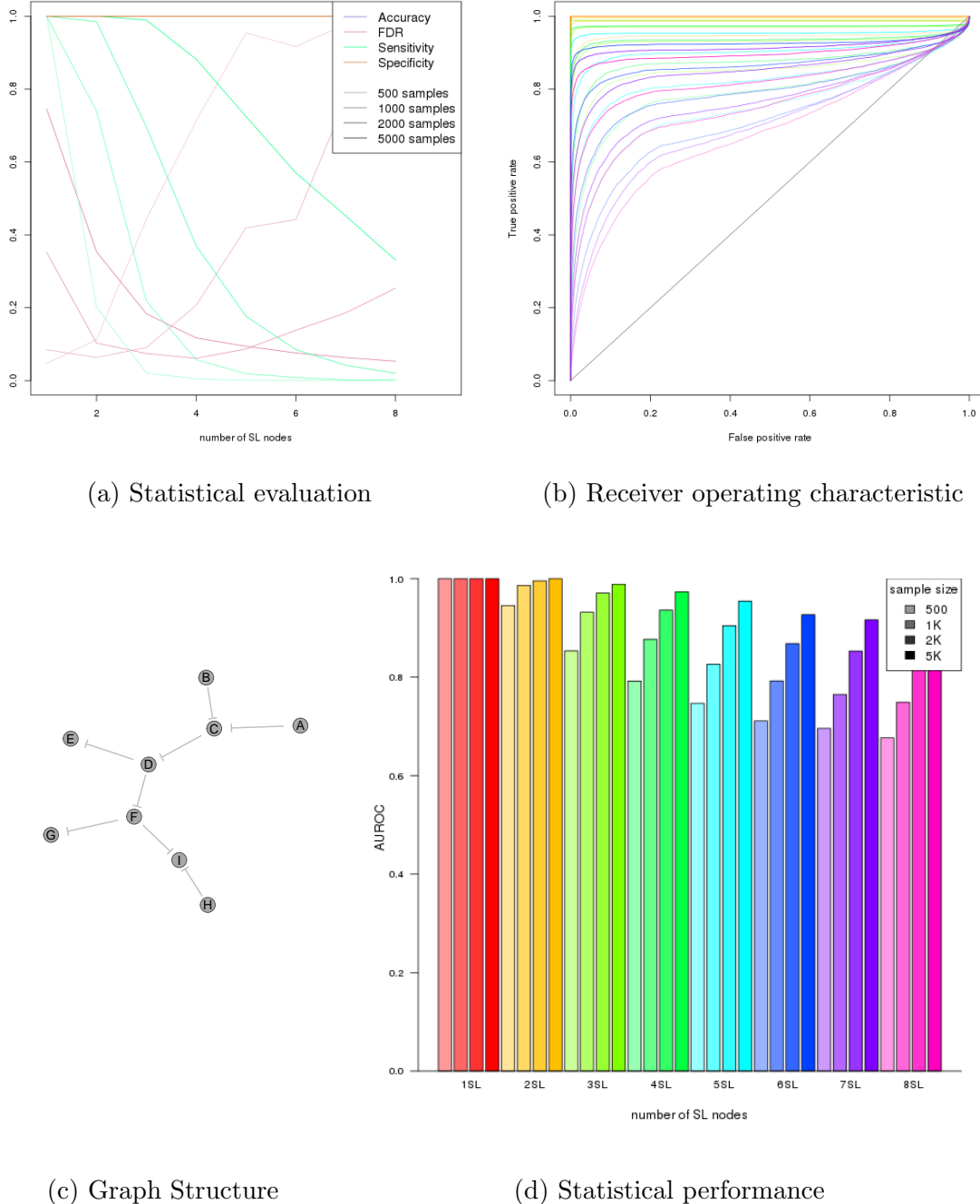
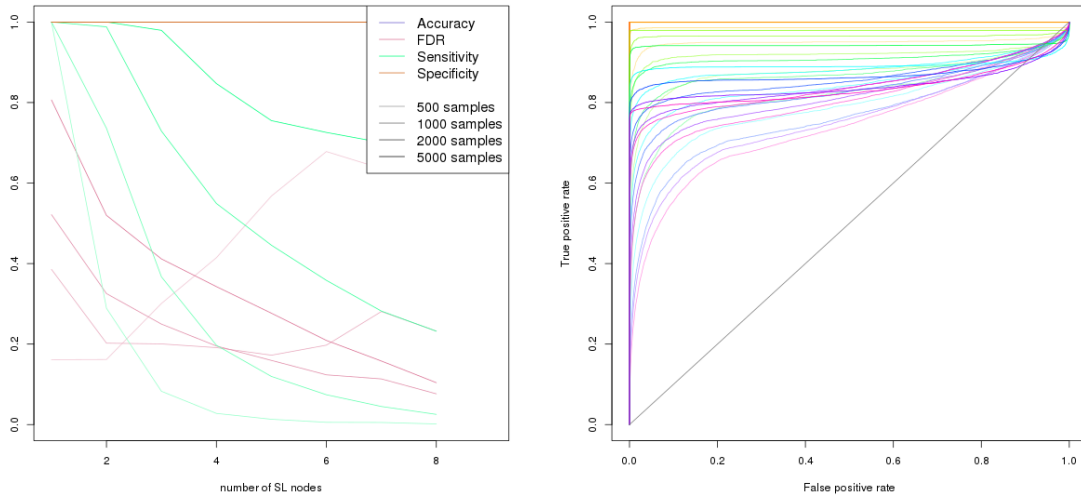
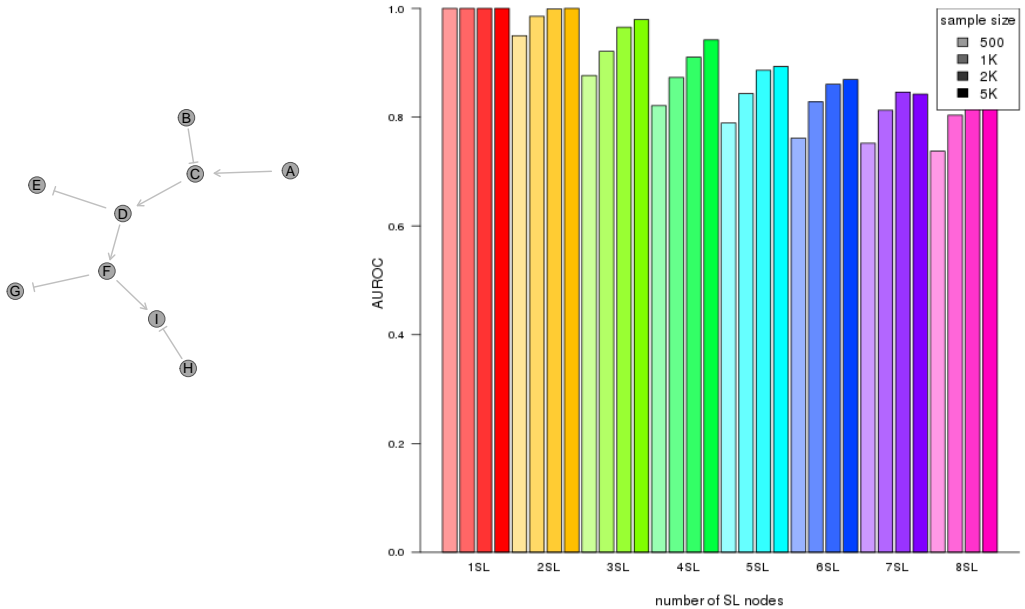


Figure O.32: Performance of simulations including a constructed graph with inhibition. Simulation of synthetic lethality was performed sampling from a multivariate normal distribution generated from Graph4 with inhibitions among 20,000 genes. Performance of SLIPT declines for more synthetic partners and lower sample sizes. For each parameter value, 1000 simulations were used.



(a) Statistical evaluation

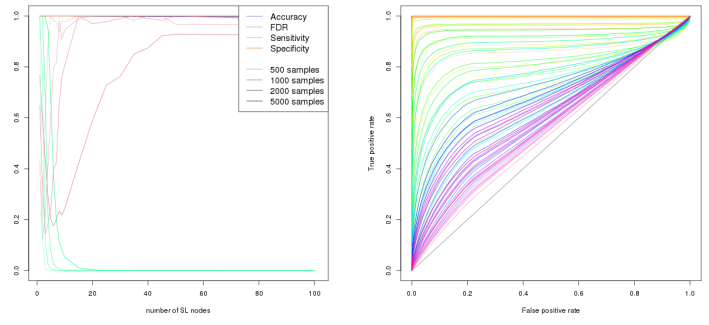
(b) Receiver operating characteristic



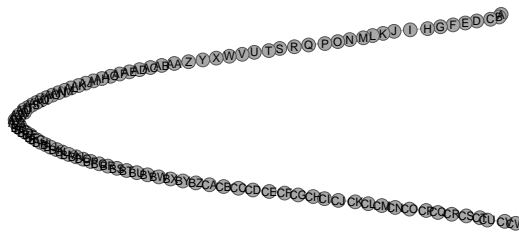
(c) Graph Structure

(d) Statistical performance

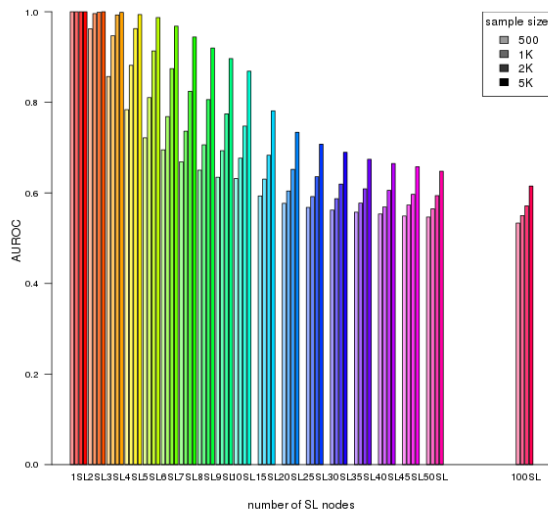
Figure O.33: Performance of simulations including a constructed graph with inhibition. Simulation of synthetic lethality was performed sampling from a multivariate normal distribution generated from Graph4 with some inhibitions among 20,000 genes. Performance of SLIPT declines for more synthetic partners and lower sample sizes. For each parameter value, 1000 simulations were used.



(a) Statistical evaluation (b) Receiver operating characteristic

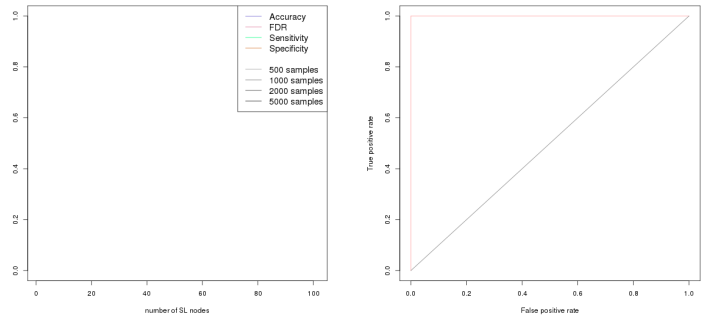


(c) Graph Structure

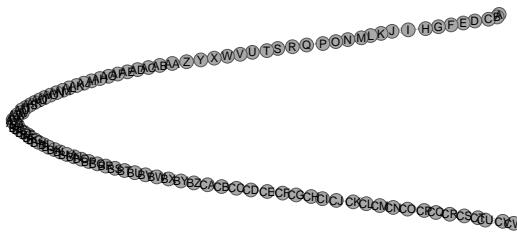


(d) Statistical performance

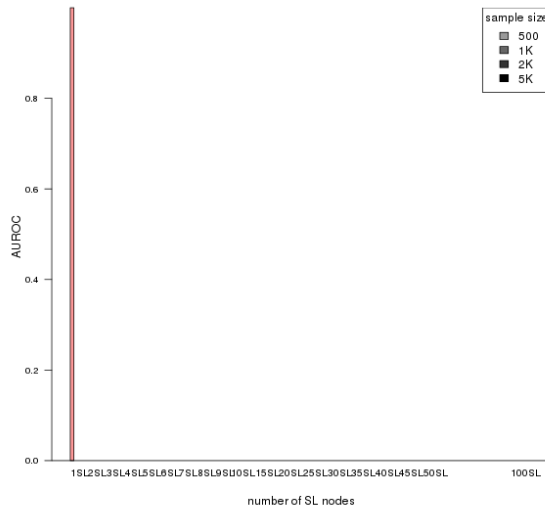
Figure O.34: **Performance of simulations including a large graph with inhibition.** Simulation of synthetic lethality was performed sampling from a multivariate normal distribution generated from Graph5 with inhibitions among 20,000 genes. Performance of SLIPT declines for more synthetic partners and lower sample sizes. For each parameter value, 1000 simulations were used.



(a) Statistical evaluation (b) Receiver operating characteristic

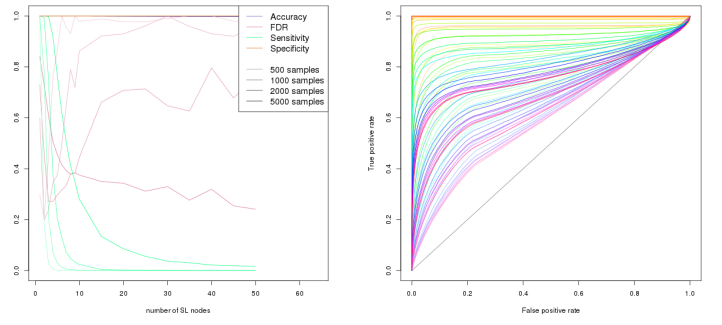


(c) Graph Structure

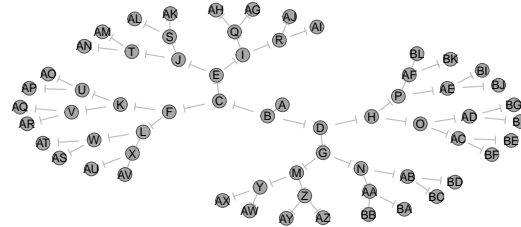


(d) Statistical performance

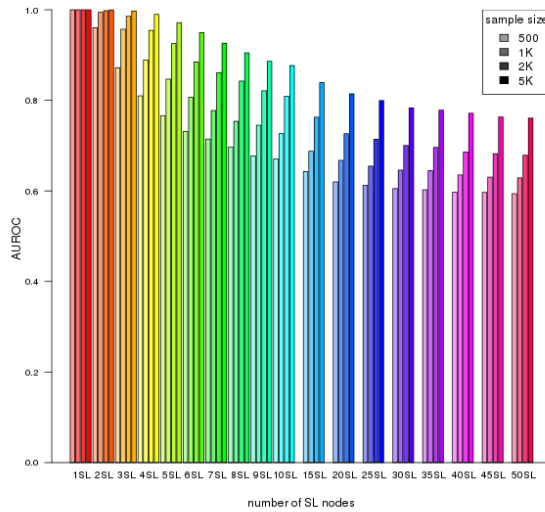
Figure O.35: Performance of simulations including a large graph with inhibition.
 Simulation of synthetic lethality was performed sampling from a multivariate normal distribution generated from Graph5 with alternating inhibitions among 20,000 genes. Performance of SLIPT declines for more synthetic partners and lower sample sizes. For each parameter value, 1000 simulations were used.



(a) Statistical evaluation (b) Receiver operating characteristic

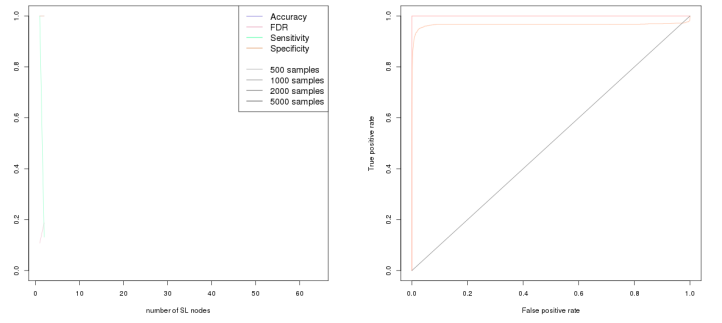


(c) Graph Structure

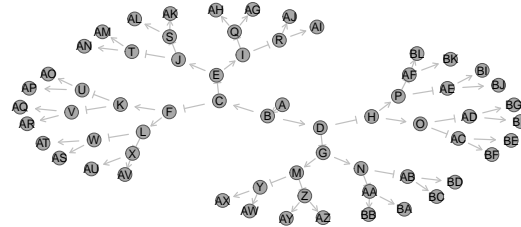


(d) Statistical performance

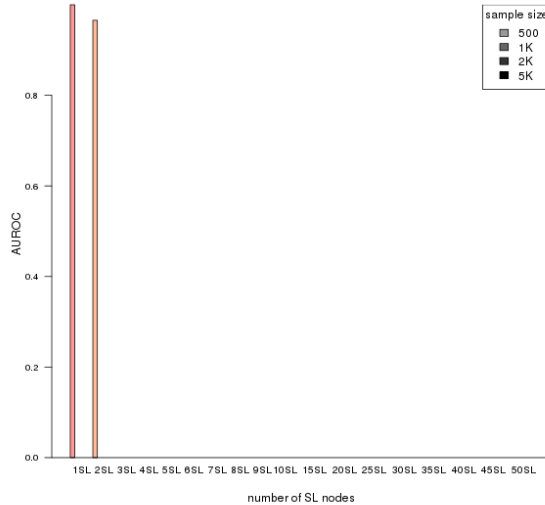
Figure O.36: Performance of simulations including a branching graph with inhibition. Simulation of synthetic lethality was performed sampling from a multivariate normal distribution generated from Graph6 with inhibitions among 20,000 genes. Performance of SLIPT declines for more synthetic partners and lower sample sizes. For each parameter value, 1000 simulations were used.



(a) Statistical evaluation (b) Receiver operating characteristic

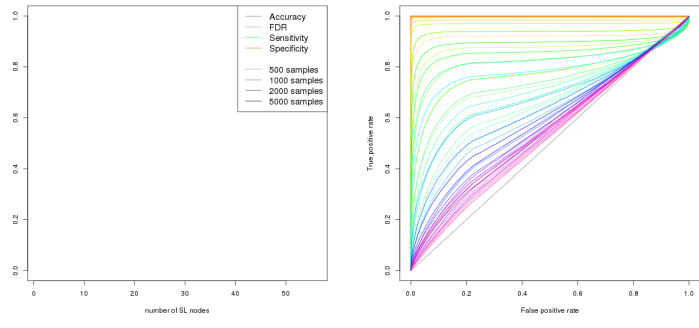


(c) Graph Structure

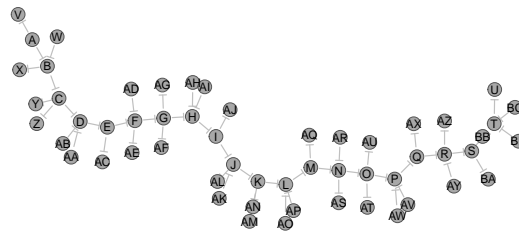


(d) Statistical performance

Figure O.37: **Performance of simulations including a branching graph with inhibition.** Simulation of synthetic lethality was performed sampling from a multivariate normal distribution generated from Graph6 with alternating inhibitions among 20,000 genes. Performance of SLIPT declines for more synthetic partners and lower sample sizes. For each parameter value, 1000 simulations were used.



(a) Statistical evaluation (b) Receiver operating characteristic

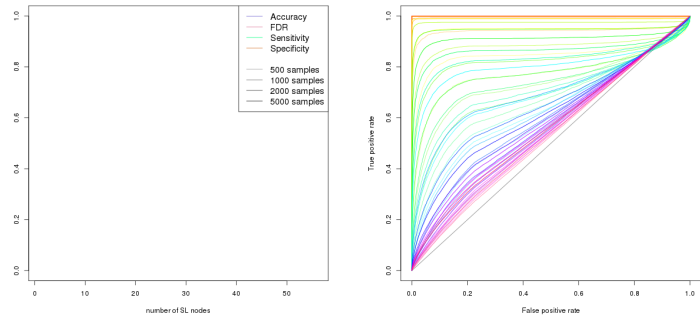


(c) Graph Structure

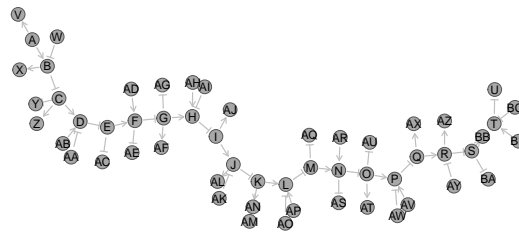


(d) Statistical performance

Figure O.38: Performance of simulations including a complex graph with inhibition. Simulation of synthetic lethality was performed sampling from a multivariate normal distribution generated from Graph7 with inhibitions among 20,000 genes. Performance of SLIPT declines for more synthetic partners and lower sample sizes. For each parameter value, 1000 simulations were used.



(a) Statistical evaluation (b) Receiver operating characteristic



(c) Graph Structure



(d) Statistical performance

Figure O.39: Performance of simulations including a complex graph with inhibition. Simulation of synthetic lethality was performed sampling from a multivariate normal distribution generated from Graph7 with some inhibitions among 20,000 genes. Performance of SLIPT declines for more synthetic partners and lower sample sizes. For each parameter value, 1000 simulations were used.

O.5 Simations from Pathway Graph Structures

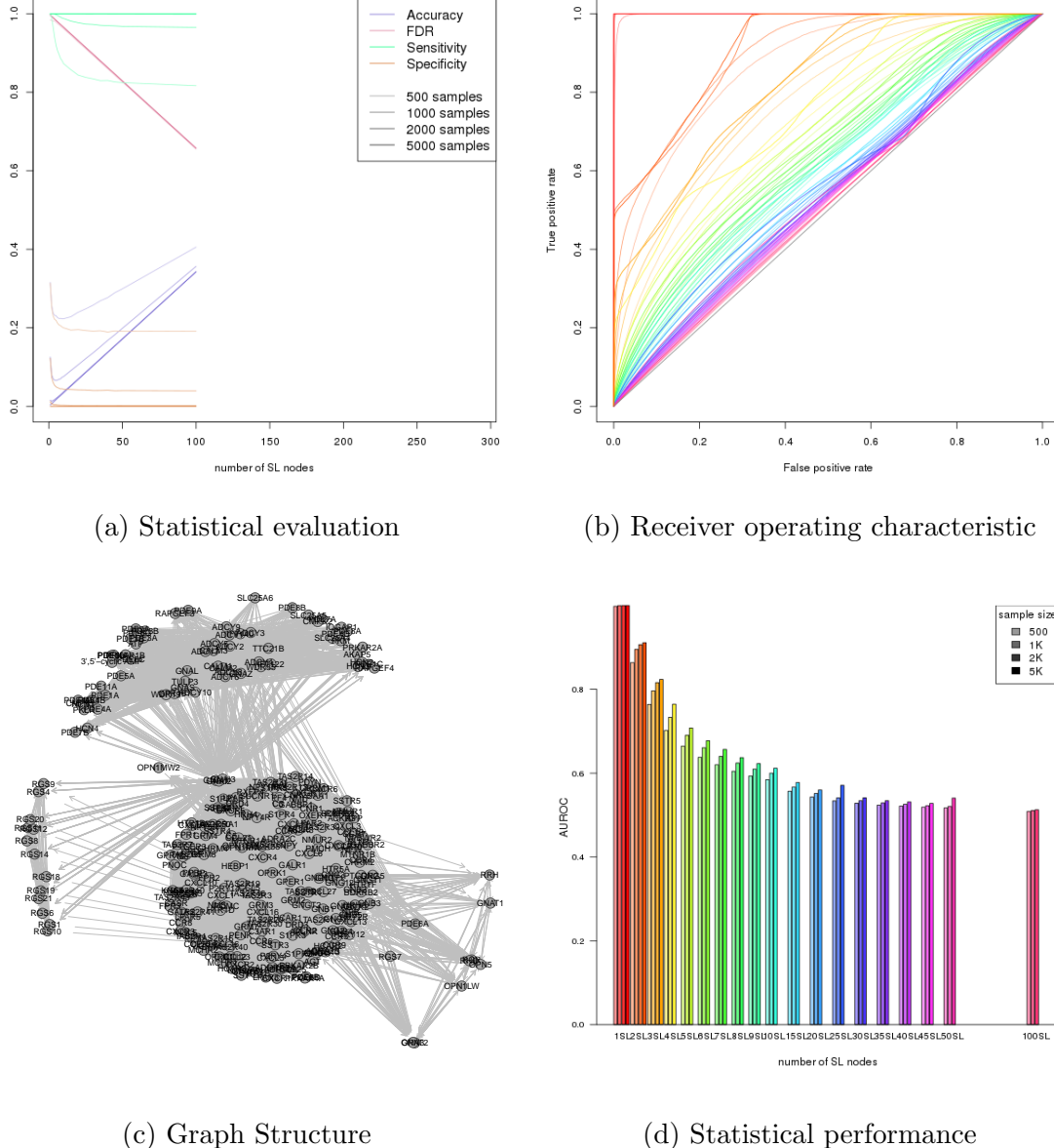
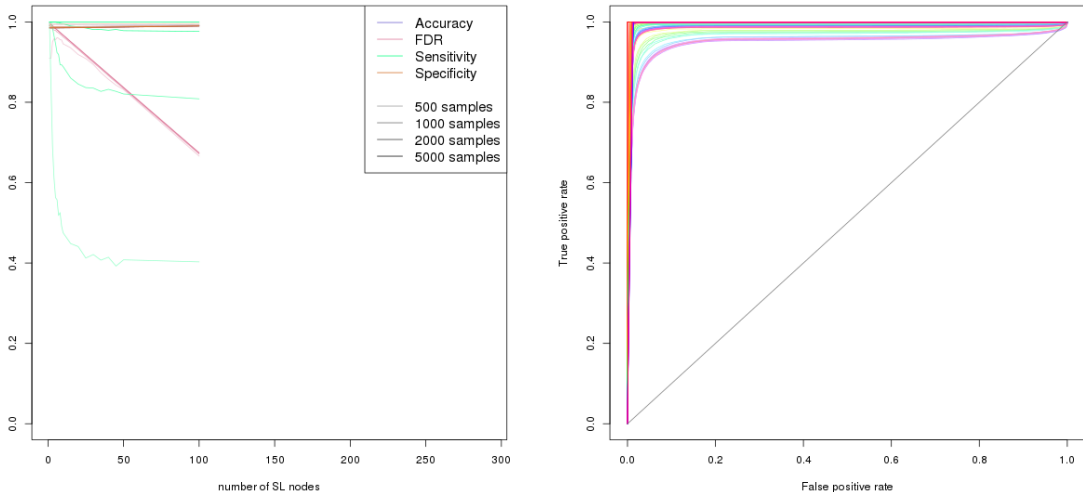
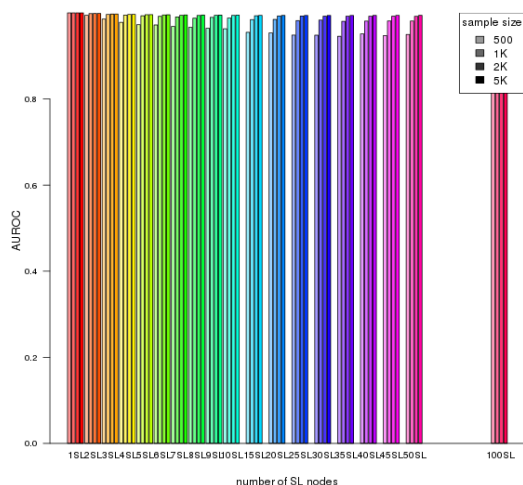


Figure O.40: Performance of simulations on the $G_{\alpha i}$ signalling pathway. Simulation of synthetic lethality was performed sampling from a multivariate normal distribution based on the Reactome $G_{\alpha i}$ signalling pathway. Performance of SLIPT was high across parameters for detecting synthetic lethality in the graph structure within a larger dataset. The performance decreases for a greater number of true positives to detect but the accuracy increases with a low false discovery rate.



(a) Statistical evaluation



(d) Statistical performance

Figure O.41: **Performance of simulations including the $G_{\alpha i}$ signalling pathway.**
 Simulation of synthetic lethality was performed sampling from a multivariate normal distribution (without correlation structure apart from the Reactome $G_{\alpha i}$ signalling pathway. Performance of SLIPT was high across parameters for detecting synthetic lethality in the graph structure within a larger dataset. The sensitivity decreases for a greater number of true positives to detect but the specificity remains high with a low false discovery rate.